The evolution of the sediment regime in a large open coast managed realignment site: a case study of the Medmerry Managed Realignment Site, UK

Jonathan Dale

A thesis submitted in partial fulfilment of the requirements of the University of Brighton for the degree of Doctor of Philosophy

May 2018

Abstract

Coastal wetlands are of global importance, but are threatened by rising sea levels and anthropogenic activity. This thesis focuses on a method of compensating for intertidal habitat loss, known as managed realignment (MR); the process of re-locating the land / sea border by allowing inundation of the coastal hinterland. However, there is growing evidence that saltmarshes in MR sites have lower biodiversity and ecosystem service delivery than anticipated, which may have consequences for the level of coastal flood defence and ecosystem functioning. Differences in the physical sediment characteristics, structure, hydrology and geochemistry have been proposed as possible explanations for these differences, which relate to the former land use and site design. This thesis aims to evaluate how former land use, site design and construction influence the evolution of the sediment regime in managed realignment sites, using as a case study the Medmerry Managed Realignment Site, West Sussex, United Kingdom, the largest open coast MR site in Europe (at the time of site inundation). A novel combination of surface sediment, hydrodynamic, creek morphogenesis, and subsurface structure and physiochemical datasets are analysed from a two year monitoring period. Results indicate that sediment was mainly imported into the Medmerry site (apart from during large freshwater discharge events), although greater concentrations of suspended sediment were measured being redistributed internally. Different patterns of sedimentation were observed at two spatially contrasting, but similarly designed, sites. At an exposed near-breach site, 15.2 cm of accretion were measured over a one year period, whereas rhythmic periods of accretion and erosion were measured at a sheltered location in the centre of the site. Measurements of embryonic creek development suggested that creek formation will occur relatively quickly (< 3 years), but is influenced by the subsurface sediment characteristics. Differences in the subsurface sediment conditions were found to relate to the former land use and changes following site inundation. These findings are discussed relative to the design and construction of MR sites, to improve the success of future schemes in terms of compensating for habitat loss and the provision of coastal flood defence. This is of particular importance as global communities face the implications of future climate change and attempt to sustainably defend against sea level rise, whilst compensating for habitat loss and degradation.

Table of Contents

List of Figures

List of Tables

List of Acronyms

µCT:	Microtomography
AD:	Anno Domini
B.P:	Before present
CIRIA:	Construction Industry Research and Information Association
CRM:	Certified Reference Material
CSM:	Cohesive Strength Meter
CTD:	Conductivity, temperature, depth
d_{50}:	Median grain size
DEFRA:	Department for Environment, Food and Rural Affairs
dGPS:	Differential Global Positioning System
DO:	Drainage Outlet
DTM:	Digital Terrain Model
EPS:	Extracellular polymeric substances
EU:	European Union
FNU:	Formazin Nephelometric Units
GPS:	Global Positioning System
ICP-OES:	Inductively Coupled Plasma-Optical Emission Spectrometer
LiDAR:	Light Detecting and Ranging
MAE:	Mean-absolute error
MHWN:	Mean high water neaps
MHWS:	Mean high water springs
MR:	Managed realignment
mS:	MicroSiemens
OD:	Ordnance Datum
PCA:	Principle component analysis
PPM:	Parts per million
PSI:	Pounds per square inch
P_{stag}:	Stagnation Pressure
PSU:	Practical Salinity Units
RMSE:	Root-mean-square error
s:	Seconds
SfM:	Structure-from-Motion
SSC:	Suspended Sediment Concentration
UAV:	Unmanned aerial vehicle

Acknowledgments

First, I would like to thank my supervisors; Heidi Burgess, Andy Cundy, Dave Nash and Callum Firth. Despite Andy and Callum moving on to pastures new during my project, they have all supported me and helped me to develop academically. I will always be appreciative for the time and support they have invested in me. I am grateful to the Environment Agency for funding my project, supplying additional data and giving me the opportunity to study such an amazing site, and for the support from the RSPB (particularly Tim Callaway and Peter Hughes) and everyone else working and involved at Medmerry.

I would also like to thank Niall Burnside (University of Brighton) for his time and support with the UAV survey, Kate Spencer, Simon Carr and Lucy Diggens (all Queen Mary, University of London) for providing the microtomography data, and Ian Croudace (University of Southampton) for the ITRAX data. My thanks also go to all the academics and colleagues from other institutions that I have had the opportunity to engage and discuss my project with, including Rolf Riethmuller (Helmholtz-Sentrum Geesthacht) and everyone involved with the Estuarine and Coastal Sciences Association.

I wish to acknowledge my appreciation for the support provided by the School of Environment and Technology and the Doctoral College at the University of Brighton, including the financial and administrative support. A big thank you goes to everyone I have had the pleasure to teach and lecture with, especially everyone on the Greece field trip. I would like to thank Pete Lyons, Pete Mathers, Dave Harker, Linda Barber and Bill Whitney for their technical support. I am also grateful and appreciative of everyone who came on site with me, especially Magda, Matt, Dom and Fabio. Thank you to everyone I have had the pleasure to share an office and the PhD journey with, particularly Paul, Sam, Rob, Eva, Mariana, Matt and Sarah, your support, guidance and encouragement along the way has always been appreciated.

I would like to thank my friends and family. My parents, who have always been there and encouraged me from an early age (“you haven’t had fun unless you come home covered in mud”), Simon, Nana and the rest of my family. Finally, I would like to thank Sophie for her support, and for putting up with all the mud.

Author’s Declaration

I declare that the research contained in this thesis, unless otherwise formally indicated within the text, is the original work of the author. The thesis has not been previously submitted to this or any other university for a degree, and does not incorporate any material already submitted for a degree.

Signed:

Dated:

1 Introduction: The Nature of Coastal Wetlands

Intertidal wetlands, consisting of saltmarsh, mudflat and mangrove habitats, form a transition between marine and terrestrial systems (Figure 1.1) and provide a range of ecosystem services (e.g. Barbier et al., 2011; Costanza et al., 1997; Granek et al., 2010; Turner and Daily, 2008). In recognition of the importance of these environments, the global value of saltmarshes and mangroves has been estimated to be $1,648 billion per annum (Costanza et al., 1997). Mangroves are located on tropical shorelines, whereas saltmarshes are found on low energy, mid to high latitude coastlines (e.g. Mitsch and Gosselink, 2000). Saltmarshes occupy around 5.1 Mha of the Earth's surface (Pendleton et al., 2012) and develop in areas where fine sediment can accumulate due to limited tidal currents and wind-wave action. Wetland environments provide important ecosystem services (Costanza et al., 1997), such as the provision of nursery habitats, water quality regulation and coastal flood defence (Barbier et al., 2011).

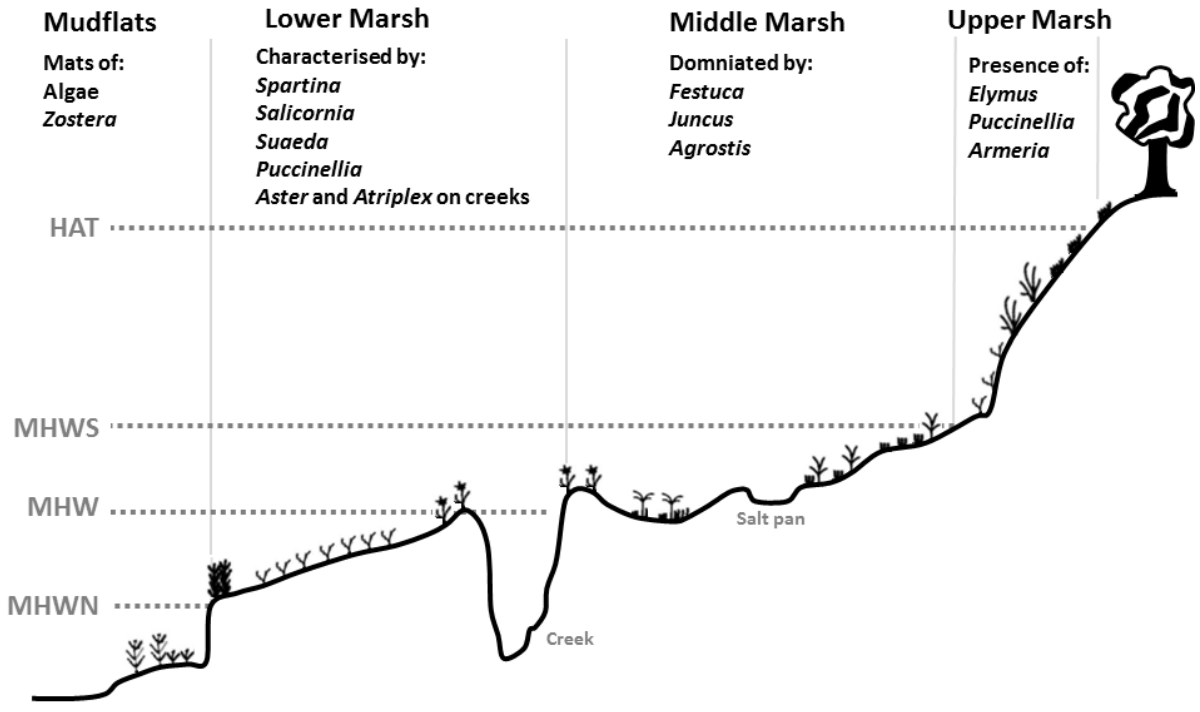

Figure 1.1: Typical profile of a United Kingdom intertidal mudflat and saltmarsh (adapted from: Foster et al., 2013; Rodwell, 2001).

Despite their importance, coastal wetlands are under threat from rising sea levels, pollution, reclamation and other anthropogenic activities (e.g. Kennish, 2002), causing degradation and habitat loss on a global scale. Pye and French (1993) estimated that, between 1993 and 2013, 8000 to 10,000 hectares (ha) of intertidal mudflat for England alone would be lost as a result of erosion caused by rising sea levels. There are a number of approaches to rehabilitate and compensate for the loss of intertidal habitat, including managed realignment (MR). This technique describes the process of re-locating the land / sea border (French, 2006) by lowering, de-embanking or breaching the previous defences, and constructing new or maintaining previous secondary defences. MR is the focus of this study, which investigates the following research questions;

1) How does surface sediment properties change in MR sites following tidal inundation?
2) To what extent are the rates and rhythms of sediment accretion and erosion controlled by the fluxes of suspended sediment transport and hydrodynamic variability in MR sites?
3) What factors control the formation and subsequent evolution of creek networks in MR sites?
4) Following site inundation, what are the causes of any differences and changes in the subsurface physicochemical and structural evolution of MR sites?

1.1 Geomorphological Characteristics

The substrate of low-energy saltmarshes and mudflats tends to be dominated by cohesive sediment, a complex mixture of flocculated clay and inorganic minerals, organic material, liquids and gases, and forms as a result of biological processes, weathering and transportation of material (e.g. Grabowski et al., 2011). Sediment is, by definition, formed of material that can settle in water due to gravity and has been deposited following the processes of erosion and transportation, as opposed to soils which are subjected to pedogenesis (soil formation processes). The mineral solids in cohesive sediments consist of a clay fraction (< 2 μm), a silt fraction (2 μm to 63 μm), and a sand fraction (> 63 μm). The surface of the plate-like clay minerals have an ionic charge equal to, or greater than, the force of gravity (Dyer, 1986), creating an

electrostatic interaction between the particles. As a result, particles stick together, or flocculate, rather than acting as individual particles. The strength of the inter-particle cohesive force increases with decreasing particle size (Mehta et al., 1989), therefore the clay content is predominantly the controlling factor determining whether sediments behave cohesively or not.

The behaviour and characteristics of saltmarshes and mudflats are determined by the tidal range, the wind-wave climate, sediment supply, relative sea level change and biological (floral and faunal) activity (Allen and Pye, 1992; Pethick, 1992). Once the surface of the intertidal zone reaches a sufficient elevation, relative to mean sea level, halophytic vegetation can colonise creating a saltmarsh which adds organic matter and, in turn, traps and binds sediment, increasing the rate of sedimentation (Allen and Pye, 1992). Saltmarshes develop between the elevations of mean high water spring (MHWS) tides and mean high water neap (MHWN) tides (Figure 1.1) and are periodically inundated by seawater, which infiltrates the sediment during high water and drains during low water. The abundance of difference species of halophytic vegetation varies across the marsh profile (e.g. Rodwell, 2001) depending on the hydroperiod; the duration and frequency of tidal inundation (Mitsch and Gosselink, 2000). This creates different vegetation zones, as illustrated in Figure 1.1.

Intertidal wetlands are ecologically active zones with biological processes affecting the sediment in numerous ways (Whitehouse et al., 2000), including the reworking and mixing of deposited sediment; a process known as bioturbation. These biological processes can act to stabilise the sediment through the secretion of adhesive mucous compounds called extracellular polymeric substances (EPS). EPS are secreted by bacteria, microalgae and microfauna, and act to bind together the sediment particles together. However, biological activity can also make sediment more susceptible to erosion as a result burrowing and digging weakening the sediment structure.

Most saltmarshes are dissected by salt pans and creek networks (Allen, 2000), which are often dendritic and extend the mudflat into the upper intertidal zone (Pethick, 1992), acting as conduits for tidal waters, sediment and nutrients between the marsh and the

adjacent coastline. There are a number of conceptual models used to predict saltmarsh accretion, and therefore evolution, over time (e.g. Allen, 2000). These models typically portray an asymptotic relationship between the elevation of the marsh and time, with initially high sedimentation rates that slow as the elevation increases and the hydroperiod decreases. However, these models tend to be simplified and fail to incorporate mass erosion events, such as storms (e.g. Pethick, 1992), which can interrupt the long-term evolution of the marsh surface.

1.2 Importance of Saltmarsh and Mudflat Habitat

Intertidal wetlands are of global importance as they provide a range of ecosystem, economic and cultural services such as wildlife habitat and species diversity, carbon sequestration, immobilisation of pollutants, water quality improvements, social and recreation opportunities, and protection from coastal flooding (e.g. Costanza et al., 1997; King and Lester, 1995; Moller et al., 2014; Moller et al., 2001; Stark et al., 2016). They are biologically highly productive; they support, and provide nursery grounds for, a number of commercial fish and shellfish species (Boorman and Hazelden, 1995), including oysters, grey mullet, bass and flat fish such as plaice and flounders (King and Lester, 1995). A large number of migratory and over-wintering wildfowl and wading birds graze, nest and roost on marshes, and passerines feed on seeds from the vegetation (Boorman and Hazelden, 1995). Furthermore, a range of invertebrates are found in these environments which provide an important food source for various species of fish, shellfish and birds (Boorman, 1992). The ecological importance of the intertidal zone is evident in national and international conservation policies; in the United Kingdom, more than 80 % of saltmarshes are protected by designations owing to their nature conservation interest (Burd, 1989; Foster et al., 2013).

In addition to their ecological importance, saltmarshes provide an enhanced level of coastal flood defence through the attenuation of wave height and dissipation of wave energy (Cooper, 2005; Moller, 2006; Moller et al., 2014; Moller and Spencer, 2002; Moller et al., 1999; Stark et al., 2016). Defence is provided by increased friction, in addition to a decrease in water depth, over the marsh surface (Moller et al., 1999).

Brampton (1992) used scaled physical models to predict an approximate 40 % reduction in wave height over an 80 m wide saltmarsh, although recent field and flume experiments have suggested a greater reduction in wave energy (Moller et al., 2014; Moller and Spencer, 2002). Furthermore, these environments also protect and reduce the cost of maintaining engineered defences, such as sea walls (e.g. King and Lester, 1995), which are becoming a growing concern due to questions over their medium to long term integrity (French, 2006).

1.3 Coastal Squeeze and the Loss of Intertidal Habitat

Intertidal habitats are under significant pressure and are being lost and degraded, partly due to alterations and influences caused by human activities (e.g. Gedan et al., 2009). Approximately 50 % of saltmarshes have been lost globally (Barbier et al., 2011) as a result of a reduction in water quality, climate change and sea level rise. Furthermore, saltmarshes and mudflats have been reclaimed (embanked and drained) for agriculture, industry and recreational use, and coastal development through the construction and expansion of ports and marinas, dredging activities and the construction of coastal defences (e.g. Esteves, 2014; Jacobs et al., 2009; Kennish, 2002). With sea levels predicted to rise between 0.4 and 1.2 m by 2100 (Horton et al., 2014), depending on the future temperature scenario, coastal defences and other developments create a 'fixed' coastline (Figure 1.2), resulting in a process known as coastal squeeze (Doody, 2004; Doody, 2013).

Under natural conditions intertidal habitats would adjust dynamically to relative sea level rise by migrating inland to occupy the same position in the tidal frame (French, 1999), depending on numerous interacting physical and biological variables such as: sediment supply, rate of sea level rise, topography and vegetation type (e.g. Esteves, 2014). Hard engineered structures prevent this migration from happening, intensifying the marsh instability as waters deepen and the duration and frequency of tidal inundation increases, resulting in enhanced marsh edge erosion, widening of creeks and a loss of intertidal habitat (e.g. French, 1999).

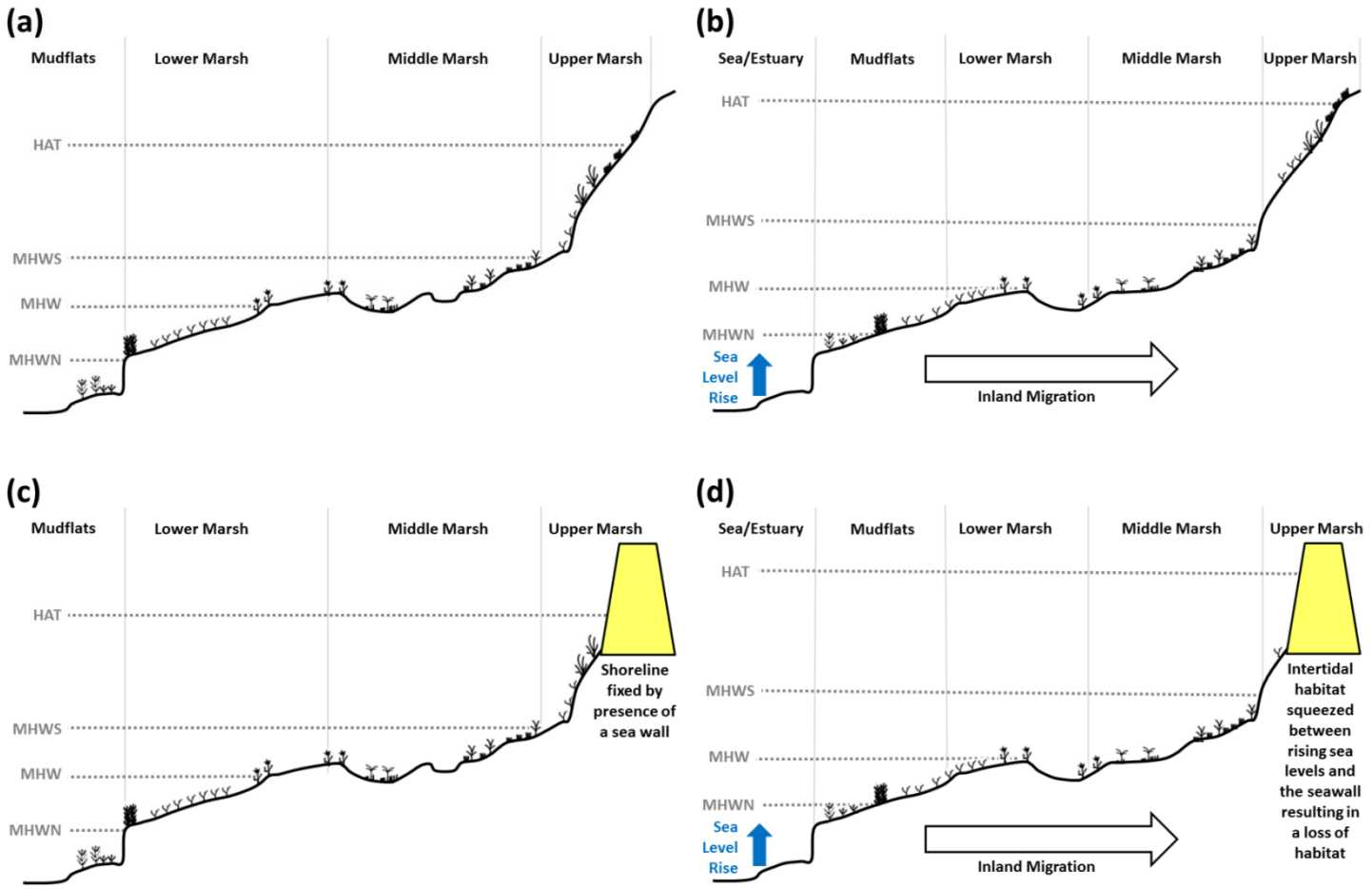

Figure 1.2: The loss of intertidal habitat through coastal squeeze. (a) The zonation of intertidal habitat in relation to tidal range. (b) Intertidal habitats tend to migrate inland in response to rising sea levels, however (c) when hard engineered structures such as sea walls are present the shoreline becomes fixed. (d) This prevents the inland migration of the intertidal zone resulting in habitat loss as the saltmarsh and mudflat are forced against the defences and squeezed between the fixed shoreline and rising sea levels.

The influence of coastal squeeze is such that it is widely considered to be the main cause of intertidal habitat loss (e.g. Doody, 2013). However, there are a number of mechanisms driving habitat loss (e.g. Pontee, 2013), including changes in the wind / wave climate and changes in sediment supply. In a study of pioneer marshes in the south-east of England, Hughes and Paramor (2004) related an increased abundance of the polychaete *Nereis diversicolor* to habitat loss rather than coastal squeeze. Furthermore, it has been suggested by Kirwan et al. (2016) that current predictions overestimate rates of marsh vulnerability as they do not account for biophysical processes, which can accelerate the build-up of marshes vertically. These authors also argued that current estimates do not account for the ability of marshes to migrate inland. Nonetheless, their study primarily focused on marshes in the United States that are not backed by hard coastal flood defences. As the prevention of inland marsh migration by hard defences forms the fundamental basis of the coastal squeeze theory, it is probable that in areas where coastal squeeze is occurring estimates of marsh vulnerability are more accurate than Kirwan et al. (2016) proposed.

Recognition of the importance of, and threats to, intertidal habitats has resulted in calls for an approach to coastal management that protects and allows for the sustainable use of these environments, termed an ecosystem services approach (e.g. Balmford et al., 2002; Bockstael et al., 2000; Costanza et al., 1997; Turner and Daily, 2008). The ecosystem services approach is a conceptual framework which provides a collection of methods to support sustainable ecosystem management, and delivers a range of pathways for coastal managers to consider the options available, and to effectively communicate the consequences to various stakeholder groups (Granek et al., 2010).

Environmental regulations now enforce mitigation and compensatory measures for habitat loss (van Loon-Steensma and Vellinga, 2013). For Europe, this is exemplified by the European Union Habitats Directive (European Parliament and the Council of the European Commission, 1992), which protects against any development that might pose a threat to the integrity of designated Special Areas of Conservation (Leggett et al., 2004; Pethick, 2002). In addition, intertidal environments are protected by Nature 2000 designations (Esteves, 2014) and the Ramsar convention (Leggett et al., 2004). In the United Kingdom, this protection is implemented through the Habitats Directive, which

is transposed through the Habitats Regulations to determine the effects of any plan or project on protected habitats.

1.4 Compensating for Habitat Loss

There have been a number of rehabilitation schemes to (partially, or fully) replace the structural or functional characteristics of a lost or reduced ecosystem, either through the creation of new habitat or re-creating and restoring habitat (cf. Elliott et al., 2007). These schemes use ecological engineering approaches to either enhance the physical-biological links through habitat creation or modification, such as replanting schemes, or by engineering the physical processes to create the desired conditions for habitat creation (Elliott et al., 2016). For example, it may be necessary to increase the rate of sedimentation by decreasing current velocities over the intertidal zone or increasing the suspended sediment concentration (Boorman and Hazelden, 1995). Several methods of protecting saltmarshes were reviewed by Doody (2008), including engineered structures such as offshore breakwaters and riprap at the eroding marsh edge to reduce current velocities over the marsh, allowing vegetation to become rooted and established, and increasing marsh stability. On the other hand, sediment lost via erosion can be replenished by sediment recharge projects using dredged material and soils removed from elsewhere (Doody, 2008). For example, materials excavated from central London during the Crossrail project were used for a habitat creation scheme as part of Wallasea Island project (Tucker, 2017). However, the suitability of this technique is questionable as the available material may not be representative of the original marsh sediments and could contain contaminants such as heavy metals. Alternatively, it is possible to offset reductions in the extent of saltmarsh and mudflat through habitat recreation schemes, inundating areas that have previously been reclaimed through the construction of embankments and drained, usually for agriculture; a technique known as managed realignment (MR).

MR as a technique for restoring and compensating for intertidal habitat loss is reviewed in Chapter 2. It has become increasingly popular in Europe and America (Esteves, 2014; Mazik et al., 2010), and in the United Kingdom has been the preferred approach to

coastal management for just over a decade (Esteves, 2013). The process involves inundating the previously defended low-lying coastal hinterland by re-locating the land / sea border (French, 2006), by lowering, de-embanking or breaching the former defences and constructing new or maintaining secondary defences. However, there is increasing evidence that MR sites have lower biodiversity and delivery of ecosystem services than anticipated (e.g. Mossman et al., 2012). These shortcomings have been linked to physical disturbances, such as changes in sediment structure, compaction, and the collapse of pore space, to the sediment caused by the former land use (see Chapter 2). These alterations may lead to reduced hydrological connectivity, poor drainage and anoxia (Crooks et al., 2002; Tempest et al., 2015), preventing species colonisation. Despite this, there remains a lack of understanding of the impact MR has on subsequent sedimentary processes (Esteves, 2013). This is particularly the case for the influence of different former land uses, the site design and the site construction processes on the evolution of the sediment regime; the key sediment erosion, transportation, deposition, and consolidation characteristics.

1.5 Thesis Aims, Approach and Structure

This thesis aims to evaluate how the former land use, site design and construction influence the evolution of the sediment regime in MR sites. The research presented comprises a novel combination of field based and laboratory approaches, examining measurements taken over varying temporal and spatial scales at the Medmerry Managed Realignment Site, West Sussex, United Kingdom (see Chapter 3 for site description and history). Breached in September 2013 and occupying 450 ha, the Medmerry site is the largest open coast MR site in Europe (at the time of site inundation), and is predicted to create 300 ha of intertidal and transitional habitat (Pearce et al., 2011). Measurements were taken over a two year period (November 2014 – October 2016), during the second and third years after site inundation. Specifically, the objectives for the research presented are to:

5) Regularly monitor the surface sediment properties to assess changes during the study period;
6) Assess rates and rhythms of sediment accretion and erosion in response to the fluxes of suspended sediment transport and hydrodynamic variability;

7) Analyse formation and subsequent evolution of creek networks;
8) Identify differences and changes in the subsurface physicochemical and structural evolution;
9) Evaluate the evolution of the sediment regime in terms of Objectives 1 to 4 in response to the former land use, site design and construction, to inform the design and construction of future MR schemes.

The thesis is comprised of ten main chapters including four results chapters, with measurements and findings discussed within each results chapter. Following this introduction:

- **Chapter 2:** Reviews the current knowledge and approaches to managed realignment with a focus on the evolution of the sediment regime.
- **Chapter 3:** Presents the wider study area, the coastal management issues, and the study site for this thesis.
- **Chapter 4:** Details the methods and equipment used to investigate the evolution of the sediment regime at the study site, both in the field and the laboratory.
- **Chapter 5:** Provides the principle monitoring data on the evolution of the sediment regime during the second and third year of site inundation through measurements of the change in bed elevation, surface sediment properties and cohesive strength from the six study sites.
- **Chapter 6:** Evaluates the rhythms of sedimentation and fluxes of suspended sediment in response to hydrodynamic variability.
- **Chapter 7:** Reports observations of the morphogenesis and evolution of embryonic creek networks at three locations within the Medmerry site. The change in creek position and elevation are also assessed.
- **Chapter 8:** The subsurface physicochemical and structural changes are examined through broad-scale (centimetre to decimetre) and intensive-scale (sub-millimetre) analysis.
- **Chapter 9:** Synthesises findings, discussing the influence the former land use, site design and construction have on the evolution of the sediment regime, includes a critique of this study, and gives overall conclusion, providing suggestions for future work.

2 Review of Managed Realignment as an Intertidal Habitat Restoration Technique

Managed realignment (MR) is a soft ecological engineering (or ecoengineering) technique (Bergen et al., 2001), which involves the rehabilitation of the estuarine and coastal system to restore it from historic reclamation and degradation (Elliott et al., 2016), and compensate for present day habitat losses elsewhere (as outlined in Chapter 1). Ecoengineering is based around the principles of ecohydrology (Wolanski and Elliott, 2016), which consider the relationships between the physical functioning of the system and the creation of appropriate ecological functioning of an intertidal environment (Elliott et al., 2016). In the case of MR, this involves a regulated shift in the land / sea border and the (re)introduction of inter-tidal conditions.

2.1 Definitions of Managed Realignment

Although MR is a globally established practice, much ambiguity remains with regards to what processes, techniques and management strategies the term actually defines. This is due to the array of definitions that exist and the spatial and temporal variations in the terminology used to describe the same process. These include: managed realignment, managed retreat, setback, de-embankment, depoldering, regulated tidal exchange and controlled reduced tides. For example, in the United Kingdom the process was initially called setback and then managed retreat, but the public perception of these terms were considered to be too negative. More recently, the term managed realignment has been used as it is considered to be a positive coastal management approach (Pethick, 2002; Wolanski and Elliott, 2016).

Most definitions of the MR processes (e.g. Blackwell et al., 2010; French, 2006; Mossman, Davy, et al., 2012; Rupp-Armstrong and Nicholls, 2007; Wolters et al., 2008) consider only the landwards movement of the shoreline through the removal or breaching of flood defences. These, therefore, fail to consider schemes where

realignment is carried out using alternative methods, such as regulated tidal exchange or controlled reduced tide schemes (see below). In order to consider the various definitions and understandings of what MR involves, Esteves (2014) suggested a more applicable definition:

> "*managed realignment is a soft engineering approach aiming to promote… sustainability of coastal erosion and flood risk management by creating opportunities for the realisation of the wider benefits provided by the natural adaptive capacity of coastlines that are allowed to respond more dynamically to environmental change*" (Esteves, 2014, p. 28).

This definition, whilst extremely generalised, recognises the importance of ecosystem services in managing and restoring intertidal environments to compensate for habitat loss and increase the level of coastal flood defence. It also considers the terminology for different methods of realignment which have previously been used by industry, government and policy makers, and the scientific community inconsistently and without clarity.

2.2 Methods of Managed Realignment

The physical, topographic and geographical design of MR sites is fundamental to ensure a fully functioning intertidal system. The design of the schemes should, according to the Construction Industry Research and Information Association (CIRIA), be a dynamic process, and must also consider: the specific aims and objectives, the potential opportunities and constraints, the technical feasibility, the economic viability and the environmental and social acceptability (Leggett et al., 2004).

The traditional method of MR involves removing or breaching flood defences in estuarine and coastal environments. However, in some locations, the terrestrial land behind the flood defences is significantly lower than the pre-existing marshes (Figure

2.1), as a result of dewatering, deflation due to the breakdown of organic matter, compaction caused by agricultural activities landwards of the defences, and sedimentation on the seawards side (e.g. Cox et al., 2006; Temmerman et al., 2003). Consequently, breaching or removing defences may not be suitable at these sites as the lower elevation will result in inundation of the entire site during every tide cycle, and therefore prevent a range of intertidal vegetation from becoming established (Jacobs et al., 2009). Alternatively, the shoreline, but not the defences, can be realigned through regulated tidal exchange or controlled reduced tide schemes.

Regulated tidal exchange schemes, such as Polder de Sébastopol, Vendée, France, allow a controlled tidal flow through culverts and sluices through the embankments and defences (e.g. Esteves, 2014). Controlled reduced tide schemes have been implemented along the Scheldt estuary (Figure 2.1) in Belgium as part of the Sigma Plan (e.g. Jacobs et al., 2009). They include flood control areas and sluices to allow regulated tidal flows, recreating the spring and neap tidal cycles and promoting the development of intertidal habitat in the flood control area. The flood control areas can be used to store water during storm events, reducing the flood risk elsewhere, which then drain once the water level lowers outside (e.g. Cox et al., 2006; Jacobs et al., 2009; Maris et al., 2007).

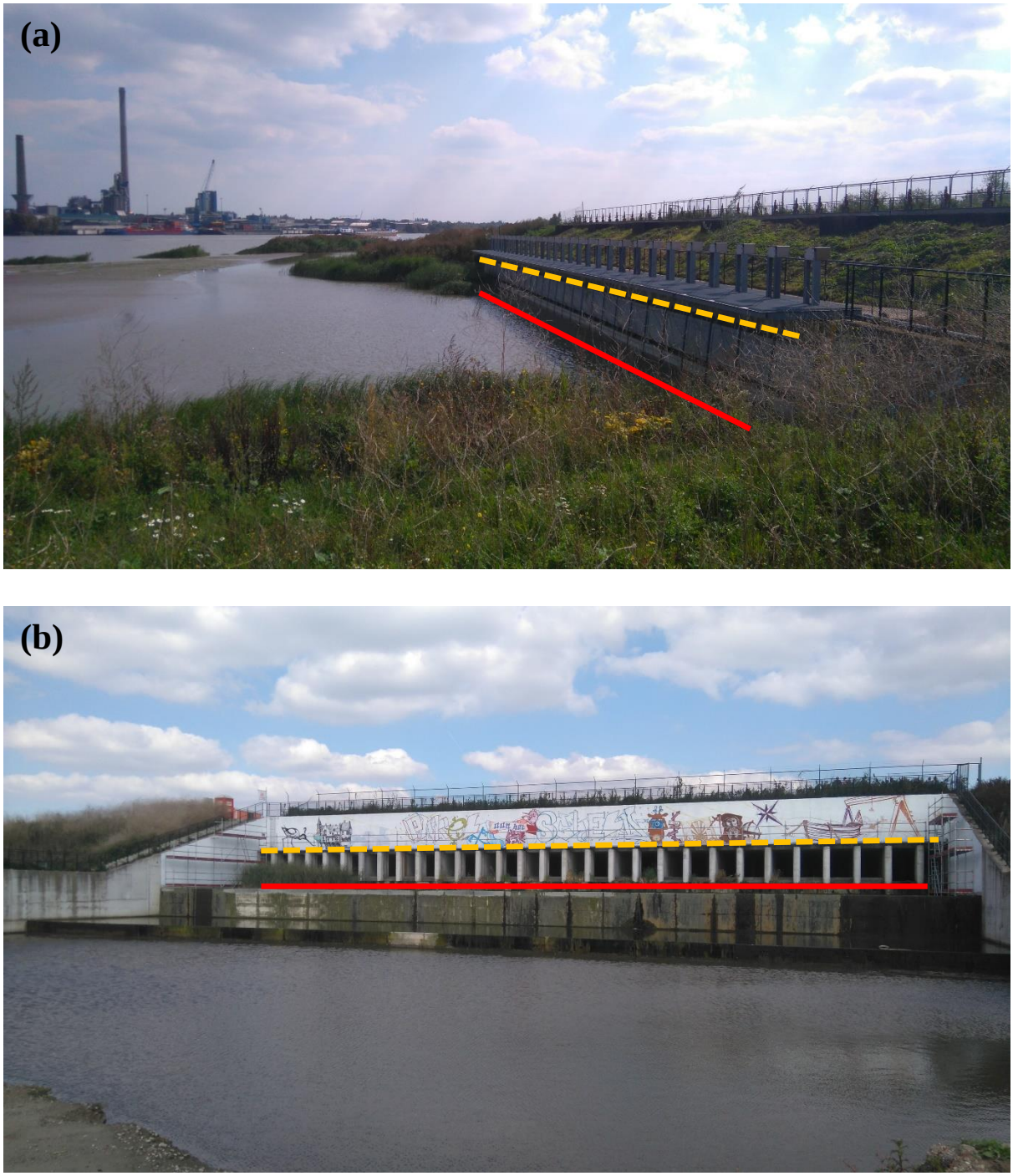

Figure 2.1: (a) The estuarine side, looking upstream, and (b) the landwards side, looking towards the estuary, of the sluices for a controlled reduced tide scheme to be implemented on the Scheldt estuary, Belgium as part of the Sigma Plan. Note the large difference in elevation between the two sides of the sluice. The water level in (a) is approximately level with the bottom of the white pillars in (b), marked by the solid red line, and the top of the sluices is marked on both by the yellow dashed line which is approximately 20 m long (photograph: J. Dale).

2.3 Managed Realignment in the United Kingdom

MR has become increasingly popular in economically developed countries and regions such as the United States, Europe, Australia and New Zealand, and has been partly driven by legislative requirements for improved biodiversity, such as the European Union Habitats Directive (European Parliament and the Council of the European Commission, 1992). The first realignment projects in Europe took place in France and Germany in the early 1980s, but at present the United Kingdom has the highest number of MR sites (Esteves, 2014). Saltmarsh and mudflat habitats are of high importance in the United Kingdom; there are approximately 45,300 ha of saltmarsh (Burd, 1989) surrounding 2000 km (Doody, 1992) of the United Kingdom's coastline, with the ecosystem valued at £48 billion (UK National Ecosystem Assessment, 2011). However, it has been recognised that these environments are under threat from climate change and habitat loss (Esteves, 2014). Furthermore, the majority of the current sea defences in the United Kingdom were constructed following the 1953 North Sea storm surge, which resulted in the death of 307 people in the United Kingdom (Baxter, 2005; McRobie et al., 2005), and are coming towards the end of their design life. Consequently, these defences require new investment and expensive upgrades and maintenance (e.g. Moller et al., 1999), which in some cases can be considered unsustainable and uneconomical as the expenditure on the defences is more than the value of the land being protected (Hughes and Paramor, 2004).

MR has been the preferred coastal management strategy in the United Kingdom since the *Making Space for Water* strategy was published by the Department for Environment, Food and Rural Affairs (DEFRA, 2005). *Making Space for Water* represented a movement away from hard engineered structures, with a fixed shoreline, towards soft engineering techniques and a more dynamic approach to coastal management. MR is considered to be the most appropriate solution, aiming for a 'triple-win'; to ensure the needs for coastal protection (safety), to reduce the cost of maintaining unsustainable hard defences such as sea walls (economic), and to compensate for habitat loss and adaption to climate change (ecology) (Edwards and Winn, 2006). MR schemes undertaken in the United Kingdom, reported in the Online Marine Registry (ABPmer, 2017) and by Esteves (2014), are listed in Table 2.1.

Table 2.1: Existing managed realignment projects in the United Kingdom, listed in age order and indicating the location, implementation method, and size (after ABPmer, 2017; Esteves, 2014). Note that historic, naturally breached, unmanaged realignment sites, such as Pagham Habour (e.g. Cundy et al., 2002), are not included here.

Site Name	Location	Method	Year	Area (ha)
Northey Island	Blackwater	Manged realignment	1991	0.8
Seal Sands (Northwest Enclosure)	Tees	Controlled tidal restoration	1993	9
Pawlett Hams	Parret	Managed realignment	1994	4.8
Horsey Island	Hamford Water	Controlled tidal restoration	1995	1.2
Orplands Farm	Blackwater	Manged realignment	1995	38
Ryan's Field	Hayle	Controlled tidal restoration	1995	6.23
Saltram (Blaxton Meadow)	Plym	Controlled tidal restoration	1995	5
Tollesbury	Blackwater	Manged realignment	1995	21
Abbotts Hall	Blackwater	Controlled tidal restoration	1996	84
Porlock Bay	North Somerset Coast	Unmanaged realignment	1996	75
Montrose Basin	Montrose Basin	Managed realignment	1997	0.3
Thornham Point	Chichester Harbour	Breach of defence	1997	6.9
Millennium Terraces	Thames	Manged realignment	1998	0.5
Lantern Marsh (North)	Ore	Managed realignment	1999	29
Upper Lantern Marsh	Ore	Breach of defence	1999	37
Annery Kiln	Torridge	Breach of defence	2000	3.8
Black Devon Wetlands	Forth / Black Devon	Managed realignment	2000	28
Chalkdock Marsh	Chichester Harbour	Controlled tidal restoration	2000	3.2
Havergate Island	Ore	Manged realignment	2000	8.1
Pillmouth	Torridge	Manged realignment	2000	12.9

Trimley Marsh	Orwell	Breach of defence	2000	16.5
Watertown Farm	Yeo	Breach of defence	2000	1.5
Bleadon Levels	Axe	Breach of defence	2001	13
Cone Pill	Severn	Breach of defence	2001	50
Abbotts Hall	Blackwater	Breach of defence	2002	84
Brancaster West Marsh	North Norfolk	Manged realignment	2002	7.5
Brandy Hole	Crouch	Breach of defences	2002	12
Freiston	The Wash	Manged realignment	2002	66
Nigg Bay	Cromarty Firth	Manged realignment	2003	25
Paull Holme Strays	Humber	Manged realignment	2003	80
Clapper Marshes	Camel	Controlled tidal restoration	2004-2011	10
Goosemoor	Clyst	Regulated tidal exchange	2004	6.3
Lower Clyst (Goosemoor)	Exe Estuary	Controlled tidal restoration	2004	6.2
Man Sands	South Devon Coast	Removal of defence	2004	2
Thorness Bay	The Solent	Breach of defence	2004	7
Walborough	Axe	Controlled tidal restoration	2004	4.5
Glasson	Conder	Controlled tidal restoration	2005	6.4
Halvergate	Yare	Manged realignment	2005	5
Alkborough	Humber	Breach of defence	2006	440
Allfeet's Marsh (Wallasea Island)	Crouch	Managed realignment	2006	113
Alnmouth	Aln	Breach of defences in two adjacent areas, one breach in each	2006	8
Barking Creek	Barking Creek	Removal of defence	2006	0.3
Barking Creek Tidal Barrier	Barking Creek	Breach of defence	2006	1
Chowder Ness	Humber	Manged realignment	2006	15

Vange Marsh	Thames	Controlled tidal restoration	2006	1
Wallasea	Crouch	Manged realignment	2006	115
Welwick	Humber	Manged realignment	2006	54
Great Orcheton Fields	Erme	Unmanaged realignment	2007	24
Lepe/Darkwater	Dark Water	Controlled tidal restoration	2007	5
Treraven Meadows	Camel	Controlled tidal restoration	2007	15
Alnmouth	Aln	Breach of defence	2008	20
Hesketh Out Marsh	Ribble Estuary	Manged realignment	2008	168
Kennet Pans	Firth of Forth	Manged realignment	2008	8.2
Black Hole Marsh	Axe	Controlled tidal restoration	2009	6
Lymington Estuary	Lymington	Regulated tidal exchange	2009	21
Skinflats Tidal Exchange Project – STEP Forth	Firth of Forth	Controlled tidal restoration	2009	11
Warkworth	Coquet	Breach of defence	2009	0.4
Amble Marshes	Camel	Controlled tidal restoration	2010	56
Devereux Farm	Hamford Water	Breach of defence	2010	6
Goswick Farm	South Low River	Controlled tidal restoration	2010	4.5
London Gateway Wildlife Reserve	Thames	Manged realignment	2010	27
Stanford Wharf	Thames	Managed realignment	2010	27
Ynys-hir	Dyfi	Managed realignment	2010	6
Castles Dike	Coquet	Managed realignment	2011	8
Rye Harbour Farm	Rother	Regulated tidal exchange	2011	17

South Efford Marsh	Avon	Regulated tidal exchange	2011	17
Titchwell Marsh	Norfolk Coast	Managed realignment	2011	11
Tutshill	Congresbury Yeo	Managed realignment	2011	2
Lytchett Fields	Poole	Unmanaged realignment	2012	23
Washington	Wear	Managed realignment	2012	1.2
Cobnor Point	Chichester Harbour	Managed realignment	2013	6.5
Greatham	Tees	Managed realignment	2013	40
Hazlewood Marshes	Alde	Unmanaged realignment	2013	69
Medmerry	West Sussex	Manged realignment	2013	320
West Wittering	Chichester Harbour	Regulated tidal exchange	2013	6
Cwm Ivy	Loughor	Unmanaged realignment	2014	39
Otterhampton Marsh	Parrett	Regulated tidal exchange	2014	84
Steart Peninsula	Parrett estuary	Manged realignment	2014	416
The Saltings	Rother	Managed realignment	2014	1
Fingringhoe Wick	Colne Estuary	Managed realignment	2015	22
Salt Fleet Flats Reserve	Thames	Managed realignment	2016	65
Bowers Marsh	East Haven Creek	Regulated tidal exchange	Unknown	10

2.4 The Structure and Functioning of Managed Realignment Sites

Following the principles of ecohydrology (Wolanski and Elliott, 2016), MR presumes that, providing the physical and / or chemical structure of the system is restored, saltmarsh colonisation will follow (Borja et al., 2010). Surface elevation is regarded as the most important factor in the design of MR schemes (Howe et al., 2010), as bed elevation controls the hydroperiod, the frequency and duration of tidal inundation, hence directly influencing the zonation and colonisation of saltmarsh vegetation. However, rapid sedimentation and erosion processes post-breaching, and internal sediment reworking, can significantly impact local site elevation and thus vegetation colonisation. For example, at Paull Holme Stays, Humber Estuary, United Kingdom, sediment accretion has been greater than expected, resulting in the formation of upper saltmarsh and not the intended mudflat habitat (Wolanski and Elliott, 2016). There is also increasing evidence that restored saltmarshes do not have the same biological or ecological characteristics, and have lower biodiversity, than their natural counterparts (Edwards and Proffitt, 2003; Mossman, Brown, et al., 2012; Mossman, Davy, et al., 2012; Spencer et al., 2012), which may have consequences for the ecosystem services provided (Doherty et al., 2014).

It is, therefore, critical to understand the factors influencing the physical structure and functioning of MR sites in order to improve the delivery of ecosystem services (Spencer et al., 2017). However, there is an overall lack of understanding regarding the impact MR has on sedimentary processes (Esteves, 2013). This is particularly true of the factors influencing the evolution of the sediment regime, which defines the key spatial and temporal characteristics of the sediment erosion, transportation, deposition and consolidation processes (reviewed below). This shortage of knowledge has been explained by a lack of long-term monitoring data (Spencer and Harvey, 2012), with the monitoring that has been carried out focusing on vegetation change, which occurs on a comparatively short timescale (Kentula, 2000). In addition, research has tended to be published in grey literature rather than peer-reviewed scientific publications (Esteves, 2013). Figure 2.2 presents an overview of the factors influencing the evolution of the sediment regime in MR sites (which are discussed in Sections 2.4.1 to 2.4.3).

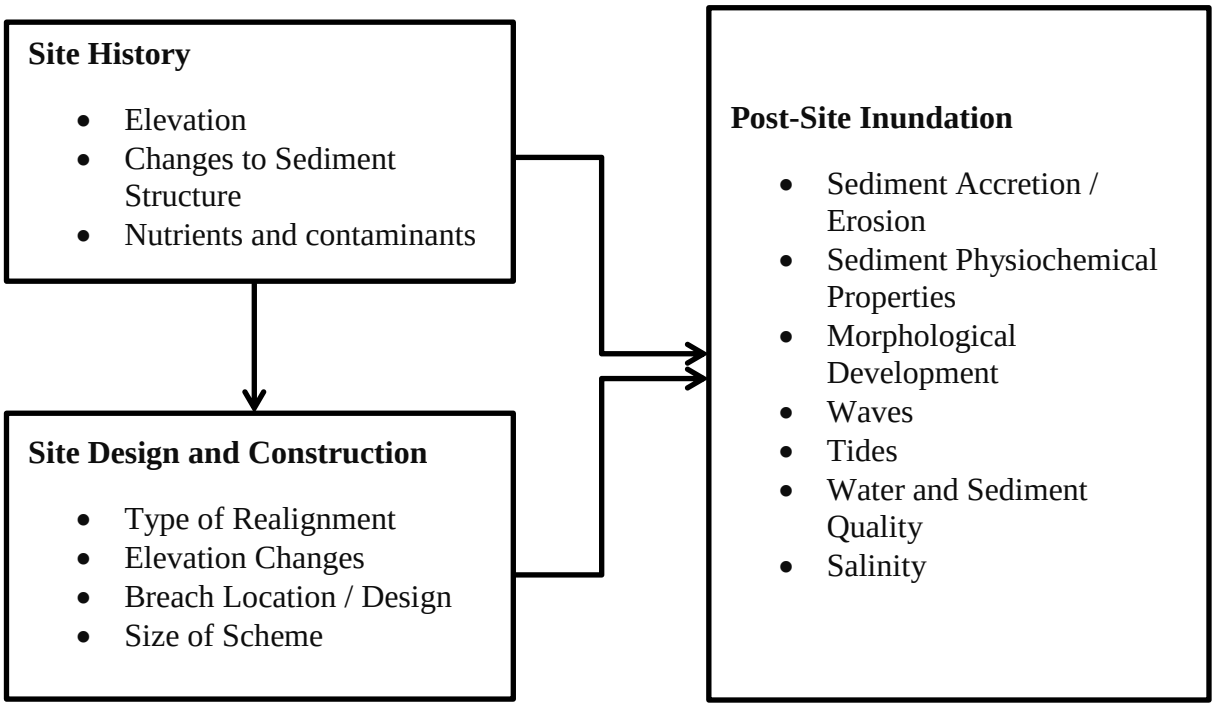

Figure 2.2: An overview of factors influencing the evolution of the sediment regime in managed realignment sites (see text for discussion).

2.4.1 The Influence of Site History

The fundamental rationale of MR is to create new areas of intertidal saltmarsh and mudflat. Therefore, inundating reclaimed land which has previously demonstrated an ability to support these habitats (French, 2006) is often considered to be the most suitable approach to MR. Whilst selecting areas for potential MR based on the criteria of restoring former saltmarshes and mudflats is a reasonable approach, post-reclamation changes to the sediment also need to be considered in the site selection criteria. Many sites are lower in elevation than surrounding natural saltmarshes, as they have been drained and dewatered, and not subjected to sediment accretion occurring on the non-reclaimed marshes (e.g. Cox et al., 2006; Temmerman et al., 2003). Reclaimed saltmarshes have also been flushed by percolating rainwater which has a desalinating effect, and irreversibly altered by physical disturbances (French, 2006; Spencer et al., 2017; Spencer and Harvey, 2012; Viles et al., 2008). Such disturbances have been associated with compaction caused by agricultural machinery (Hazelden and Boorman, 2001) resulting in a decrease in porosity and an increase in the sediment density (Alaoui

et al., 2011). Dent et al. (1976) found that, post-reclamation, sediments experienced distinct changes in soil density, porosity and organic content, with ploughing for arable use accelerating the rate of change. Ploughing appeared to enhance the changes due to an increased breakdown in sediment structure and enhanced aeration and oxidation of organic matter. It has been proposed that these changes are the cause of reduced hydraulic conductivity, leading to the poor drainage and anoxia observed within MR sites (e.g. Crooks et al., 2002; Tempest et al., 2015). Drainage, generally through macropores, is considered to be an important parameter in determining the ecological functioning of a saltmarsh (Howes and Goehringer, 1994; Schile et al., 2011); changes to the sediment structure through compaction and agricultural activity could therefore have negative implications for the delivery of ecosystem services in newly created saltmarshes and mudflats.

Further negative implications may occur through the release of metals and herbicides stored in the agricultural soil following initial site inundation. Kadiri (2010) found a greater potential for metals to be released at higher salinities due to the reaction between the seawater cations and the metals within a former agricultural soil. The introduction of intertidal conditions was also found to contribute to contaminate release; the author associated periodic wetting and drying to increased mineralisation of organic matter due microbial activity and the release of dissolved organic carbon (Kadiri, 2010). Therefore, in sites with a history of intensive agricultural activity, there is an increased probability of metals and herbicides being introduced into the water column following site inundation, rather than the desired water quality regulation being attained.

2.4.2 The Influence of Site Design and Construction

Deciding whether a site is suitable for MR is often determined by the aims of the project. CIRIA (Leggett et al., 2004) stated that where the primary aim is flood defence there should be a high level of confidence that the existing defences are in a poor condition and are unsustainable. MR should also be an economically viable option and there should be financial support for the scheme. Where habitat creation is the major

driver then the wider environment should be considered, such as the location relative to pre-existing saltmarsh to provide a supply of seeds to accelerate saltmarsh colonisation.

The impact of site construction also plays a major role in the ability of intertidal habitat to become established. This includes the influence of physical disturbances (Viles et al., 2008), such as changes in slope angle and compaction of sediment, caused by the heavy plant machinery used during site construction, which can also result in poor drainage, leading to anoxia (Davy et al., 2011) and limited biogeochemical cycling within the sediment (e.g. Spencer et al., 2008). The pre-breach design of MR sites is intended to encourage the development of a range of saltmarsh and mudflat habitat (Burgess et al., 2016). Elevation and hydroperiod can be varied to modify conditions for specific habitat development by applying additional sediment, or excavating areas (Spencer and Harvey, 2012) creating features known as 'borrow pits'. Suitable and affordable land must be available, and the land must not be contaminated by, for example, pollutants from former or current landfill sites within or near the proposed realignment area (e.g. Hodge and Johnson, 2007).

2.4.2.1 Breach Design and Location

The size and design of the breach plays an important role in regulating post-breach tidal inundation. Removing all of the previous flood defences has, in some cases, resulted in sites having no protection from fast tidal flows, drowning the newly inundated area (Anisfeld et al., 1999). However, if the breach is too small the accommodation space will increase without increasing the cross sectional area of the original channel, potentially leading to increased erosion and the loss of saltmarshes elsewhere (Townend and Pethick, 2002). At MR sites in highly turbid estuaries, such as Paull Holme Stays in the Humber on the east coast of the United Kingdom, insufficient breach width has prevented natural in / out tidal flow dynamics. This has results in greater levels of accretion than anticipated, resulting in secondary degradation through the formation of upper saltmarsh which will eventually become dried out high elevation marsh and terrestrial land, and not sustain the desired range of mudflat and saltmarsh habitat (Wolanski and Elliott, 2016). The possibility of breaching a site in two or more

locations has also been suggested, but this idea has generally been dismissed as it could lead to a high energy channel forming through the site as the tidal waters enter through one breach and exit through the other (French, 1999).

2.4.2.2 Size of Scheme

MR sites are located in areas where farmland is available to buy and there are no houses to relocate, which often influences the size of the realignment area (Wolanski and Elliott, 2016). Whilst economic and social restrictions may reduce the size of the MR schemes, it is important that the site is large enough to operate as a self-sustaining system, creating sufficient intertidal habitat to compensate for losses elsewhere and providing a suitable level of coastal flood defence. This is highlighted by Wolters et al. (2005) in a review of 70 European MR sites, which concluded that a site should be at least 30 ha to sustain at least 50 % of the target saltmarsh species, with best results found in sites larger than 100 ha. These authors found that sites that occupy a greater distance inland (i.e. the line perpendicular to the coastline, compared to the line parallel to the coastline) had greater species diversity due to the greater allowance for zonational processes.

2.4.3 Post-Site Inundation Influences

Following site inundation, the terrestrial soils in MR sites are inundated and intertidal sediments start to accumulate. Rapid accumulation of sediment occurs, providing sediment is readily available, if the elevation needs to adjust relative to mean sea level, as would be expected if the previously protected land had been reclaimed and subsequently lowered through dewatering and compaction processes (Crooks and Pye, 2000; French, 2006). The accommodation space for sediment accumulation provided by MR sites also means they act as a sink for heavy metals and contaminants (Andrews et al., 2006) which are found extensively in polluted estuarine sediments (e.g. Cundy et al., 2003; Spencer et al., 2003). Nonetheless, some contaminants are not permanently bound to cohesive sediments and may be released due to physical and chemical sedimentological changes (Gambrell et al., 1991). There is also the possibility that

contaminants in the inundated terrestrial soil, such as herbicides and pesticides, may be released following inundation (Kadiri, 2010).

2.4.3.1 Sediment Accretion and Erosion

In MR sites, variations in supply of sediment after site inundation would be expected as sediment is re-distributed around the site and intertidal morphology develops (Pontee, 2014). High sedimentation rates would initially be anticipated according to predictive models (e.g. Allen, 2000) and measurement data (e.g. Clapp, 2009; Dixon et al., 2008), particularly in areas of lower elevation. However, this is dependent on the site hydrodynamics, sedimentation processes, engineered morphology and surface sediment properties when initially inundated.

An understanding of the evolution of the sediment regime in MR sites would enhance the design and management, and consequently the long-term sustainability, of these newly inundated intertidal environments. Despite this, little is known of the sedimentation processes which occur in MR sites. Watts et al. (2003) measured the critical erosion shear stress at the Tollesbury MR site in Essex six years after realignment. They reported that the underlying agricultural sediment was highly resistant to erosion (τ_o = 6.23 N m $^{-2}$) and above mean high water neaps (MHWN), where vegetation had become established, the surface sediment had moderate resistance to erosion (τ_o = 2.45 N m $^{-2}$). However, below MHWN, where the greatest rates of sediment accretion were observed, the surface resistance to erosion was much lower (τ_o = 1.5 N m $^{-2}$). The authors related this to very high sediment moisture content and low bulk densities resulting from poor consolidation due to the high accretion rates (Watts et al., 2003). Further research is required to investigate the spatial and temporal changes in sedimentary processes in MR sites to improve site design, construction processes and pre-inundation landscaping and morphology, ensuring a sustainable and desired range of ecosystem services are delivered.

2.4.3.2 Site Morphology

The morphological evolution of MR sites has been related to the former land-use and engineering modifications during site construction (D'Alpaos, Lanzoni, Marani, Bonornetto, et al., 2007; Spencer and Harvey, 2012). The development of creek networks is thought to be related to the pre-existing landscape (French and Stoddart, 1992), including the location of terrestrial surface drainage features (Crooks and Pye, 2000) such as plough lines (Spencer and Harvey, 2012). The timescale for creek development and the characteristics, including the density, of the creek networks are also influenced by factors such as the drainage characteristics, tidal energy and marsh gradient (Cornu and Sadro, 2002; Crooks et al., 2002; D'Alpaos, Lanzoni, Marani, Bonornetto, et al., 2007; Spencer and Harvey, 2012). Consequently, the creek networks which develop in MR sites can vary considerably between sites, with the former terrestrial drainage systems being retained for many years and in some cases remaining as permanent features (e.g. Bowron et al., 2011).

Creek networks play an important role in the morphological and ecological functioning of intertidal environments, and form the main transport pathways for water, biota and nutrients (Vandenbruwaene et al., 2013). Creeks have been shown to provide a locally enhanced supply of sediment; Reed et al. (1999) found that sedimentation increased by an order of magnitude within 20 m of the newly formed creeks. Furthermore, it has been demonstrated at the Tollesbury MR site that sediment erodibility decreased with proximity to creeks, which only began to develop once there had been between 20 to 30 cm of accretion (Watts, 2008; Watts et al., 2003). Creeks become more effective at increasing drainage and tidal exchange as they develop (e.g. Symonds and Collins, 2007; Watts et al., 2003), although many MR sites remain poorly drained (e.g. Crooks et al., 2002).

Poor drainage of the sediment may influence the physical and biogeochemical cycling within MR sites and therefore has an effect on nutrient cycling, carbon sequestration and climate regulation, whereas reduced topographic variability may influence saltmarsh biodiversity (Spencer and Harvey, 2012). The formation and evolution of

creek networks is widely regarded to influence the ecological, and morphological, evolution of the surrounding intertidal area (e.g. D'Alpaos, Lanzoni, Marani and Rinaldo, 2007; Kirwan and Murray, 2007; Temmerman et al., 2007). Therefore, creating suitable creek networks, or the conditions to facilitate rapid creek development, would enhance the establishment of saltmarsh vegetation following site inundation (Wolanski and Elliott, 2016). However, investigations into the formation of creek networks has focused on morphodynamic models (e.g. Fagherazzi and Furbish, 2001; Kirwan and Murray, 2007; Temmerman et al., 2007), with few studies providing empirical field data on creek formation and evolution (Vandenbruwaene et al., 2012). This is probably due to most creek networks in coastal wetlands already being in a state of quasi-equilibrium, i.e. in a state where any change happens slowly enough for the rest of the intertidal system to remain in equilibrium, (e.g. Marani et al., 2003; Shi et al., 1995). Consequently, newly inundated MR sites are important naturally-forced laboratories for investigating creek formation and development, the resulting sedimentological changes and the evolution of the sediment regime.

2.4.3.3 The Preservation of the Terrestrial Surface

The problems associated with physical disturbance caused by agricultural activity may be reduced in areas of rapid sedimentation, which can bury the terrestrial surface. The presence of remnant terrestrial vegetation is, in some cases, considered to be important as it protects the terrestrial surface from erosion (French, 2006), and encourages the deposition of new sediment (Boorman and Hazelden, 1995). However, Macleod et al. (1999) found, in a post-breach investigation at the MR site at Orplands Farm, Essex, that rapid sedimentation occurred, blanketing not only the terrestrial surface but the freshwater vegetation growing on it. This vegetation layer became heavily waterlogged as it decayed, resulting in a buried layer of sodium rich anoxic mud which could potentially inhibit the establishment of saltmarsh vegetation. As a result, questions regarding the best practice for preparing the sediment surface prior to breaching MR sites remain unanswered and require further investigation.

In the design of early MR sites it was assumed that in order for there to be accretion of sediment tidal currents need to be reduced (French et al., 2000). However, nearly all MR sites are now considered to accumulate sediment (Morris, 2013) making them important sinks for organic matter, nutrients and contaminant metals. Nonetheless, it has been reported that the legacy of compacted agricultural soils remains for many years after MR sites are inundated; at the Orplands Farm MR site in Essex the underlying sediment had retained properties of a compacted agricultural soil, and a differing sediment structure from natural saltmarshes, with the terrestrial soil horizon preserved for at least two decades after inundation (Spencer et al., 2017; Spencer et al., 2008). Further evidence of a preserved reclamation soil layer was presented by Cundy et al. (2002) nearly a century after the storm-induced natural breach which occurred at Pagham Harbour in 1910 AD.

The flux of pore water through the sub-surface sediment is controlled by the sediment structure and texture (Wilson and Morris, 2012; Xin et al., 2009), and influences the sediment redox status, salinity and nutrient availability (Davy et al., 2011; Howe et al., 2010; Wilson et al., 2015; Wolters et al., 2008). In some MR sites a compact layer of sediment, representing the former terrestrial surface, has been recognised in the stratigraphy to act as an aquiclude and restrict sub-surface hydrological connectivity and drainage (e.g. Crooks and Pye, 2000; Crooks et al., 2002; Hazelden and Boorman, 2001; Spencer et al., 2008; Tempest et al., 2015). A compacted sub-surface sediment layer can have serious long-term detrimental effect on plant colonisation and growth by inhibiting the development of root systems, and can also prevent penetration by burrowing invertebrates (Spencer et al., 2017). Further research is required to advance the understanding of the preservation of terrestrial soils in response to the sedimentary processes in newly inundated MR sites.

2.5 Identified Knowledge Gaps

On the basis of the preceding review, there are a number of gaps in knowledge regarding the evolution of the sediment regime in MR sites. To date, research undertaken on MR sites has tended to be short-term and there is a general lack of

understanding of the sediment processes (Esteves, 2013). This is despite the fact that sedimentological factors, such as differences in the sediment structure leading to anoxia and poor drainage, have been suggested as possible explanations for the ecological differences that have been observed between natural and restored sites (e.g. Crooks et al., 2002; Spencer et al., 2017; Tempest et al., 2015). These differences could be due to physical disturbances resulting from the former land-use and site construction. Further research is required to evaluate the success of MR as a long-term sustainable coastal management strategy. At present, work is required to:

- Provide and evaluate long-term data to enhance understanding of the evolution of the sediment regime in MR sites.
- Determine the role played by different physical disturbances caused by former land use, site design and construction activities in sedimentary processes in MR sites.
- Consider the functioning and evolution of the sediment regime, including the influence of physical disturbances, to inform the design and implementation of MR schemes and aid the wider management of intertidal environments.

The following chapters in this thesis address these knowledge gaps through measurements of the sedimentary processes at the Medmerry Managed Realignment Site (reviewed in Chapter 3). The resulting data are analysed to gain a greater understanding of the evolution of the sediment regime in MR sites and facilitate advances in improving the design and implementation of saltmarsh restoration schemes. Data of this type are site specific and dependent on the site construction, such as the morphology, topography, and inlet / outlet design (Wolanski and Elliott, 2016), which in turn are controlled by the specific aims of the site and finances available, and therefore the site design and pre-breach landscaping. Nonetheless, MR sites provide important naturally-forced laboratories within which the evolution of the sediment regime in newly breached or flooded intertidal areas can be analysed. This analysis can provide valuable information, which can then support investigations of the ecological development and facilitate improved site design and construction to maximise the delivery of ecosystem services in intertidal and estuarine restoration schemes.

3 The Study Site: The Solent and the Medmerry Managed Realignment Site

To evaluate the influence of the former land use, site design and construction on the evolution of the sediment regime in managed realignment (MR) sites, this study assesses the sedimentary processes at the Medmerry Managed Realignment Site during the second and thirds years after site inundation, addressing the knowledge gaps identified in Chapter 2. The Medmerry scheme is the located on the Manhood Peninsula, in the eastern Solent on the south coast of the United Kingdom. The Solent is the stretch of water from Hurst Spit, Hampshire in the west to the Selsey Bill headland on the Manhood Peninsula, in West Sussex to the east, and includes the north coast of the Isle of Wight (Figure 3.1). The main Solent channel forms part of the course of the former Solent River. The Solent River used to flow from west to east through Poole Harbour and into the present day English Channel during stadials and periods of low sea level in the Late Quaternary (Allen and Gibbard, 1993), but was flooded and subsequently partly infilled during the early Holocene sea level transgression, up to 5,000 years before present (B.P) (Carter and Bray, 2004).

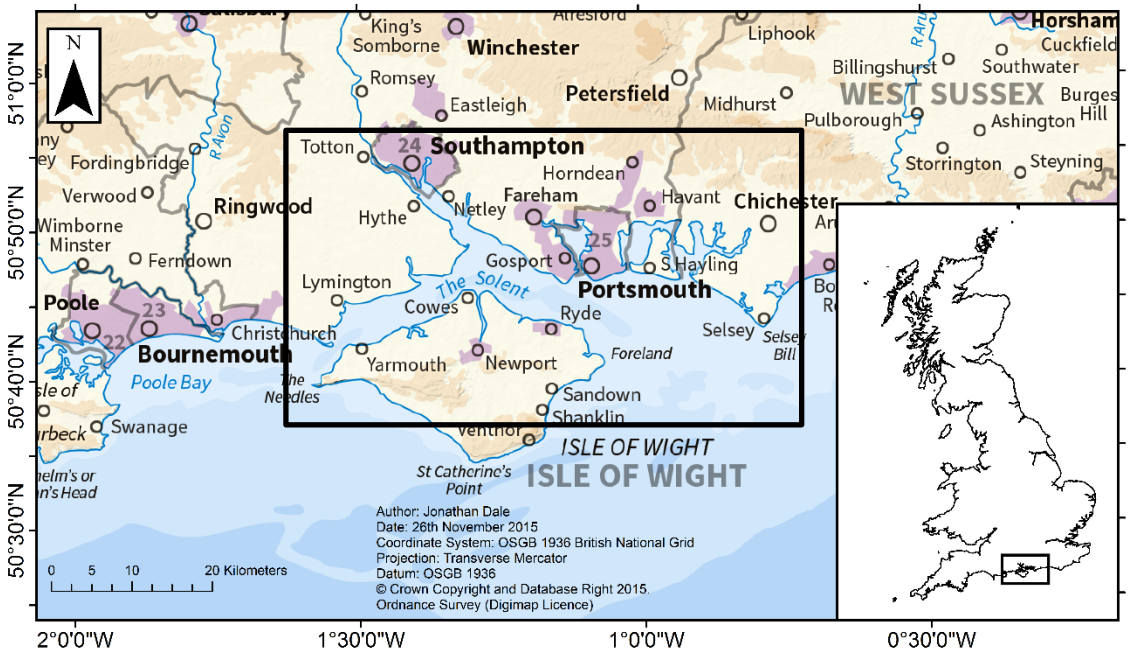

Figure 3.1: The location of the Solent on a local (black rectangle) and national (insert) scale including the location of Southampton and Portsmouth.

Since 5,000 B.P, relative sea level change had been the predominant control on the form and extent of the Solent, until progressive land claim and development began in the eighteenth century, particularly around Southampton and Portsmouth where over one million people currently live (Wadey et al., 2013). Consequently, there is a need for extensive coastal flood defences to protect the Solent's coastline; without the coastal defences, and not considering the flooding dynamics, more than 24,000 properties would be exposed to flooding in a 1 in 200 year still water level coastal flood event (Wadey et al., 2012). At present, 76 % of the Solents coastline is protected by coastal flood defences, although an estimated 75 % of these defences will reach the end of their residual or engineered design life time in the next 20 years (Foster et al., 2014). Therefore, there is a need to maintain the level of coastal flood defence in the region, whilst evaluating the methods used to ensure the Solents coastline is protected sustainably and economically.

The tidal range in the Solent varies from approximately 2 m at Hurst Spit to 5 m at Selsey Bill. Inland from Weymouth, to the west of the Solent, there is a degenerate amphidromic point; although close to the amphidrome the semi-diurnal tidal constituent is relatively weak. However, a double high water is experienced in Southampton Water due to the relatively large amplitude of the tidal constituents influenced by local shallow water effects (M_4 and M_6 tidal harmonics) due to the configuration of Christchurch Bay (to the west) and resonance in the English Channel (Wadey et al., 2013). Further east there is a phase change in the relationship between the tidal constituents, resulting in an extended, rather than double, high water.

3.1 Coastal Management Issues in the Solent

Over 80 % of the coastline within the Solent is designated for its nature conservation interest (Foster et al., 2014). However, the shoreline management plans for the Solent (littoral sediment cell 5) quantified changes in the extent of intertidal habitat within the region (Environment Agency, 2010), estimating that 40 % (approximately 670 hectares) of saltmarsh in the region were lost through erosion between 1971 and 2001 (Cope et al., 2008). The erosion of saltmarsh in the Solent has been explained by the combined

effect of *Spartina* dieback, restricted sediment supply, pollution, sea level rise and coastal squeeze (Baily and Pearson, 2007); records of mean sea level from Southampton (1935-2005) and Portsmouth (1962-2007) indicate a rise of 1.19 ± 0.24 mm / year and 1.73 mm / year respectively (Haigh et al., 2009), whilst cored saltmarsh records indicate a rate of 4 to 5 mm / year over the last 100 years (Cundy and Croudace, 1996).

Coastal flooding, according to analysis of extreme water level events and newspaper records, is experienced relatively frequently in the Solent (Ruocco et al., 2011). Furthermore, there are growing concerns regarding the risk of coastal flooding as a result of rising sea levels (Haigh et al., 2009, 2011). Since records began in 1935, the highest tide levels recorded at Southampton occurred on 10th March 2008 due to a storm surge caused by a strong jet stream across the north Atlantic creating a deep low depression off south-east Greenland, which deepened as the storm moved south-east (Haigh et al., 2011). Over 7 km^2 of land, in 37 separate areas, were flooded across the Solent region during the 10th March event, with a breach in the shingle barrier beach at Medmerry (Figure 3.2), approximately 10 km south-east of Chichester Harbour (Pearce et al., 2011), near the town of Selsey (Figure 3.3) responsible for 90 % of flooding (Wadey et al., 2013). It is the location of, and response to, the flooding at Medmerry that will be the focus of this investigation.

Figure 3.2: Flooding to a caravan site at Medmerry, on the Manhood Peninsula, in during the 10th March 2008 storm surge (looking southwards) caused by a breach in shingle barrier beach defences (source: Daily Mail, 2008).

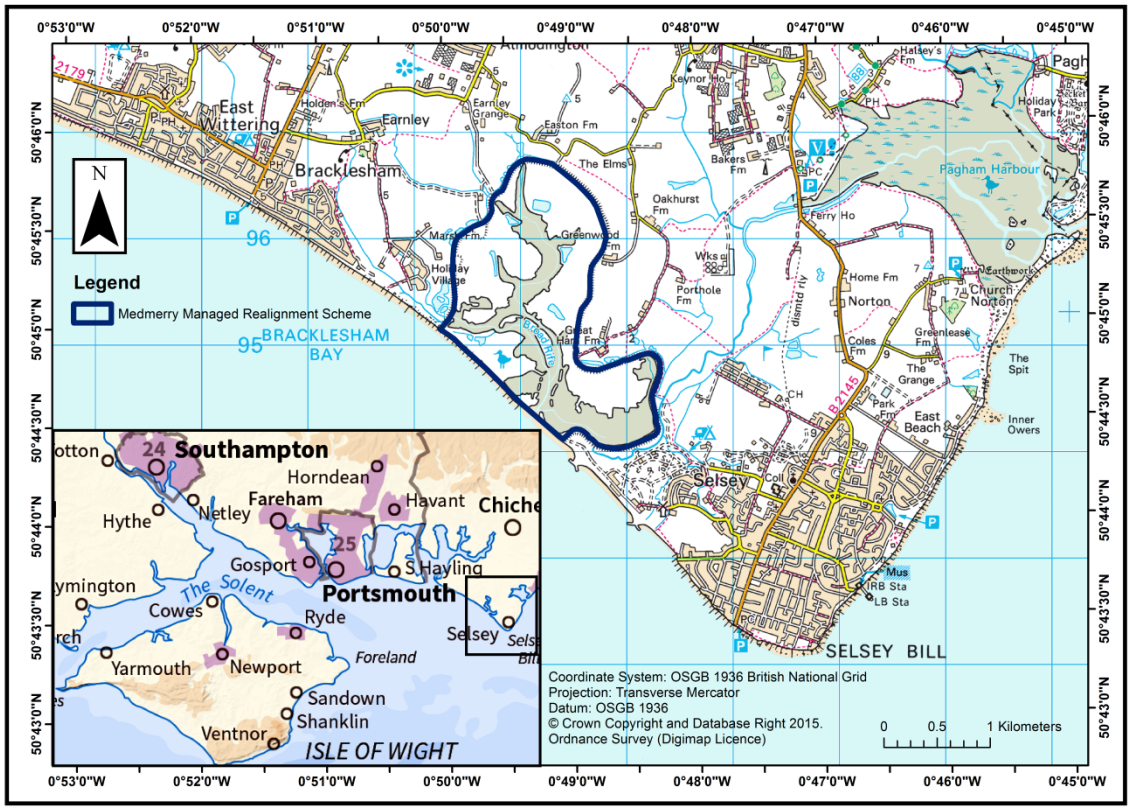

Figure 3.3: The Manhood Peninsula and the location of the Medmerry Managed Realignment Site.

3.2 The Medmerry and Selsey Bill Region

3.2.1 Late Quaternary and Holocene Evolution of the Region

The Medmerry region is located on an underlying bedrock of undifferentiated Bracklesham Group and Barton Group sand, silt and clay with superficial clay, silt and sand alluvium deposits (British Geological Survey, 2017). Fluctuations in relative sea level are, geologically, not uncommon in the Medmerry region; evidence of five occasions during the Middle and Upper Pleistocene when relative sea levels were higher than the current day were presented from the West Sussex coastal plain by Bates et al. (1997). Prior to the early Holocene sea level transgression, the Medmerry region consisted of a freshwater wetland (Krawiec, 2017; Krawiec, in press). However, during the early Holocene, rising sea levels swept up large quantities of sand and shingle. This resulted in the formation of large shingle spits, barrier beaches, offshore shoals and

forelands several kilometres seawards of the present coastline (Carter and Bray, 2004), although the exact location of the early Holocene coastline at Medmerry remains unknown (Krawiec, 2017). As sea levels continued to rise the former tributary systems of the River Solent were drowned, creating tidal inlets such as Pagham Harbour on the eastern side of the Manhood Peninsula. The spit and barrier formations migrated landwards, 2,000 to 3,000 B.P (Cope, 2004), but evidence of these features remains in the Owers and Mixon rocks and the Hounds Bank relict barrier islands found offshore of Selsey Bill (Carter and Bray, 2004).

Archaeological and sedimentological evidence suggests that once there was a continuous marine channel, known today as Broad Rife, which connected Pagham Harbour to Bracklesham Bay, on the western side of the peninsula (Bone, 1996; Castleden, 1998). This channel would have isolated the end of the peninsula, where Selsey is now, as an island, probably contained brackish water and was lagoonal in morphology, similar to the present day Fleet Lagoon behind Chesil Beach in Dorset (Krawiec, in press). The channel may have formed as a result of a breach in the barrier beach, caused by multiple storm events rather than rising sea levels (Krawiec, 2017). It is likely that the barrier beach, which was protected by the Hounds Bank offshore (Goodburn, 1987), has been subsequently breached in this way and reformed many times since (Carter and Bray, 2004; Krawiec, in press). Figure 3.4 schematically illustrates the Holocene evolution of the coastline.

3.2.2 Human Activity in the Region

Despite there being archaeological evidence suggesting that early settlers were present in the region during the Bronze and Iron Age, it is not until the Saxons invaded post-Romanic Britain that documented evidence is available of people living in the Medmerry area (Brossler, 2010). The main evidence supporting the establishment of settlements during this time period comes from place names in Saxon Charters, which relate to villages in the surrounding area. Ekwall (1960) stated that Earnley, to the north-west of Medmerry, was first referred to in 730 AD and originates from the term *Earnaleach* meaning ‘Eagles Wood’. In 780 AD, Selsey was known as *Siolesia*

meaning ‘Seal Island’, supporting suggestions that the area was separated from the mainland (Ekwall, 1960).

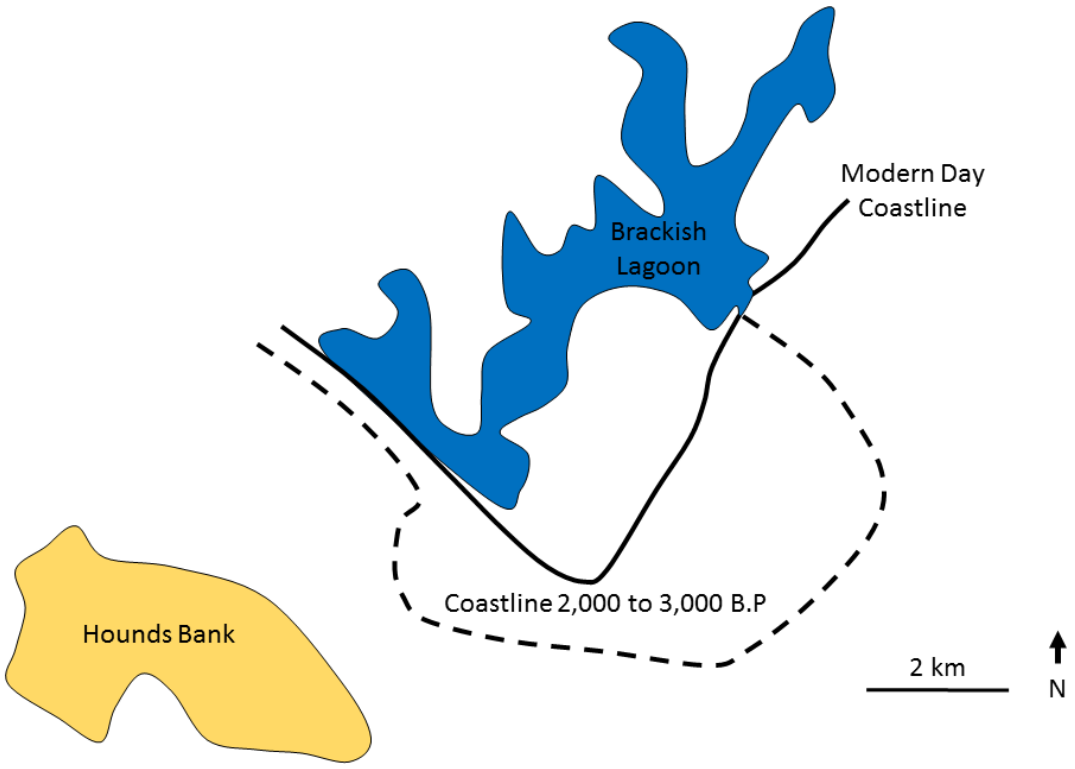

Figure 3.4: Schematic of the Holocene evolution of the Manhood Penisular and the Medmerry region (adapted from Goodburn, 1987). The black solid line represents the modern day coastline, the dashed line the coastline following the early Holocene sea level transgression, and the approximate location of the brackish lagoon and the Hounds Bank offshore are marked.

Early maps of the region, such as Yeakell and Gardner’s 1778-1783 map of Sussex (Figure 3.5), indicate that Selsey was divided from the mainland by a series of channel networks flanked by wetland up until the early 19th century. Access to the mainland came from a ferry crossing until the Lord of Selsey Manor, Sir James Peachey, ordered the construction of a 460 m long bank to provide a crossing in 1805. Subsequently, 126 hectares of land were reclaimed to the west of the bank by draining the land through an outfall fed by a sluice constructed in 1810; one of the earliest examples of land reclamation in the region (Bone, 1996). The line of this bank is still used today by the B2145 access road to Selsey. Large scale Tithe Maps of the area dating from 1842 to 1846 and the first Ordnance Survey map of the area (1875) held in the West Sussex Records Office, Chichester[1], indicate that some of the drained and claimed saltmarshes

[1] Record Office, 3 Orchard Street, Chichester, PO19 1DD

to the west of the bank were suitable for arable cultivation. Further reclamation occurred when the mouth of the Broad Rife channel was blocked in 1880 and construction of the Medmerry Sluice, later known as Broad Rife Sluice (Bone, 1996), took place in 1884, reclaiming approximately 120 hectares of saltmarsh (Carter and Bray, 2004).

Further changes occurred in the region as a result of the First and Second World Wars. Numerous lines of strategic defences, known as Stop Lines, were constructed, and the legacy of these defences remains today. These include anti-tank blocks and traps, minefields and machine gun emplacements. The post-war landscape has remained predominantly agricultural, with the development of holiday caravan parks along the back-barrier hinterland (such as the one presented in Figure 3.2) and the presence of small patches of marshland due to seepage and over-washing, colonised by *Salicornia* (Cope, 2004).

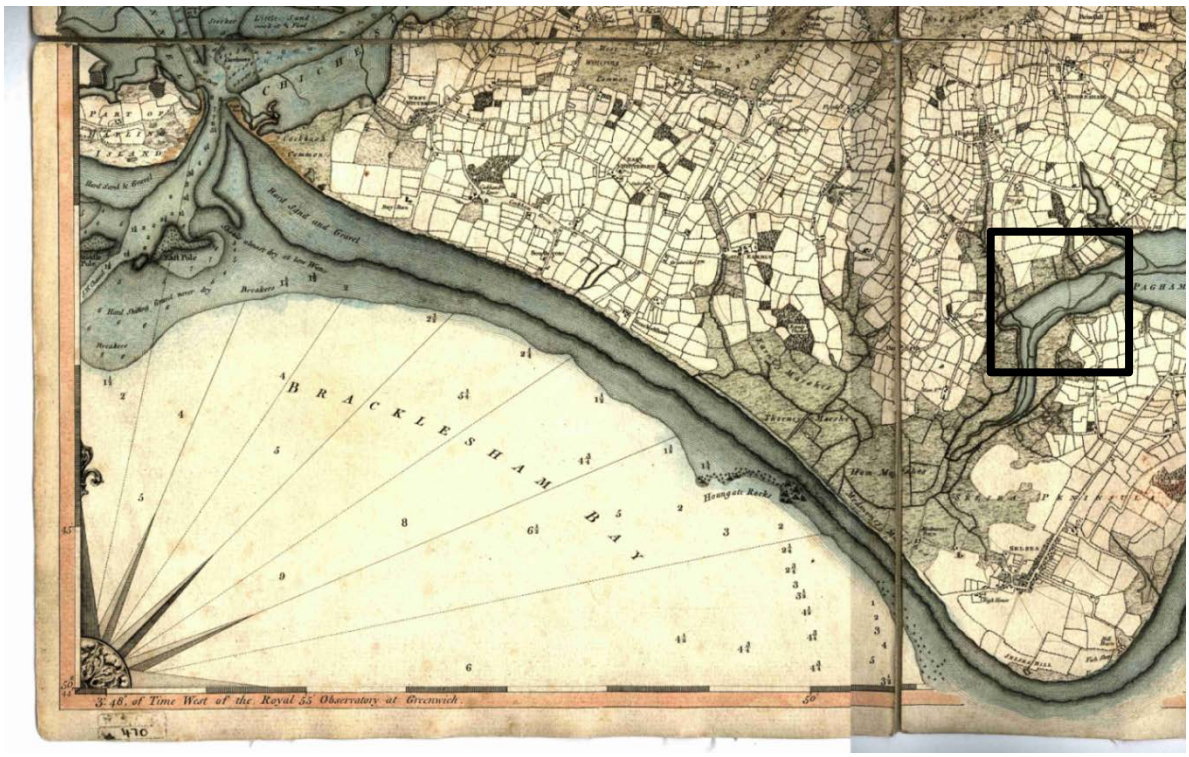

Figure 3.5: Bracklesham Bay and the Manhood Peninsula recorded in Yeakell and Gardner's 1778-1783 map of Sussex. The black square marks the position of the ferry route; now the position of the Ferry Bank, one of the earliest attempts of saltmarsh reclamation in the region.

3.2.3 Coastal Flood Defence Issues at Medmerry

Coastal flood defence at Medmerry was provided by the shingle barrier beach, which was actively managed by the Environment Agency; in order to maintain the necessary defence standard to protect the coastal hinterland constant work was required each winter to recycle and re-profile the shingle bank. Nevertheless, the defences remained vulnerable during storm events; the bank was breached 14 times between 1994 and 2011, flooding homes, the local holiday caravan parks (Figure 3.2) and agricultural land. Around 350 homes and businesses, thousands of caravans and holiday chalets, the local sewage works and the B2145, the only access road for the 5,000 homes in Selsey, were considered to be at risk of coastal flooding (Pearce et al., 2011). The coastal flooding and erosion risk was reviewed in the Pagham to East Head Coastal Defence Strategy in 2009, concluding that the existing defences were unable to prevent flooding and would no longer be effective beyond the short-term. MR was endorsed, after a review of the available options, as the most suitable method of managing the risk of coastal flooding (Environment Agency, 2007).

3.2.4 The Medmerry Managed Realignment Site

Realigning the coastline at Medmerry was intended to provide not only a sustainable and cost-effective method of coastal flood and erosion risk management, but to compensate for the loss of saltmarsh and mudflat habitat elsewhere in the Solent. It was estimated that up to 300 hectares of new intertidal and transitional habitat would form over a hundred years following construction of the site (Pearce et al., 2011). The Medmerry scheme (Figure 3.3) is the largest open coast MR site in Europe and is one of the first examples of open coast realignment in the United Kingdom; most other schemes have been carried out within rivers or estuaries. Similarities have been highlighted between Medmerry and the natural realignment caused by a storm at Porlock, Somerset in 1996.

Material for the new defences were sourced from within the site, creating borrow pits, leading to the construction of an earth ‘bund’ 6.7 km long and extending 3 km inland.

These defences were designed to initially provide a 1 in 1000 year (0.1 % chance of flooding in any year) standard of protection, decreasing to 1 in 100 year (1 %) in 100 years' time (Pearce et al., 2011), allowing for sea level rise and climate change. The surrounding land drains through four drainage outlets (DOs), with tidal gates attached, into the realignment area. Construction began in autumn 2011, with the site being breached through a single opening in the shingle barrier on 9th September 2013, forming a semi-diurnal, mesotidal semi-enclosed estuarine system.

Current velocities in the breach (Figure 3.6), measured using an Acoustic Doppler Current Profiler (provided by the Channel Coastal Observatory), showed spring tide current velocities peaked almost 1 m/s higher than peak neap tide current velocities. Selected individual tidal events (Figure 3.7), characteristic of typical spring and neap tides, indicated that during spring tides the flood tide current velocities begin to increase four hours before high water, peaking approximately 20 minutes before high water. Ebb tidal currents initially increased 20 minutes after high water and were greater in velocity than flood tidal currents. Maximum ebb current velocity occurred three hours after high water. Current velocities then decreased until four hours before the next high water. A similar pattern was observed in the neap tidal currents, although with less tidal asymmetry.

There has been a considerable amount of change in the area since the site was breached. In the winter following inundation the terrestrial flora rotted and decayed, most being flushed out of the system. The width of the barrier beach has decreased, with the beach to the east of the breach rolling back by 50 m and the distal end being prograded towards the north-east by 80 m (Figure 3.8). The barrier beach to the west of the breach has rolled back by 70 m, with the hinge receding westerly by around 150 m and the beach pivoting on the breach side from the hinge resulting in an 80 m roll back. This has significantly altered the breach and the position of the drainage channels inside the site. As the beach has rolled back, it has exposed reclaimed, *Scrobicularia plana* rich, organic poor, Fe-stained, apparently intertidal sediments (Figure 3.9). In general, the site has also been reported to be attracting a range of bird and fish species, and is also beginning to support intertidal saltmarsh vegetation (Environment Agency, 2015).

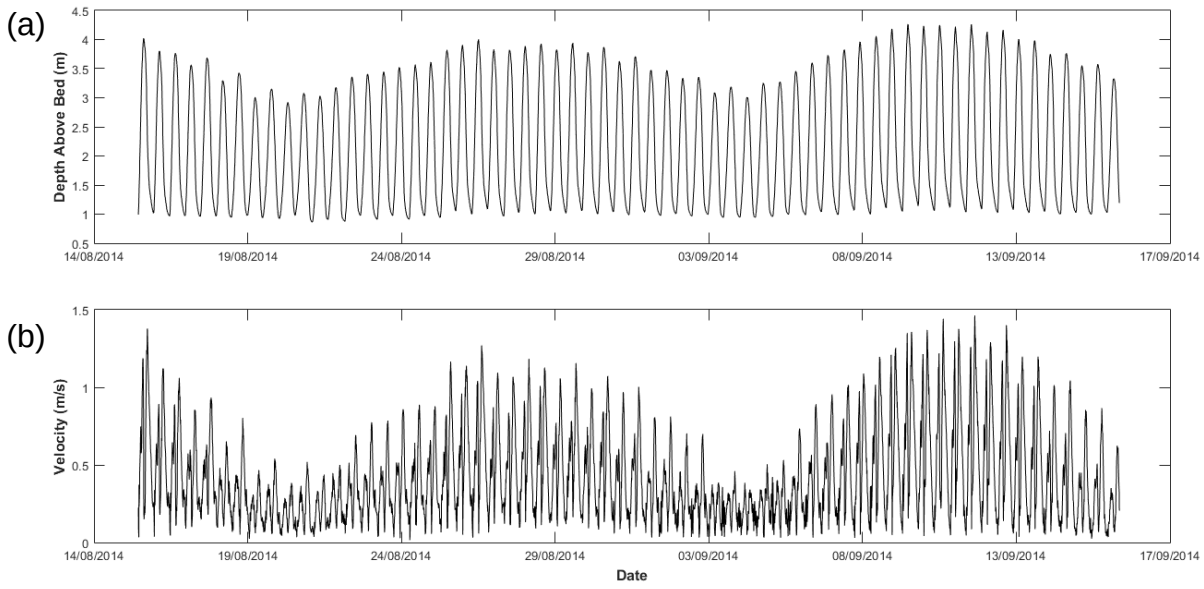

Figure 3.6: Acoustic Doppler Current Profiler Current measured (a) depth and (b) depth averaged current velocities in the breach at the Medmerry Managed Realignment Site between 15th August and 16th September 2014.

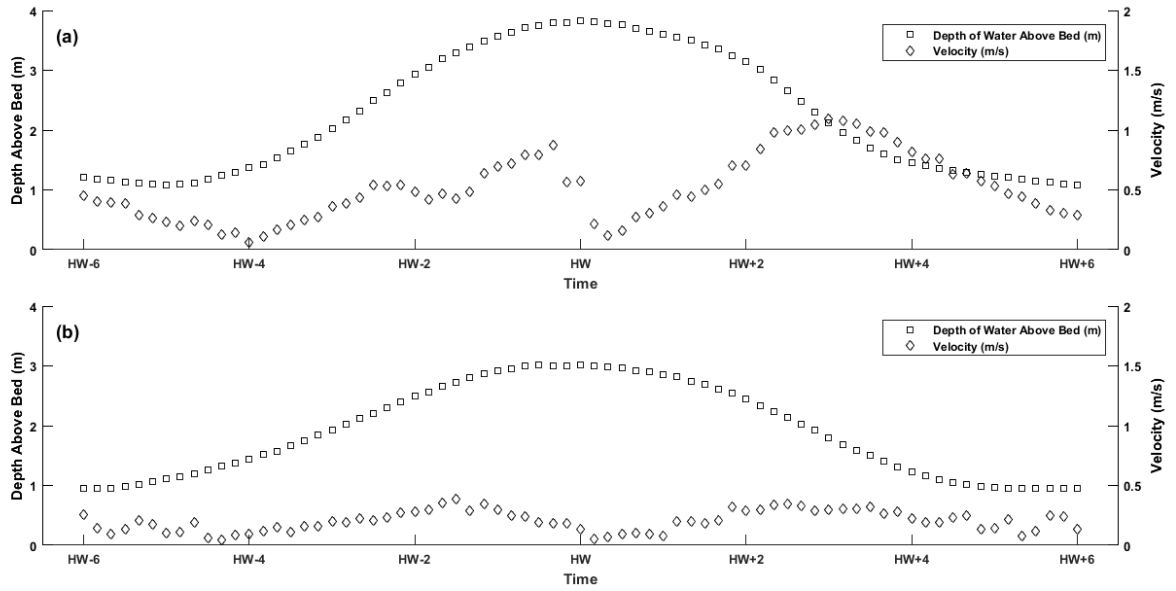

Figure 3.7: Example depth averaged current velocities in the breach during (a) a spring tide on 26th August 2014 and (b) a neap site on 4th September 2014.

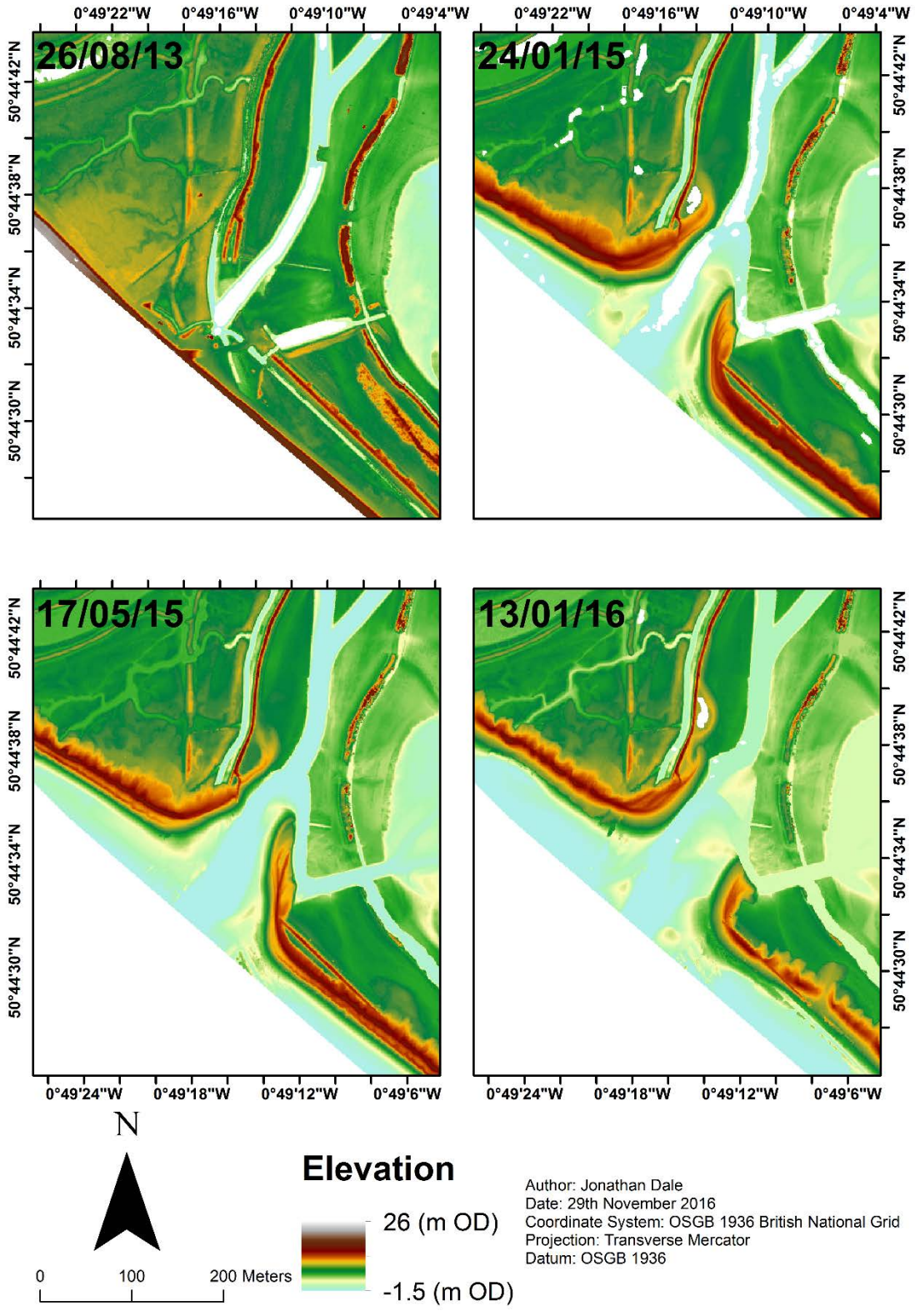

Figure 3.8: Changes in breach morphology following site inundation, examined via elevation data derived from Light Detection and Ranging (LiDAR) measurements on 26th August 2013 (pre-breach), 24th January 2015, 17th May 2015, and 13th January 2016. Data provided by the Environment Agency (United Kingdom).

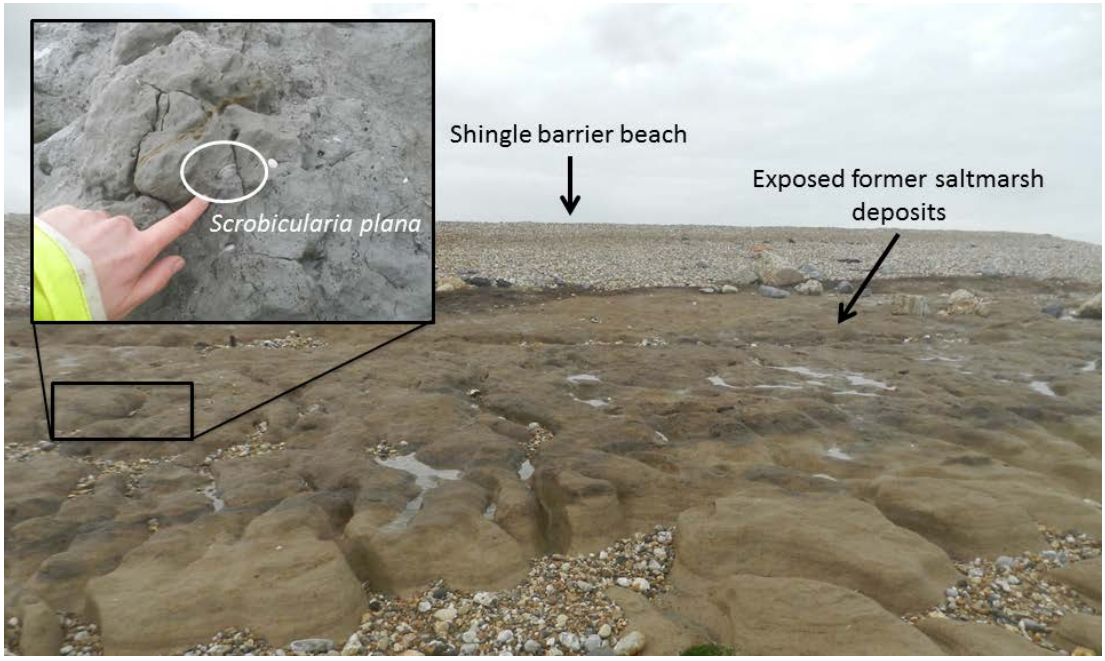

Figure 3.9: The Fe-stained former salt marsh underlain by mudflat deposits (looking north-eastwards), with *Scrobicularia plana* shell (insert), exposed as the shingle barrier beach has rolled back following the breach and site inundation (photograph; J. Dale and A. Cundy (insert)).

3.3 Study Sites

In order to investigate the evolution of the sediment regime at the Medmerry Managed Realignment Site (Figure 3.10) six sites were selected based on an evaluation of changes in land use practice and different site construction processes through analysis of historic maps, photographs and records stored at the West Sussex Records Office and discussion with the Environment Agency. Five monitoring sites were initially investigated at Medmerry by Burgess et al. (2016). An additional monitoring site, Site 2b, has been considered in this study.

Sites 1, 2a and 2b are at the landward extremities of the site, located near the newly constructed tidal gates which drain freshwater into the Medmerry site. Sites 3 and 4 are at the entrance and towards the back, respectively, of a borrow pit and are near the centre of the site, halfway along the main channel flowing through the site; Easton Rife. Site 5 is at the back of a borrow pit in close proximity to the breach. Each site is described here, based on the former land use and landscape construction techniques

(summarised in Table 3.1) and the location where samples and measurements were taken (as outlined in Chapter 4) are indicated. Measurements were also taken from within the breach.

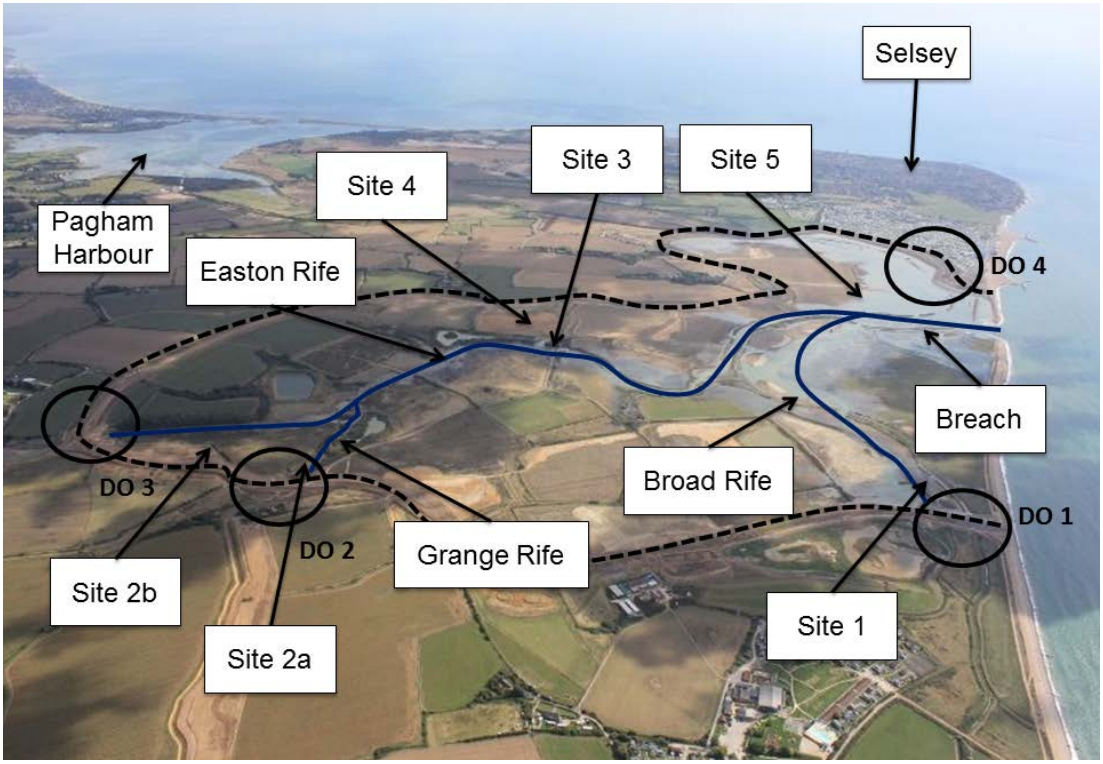

Figure 3.10: The location of the monitoring sites (looking south-eastwards), the new defences (black dashed line), the drainage networks (blue line) and the drainage outlets (DOs) at the Medmerry Managed Realignment Site, in context with Pagham Harbour and Selsey (photograph: John Akerman).

Table 3.1: Summary of the former land use, design and construction processes at each study site at the Medmerry Managed Realignment Site investigated in this thesis.

Site	Former Land Use, Design and Construction Processes
Site 1	Pastoral grassland used to store excavated material during site construction. Area was cleared and levelled prior to site inundation.
Site 2a	Freshwater drainage channel cut and re-profiled during site construction.
Site 2b	Low quality arable / pastoral land characterised by remnant tyre tracks from the heavy plant used during site construction.
Site 3	Pastoral land with channel cut during site construction leading up a borrow pit.
Site 4	Borrow pit that is only inundated on extreme spring tides (approximately 3 to 4 times a year).
Site 5	Intensive arable field last harvested the week before site inundation, behind a borrow pit.

3.3.1 Site 1

Previously known as Robinson's Marsh, and classified as pastoral land in the 1842 Wittering East Tithe Map, this site is located at the western extremity of the Medmerry site. The site is located on a cut channel, which intersects the relict Broad Rife drainage channel, and is downstream from DO1 (Figure 3.11). Post-reclamation, the area remained pastoral grassland with marsh like morphology until the construction of the realigned defences, when the area was used to store material excavated from the borrow pits but considered unsuitable for use in constructing the new defences. The site was then cleared and levelled prior to site inundation, inevitably causing a high degree of compaction to the sediment surface. The site is inundated during most tides, draining as sheet flow into the channel, and the sediment is continuously saturated with some pooling of tidal and pluvial water.

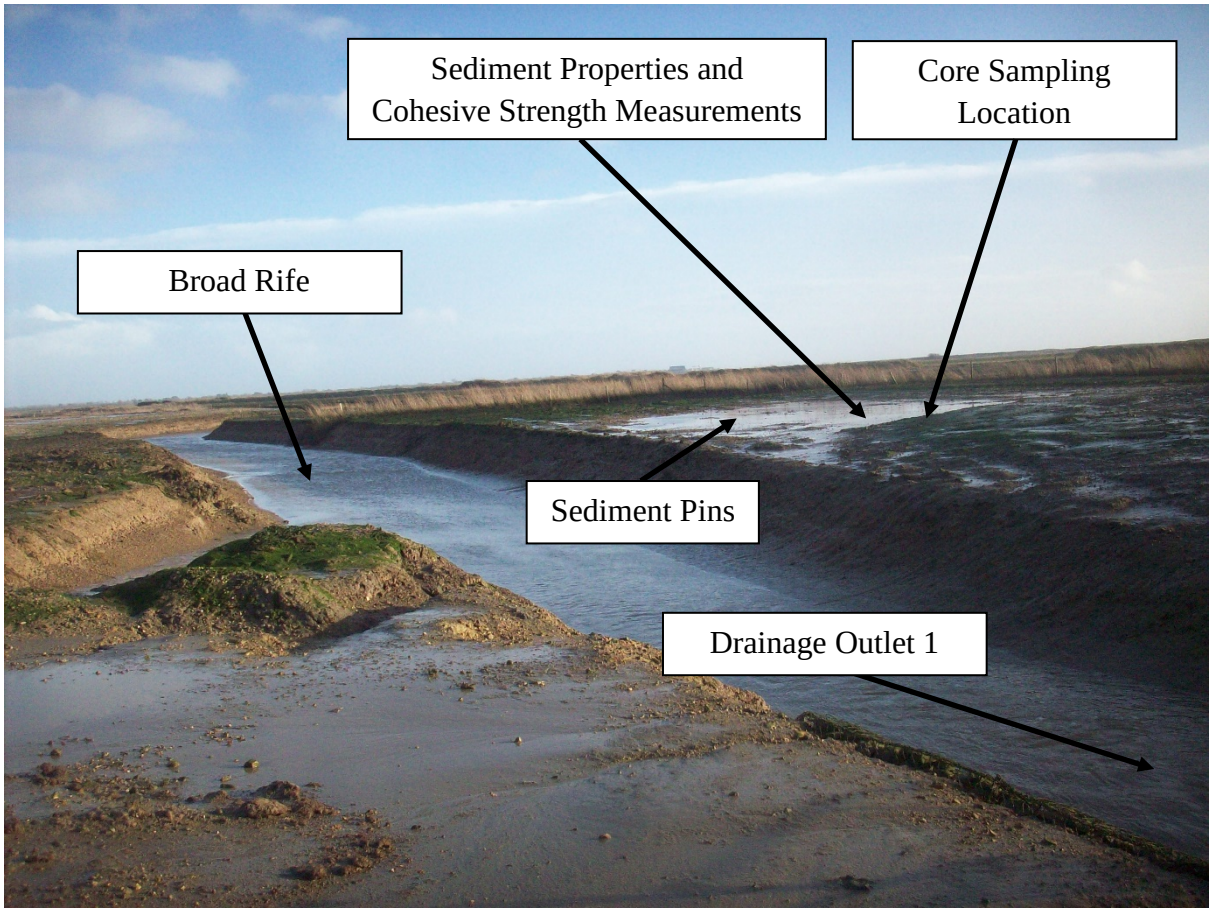

Figure 3.11: Site 1 consists of the flattened and compacted bank on the opposite side of the channel, looking downstream (south-eastwards) from Drainage Outlet 1 on 15th January 2015 (photograph: J. Dale).

3.3.2 Site 2a

Site 2a is between DO2 and an older culvert used for vehicle access (Figure 3.12). The channel, Grange Rife, is a tributary to Easton Rife and existed prior to site construction, but was cut, re-profiled and heavily engineered to allow for the transition into DO2. In a map of Earnley Farm dating from 1827, this area was named Barn Marsh and was identified as being pastoral land in the 1845 Earnley Tithe Map. The area surrounding the channel remained pastoral until site construction. The site itself is within the channel, but located on a scoured beach above the level of the usual freshwater flow. The entire site, including the surrounding banks and the old culvert, is inundated at high water and the sediment is constantly saturated.

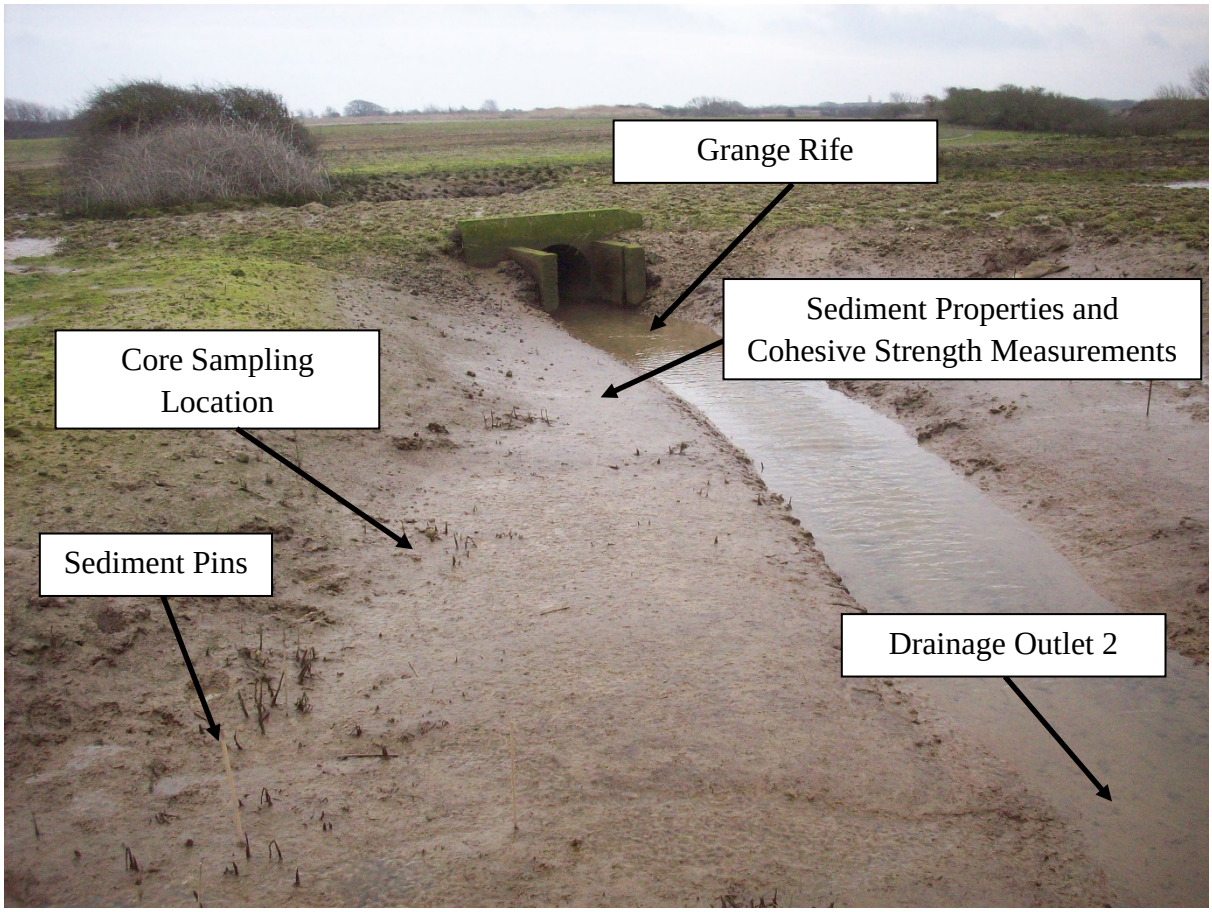

Figure 3.12: Looking downstream (south-eastwards) of Drainage Outlet 2 at Site 2a on 13th February 2015. Measurements were taken on the flat scoured beach to the left of the channel (photograph: J. Dale).

3.3.3 Site 2b

Located at the furthest point inland, Site 2b consists of an intertidal floodplain and adjacent Easton Rife channel, the main drainage channel running through the site, which feeds into the site through DO3. The 1827 Earnley Farm map refers to this area as Six Acre Marsh, with aerial photography indicating that the land-use fluctuated between arable and pastoral practices since the 1930s. Attempts to grow crops at this site were usually unsuccessful due to the soil quality. The site is characterised by the remnants of tyre tracks from the heavy machinery used during the construction phase which ran parallel to the Easton Rife channel (Figure 3.13). Within these tracks, which initially acted as the drainage network for the site, pooling of tidal and pluvial water tended to occur resulting in the sediment usually being saturated. Desiccation cracks frequently formed on the ridges either side of the tracks.

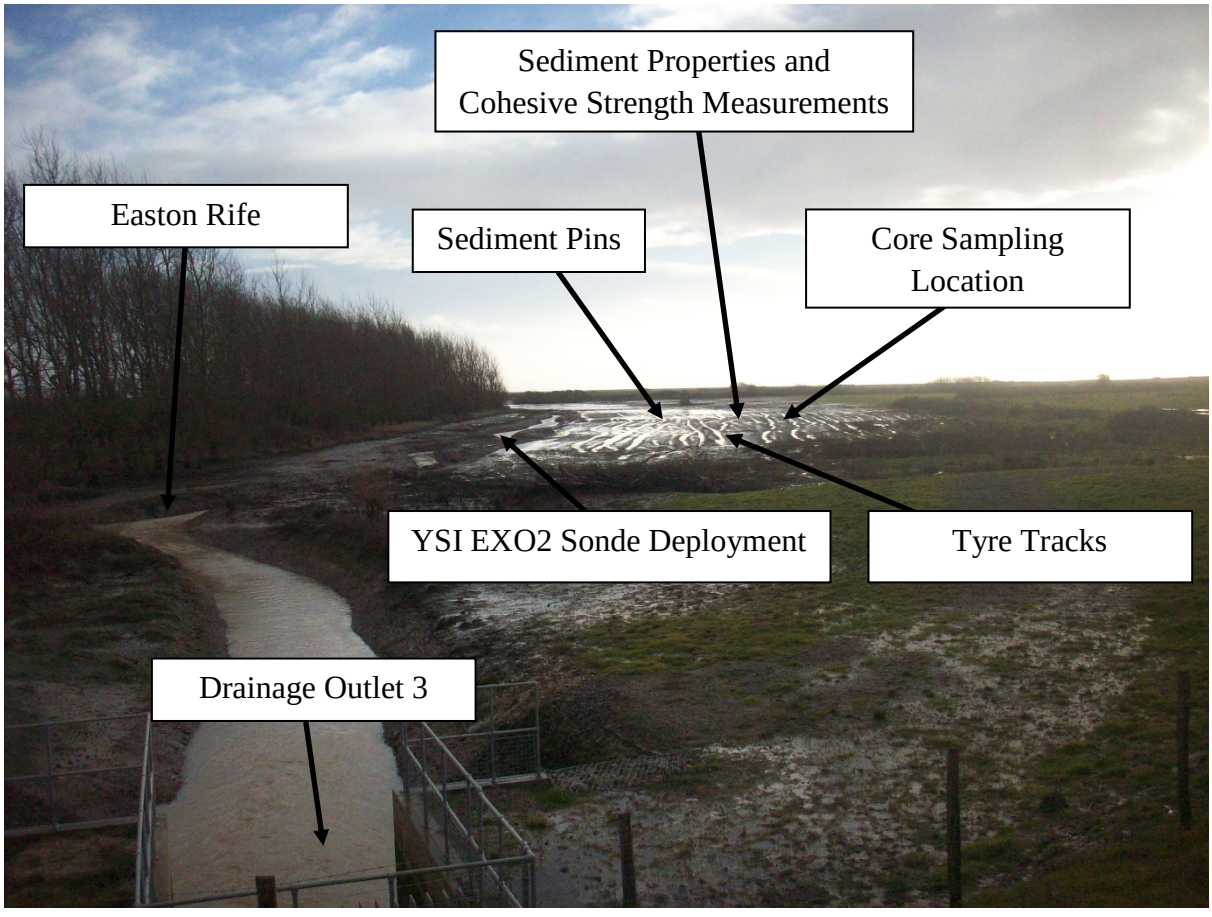

Figure 3.13: Site 2b, downstream (southwards) of Drainage Outlet 3, on 15th January 2015 characterised by tyre tracks left by the machinery used during site construction (photograph: J. Dale).

3.3.4 Site 3

Situated at the centre of the Medmerry Managed Realignment Site, Site 3 historically was an area of pastoral land, with vegetation growth increasing during the 20th century. The site marks the entrance to a borrow pit, Borrow Pit 6 (see Site 4), where a channel was cut through the eastern bank of Easton Rife, which gently slopes up to the borrow pit behind the remains of a row of trees. The hedgerow was cut and up to 1.5 m of sediment were excavated during site construction exposing soils compacted by the removed large overburden, with the heavy construction machinery causing additional compaction within the channel (Figure 3.14). An incised meandering pluvial creek formed within the channel following a period of heavy rain in January 2014 (Burgess et al., 2016). Tidal waters only enter the upper reaches of the entrance channel during extreme spring tides (see Site 4), and the borrow pit was known not to be inundated during the period in which the embryonic creek formed.

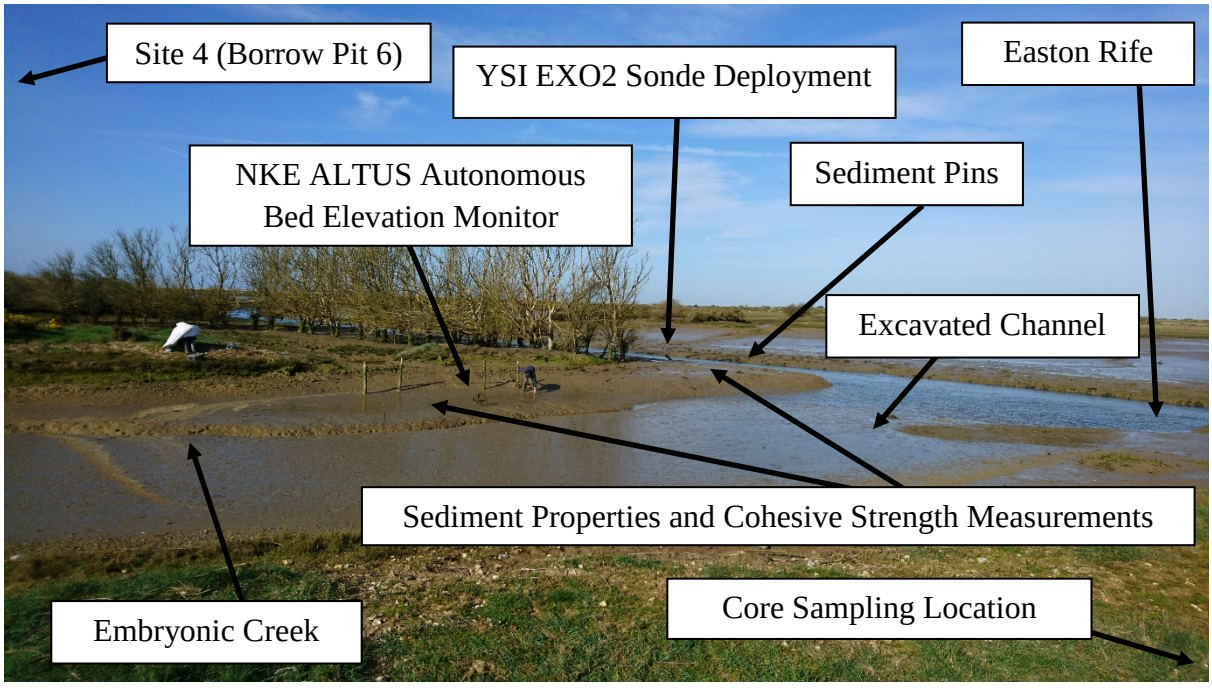

Figure 3.14: The remains of the terrestrial vegetation, the cut channel and within it the pluvial embryonic creek which has formed post-breach at Site 3 (looking westwards) on 18th May 2015 (photograph: J. Dale).

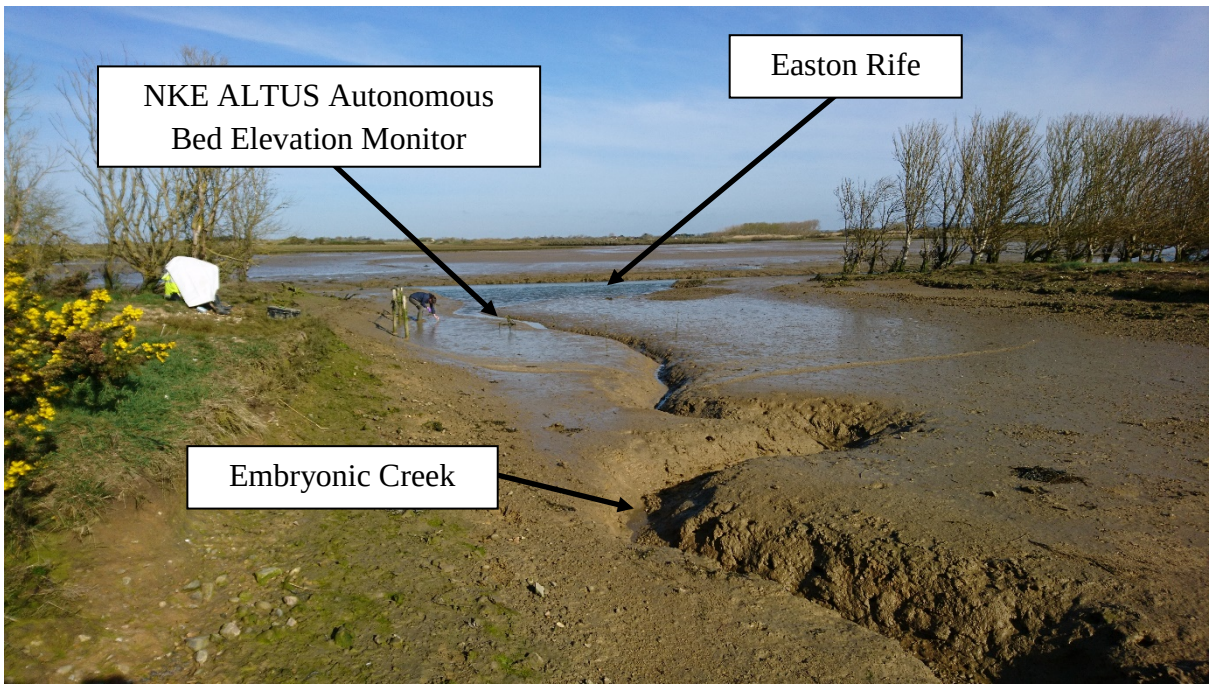

Figure 3.15: The pluvial embryonic creek which has formed post-breach at Site 3 (looking north-westwards) on 18th May 2015 (photograph: J. Dale).

3.3.5 Site 4

Site 4 is towards the back of Borrow Pit 6, leading up from Site 3 (Figure 3.16). However, this site is only inundated during extreme spring tides (approximately 3 to 4 times a year) owing to the relatively high elevation in comparison to mean high water. Although this area was previously used for arable farming, the surface sediment at the time of breaching was heavily compacted due to the excavation of material creating the borrow pit. The low frequency of inundation and compact sediment have reduced the possibility of saltmarsh vegetation becoming established, with the surface often inundated by standing freshwater pools, which drain through the pluvial creek at Site 3.

Figure 3.16: Looking (eastwards) towards the back of the borrow pit in which Site 4 is located on 18th May 2015. The water present in the borrow pit is freshwater pluvial run off (photograph: J. Dale).

3.3.6 Site 5

This site is located towards the back of a borrow pit, Borrow Pit 8, and in a remnant barley field near the breach, which is inundated during every tide and faces the prevailing wind from the south-west. The barley field was last harvested the week before the breach, in September 2013, and had previously been used consistently for agricultural purposes. The area excavated for construction of the borrow pit was not used for arable farming until the end of the 1960s, when aerial photographs show plough lines replacing the pastoral vegetation. Tidal levels at the site, particularly at low water, are controlled by morphological changes at the mouth of the borrow pit. At this site, measurements were taken in the borrow pit (Figure 3.17) and from the bank (Figure 3.18), where two embryonic creek networks had formed on the edge of the borrow pit.

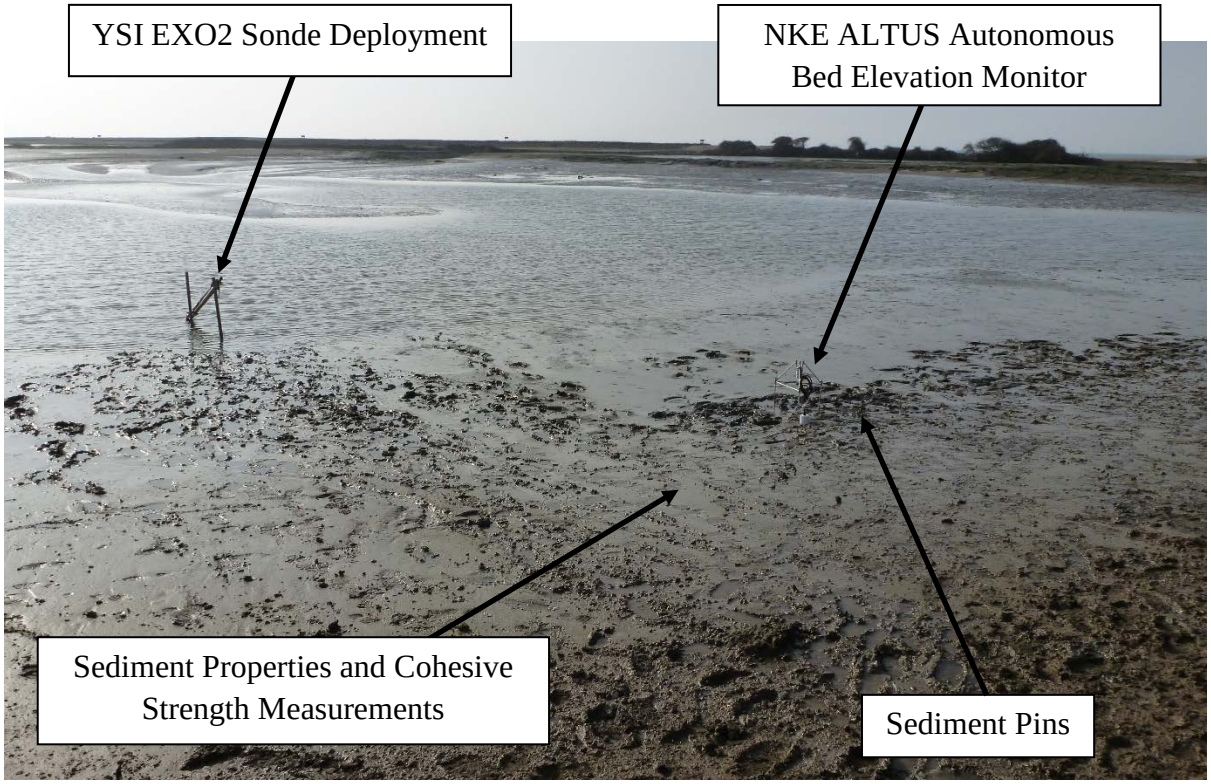

Figure 3.17: Looking (westwards) towards the breach into the borrow pit at Site 5 on 30th October 2014 (photograph: J. Dale).

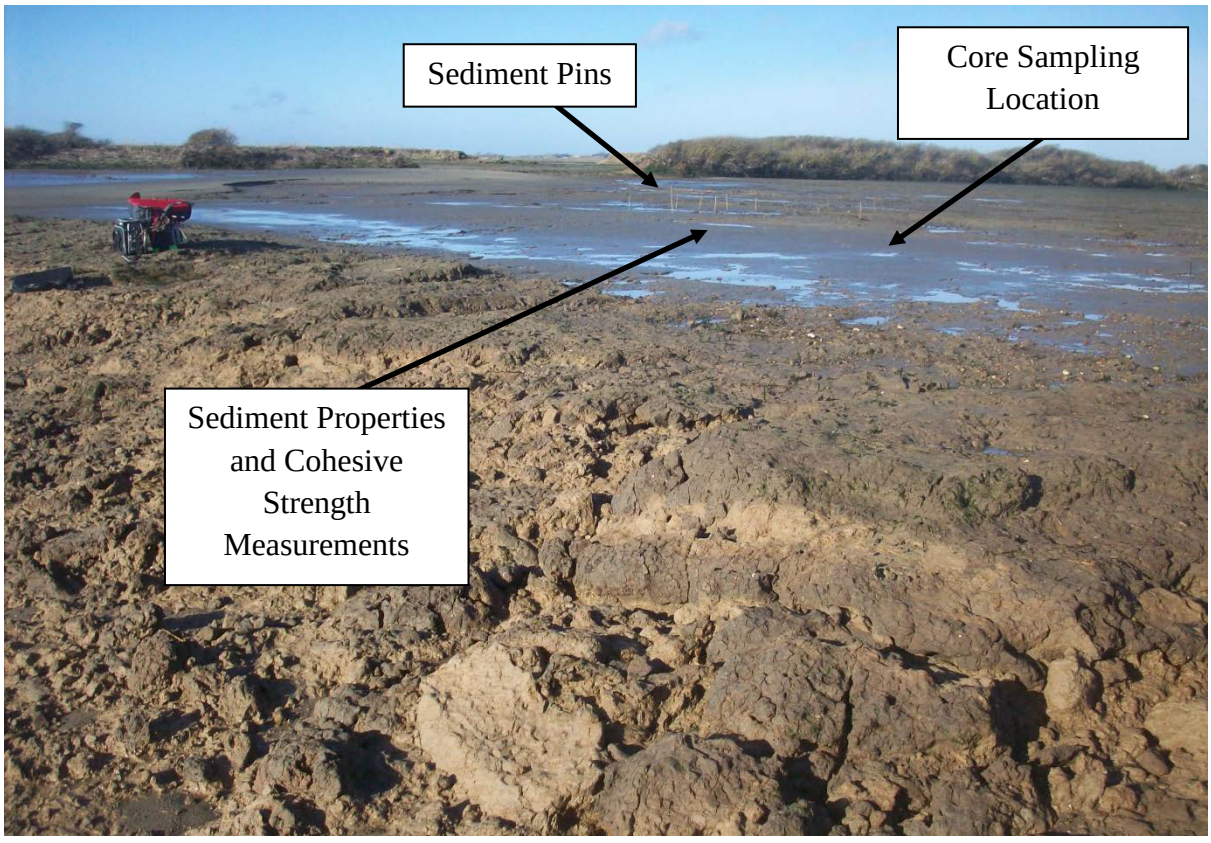

Figure 3.18: Looking (northwards) inland from the edge of the borrow pit at Site 5 on 14th January 2015 (photograph: J. Dale).

3.4 Summary

Managed realignment was carried out at Medmerry to enhance the sustainability and protection given by coastal flood defences in the region, and to compensate for habitat loss elsewhere in the Solent. The scheme is predicted to create up to 300 hectares of intertidal and transitional habitat, which have started to colonise following site inundation, restoring tidal inundation to an area previously reclaimed during the 19th century. The monitoring sites investigated at Medmerry include a range of former land uses and engineered landscape construction techniques. The evolution of the sediment regime has been investigated at these sites, addressing the knowledge gaps identified in Chapter 2, assessing the influence of the differences in site history (former land use, site design and construction), using the methods outlined in Chapter 4.

4 Materials and Methods

4.1 Introduction

This chapter details the development of techniques and the choice of equipment used to investigate the evolution of the sediment regime at the Medmerry Managed Realignment Site. The methodology of this investigation employed a variety of quantitative field measurement techniques and equipment, supplemented by laboratory analysis, frequently used in the fields of geomorphology, oceanography and civil engineering. Observations and measurements of the evolution of the sediment regime were made continuously, and during regular visits, over a two year period from November 2014 until October 2016 (during the second and third years of site inundation). Figure 4.1 presents an overview of the method used and parameters measured for each results chapter, and the methods deployed at each site (see Chapter 3 for site descriptions) are outlined in Table 4.1.

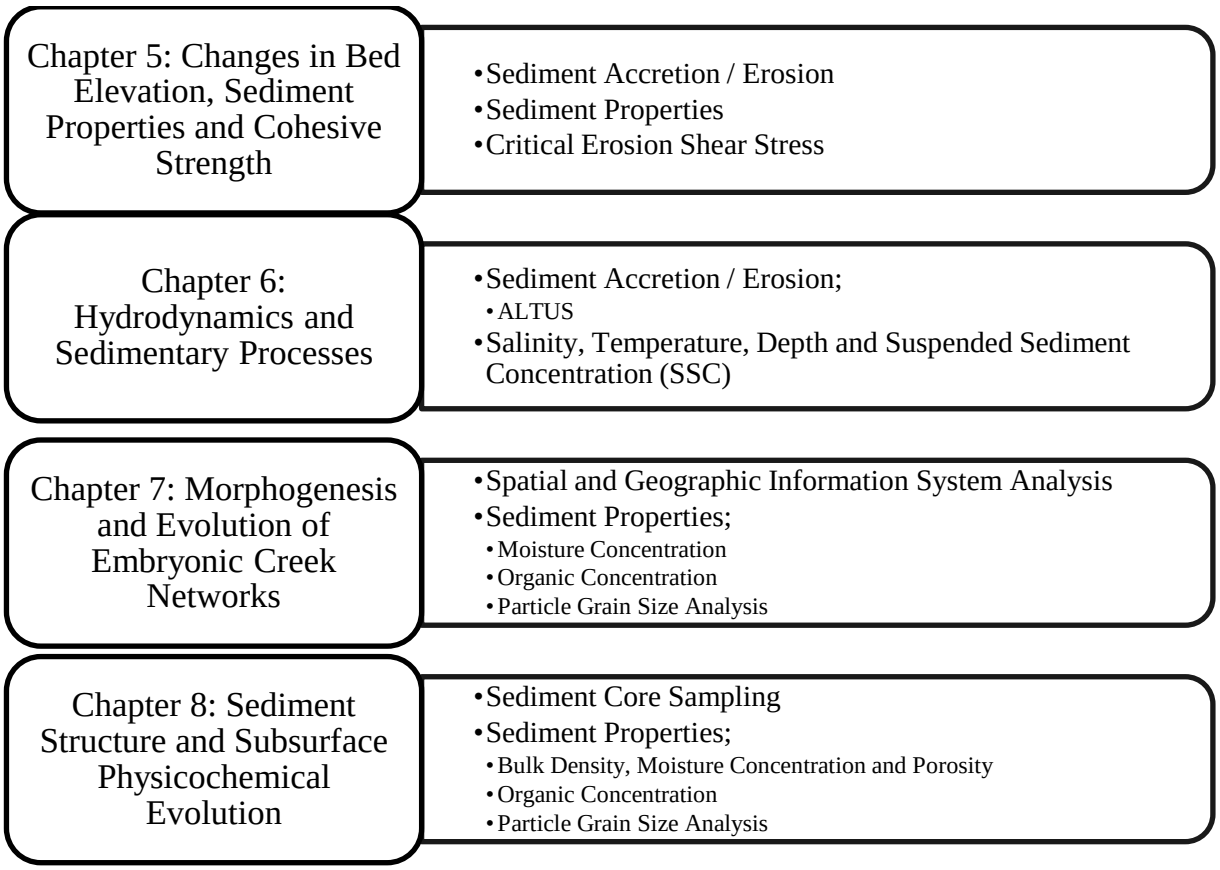

Figure 4.1: The methods used and / or the parameters measured for each results chapter in this thesis.

Table 4.1: Overview of equipment, methods and materials used at each site (described in Section 3.3) as part of this study.

	Site 1	Site 2a	Site 2b	Site 3		Site 4	Site 5		Breach
				Bank	Channel		Bank	Borrow Pit	
ALTUS					X			X	
Sediment Pins	X	X	X	X			X	X	
Surface Sediment Properties	X	X	X	X	X	X	X	X	
Surface Sediment Properties – Local Heterogeneity Analysis			X	X	X		X	X	
Critical Erosion Shear Stress	X	X	X	X	X		X	X	
Critical Erosion Shear Stress – Local Heterogeneity Analysis			X	X	X		X	X	
Creek Development – dGPS							X		

	Site 1	Site 2a	Site 2b	Site 3		Site 4	Site 5		Breach
				Bank	Channel		Bank	Borrow Pit	
Creek Development – Drone							X		
CTD and SSC – Near-Bed Continuous Monitoring			X		X			X	X
CTD and SSC – Profiling			X		X				
CTD and SSC – Longitudinal Profiling				Measurements taken along Easton Rife					
Broad-scale Sediment Core Sampling – Physical Properties	X	X	X		X[1]		X		
Broad-scale Sediment Core Sampling – Geochemical Properties			X		X[1]		X		
Broad-scale Sediment Core Sampling – Repeat Physical and Geochemical Properties Analysis			X		X[1]		X		
Intensive-scale X-Ray Microtomography and ITRAX Analysis			X				X		

[1] Cores taken from a vegetated and non-vegetated surface.

4.2 Sediment Accretion and Erosion

Changes in bed elevation were measured to monitor the rates of accretion and erosion of sediment. There are a variety of techniques available to measure the accretion or erosion of sediment, both continuously and intermittently, over a range of spatial and temporal scales (Thomas and Ridd, 2004). A number of methods used in previous studies are reviewed in Appendix 1, these include: Light Detecting and Ranging (LiDAR), Sediment Erosion Table, Sediment Pins and ALTUS systems. The choice of equipment and technique used is typically a balance between the available spatial and temporal coverage and the cost, accuracy and time available.

4.2.1 ALTUS

Following an evaluation of each potential method, NKE ALTUS autonomous bed elevation monitors were selected to collect continuous high frequency altimetry data. ALTUS systems measure changes in bed elevation when the sensor head, located in the centre of a tripod above the sediment surface, is submerged. However, the sensor only measures the area directly beneath it, an area 2.5 cm in diameter, and there is the risk of fouling around the frame which could bias the results and disturb the sediment beneath the sensor.

Two ALTUS systems were deployed in the cut channel at Site 3 at 0.60 mOD and the other in the borrow pit at Site 5 at 0.17 mOD (Figure 4.2), taking care not to disturb the area underneath the sensor. Both ALTUS systems were set to log at 10 minute measurement frequencies from 1st November 2014 and data were utilised to monitor the change in bed elevation (Chapter 5) and analyse the rhythmic patterns of sedimentation in response to site hydrodynamics (Chapter 6). Measurements were taken until 31st October 2016 at Site 3. During a site visit on 19th January 2016 the ALTUS at Site 5 was found to have sustained irreparable damage, resulting in a loss of data from November 2015 until the ALTUS was replaced by sediment pins (see Section 4.2.2) on 2nd February 2016. The equipment and measurement specifications

are outlined in Appendix 2. Data were downloaded on site using WinMemoII software and saved as a text file for subsequent data manipulation.

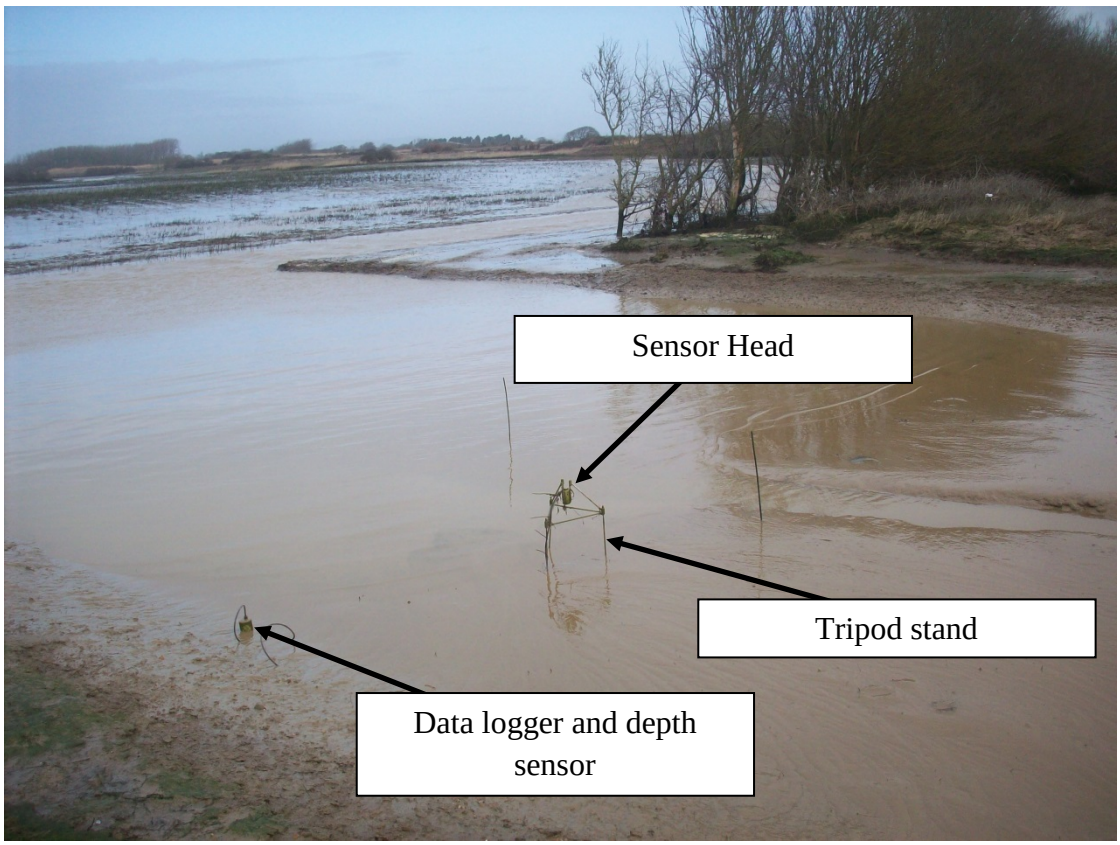

Figure 4.2: The ALTUS system deployed in the cut channel at Site 3 on 15th January 2015 and annotations (photograph: J. Dale).

4.2.2 Sediment Pins

Although ALTUS systems capture valuable data of the changes in bed elevation in response to short-term variations in the hydrodynamics they are relatively expensive and spatially limited to the area directly underneath the sensor. Therefore, sediment pins (Figure 4.3) were deployed in January 2015. At each deployment, a central bamboo pin was inserted into the sediment, with pins placed 1 m from the central pin at 90° giving a 2 m by 2 m cross formation with three pins in a cross-shore and three pins in a long-shore direction (after Ni et al., 2014). To reduce the impact of scour around the pins themselves, which could give misleading results, a 1 m bar with holes at 20 cm intervals was placed on top of the pins. Care was taken not to disturb the area under the bar. A pin was inserted through each of these holes and carefully lowered so

that it sat flush on the sediment surface. The pin was then measured, quantifying the distance between the bottom of the bar and sediment surface for each site, giving a total of 12 measurements which were then averaged to calculate the mean change in bed elevation over an area of 4 m^2. Changes in elevation were measured using pins from February 2015 and results are reported relative to the height above ordnance datum Newlyn (m OD) of the central pin.

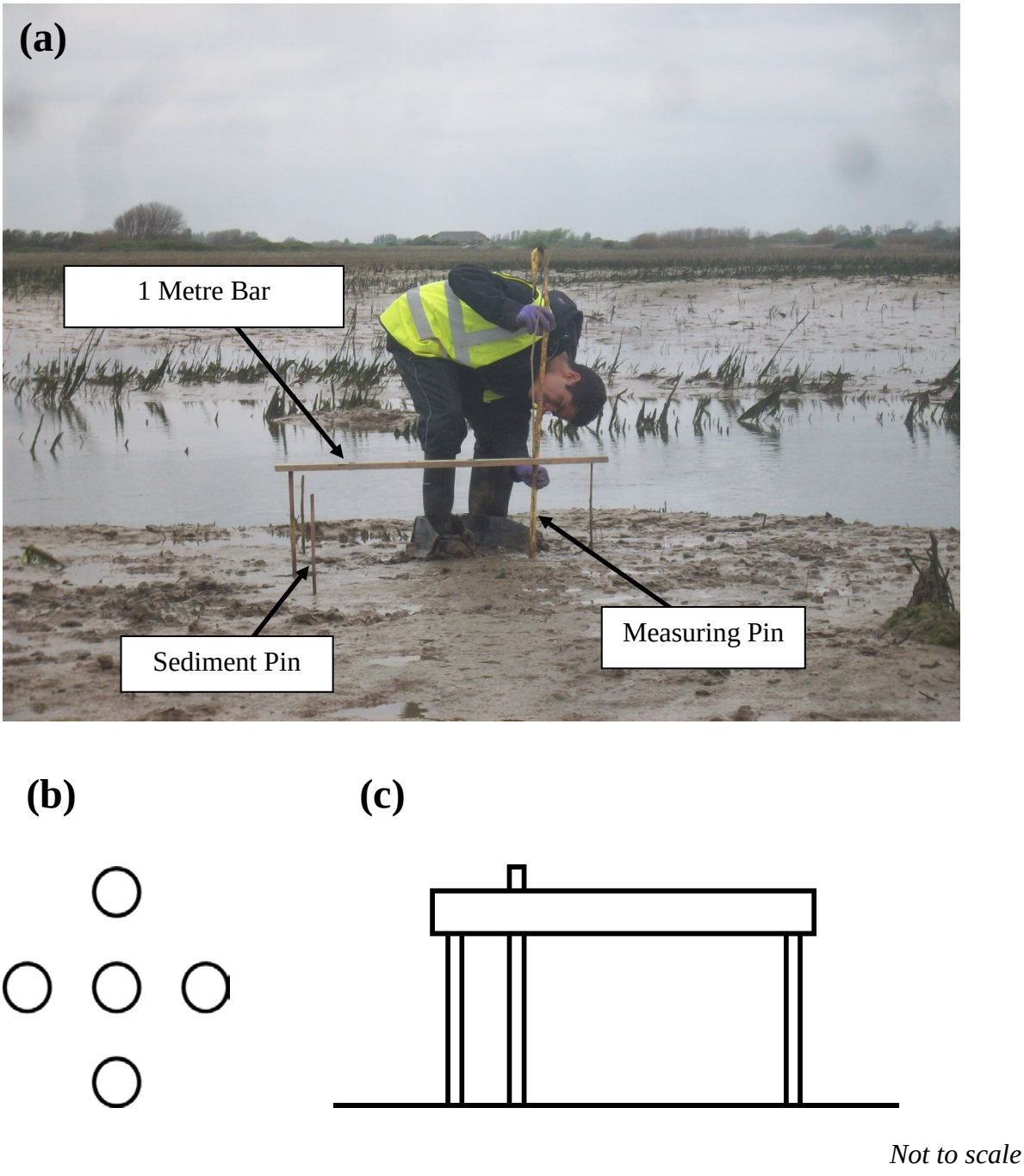

Figure 4.3: Sediment pins set up in a cross formation including the 1 m bar with 20 cm measuring intervals and measuring pin in the tidal zone (a) annotated at Site 3 on 5th May 2015 and sketches (not to scale) of (b) the aerial view and (c) the lateral view (photograph: J. Dale).

There are a number of advantages and disadvantages to this approach. Using bamboo pins means they are susceptible to damage such as snapping, resulting in a loss of data. Additionally, data are temporally limited by the measurement frequency and can be biased due to vegetation, such as seaweed, which can become wrapped around the pins. Vegetation can also influence measurements as it can disturb the sediment between the pins and can cause the pins to lean changing the measurement position between the pins, although in most cases vegetation can be easily removed minimising the disturbance.

4.3 Sediment Properties

To monitor the changes in sediment properties as the site develops and the sediment regime evolves, regular surface samples were taken at each site and analysed for the following physical and geochemical properties:

- Physical: Wet bulk density, moisture concentration, porosity, median grain size, mud (clay + silt) concentration
- Geochemical: Organic concentration (loss on ignition) and pore water salinity (chloride concentration).

At Site 4, at the back of Borrow Pit 6, only the moisture concentration, loss on ignition, median grain size and mud concentration were measured as this site is only occasionally inundated (approximately 3 to 4 times a year) due its high elevation compared to mean high water. To investigate the within-site spatial variability and local heterogeneity of the surface sediment properties, measurements were taken from separate plots in transects at Sites 2b, 3 and 5 (Table 4.2) on three occasions; August 2015, November 2015 and June 2016. These sites were selected based on the different former land use and site design, that the sites include the near-breach environment, the centre of the site and the furthest point inland, and that these sites have the largest range of intertidal zonation (mudflat to upper saltmarsh and marginal terrestrial). All laboratory analysis was performed in the Geochemical Preparation Laboratories at the University of Brighton.

Table 4.2: Length of transect and number of individual plots sampled for analysis of local heterogeneity.

Site	Length of transect (m)	Number of plots
Site 2b	30	5
Site 3	10	4
Site 5	50	6

4.3.1 Bulk Density, Moisture Concentration and Porosity

To determine changes to the bulk density, moisture concentration and porosity, copper cylinders (height = 4 cm, radius = 1 cm) were driven into the sediment until approximately 3 mm of sediment extruded beyond the cylinder. The cylinders were then excavated and placed in a sealed, labelled polythene sample bag and carefully transported back to the laboratory. Care was taken whilst extracting and transporting samples to reduce compaction and disruption to the sediment and, in order to reduce the influence of any disturbance, five replicates were taken at each site. Upon return to the laboratory, samples were trimmed so they were flush with the ends of the cylinder and carefully transferred into glass beakers which had been pre-dried and weighed to the nearest 0.0001 g. To assess temporal changes to the bulk density, samples were weighed to the nearest 0.0001 g with the wet bulked density calculated as:

$$\boldsymbol{Bulk\ Density} = \frac{\boldsymbol{m_2 - m_1}}{\boldsymbol{v}} \quad \textbf{1}$$

where m_1 is the mass of the beaker, m_2 is the mass of the wet sample and beaker and v is the volume of the cylinder (adapted from Rowell, 1994). Samples were then oven dried at 105 °C for 48 hours, cooled in a desiccator and reweighed once cool to the nearest 0.0001 g. Weighing was not carried out whilst samples were hot as the currents caused by the warm air can lead to inaccuracies in the measurements (Head, 1992). The moisture concentration was calculated as a percentage of the dry mass:

$$\boldsymbol{Moisture\ Concentration} = \frac{\boldsymbol{m_2 - m_3}}{\boldsymbol{m_3 - m_1}} \times \mathbf{100}\ \%$$

2

where m_1 = mass of beaker; m_2 = mass of beaker and wet sample; m_3 = mass of container and dry sample (BS 1377: Part 2:1990:3.2). The porosity was then calculated using the dry bulk density and particle density as:

$$\boldsymbol{Porosity} = \frac{\mathbf{1} - \boldsymbol{Dry\ Bulk\ Density}}{\boldsymbol{Particle\ Density}}$$

3

with the dry bulk density derived from Equation 1 where m_2 is the mass of the dry sample. The particle density was assumed to be 2.65 g cm^{-3} as stated by Rowell (1994) based on typical data.

4.3.2 Organic Concentration

There are several methods of calculating the organic concentration of the sediment including loss on ignition or wet oxidation using hydrogen peroxide (Rowell, 1994). Loss on ignition was used in this investigation (adapted from BS 1377: Part 3:1990:4) as it was considered to be rapid and relatively inexpensive compared to other methods. Samples were dried for 48 hours at 105 °C, cooled to room temperature in a desiccator, weighed and placed in a muffle furnace at 450 °C for six hours. Once ignited, carbon dioxide, water and ash are produced by the oxidisation of the organic portion of the sample, although the loss of other components, such as volatile salts, inorganic carbon and structural water adsorbed to clay particles can lead to an over-estimation of the organic concentration (Rowell, 1994).

After ignition, samples were removed from the furnace, left to cool to room temperature in a desiccator and weighed to the nearest 0.0001 g. The relative

proportion of the organic portion lost from the sample was calculated from the mass difference before and after ignition as a percentage of the dry mass:

$$\boldsymbol{LOI = \frac{m_3 - m_4}{m_3 - m_1} \times 100\ \%} \quad \textbf{4}$$

where m_1 = mass of beaker; m_3 = mass of container and dry sample; m_4 = mass of container and sample after ignition.

4.3.3 Particle Grain Size Analysis

The particle grain size distribution and descriptive characteristics of the sediment samples were analysed using a Malvern Instruments Mastersizer Hydro 2000G Laser Diffraction Particle Size Analyser. Laser diffraction was selected over alternative grain size analysis techniques, such as sieve shaking, as it is a rapid technique which covers a range of particles sizes; in this case 0 to 2000 µm. Samples were taken at each site by carefully scraping away approximately the upper 5 mm of the sediment surface which was sealed in a labelled polythene bag and stored in the University of Brighton walk-in cold store at 3.6 °C until analysis.

It has been recognised that organic matter can bind particles together, resulting in an overestimation of the grain size (Rowell, 1994). Consequently, organic matter was removed prior to analysis. Wet oxidation using hydrogen peroxide (H_2O_2) was selected instead of other methods which remove organics, such as ignition in a furnace, as the loss of water from the structure of clay particles during ignition may result in a change in the size of the clay particles. Analysis showed a decrease of 6.03 µm in the medium grain size (d_{50}) after organics had been removed from a sample taken from Site 1 at Medmerry in February 2015 (Table 4.3).

Table 4.3: Changes in measured grain size after various pre-analysis treatments (n = 3).

Treatment	**d_{50} (µm)**	**Clay Concentration (%)**	**Silt Concentration (%)**	**Mud Concentration (Clay + Silt) (%)**	**Sand Concentration (%)**
No treatment	32.81 ± 2.38	3.70 ± 0.10	60.34 ± 0.68	63.04 ± 0.96	36.97 ± 0.96
H_2O_2	26.78 ± 0.59	4.66 ± 0.11	70.44 ± 0.56	75.10 ± 0.66	24.90 ± 0.66
H_2O_2 + $(NaPO_3)_6$	20.85 ± 0.48	6.47 ± 0.26	74.57 ± 0.46	81.04 ± 0.13	18.97 ± 0.13
H_2O_2 + $(NaPO_3)_6$ + One hour shaking	14.98 ± 0.39	9.74 ± 0.75	77.00 ± 2.94	86.74 ± 2.23	13.26 ± 2.23
H_2O_2 + $(NaPO_3)_6$ + Two hours shaking	8.42 ± 0.18	15.42 ± 0.31	82.87 ± 0.41	98.29 ± 0.13	1.72 ± 0.13
H_2O_2 + $(NaPO_3)_6$ + Three hours shaking	8.38 ± 0.19	15.43 ± 0.15	82.8 ± 0.11	98.23 ± 0.05	1.77 ± 0.05
H_2O_2 + $(NaPO_3)_6$ + Four hours shaking	8.36 ± 0.16	15.49 ± 0.30	82.75 ± 0.47	98.20 ± 0.20	1.80 ± 0.20

A beaker containing 1 ± 0.1 g of sediment was placed on a hotplate set at 50 °C and hydrogen peroxide at 30 % concentration was added regularly until no further reaction occurred. The temperature of the hotplate was then increased to 105 °C to burn off any excess moisture and samples were re-suspended in the dispersant sodium hexametaphosphate ($(NaPO_3)_6$). Samples were shaken on a flatbed shaker to ensure all the clay particles were fully dispersed. Analysis found that two hours were required to ensure all particles were fully dispersed, given that minimal differences were found between the sample taken from Site 1 at Medmerry when shaken for two, three or four hours (Table 4.3). Samples were pipetted into the particle size analyser ensuring sufficient sample was inserted to be within the detectable range of the equipment and measured in the metric scale (µm). Three replicate measurements were taken for each sample to check for consistency and repeatability.

4.3.4 Porewater Chloride Concentration

To measure changes in the salinity of the intertidal sediment, the porewater chloride ion concentration was used as a proxy. Although the total salt content can vary, more than 55 % of the total dissolved salts in seawater are chloride ions with the concentration ratios of major elements usually remaining constant. The occasions when typical concentration ratios are not found include the precipitation and dissolution of carbonate minerals, the freezing of seawater and in some estuaries and landlocked seas (Chester, 2009). Nonetheless, the chloride concentration was considered to be a suitable representation of the salinity of the sediment and has been used in this way in previous comparable studies (e.g. Kadiri, 2010).

Porewater was extracted at each site using a Rhizon sampler (Seeberg-Elverfeldt et al., 2005), a hydrophilic porous polymer tube with wire support extended with a polyvinyl chloride tube (Figure 4.4). The typical pore diameter of a Rhizon is 0.1 µm and the outer diameter is 2.4 mm. Rhizons were selected as they can be used *in situ* and, due to the small diameter, cause minimal disturbance to the sediment. In this study Rhizons were attached to 10 ml luer-lock syringes, with a vacuum forming once the

porous polymer had been inserted into the sediment, using a wooden block to hold the syringe plunger in place.

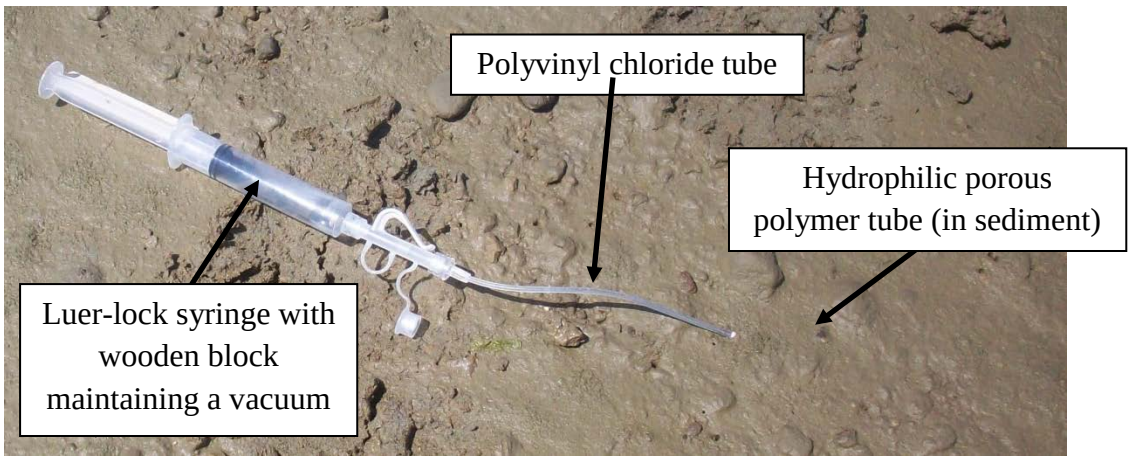

Figure 4.4: Rhizon sampler deployed *in situ* to extract porewater from the sediment (photograph: J. Dale).

Chloride concentrations were analysed using a Thermo Scientific Dionex ICS-1100 Ion Chromatograph System with a 4 x 250 mm Thermo Scientific Dionex IonPac® AS23 analytical column, a 4 x 50 mm Thermo Scientific Dionex IonPac® guard column and a Thermo Scientific Dionex ASRS 300 4 mm suppressor. The eluent used was Thermo Scientific Dionex AS23 which, after diluting to a 1 in 100 concentration, consisted of 4.5 mM Soidum Carbonate and 0.8 mM Sodium Bicarbonate. A Thermo Scientific Dionex AS-DV autosampler was used for automated sample injection and Chromeleon® software (Version 7) was used for system control and data processing. Data were downloaded from Chromeleon® as Microsoft Excel Spreadsheets. The system was calibrated using a set of five Thermo Scientific Dionex Seven Anion Standard II standards of varying concentration. Samples were diluted to 1 in 100 concentrations to ensure the chloride concentrations were within the detectable range, which was then accounted for when calculating the final concentration. The precision of the measurements was analysed through duplicate measurements, and indicated measurements were within ± 10 %.

4.3.5 Statistical Analysis

To assess the relationship between variables, Pearson correlation coefficients (*r*) were calculated. Correlation coefficients quantify the strength of a linear relationship, assuming variables are distributed normally (i.e. distributed around a central value with no bias or skew). The statistical significance of the relationships (*P*) was also assessed to determine the confidence that a given correlation coefficient will occur, given no relationship within the data. Pearson correlation was selected, after assessing the normality of the distribution, over alternative analysis such as multivariate analysis due to the number of measurements and data points available.

4.4 Critical Erosion Shear Stress

To evaluate how the resistance of the sediment to erosion changes as the sediment regime develops, and the influence of surface sediment properties, frequent measurements of the erodibility of the sediment were taken. The erodibility is expressed as either a threshold for erosion or as an erosion rate (Sanford, 2008). The threshold for erosion is a measure of the resistance to the shear stress, the erosional forces applied parallel to the sediment surface, expressed as the critical shear stress at which erosion occurs (τ_{cr}). The erosion rate is the mass of sediment eroded per unit time once the critical shear stress has been exceeded (Grabowski et al., 2011). Due to the complex range of variables influencing sediment stability it is very difficult to predict and model the erodibility of cohesive sediment, and instead it must be measured site specifically for the sediment in question (Black and Paterson, 1997; Defew et al., 2002; Winterwerp and van Kesteren, 2004). At present, there is no standard method of measuring sediment erodibility, instead there are a range of laboratory and *in situ* based techniques available which try to replicate the shear stress applied by tidal currents and wave action (Tolhurst, Defew, de Brouwer, et al., 2006).

4.4.1 Laboratory versus *In Situ* Analysis

Historically, erosion thresholds and rates were measured using sediment cores in laboratory flumes (Grabowski et al., 2010). However, sediments were often disturbed during the acquisition and transportation of the samples. Compaction and changes in the water concentration of the sediment can alter the resistance of the sediment to erosion, as demonstrated by Tolhurst, Riethmuller, et al. (2000) who associated drying of the sediment during transportation with increased stability in a comparative study between laboratory and *in situ* measurements. Furthermore, laboratory analysis fails to account for small scale and site specific variability caused by the complex interactions between various field physical, chemical and biological influences (e.g. Defew et al., 2002; Tolhurst, Defew, de Brouwer, et al., 2006), which can be altered whilst transporting and reforming samples (Black and Paterson, 1997).

Consequently, in recent years there have been advances in the techniques which allow quick *in situ* measurements of the erodibility (Grabowski et al., 2010) in order to develop predictive models of cohesive sediment dynamics (Vardy et al., 2007). Several devices exist for the *in situ* measurement of the critical erosion threshold (Black and Paterson, 1997). These are generally categorised into two groups: field deployable flumes such as the Sea Carousel or the Gust erosion chambers, or small portable erosion devices like the cohesive strength meter (CSM) or EROMES (e.g. Amos et al., 2003; Grabowski et al., 2010; Tolhurst, Black, et al., 2000) which apply stress to the sediment through a vertical jet of water fired onto the bed.

4.4.2 The Cohesive Strength Meter (CSM)

Of the available devices for measuring the critical erosion shear stress the CSM was selected for this study. There are several advantages of using a CSM to measure the erosion threshold of cohesive sediment; it is relatively light weight making it easy to carry, can be quickly set up with a rapid measurement time, and is simple to operate (Vardy et al., 2007). Additionally, it has a small footprint meaning it reduces the disturbance to the sediment, can be easily placed between saltmarsh vegetation which

can prevent deployment of other devices (Paterson and Black, 2000), and provides a high spatial resolution (Vardy et al., 2007). Although this is the case for several of the available devices, the CSM is the only one commercially available making it more readily accessible (Grabowski et al., 2010). As a result, and despite suggestions that devices which utilise a vertical jet stress mechanism are unable to detect significant variations in softer estuarine sediments (Widdows et al., 2007), the CSM has become widely used in studies of the relative stability of many intertidal sites (e.g. Tolhurst, Defew, Perkins, et al., 2006; Tolhurst, Defew, de Brouwer, et al., 2006; Tolhurst, Friend, et al., 2006; Watts et al., 2003).

4.4.2.1 CSM Deployment Procedure

The initial CSM was designed and described by Paterson (1989), with the current design remaining relatively unchanged from the one described by Tolhurst et al. (1999). The CSM measures the erosion threshold by firing a vertical jet of water, driven by air pressure, downwards at increasing pressure increments onto the sediment surface. The sediment erosion is monitored using a transmissometer in a small water filled chamber, which measures sediment resuspension 1 cm above the bed (Figure 4.5). An on-board microprocessor controls the jet firing time, the pressure increment and the data logging duration and frequency, with the CSM containing over 40 pre-set test routines.

In this study the Sand 1 routine on a Mark IV CSM (Partrac) (Figure 4.6) was used, as it has the lowest initial jet pressure (0.3 PSI), small pressure increments (0.3 PSI), a high maximum jet pressure (12 PSI), a short jet duration (0.3 seconds), a frequent data logging frequency (0.1 seconds) and a short data logging duration (3 seconds). Average transmission was calculated from the 2^{nd} to 12^{th} data logged per pressure increment which, for the Sand 1 test, corresponds to 1 second. The erosion threshold was defined as the pressure at which the average transmission dropped by 10 % of the initial transmission value (Grabowski et al., 2010). Data were downloaded as Comma Separated Values (CSV) files using CSM Application software (Version 3.0.0.3).

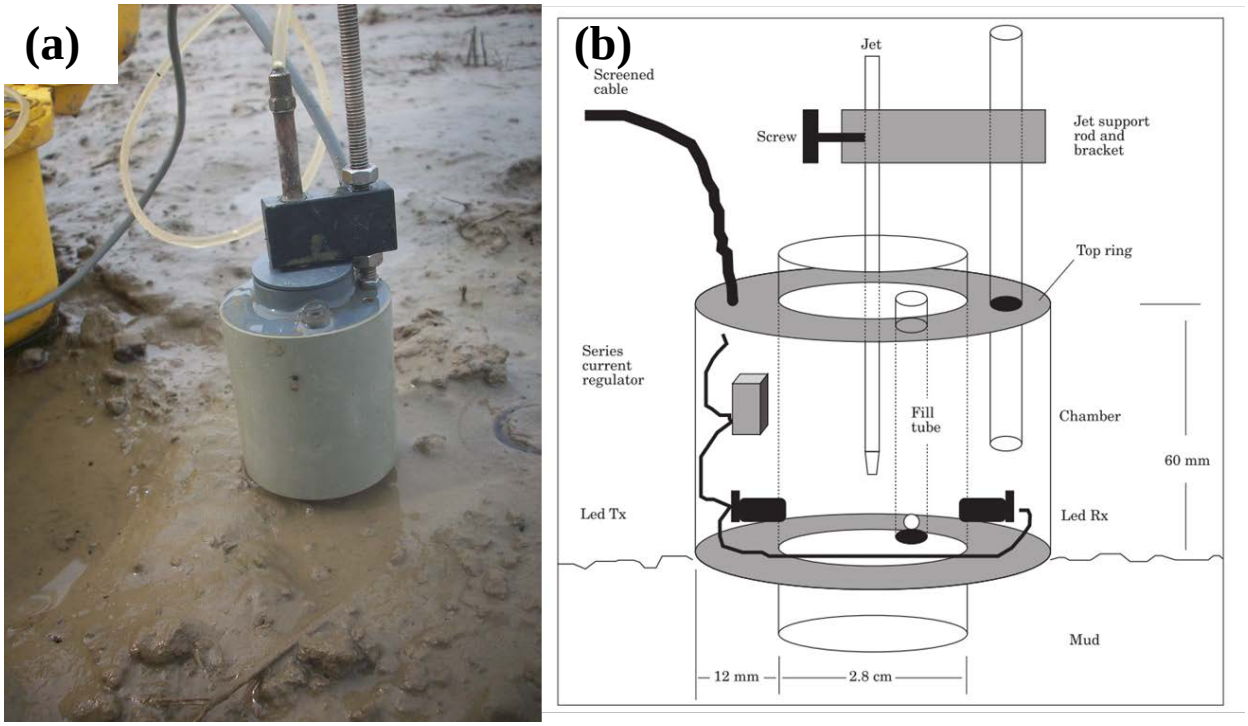

Figure 4.5: CSM test chamber (a) deployed in the field (photograph: J. Dale) and (b) illustrated including cross sectional view and details, after Tolhurst et al. (1999).

Figure 4.6: The Mark IV CSM deployed at Site 1 on 18th May 2015 (photograph: J. Dale).

Regular CSM measurements were made from March 2015. Locally sourced water, which had been filtered through a 63 µm sieve to increase the initial transmission and reduce the influence of additional sediment added in the water, was used. Measurements were made in separate plots across the intertidal zone at Sites 2b, 3 and 5 in August 2015 and June 2016 (Table 4.2), to allow assessment of the spatial heterogeneity in cohesive strength. The relationship between the sediment properties and CSM measurements were assessed through correlation analysis (see Section 4.3.5 for description).

4.4.2.2 CSM Calibration Procedure

To equate the eroding force of the jet to the equivalent horizontal shear stress, Tolhurst et al. (1999) proposed a theoretical calibration based on the resuspensions of uniform sandy beds of varying grains sizes greater than 200 µm. The equivalent horizontal bed shear stress was then calculated from the Shield's criterion derived from the relationship between the critical CSM jet pressure and the grain size. However, this calibration fails to consider how sediments with a grain size less than 200 µm respond to the jet, thus should be used cautiously when applying the CSM method to cohesive sediments (Grabowski et al., 2010). Alternatively, Vardy et al. (2007) suggested a calibration based on pressure of the jet on the sediment surface, the stagnation pressure (P_{stag}), which can vary for different CSM units even at the same internal pressure (P_I) depending on the specifics of the individual CSM model. The P_{stag} varies depending on the sampling routine, the height of the jet orifice above the sediment and the diameter and length of tubing (Vardy et al., 2007). Consequently, by reporting measurements of the critical erosion threshold as the P_{stag}, results from different CSM units can be compared. P_{stag} values were calculated from the logged P_I and the erosional force of the jet, devised by Vardy et al. (2007) as:

$$\boldsymbol{P_{stag} = \frac{1}{2}\frac{\rho_w (7.0)^2 4Q^2}{d^2 (z - z_0)^2 \pi}} \quad \textbf{5}$$

where ρ_w is the fluid density (kgm^{-3}), Q is the volume of the jet fired (m^3/s), d is the orifice diameter (m) and z is the vertical distance of the bed from the jet source (m). Given that under normal operating and calibration procedures all values are constants with the exception of Q, Equation 5 can be simplified to:

$$\boldsymbol{P_{stag} = (7.79859 \times 10^{13}) \times Q^2} \quad \textbf{6}$$

Furthermore, as Q is obtained from the mass of water produced by an individual jet per second, Equation 6 can be simplified further to give:

$$\boldsymbol{P_{stag} = 7.79859 \times 10^{13}(0.000001 \times Q_g)^2} \quad \textbf{7}$$

where Q_g is the jet volume in grams per second (Saunders, 2008). P_{stag} values were calculated based on five replicates and expressed for the Mark IV CSM used as:

$$\boldsymbol{P_{stag} = 1.3114x^2 + 52.209x - 34.603} \quad \textbf{8}$$

4.5 Salinity, Temperature, Depth and Suspended Sediment Concentration (SSC)

Measurements of the variations in hydrodynamics and suspended sediment were taken using YSI EXO2 Sondes containing conductivity, temperature, depth (CTD) and turbidity probes (Figure 4.7). The specification for each probe is outlined in Appendix 3. Probes were protected against biofouling using disposable copper tape and cleaned during deployment to avoid fouling and maintain accuracy by YSI EXO2 Central

Wipers. Sondes were calibrated (see below), controlled and data were downloaded using KOR-EXO software, with data saved in Microsoft Excel Spreadsheets.

4.5.1 YSI EXO2 Sondes

4.5.1.1 Sonde Sensors Overview

YSI EXO combination Conductivity and Temperature Sensors were installed (Figure 4.7). The temperature sensor utilises a thermistor and an algorithm is used to convert the measured resistance to temperature (°C). No calibration for temperature or maintenance of the sensor is required, although the accuracy was checked on a regular basis through comparisons with other probes and sensors.

Conductivity measurements, in microSiemens per centimetre, were used to calculate the salinity of the water, with results recorded in Practical Salinity Units (PSU). The conductivity of solutions of ionic species is heavily dependent on the temperature. Changes in the salinity were, therefore, determined through measurements of the conductance and temperature of the water utilising the methods stated in the Standard Methods for the Examination of Water and Wastewater (American Public Health Association and American Water Works Association, 1981). The probes were calibrated regularly for salinity measurements using YSI 3169 Conductivity Calibration Solution.

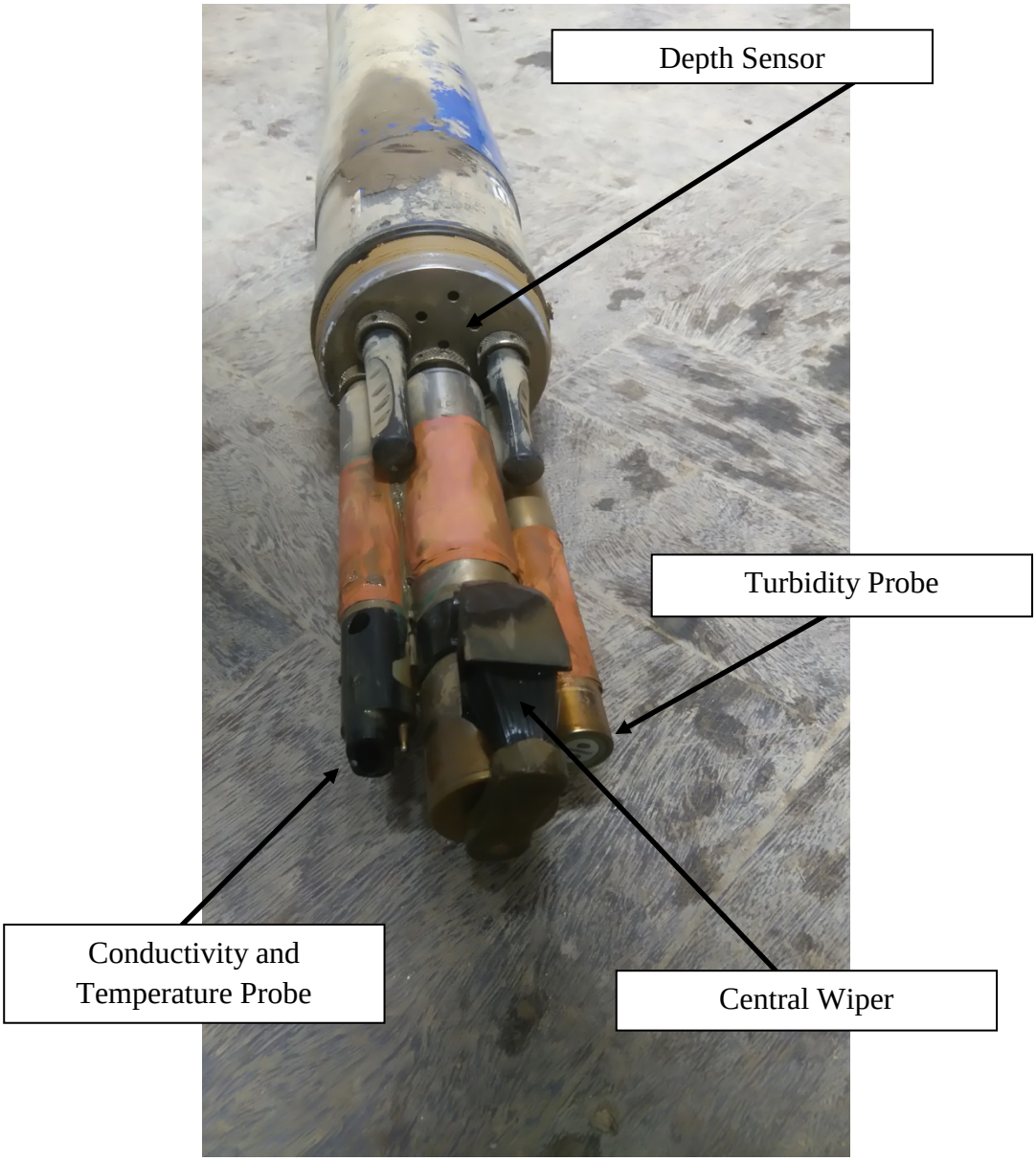

Figure 4.7: Sonde bulkhead with annotated central wiper and conductivity and temperature, depth and turbidity sensors (photograph: J. Dale).

To measure changes in water depth, the Sondes contained non-vented strain gauges fed by two small intake openings on the face of the bulkhead (Figure 4.7). Pressure changes were measured by a differential strain gauge transducer, with one side of the transducer exposed to the water and the other exposed to a vacuum. Depth measurements were calculated using the pressure exerted by the water minus the atmospheric pressure. Nonetheless, depth measurements can still be influenced by factors such as the local barometric pressure, water density and temperature, although the Sonde can be calibrated in respect to the local barometric pressure.

The Sondes were fitted with YSI EXO Turbidity Sensors (Figure 4.7). Turbidity is used as an indirect measurement of the fluxes in suspended sediment concentration (SSC), determined by measuring the scattering of a beam of light by the particles suspended in solution. The EXO Turbidity Sensor uses a near-infrared light source, and detects the scattering 90° of the light beam with values reported in Formazin Nephelometric Units (FNU). The turbidity probes were calibrated regularly using YSI 6073 Turbidity Standard, and turbidity readings were calibrated for the appropriate SSC by correlating the optical backscatter with measurements of the amount of particulate matter in suspension (see below).

4.5.1.2 Calibrating Suspended Sediment Concentration and Turbidity

Optical backscatter has been demonstrated to have a very close site specific relationship to the SSC concentration in freshwater environments (e.g. Vant and Daviescolley, 1984; Wass and Leeks, 1999), making it a suitable technique for continuously measuring the SSC in lakes and rivers. However, this relationship has been found to be much lower in more dynamic and turbulent environments (Weeks et al., 1993), as estimates of the SSC using optical backscatter are strongly influenced by the floc properties.

Therefore, EXO Turbidity Sensors were calibrated based on the relationship between the optical backscatter and total suspended solids using sediment re-suspended in seawater and freshwater. Sediment was sourced from Site 3 at Medmerry, resuspended in local seawater and gradually diluted using freshwater collected at Medmerry, comparing the backscatter turbidity value measured by the probe to the actual suspended sediment concentration. Comparisons were supported by *in situ* measurements through bottled suspended sediment samples collected in the field and the corresponding turbidity value.

The suspended sediment concentrations were measured using pre-washed, dried and weighed 0.7 µm glass microfiber filters following the United States Environmental Protection Agency Environmental Sciences Section Method 340.2. Water samples were gravimetrically pumped through the filter papers, dried for one hour in an oven at 105°C, cooled in a desiccator and weighed. The SSC concentrations were calculated as a function of:

$$\boldsymbol{SSC = (M_2 - M_1) \times \left(\frac{1000}{V}\right)} \quad \textbf{9}$$

where M_1 is the dry filter paper weight, M_2 is the dry filter paper and sediment residue and V is the volume of water filtered.

4.5.2 Near-Bed Monitoring

Long-term high-frequency near-bed *in situ* measurements were made by deploying the Sondes in a 2.5 m protective deployment tube with holes in to allow water to flow through, fixed to a scaffolding rig driven into the ground (Figure 4.8) approximately 2 cm from the bed. Data logging frequency was set at 10 minutes for each deployment. Over a one year period, from 1st November 2014 to 31st October 2015, measurements were taken from the entrance of the excavated channel at Site 3 (Section 3.3.4) at 0.46 mOD and the borrow pit at Site 5 (Section 3.3.6) at -0.31 mOD. These sites were selected to compare two sites of similar design and construction but contrasting in spatial position within the Medmerry site.

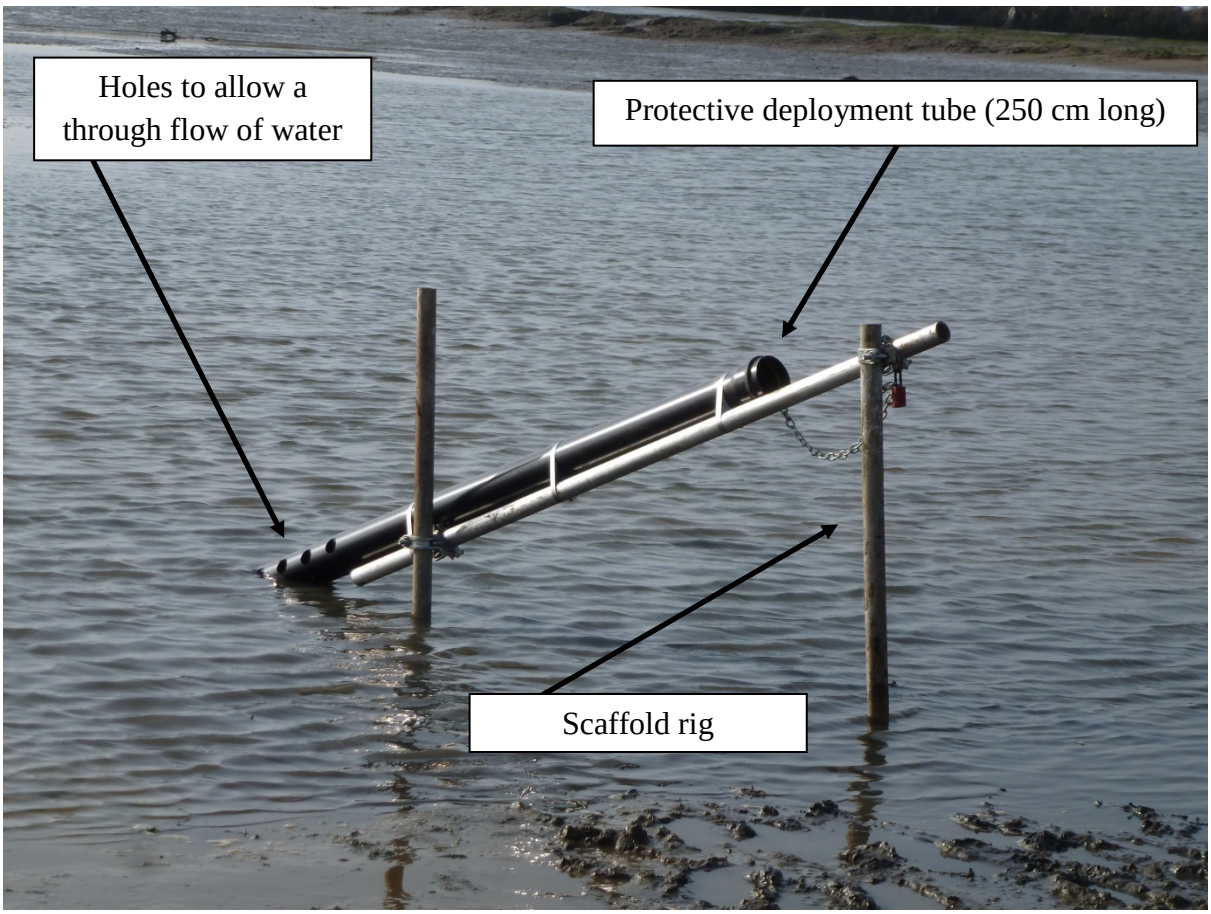

Figure 4.8: The EXO2 Sonde deployment tube and scaffolding rig in the borrow pit at Site 5 on 30th October 2014 (photograph: J. Dale).

The analysis of the data collected at Site 3 and Site 5 (Section 6.2), particularly the relationship between the SSC and the salinity values, showed the need for further consideration of the internal reworking and inputs of sediment. Measurements of the near-bed hydrodynamics were repeated at Site 3 for the period 1st November 2015 to 31st October 2016. Measurements were also taken in the breach (Figure 4.9), at 0.68 mOD, and near the culvert and tidal gates at Site 2b, at 0.41 mOD. These sites were selected along the main drainage channel, Easton Rife, to assess fluxes in sediment exported and imported, and the associated hydrodynamics, at the landward and seaward extremities of the site.

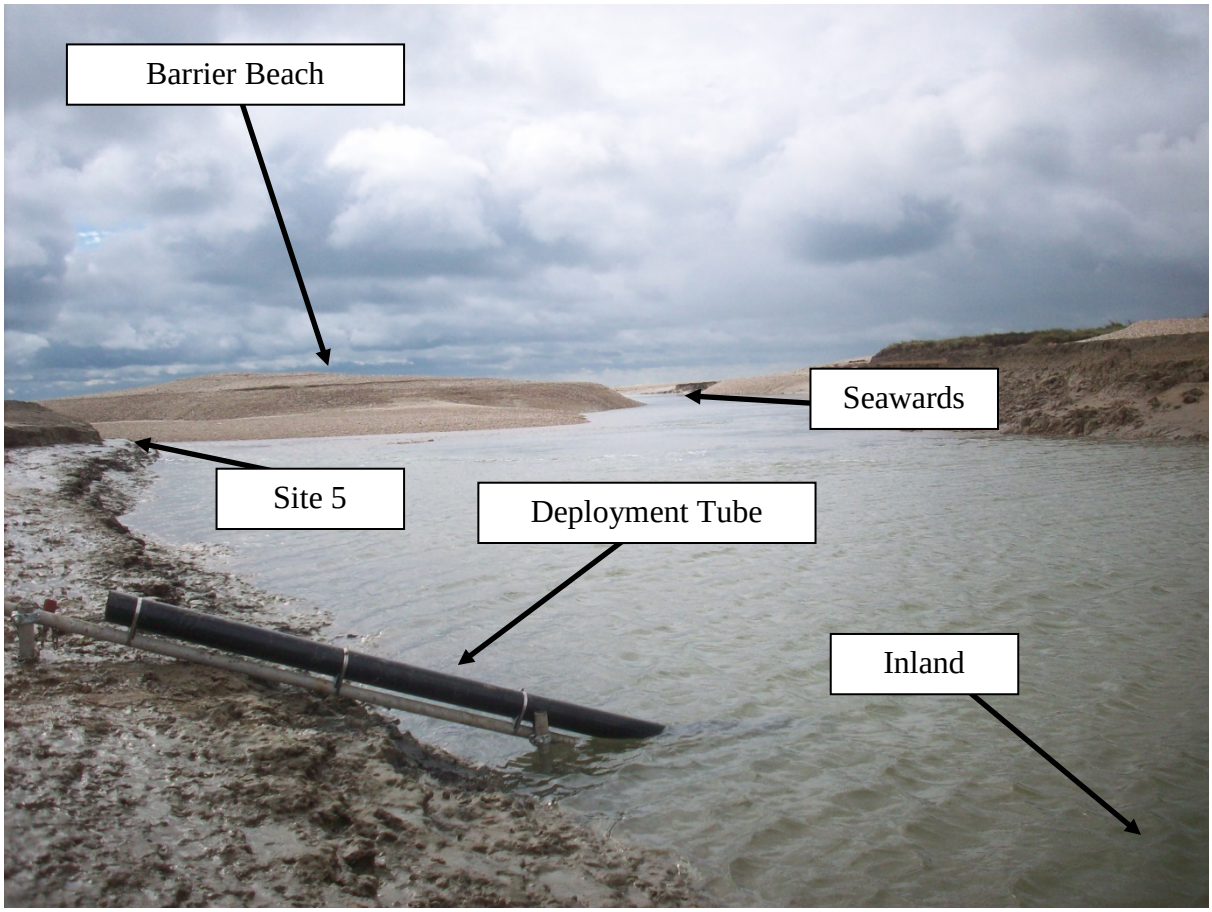

Figure 4.9: Deployment of EXO2 Sonde in the breach, looking seawards on 22nd September 2015 (photograph: J.Dale).

4.5.3 Water Column Profiling

To assess the temporal and spatial changes in SSC and salinity throughout the water column measurements were taken over the spring tide tidal cycle on 6th June 2016, and longitudinal profiling was carried out during high water ± 60 minutes on 7th June 2016.

4.5.3.1 Static Tidal Cycle Profiling

Measurements were made through the water column during the flood and ebb tide, from as soon as the water depths became adequate to sample until they became too shallow again. The Sondes were raised and lowered through the water column by a

line and pulley system suspended above the channels. At Site 2b, the Sonde was deployed from a scaffolding pole suspended over the channel (Figure 4.10), whereas at Site 3 the Sonde was attached to a pole with a tripod stand which extended over the channel (Figure 4.11). Due to the high current velocities at Site 3 an anchor and guide line were deployed prior to sampling to ensure vertical measurements of the water column.

4.5.3.2 Longitudinal Profiling

To supplement static profile measurements, longitudinal water column profile measurements were taken in transect along Easton Rife from a sit-on-top kayak (Figure 4.12). Measurements were made from surface to bed at discrete, regular, intervals. Measurements started at 60 minutes before high water at the breach, following the flooding tide along the rife to the drainage outlet at Site 2b. Measurements were repeated on the ebb tide in reverse, starting at Site 2b and finishing at the breach.

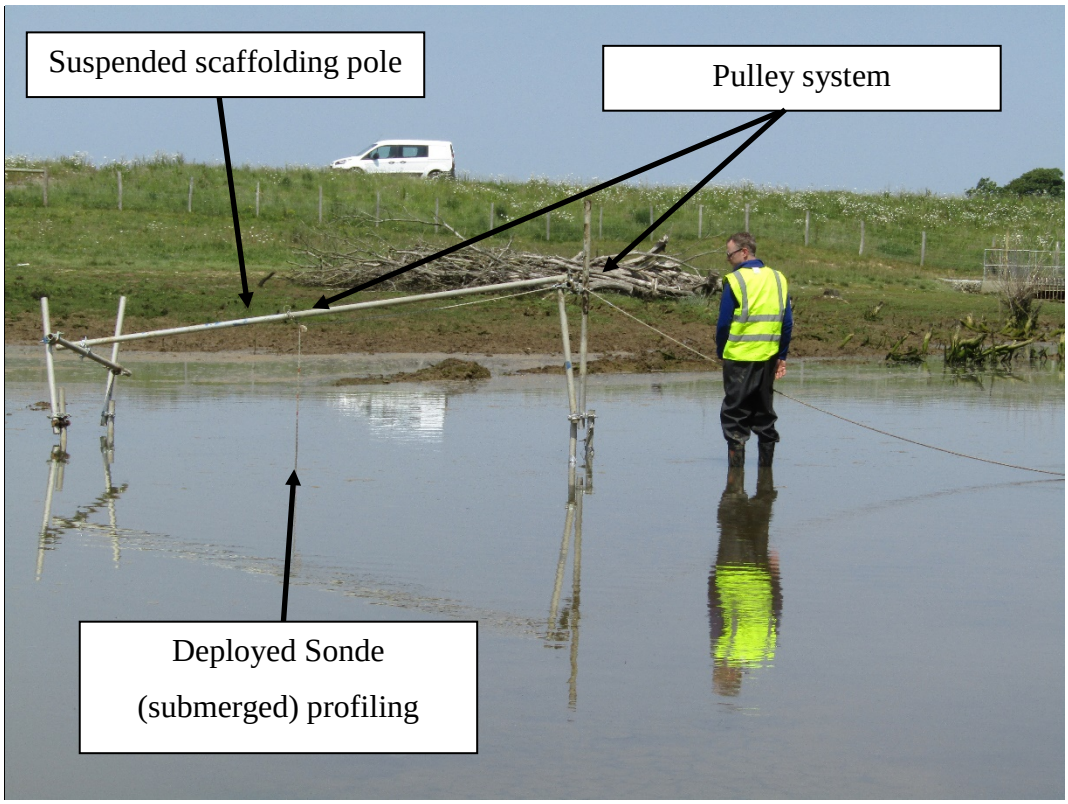

Figure 4.10: Profiling setup (looking northwards) at Site 2b on 6th June 2016 (photograph: H. Burgess).

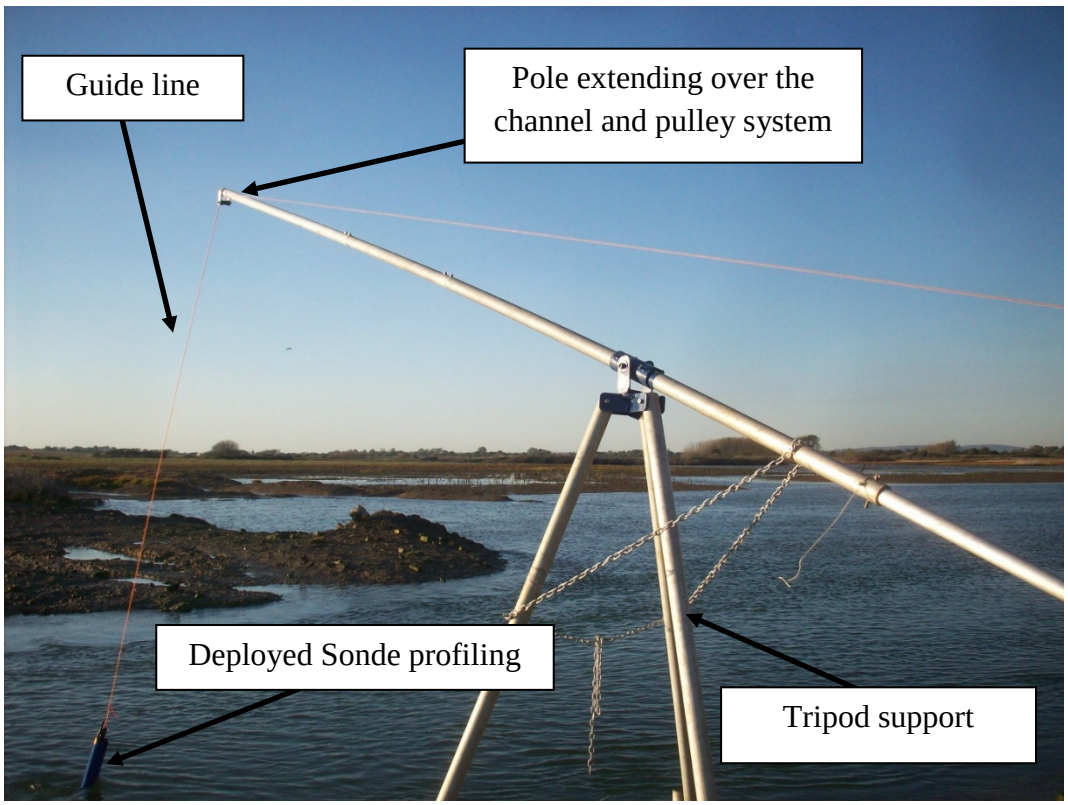

Figure 4.11: Profiling setup at Site 3 on 6th June (photograph: J. Dale).

Figure 4.12: Longitudinal profiling of the water column at the Medmerry Managed Realignment Site on 7th June 2016 (photograph: M. Grove).

4.6 Spatial and Geographic Information Systems Analysis

Measurements were taken of the morphogenesis and subsequent evolution of embryonic creek networks within the site. Embryonic creeks were considered to have formed after an elongated depression was detected in areas of sediment which previously appeared to have no or very subtle variations in surface topography, disregarding the main drainage network running through the site. Embryonic creek formation had already been observed at Site 3 (Section 3.3.4) and Site 5 (Section 3.3.6), prior to the monitoring period for this thesis.

4.6.1 Differential Global Positioning System (dGPS)

Differential Global Positioning System (dGPS) measurements were made of the evolution of the embryonic creek network at Site 5, which had experienced the greatest creek developed prior to this study, on four occasions during the study period: 8th August 2015, 22nd October 2015, 3rd March 2016 and 10th June 2016. Positional measurements were taken from within the borrow pit to the abrupt break in the longitudinal profile, known as the nickpoint, which usually characterises low-order creek networks (Symonds and Collins, 2007b). Positional data were supported by dGPS elevation data taken along three transects crossing the creek networks at the edge of the borrow pit (T1), inland (T2) and at the top of the embryonic system (T3), to evaluate changes in the width and depth of the creeks. dGPS measurements were selected as the technique allows high frequency recordings to be taken at a relatively small spatial resolution and has been proven to have a high accuracy, high spatial resolution and be relatively efficient and robust (Young, 2012), making it suitable for use in the intertidal zone.

The use of dGPS can, however, be limited due to the number of satellites required for the system to receive positional data. The more satellites available for the dGPS to receive data from the higher the accuracy, which is dependent on the position of the satellites relative to the earth and changes as the satellites move through their orbit. Despite this limitation, measurements taken using dGPS have been demonstrated to be

accurate to the centimetre level. The greater accuracy, in comparison to standard global positioning system (GPS) data, comes from the use of a reference base station, positioned at a known location which continually records its position according to the satellite network, and a roving receiver. A correction is applied to the data recorded by the roving receiver derived from the internal calculations made by the base station. The correction data can either be determined by a single or network of reference stations.

Although using a single reference station is typically the more straightforward method, setting up the base station can be time consuming. Furthermore, as the distance between the reference station and the rover increases, the accuracy of the positional data decreases. Therefore, a network of references stations, which consists of multiple, usually permanent, installations that continuously stream satellite observations, was used. Consequently, there was no need to transport, set up, secure and power a base station, with the accuracy maintained over a larger distance. The availability of reliable correction data was also higher; if one reference base station stopped working others were still available.

Measurement data were taken using a Leica AS19 GNSS antenna, a Leica Viva GS10 GPS receiver and a Leica CS15 controller. Raw GPS measurements taken by the rover were imported into Leica Geo Office (Version 8.3). Network Receiver Independent Exchange Format (RINEX) correction data were obtained from Leica Smart Net UK & Ireland (http://uk.smartnet-eu.com/rinex-download_148.htm), with the correction applied to the raw data by the Leica software. Corrected data were then exported as an American Standard Code for Information Interchange (ASCII) file. Leica Geo Office reported the positional quality (XYZ) for all dGPS points as < 0.02 m.

4.6.2 Unmanned Aerial Vehicle (UAV) Derived Digital Surface Model (DSM)

Measurements taken by dGPS are subjective (in terms of measurement location) and are spatially limited, and therefore may not be the most appropriate method of

measuring morphological development within intertidal environments. An alternative method is the use of unmanned aerial vehicles (UAVs), which are being increasingly used across a number of scientific disciplines to provide high resolution detailed imagery (e.g. James and Robson, 2014; Tonkin and Midgley, 2016). Images can be used for rapid reconstruction of surface geometry, providing there is sufficient overlap between images, without the need for camera position or orientation data through automated photogrammetric techniques (e.g. James and Robson, 2012; Javemick et al., 2014; Nolan et al., 2015; Westoby et al., 2012). The emerging, low-cost photogrammetric method Structure-from-Motion (SfM) with Multi-View Stereopsis provides a quick method for high resolution topographic reconstruction (Westoby et al., 2012). Therefore, following the four dGPS surveys of embryonic creek development, a high resolution orthomosaic and digital surface model (DSM) of Site 5 were produced after an aerial survey with a small UAV on 13th July 2016. Results were utilised to ascertain the suitability of UAV-SfM analysis and assess the appropriateness of resolution of dGPS measurements for monitoring embryonic creek development.

4.6.2.1 Data Acquisition and Analysis

Aerial imagery was acquired using a DJI Inspire 1 UAV. The UAV was flown at a target altitude of 20 m above ground level and at 5 m line spacing in consistent weather conditions (temperature, 18 °C; wind speed, 9 mph NW; sun with minor cloud cover). Following an initial test flight, aerial images were acquired during four separate flights over an hour-long period using a crosshatched flight plan to ensure maximum overlap (> 80 %) and a complete coverage of the study site. Images were captured using a DJI Zenmuse X3, 3-band RGB camera with a focal length of 20 mm.

Seven ground control points were recorded using dGPS. A total of 319 images were processed following quality assessment (> 0.70 sharpness) (Agisoft Photoscan; Version 1.2.6; Build 2834). Fisheye correction and camera alignment optimisation were applied to minimise the central ‘doming’ effect, reported in previous studies (e.g. James and Robson, 2014) and potentially amplified due to the low flight height. A

dense point cloud, derived from 319 images and comprising of 4,904,206 matched points, was produced from optimised camera locations using mild-depth filtering to ensure the preservation of small and important detail. The effective overlap of photographs was > 9 images per point within the study area. The dense point cloud output was used to generate both the orthomosaic image and the DSM. The DSM had a reported resolution of 0.0263 m per pixel, and the resolution of the RGB orthorectified image was 0.00658 m per pixel (Agisoft, 2016). All data were projected using the OSGB1936 coordinate system and datum and all analysis was conducted using ArcGIS 10.2.2.

4.6.2.2 Model Validation

The software reported a total Root-mean-square-error (RMSE) value of 0.027 m for the final orthophoto (Agisoft, 2016). Independent assessment of the UAV modelling was completed using an additional six control points, recorded using dGPS, to assess the vertical and horizontal error of the DSM (Table 4.4), indicating that the difference in position (XY) ranged between 0.017 and -0.058 m (DSM - dGPS measurements). RMSE and mean-absolute error (MAE) were calculated, with RMSE values of 0.028 m and 0.033 m, and MAE values of 0.023 m and 0.024 m, for the x and y values respectively. Vertical differences between the independent control points and the DSM varied between 0.022 m and -0.038 m. The RMSE value was 0.024 m and the MAE was 0.023 m, within the range of acceptable values for reasonable surface reconstruction reported by Tonkin and Midgley (2016).

An additional 54 positional measurements of the embryonic creek systems, along with 53 elevation measurements from three cross-profile transects, were collected using dGPS (as captured previously, see Section 4.6.1) on 27th July 2016. These measurements were analysed to assess the effectiveness of the model, and assess the appropriateness of the resolution of dGPS measurements, as a tool for evaluating the development of embryonic creek networks.

Table 4.4: Digital surface model (DSM) quality in comparison to x, y and z differential global positioning system (dGPS) measurements of six independent control points.

	Independent Control Points		
	X	**Y**	**Z**
Mean Difference (m)	-0.016	-0.021	-0.012
Maximum Difference (m)	0.017	0.006	0.022
Minimum Difference (m)	-0.057	-0.058	-0.038
RMSE (m)	0.028	0.033	0.024
MAE (m)	0.023	0.024	0.023

4.7 Sediment Core Sampling

The differences in the sediment structure and composition, in relation to the former land use, were analysed through measurements of the sediment sub-surface physical properties and geochemistry. Analysis was initially performed on a broad centimetre scale. Following this analysis additional analysis was carried out on an intensive sub-millimetre scale. All sampling was performed at low water.

4.7.1 Broad (centimetre to decimetre) Scale Subsurface Sampling

Vertical sediment cores were taken in January and February 2015, 16 to 17 months after the site was breached, from Sites 1, 2a, 2b, 3 and 5. At Site 3 samples were taken from the opposite side of the excavated channel, from a vegetated and non-vegetated surface (Figure 4.13). Two cores were taken in parallel, at approximately the same elevation and within 30 cm of each other, at each sampling location using a hand driven large gouge core, transferred to open PVC tubes and wrapped in PVC film. Sediment cores were collected at least 15 m from the channel (after Spencer et al., 2017), to minimise the influence of lateral flow (Marani et al., 2006), apart from at Site 2a where cores were taken on the scoured beach within the channel.

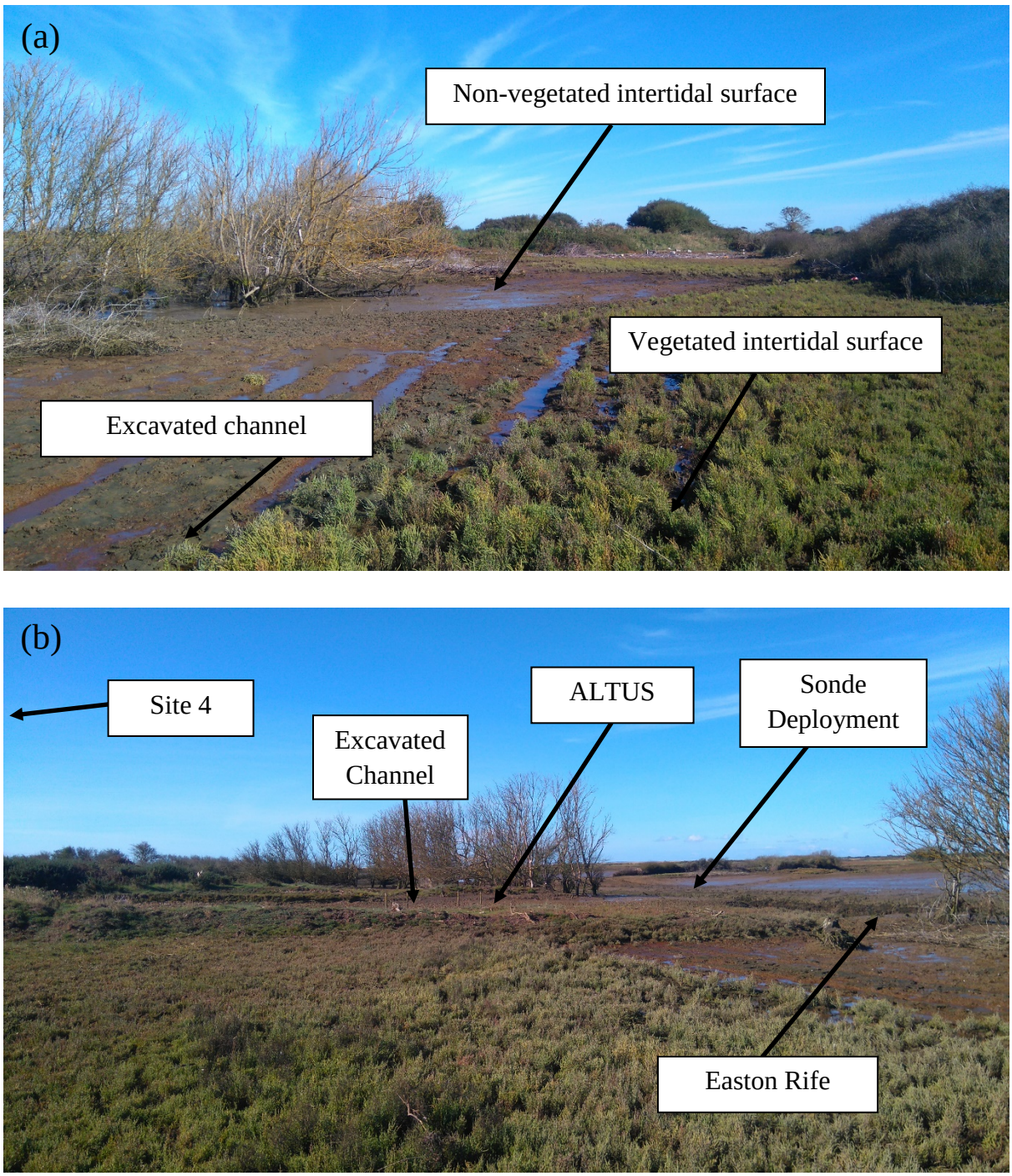

Figure 4.13: Location of sediment core sampling at Site 3 from (a) a vegetated and non-vegetated surface, and (b) in comparison to the rest of the site. Photographs were taken from the same location following a 180° rotation (photograph: J.Dale).

Samples were stored in the University of Brighton walk-in cold store at + 3.6 °C until analysis. Upon examination, initial observations in sediment properties were logged and one core from each site was subsampled at 1 cm increments and stored in sealed, labelled polythene sample bags for particle grain size analysis using the method

outlined in Section 4.3.3. For the remaining cores, a known quantity of sediment was extracted using a syringe at 1 cm intervals and analysed for wet bulk density, moisture concentration, porosity and organic concentration (refer to Sections 4.3.1 and 4.3.2 for method). Repeat samples were analysed every 20 samples to test for analytical error and were within ±10 % throughout. Following examination of the differences in physical sediment properties, the samples from Site 2b, both from Site 3, and Site 5 were also examined for a suite of elements using an Inductively Coupled Plasma-Optical Emission Spectrometer (ICP-OES, see below). Sampling was repeated in September 2016 at these sites to compare the sub-surface evolution across the different sites. To discriminate between different sub-surface sediment units, principal component analysis (PCA) was used. PCA is a data reduction technique which calculates new variables, or principle components, from linear combinations of the original parameters and has been used successfully elsewhere to (partially) discriminate geochemical data (e.g. Cundy et al., 2006). The first principal component accounts for the greatest variability, with every subsequent component accounting for less of the variability (Reid and Spencer, 2009).

4.7.1.1 Inductively Coupled Plasma-Optical Emission Spectrometer (ICP-OES)

Sediment samples were digested with Aqua Regia (modified from Berrow and Stein, 1983). Aqua Regia was prepared with 3 HCl : 1 HNO_3 (molar ratio) mixture at room temperature. 0.1 ± 0.01 g of sample, oven dried at 105 °C, were digested in 3 ml of Aqua Regia for three hours in a water bath at 80 °C. Following digestion, 7 ml of distilled water were then added to the sample. A 1:10 dilution of the solution was made with distilled water for analysis using a Perkin Elmer Optima 2100 DV ICP-OES for Al, Ca, Fe, Mn, S and Na.

Grain size and mineralogical variations have been recognised to influence the distribution of some elements within intertidal sediments (e.g. Spencer et al., 2008). To account for these variations the distribution of Al, which has previously been identified as reliable grain size proxy within the Solent (Cundy and Croudace, 1995), was measured. Ca has been used in previous studies to identify changes in pH,

resulting in dissolution in the upper layers and re-precipitation at depth (e.g. Luther and Church, 1988; Spencer et al., 2003; Vranken et al., 1990), and also the presence of carbonate (shell) material (Cundy et al., 2006). Fe and Mn are involved in bacterially-driven aquatic redox processes, with a strong peak indicating redox mobilisation and diagenetic enhancement in oxic sediment (e.g. Spencer et al., 2003; Zwolsman et al., 1993). An increase in S can indicate bacterial reduction of sulphate (Cundy and Croudace, 1995). Whilst redox potential can be measured *in situ* using probes, such as a pH/ORP meters (Spencer et al., 2008), these techniques are semi-quantitative and subject to temporal variability, whilst the use of redox sensitive elements (Fe, Mn, S) have been used successfully in previous studies (e.g. Cundy and Croudace, 1995). The distribution of Na has been analysed as it is indicative of tidal input (Spencer et al., 2017; Spencer et al., 2008).

The ICP-OES was calibrated using Perkin Elmer Quality Control Standard 21 (Ca, Fe, Mn), UV Wave Calibration Solution (S), Aluminium (Al) and Sodium (Na) calibration standards at varying concentrations (see Appendix 4 for calibration coefficients). To assess the elemental recovery of the digestion procedure (e.g. Cochran et al., 1998) the measured values were compared to the quoted values for a Certified Reference Material (CRM) digested and analysed alongside the samples. The Mess-4 Marine Sediment (National Research Council Canada) CRM was used and recovery values were generally within ± 25 % of the reported values (Table 4.5, see Appendix 5 for full values). Process blanks and repeat samples were analysed every 20 samples for quality control, and were below the detection level and within ±10 % respectfully throughout.

4.7.2 Intensive (sub-millimetre) Scale Subsurface Sampling

Smaller sediment cores were recovered from Site 2b and 5 in July 2015, taken at the same location as the samples for broad-scale analysis. Cores were taken using the advanced trimming method (Hvorslev, 1949). Clear plastic PVC tubes 44 mm in diameter were inserted into the sediment, trimming the surrounding sediment to minimise disturbance. Core lengths varied between 7.9 cm and 11.1 cm. The ends of

the sample tubes were capped and wrapped in PVC film, secured with tape, to prevent moisture loss. During transport and storage cores were kept upright to minimise any disturbance and, on return to the laboratory, were stored between + 3.6 °C and + 4 °C. Sampling was repeated in September 2016 for a comparison of the sub-surface evolution and changes in the sediment structure.

Table 4.5: Average percentage recovery values (mean ± standard deviation) of the six elements analysed, compared to the quoted value, for the Mess-4 Marine Sediment Certified Reference Material digested alongside samples.

Element	Average Recovery Value (Percent)
Al	75.89 ± 1.79
Na	77.08 ± 7.99
S	107.71 ± 10.46
Fe	76.36 ± 8.14
Mn	122.71 ± 11.34
Ca	92.16 ± 9.68

4.7.2.1 X-Ray Microtomography (µCT) Analysis

To enhance analysis of the difference in sediment structure, cores were examined to the micro-scale using x-ray computed microtomography (µCT). Using the x-ray attenuation due to the material density and atomic number, with higher attenuation representing high-density and / or high atomic number material, the x-ray µCT technique produces a three dimensional non-destructive model of the sample (Cnudde and Boone, 2013; Ketcham and Carlson, 2001). Sealed core tubes were scanned at 76 µm resolution using a Mikon Metrology XT H 225 X-ray CT system with Perken Elmer XRD 0820 CN3 16-bit flat panel detector (Nikon Metrology, Tring, Hertfordshire, United Kingdom) at Queen Mary, University of London. Inspect-X was used to perform the scans and X-radiogram acquisition (settings outlined in Table 4.6) and reconstruction was undertaken in CTPro. Dishtri 2.1 volume rendering software was used for visualisation of the reconstructed 3D models as the software has been demonstrated to allow successful segmentation of heterogeneous samples (Bendle et al., 2015). The bulk phase of each sample was visually identified and segmented following the method of Spencer et al. (2017).

Table 4.6: Settings used for x-ray microtomography scans.

Parameter	Setting
Voltage	165 kV
Ampage	240 µA
Exposure	1415 ms
Gain	12 dB
Filter	Cu
Filter Thickness	1.0 mm

4.7.2.2 Non-destructive micro-X-ray fluorescence spectrometry

Cores were photographed and analysed using ITRAX non-destructive micro-X-ray fluorescence spectrometry analysis (Croudace et al., 2006) for a range of elemental data to compare changes in geochemistry to sediment structure analysis provided by the µCT. Each core was split and loaded onto a horizontal cradle and scanned at a resolution of 200 microns. Core Scanner Navigator software was used to control the scanner and data were plotted and displayed using Q-Spec software. The ITRAX scanner combines an X-ray line camera with a narrow, parallel, high-flux X-ray beam to record the radiograph at 55 kV. XRF analysis were performed at 30 kV, analysing for Si, Zr, Cr, K and Cl in addition to Ca, Mn, Fe and S previously analysed in the broad-scale analysis. The distribution of Si, Zr and Cr were investigated as they are representative of variations in the coarser grained sediment and heavy mineral fraction (Cundy et al., 2005). Variations in K were considered to be a proxy for the distribution of clay through the samples. Cl was measured, as an alternative to Na, to investigate the extent of tidally induced saline intrusion. Data were plotted using ItraX-Plot (National Oceanography Centre, Southampton) described by Croudace et al. (2006).

5 Changes in Bed Elevation, Sediment Properties and Cohesive Strength

5.1 Introduction

This chapter provides the principal monitoring data on the sedimentary processes at the Medmerry Managed Realignment Site through measurements of the change in the bed elevation, physicochemical properties and the critical erosion shear stress. These data are then used to support analysis of the evolution of the sediment regime examined in Chapters 6 to 8. The sites investigated in this chapter are illustrated in Figure 5.1. The relationships between these properties were also assessed at each site using Pearson correlation coefficients (r) after assessing the normality of the distribution via quantile-quantile plots. Statistical significance (P) was assessed to the 90 % ($P < 0.1$) and 95 % ($P < 0.05$) confidence intervals.

5.2 Temporal Variations in Bed Elevation and Surface Physicochemical Sediment Properties

Measurements of the changes in bed elevation were made using ALTUS autonomous bed elevation monitors (see Section 4.2.1 for description) in the channel at Site 3 from November 2014 to October 2016 and in the borrow pit at Site 5 from November 2014 to October 2015 (analysed in Chapter 6). Sediment pins (see Section 4.2.2 for description) were used to measure bed elevation changes (reported in this chapter) at Sites 1, 2a, 2b and on the banks at Sites 3 and 5 from February 2015. Sediment pins were also used in the borrow pit at Site 5 from February 2016 due to damage, and subsequently failure, of the ALTUS system. Surface sediment physicochemical properties (see Section 4.3 for methods) were measured from February 2015 until October 2016 and average values are presented in Table 5.1.

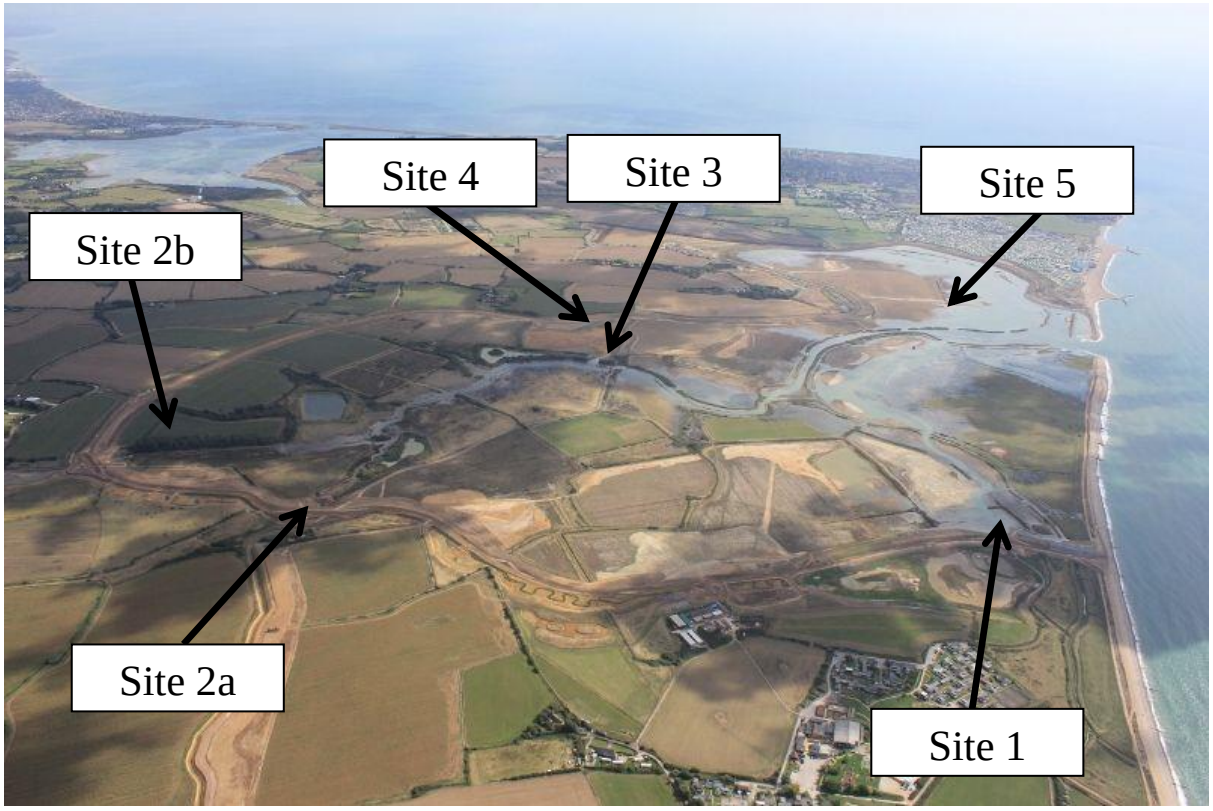

Figure 5.1: Sites analysed and discussed in Chapter 5 (looking south-eastwards, photograph: John Akerman).

5.2.1 Site 1

During the study period the area of pluvial and marine water pooling on the bank at Site 1 (the re-profiled former storage area for extracted material) decreased, although tidal waters continued to drain as sheet flow into the channel (Figure 5.2). Bed elevation, based on pin data (Figure 5.3a), increased overall by 12 mm but demonstrated evidence of seasonal variability; following an initial increase from February to March bed elevation decreased during the spring and summer until August 2015. Bed elevation then continued to increase during the winter, although the rate of increase slowed during the spring, and decreased slightly during the summer. These changes in bed elevation possibly related to an increased availability of suspended sediment, either from an external source or internal redistribution around the site, during the winter when increased erosion would typically be expected due to more energetic wave conditions and increased storm frequency.

Table 5.1: Average (mean ± standard deviation) surface sediment parameters measured at each site at the Medmerry Managed Realignment Site. Density, wet bulk density (kg m^{-3}); Moisture, moisture concentration (%); Porosity; Organic, loss on ignition (%); Cl^-, chloride concentration (PPM); d_{50}, median grain size (μm); Mud, mud (clay + silt) concentration (%).

	Site 1	Site 2a	Site 2b	Site 3 Bank	Site 3 Channel	Site 4	Site 5 Bank	Site 5 Borrow Pit
Density	1.15 ± 0.10	1.01 ± 0.11	1.04 ± 0.15	1.11 ± 0.08	1.07 ± 0.11		1.18 ± 0.11	1.02 ± 0.90
Moisture	64 ± 24	141 ± 28	73 ± 20	89 ± 16	110 ± 22	28 ± 23	43 ± 4	38 ± 4
Porosity	0.73 ± 0.06	0.84 ± 0.03	0.78 ± 0.05	0.78 ± 0.02	0.80 ± 0.03		0.69 ± 0.03	0.66 ± 0.03
Organic	2.63 ± 0.87	5.74 ± 0.59	7.34 ± 0.48	4.37 ± 0.57	3.71 ± 0.77	2.23 ± 0.93	4.36 ± 0.80	2.23 ± 0.63
Cl^-	21077 ± 9388	12749 ± 6245	16747 ± 6904	20816 ± 4821	21282 ± 9061		20168 ± 4365	19606 ± 4629
d_{50}	46.26 ± 47.99	8.37 ± 1.06	7.72 ± 0.20	20.40 ± 10.48	20.42 ± 9.66	57.51 ± 57.02	47.95 ± 35.34	112.93 ± 47.33
Mud	9.05 ± 4.05	15.49 ± 2.66	17.12 ± 2.94	11.55 ± 2.66	11.08 ± 2.86	7.21 ± 3.07	9.52 ± 4.51	5.28 ± 3.51

Wet bulk density (Figure 5.3b), moisture concentration (Figure 5.3c) and porosity (Figure 5.3d) were all highly correlated (Table 5.2), although the correlation coefficient between wet bulk density and moisture concentration was slightly lower compared to the other variables, and all fluctuated during the first six months. Despite this variability, wet bulk density demonstrated evidence of seasonality, increasing during the spring then decreasing during the summer and autumn. The inverse was found in the moisture concentration and the porosity at Site 1, following initial variability. Unusually, values decreased during the autumn and winter before increasing during the summer, whereas high moisture concentrations would be expected during the winter as a result of increased precipitation and lower rates of evaporation.

Loss on ignition values (Figure 5.3e) were variable throughout but followed a general pattern of decreasing to a minimum of 1.26 % in July 2015 and then increasing, and correlated with the sediment moisture concentration and porosity (Table 5.2; $r = 0.71$ and 0.59 respectively, $P < 0.05$). Porewater chloride concentrations (Figure 5.3f) increased during the first four months of the study before decreasing to a minimum of 8,945 PPM (0.9 %) in December 2015, and tended to be higher than other sites within Medmerry (Table 5.1), indicative of a reduced freshwater influence. Chloride concentrations subsequently increased during the remaining ten months of the study, correlating with the porosity of the sediment (Table 5.2; $r = -0.56$, $P < 0.05$).

Median grain size (Figure 5.3g) and the grain size distribution (Figure 5.3h) showed an increase in the percentage of coarse grained (sandy) sediments until January 2016. The percentage of coarse sediments subsequently decreased during the rest of the study period. This variability appeared to be driven by changes in the distribution of silt and sand as clay concentrations remained relatively constant throughout. Both median grain size and the mud (clay + silt) concentration correlated with the percentage lost on ignition (Table 5.2; $r = -0.53$ and 0.56 respectfully, $P < 0.05$).

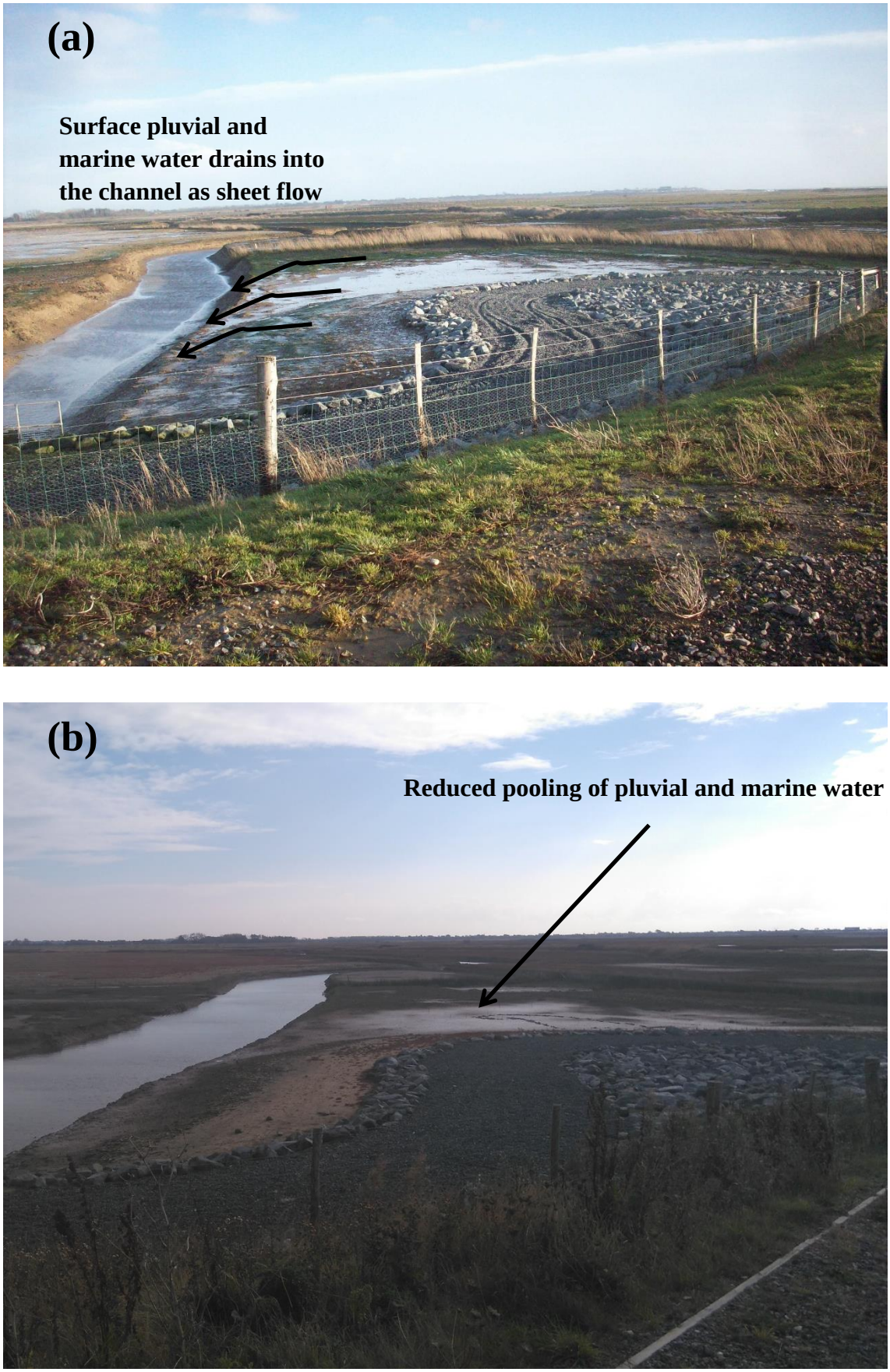

Figure 5.2: Site 1 (looking eastwards) at the Medmerry Managed Realignment Site in (a) January 2015 and (b) October 2016 (photograph: J. Dale).

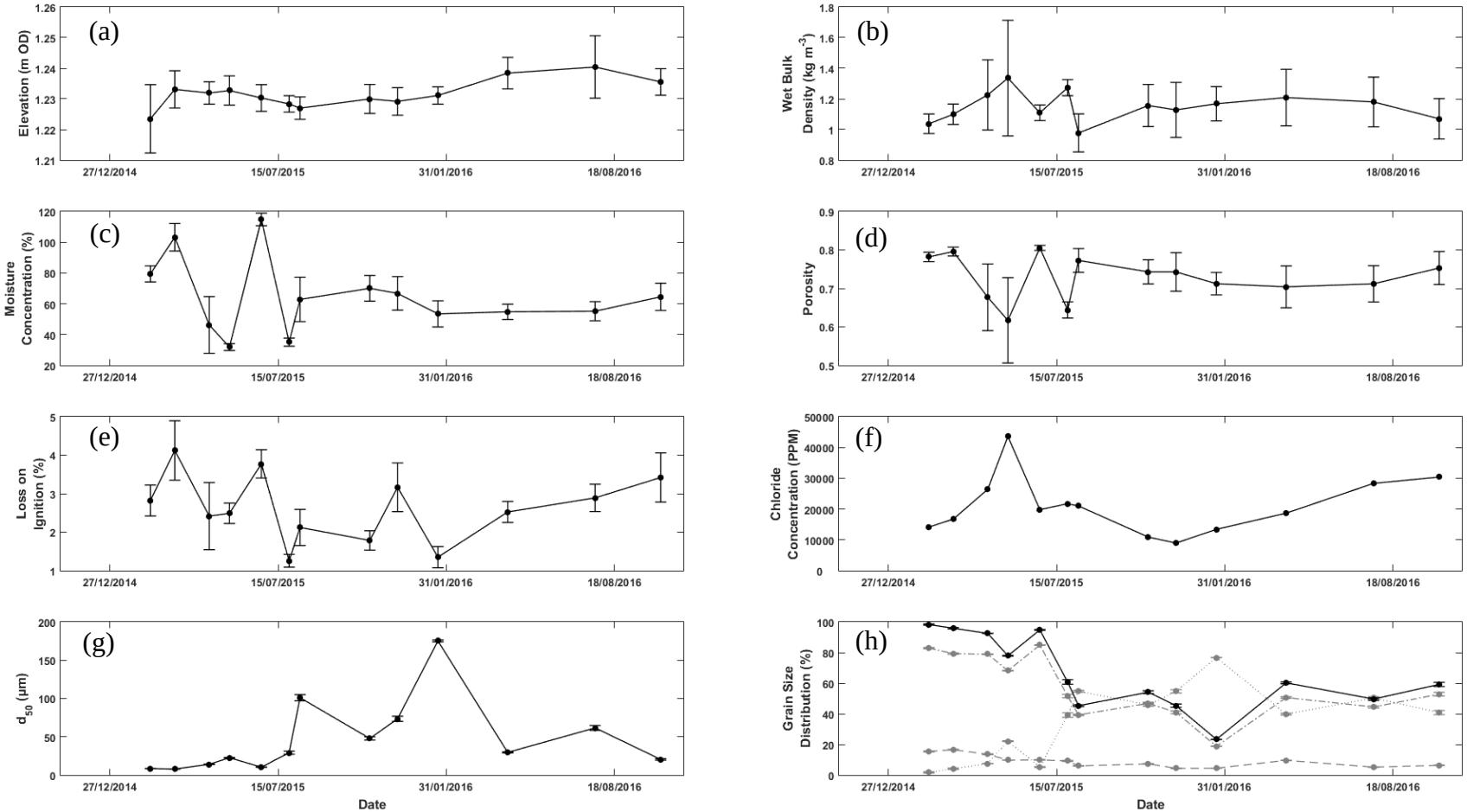

Figure 5.3: Variations (mean ± standard deviation) in surface (a) bed elevation (n = 12), (b) wet bulk density (n = 5), (c) moisture concentration (n = 5), (d) porosity (n = 5), (e) loss on ignition (n = 5), (f) chloride concentration, (g) median grain size (d_{50}) (n = 3) and (h) grain size distribution (clay, grey dashed line; silt, grey dashed-dotted line; sand, grey dotted line; mud, solid black line; n = 3) at Site 1 at the Medmerry Managed Realignment Site.

Table 5.2: Pearson correlation coefficients between physical and geochemical surface sediment properties at Site 1 at the Medmerry Managed Realignment Site. Density, wet bulk density; Moisture, moisture concentration; Porosity; Organic, loss on ignition; Cl^-, chloride concentration; d_{50}, median grain size; Mud, mud concentration (clay + silt). Numbers in bold: statistically significant at ** = $P < 0.05$.

	Density	**Moisture**	**Porosity**	**Organic**	**Cl^-**	**d_{50}**
Moisture	**-0.63****					
Porosity	**-0.89****	**0.91****				
Organic	-0.36	**0.71****	**0.59****			
Cl^-	0.47	-0.46	**-0.56****	0.07		
d_{50}	-0.13	-0.25	-0.04	**-0.53****	-0.31	
Mud	0.01	0.43	0.20	**0.56****	0.20	**-0.85****

5.2.2 Site 2a

The cut and re-profiled channel in which Site 2a is situated widened and the channel banks shallowed during the study period (Figure 5.4), flushing material into the channel and resulting in bed elevation increasing by 42 mm (Figure 5.5a). Wet bulk density measurements (Figure 5.5b) showed some evidence of seasonality, increasing during the spring, peaking in April 2015 and July 2016, and decreasing during the autumn. Wet bulk density correlated with the porosity (r = -0.67, $P < 0.05$), loss on ignition (r = 0.59, $P < 0.05$) and chloride concentration (r = 0.57, $P < 0.05$) at Site 2a (Table 5.3).

The sediment remained waterlogged with high moisture concentration in comparison to other sites (Table 5.1), which decreased during the study period and also demonstrated a degree of seasonality; moisture concentration values peaked in April 2015 and again in December 2015 (Figure 5.5c). Moisture concentration closely followed (r = 0.73, $P < 0.05$) the porosity (Figure 5.5d), whereas a negative relationship (r = -0.66, $P < 0.05$) was found between the porosity and the chloride concentration (Table 5.3). Loss on ignition values (Figure 5.5e) appeared to change seasonally, increasing during the spring then decreasing during the summer and autumn, correlating weakly with the median grain size (Table 5.3; r = -0.52, $P < 0.1$).

A high concentration of fine grained sediment was indicated throughout by the median grain size (Figure 5.5g) and the grain size distribution (Figure 5.5h).

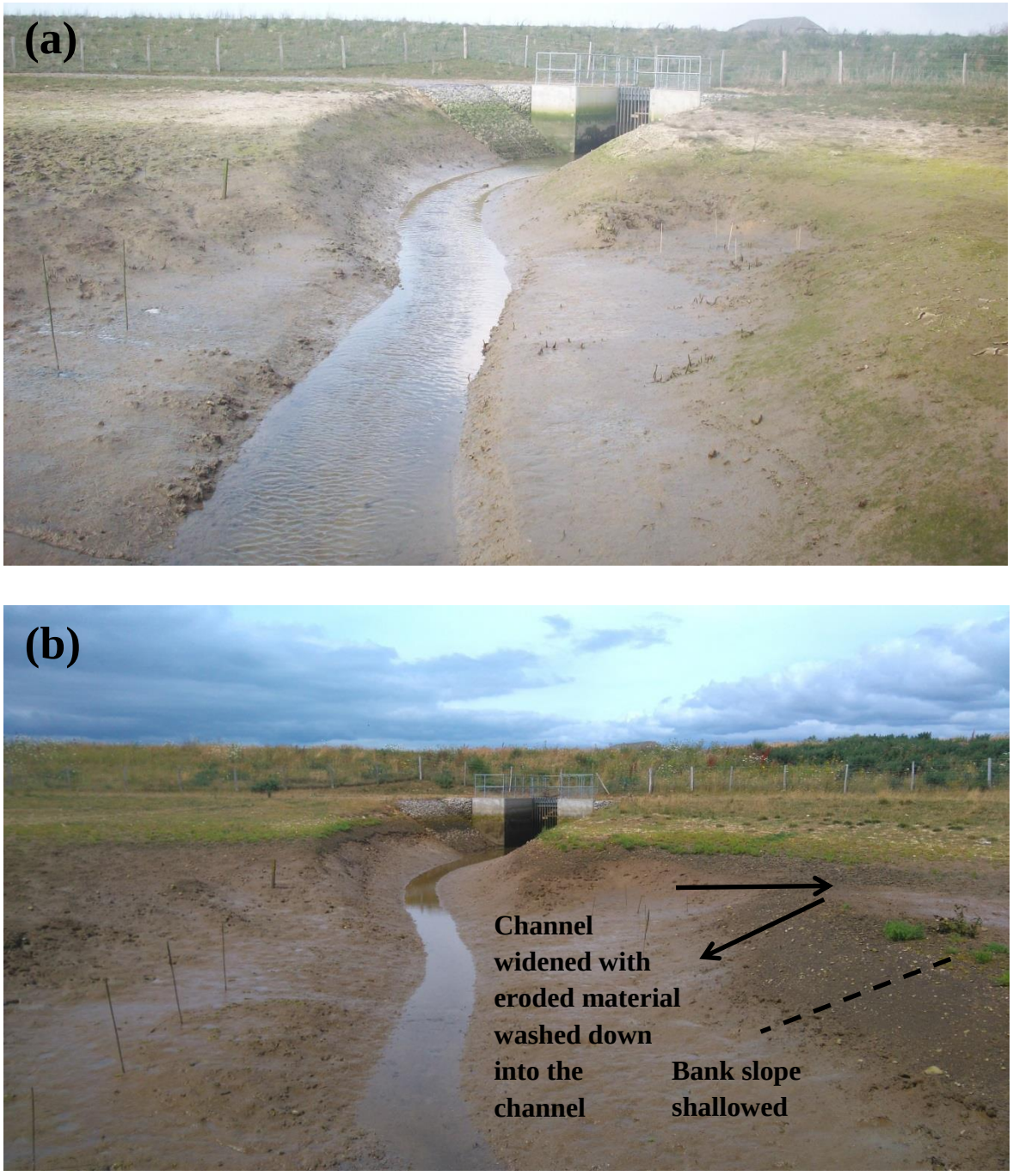

Figure 5.4: Changes within the channel at Site 2a (looking westwards) between (a) February 2015 and (b) July 2016 (photograph: J.Dale).

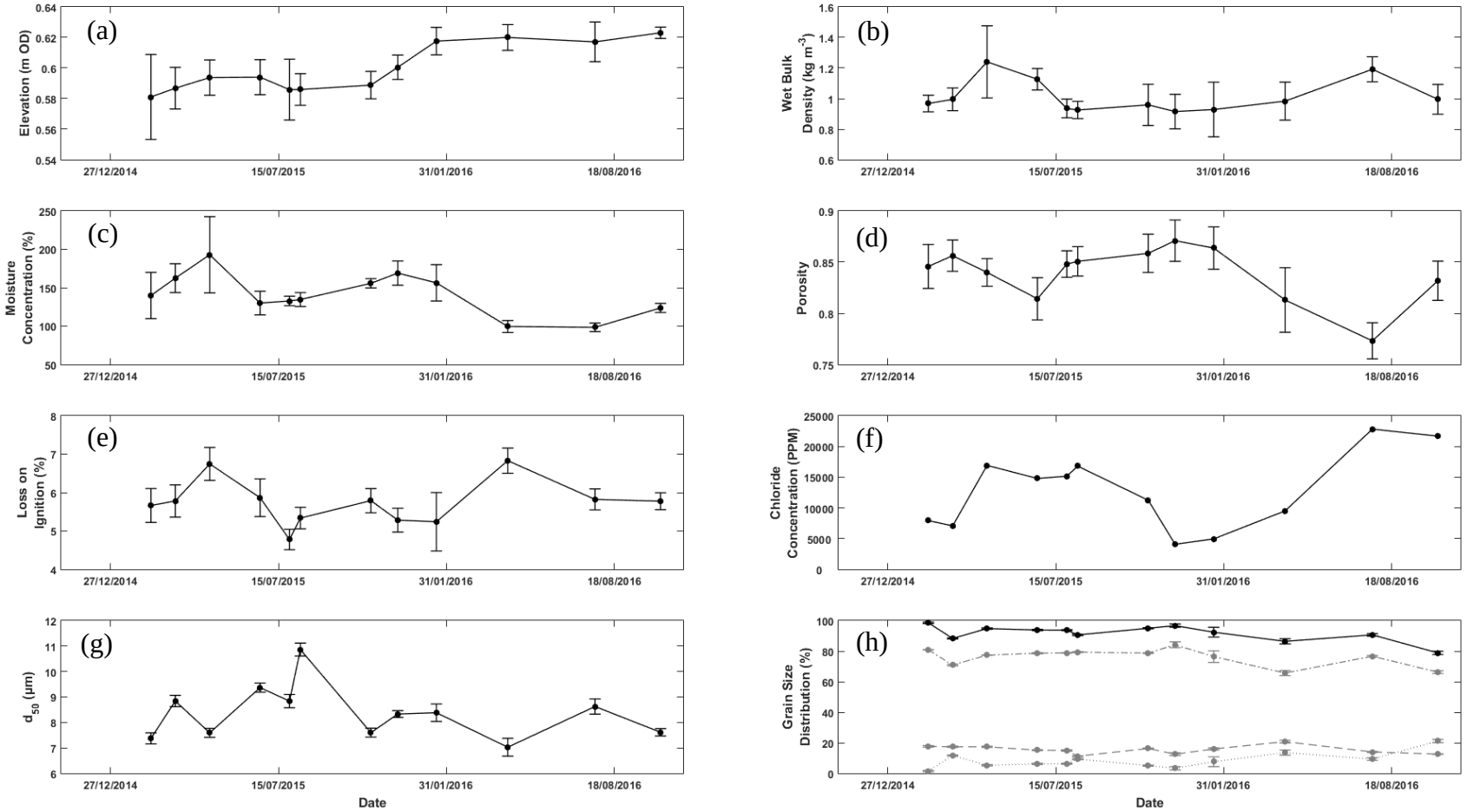

Figure 5.5: Variations (mean ± standard deviation) in surface (a) bed elevation (n = 12), (b) wet bulk density (n = 5), (c) moisture concentration (n = 5), (d) porosity (n = 5), (e) loss on ignition (n = 5), (f) chloride concentration, (g) median grain size (d_{50}) (n = 3) and (h) grain size distribution (clay, grey dashed line; silt, grey dashed-dotted line; sand, grey dotted line; mud, solid black line; n = 3) at Site 2a at the Medmerry Managed Realignment Site.

Table 5.3: Pearson correlation coefficients between physical and geochemical surface sediment properties at Site 2a at the Medmerry Managed Realignment Site. Density, wet bulk density; Moisture, moisture concentration; Porosity; Organic, loss on ignition; Cl^-, chloride concentration; d_{50}, median grain size; Mud, mud concentration (clay + silt). Numbers in bold: statistically significant at * = $P < 0.1$, ** = $P < 0.05$.

	Density	**Moisture**	**Porosity**	**Organic**	**Cl^-**	**d_{50}**
Moisture	0.01					
Porosity	**-0.67****	**0.73****				
Organic	**0.59****	-0.04	-0.43			
Cl^-	**0.57****	-0.42	**-0.66****	0.15		
d_{50}	-0.11	-0.04	0.05	**-0.52***	0.19	
Mud	0.02	0.45	0.30	-0.22	-0.43	0.06

5.2.3 Site 2b

At Site 2b, the tyre tracks remaining from the heavy plant machinery used during site construction infilled with sediment (Figure 5.6), and a slight net decrease in bed elevation of 6.5 mm was measured (Figure 5.7a). Initially, large areas of the intertidal zone were covered in an algal mat which, where possible, was avoided during sampling. The algal mat died off during the summer of 2015 and was replaced by extensive areas of *Salicornia*. Despite an initial increase, bed elevation decreased during the summer, matching the apparent seasonal variations observed at Site 1 (Figure 5.3a). The rate of bed elevation decrease slowed during the autumn, with the bed elevation increasing slightly during the winter. Bed elevation decreased again during the following spring and summer. As with Site 1, these variations could be attributed to changes in sediment supply and the relationship between erosion and accretion. However, this pattern is also reflected in the sediment moisture concentration at Site 2b (Figure 5.7c). It is, therefore, possible that changes in bed elevation are not caused by the erosion or accretion of sediment but by the sediment drying and consolidating during the warmer summer months, when rates of evaporation would be expected to be greater, and by absorption of water and swelling during the winter.

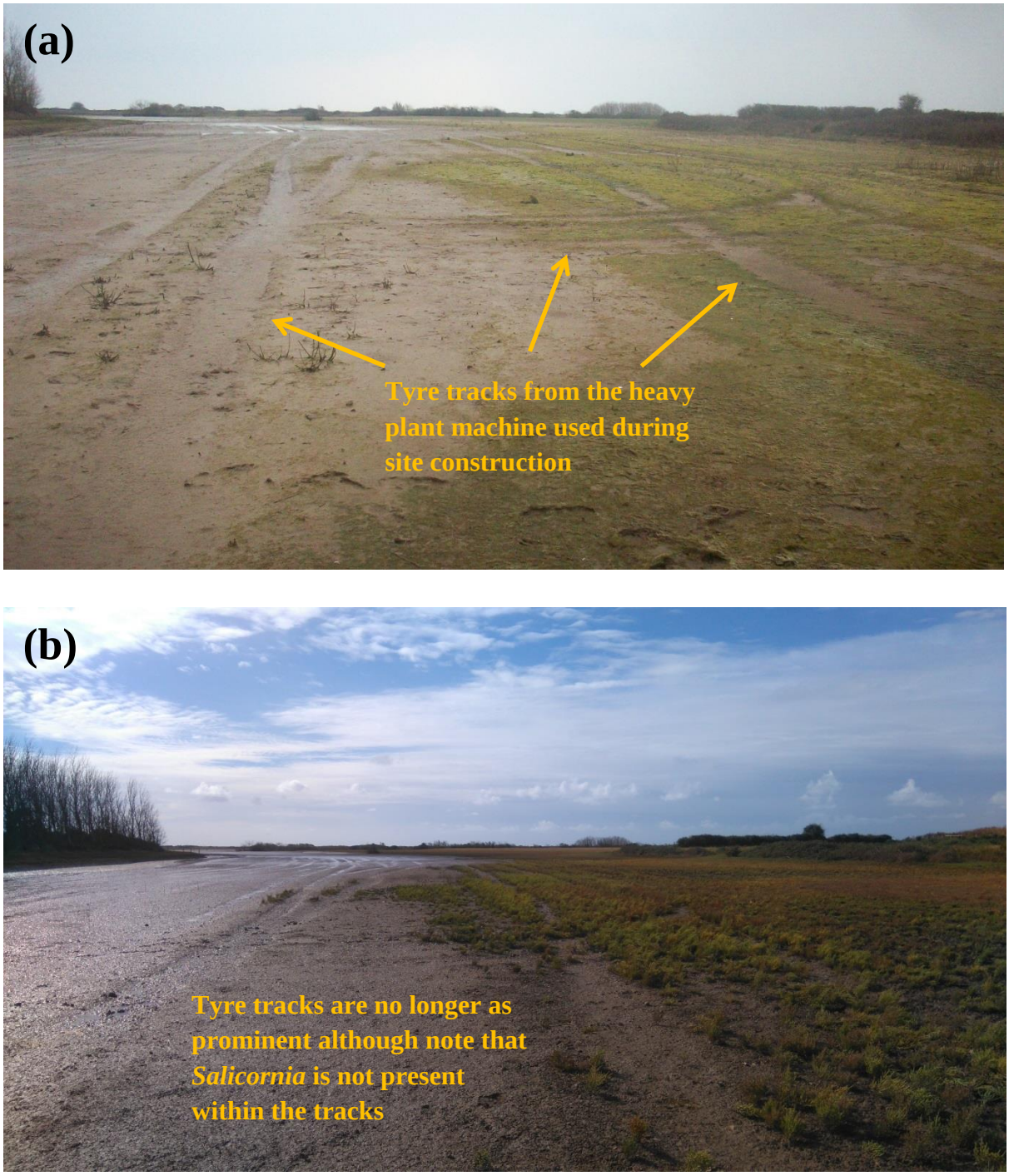

Figure 5.6: Tyre tracks remaining from the site construction (looking southwards), photographed in (a) March 2015 and (b) September 2016 have filled in during the study period (photograph: J.Dale).

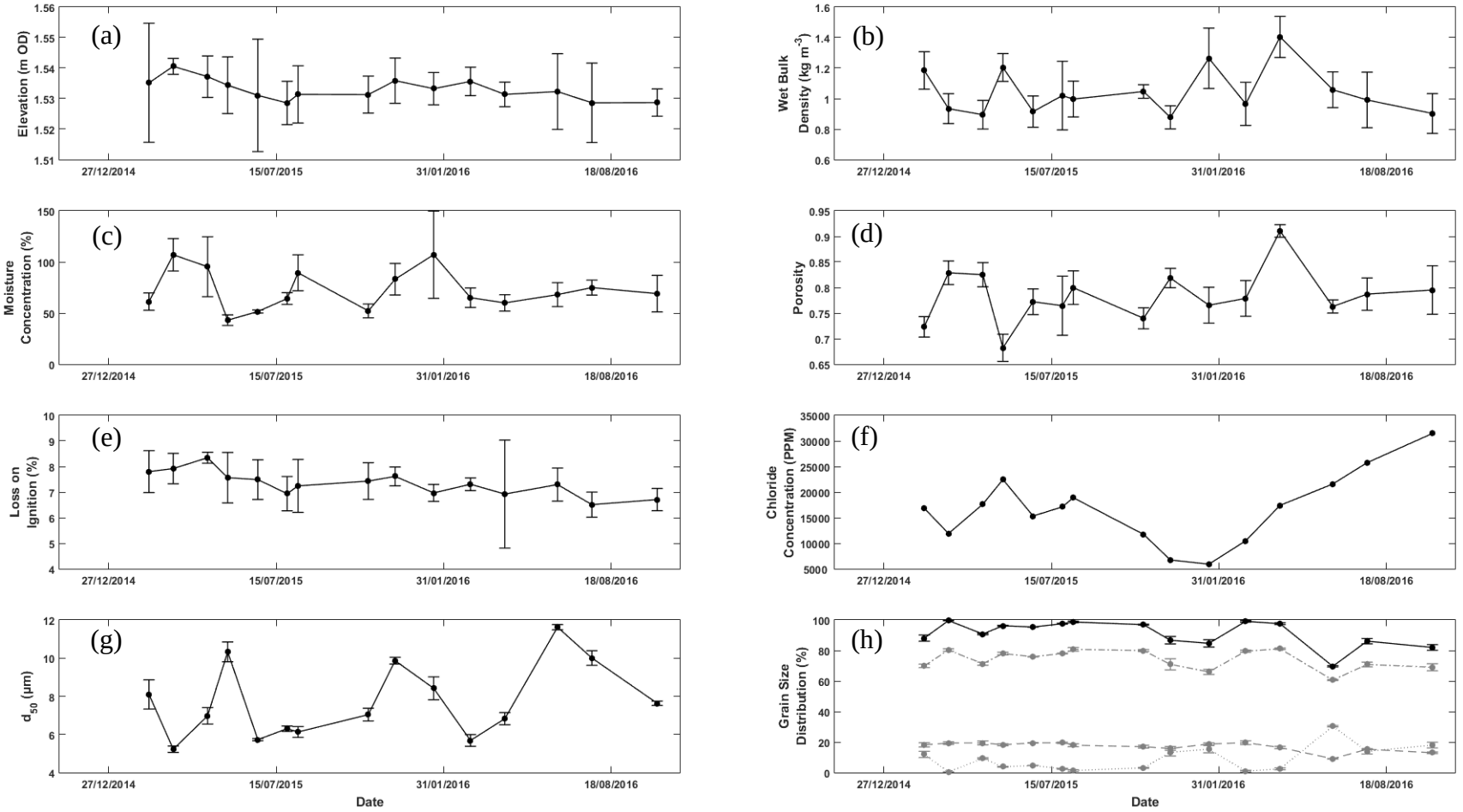

Figure 5.7: Variations (mean ± standard deviation) in surface (a) bed elevation (n = 12), (b) wet bulk density (n = 5), (c) moisture concentration (n = 5), (d) porosity (n = 5), (e) loss on ignition (n = 5), (f) chloride concentration, (g) median grain size (d_{50}) (n = 3) and (h) grain size distribution (clay, grey dashed line; silt, grey dashed-dotted line; sand, grey dotted line; mud, solid black line; n = 3) at Site 2b at the Medmerry Managed Realignment Site.

Wet bulk density (Figure 5.7b) and porosity (Figure 5.7d) fluctuated between months. Loss on ignition (Figure 5.7e), which tended to be higher at Site 2b compared to the other sites (Table 5.1), also fluctuated but followed a general pattern of decreasing over the study period. Chloride concentration (Figure 5.7f) increased and then decreased during the first year of measurements, then increased continually for the rest of the study period. As with Site 2a, the median grain size (Figure 5.7g) and grain size distribution (Figure 5.7h) were dominated by a high percentage of mud, with sediments at Site 2b having on average a higher proportion of clay and silt than the other sites (Table 5.1). No relationships were found between the surface sediment physical or geochemical properties at Site 2b (Table 5.4) with the exception of mud concentration and median grain size (r = -0.75, $P < 0.05$), although given that the two are both derived from particle grain size analysis this result is expected to occur.

Table 5.4: Pearson correlation coefficients between physical and geochemical surface sediment properties at Site 2b at the Medmerry Managed Realignment Site. Density, wet bulk density; Moisture, moisture concentration; Porosity; Organic, loss on ignition; Cl^-, chloride concentration; d_{50}, median grain size; Mud, mud concentration (clay + silt). Numbers in bold: statistically significant at ** = $P < 0.05$.

	Density	**Moisture**	**Porosity**	**Organic**	**Cl^-**	**d_{50}**
Moisture	-0.22					
Porosity	-0.01	0.41				
Organic	-0.25	0.18	-0.08			
Cl^-	-0.07	-0.34	-0.09	-0.37		
d_{50}	0.19	-0.15	-0.34	-0.18	0.27	
Mud	0.04	-0.11	0.13	0.20	-0.30	**-0.75****

5.2.4 Site 3

The remains of terrestrial vegetation and former beech tree hedgerow on the bank at Site 3 rotted and decayed, while the remains of freshwater reeds and grasses present at the start of the study period were removed by tidal currents and saltmarsh vegetation began to colonise (Figure 5.8). In contrast to Sites 1 and 2b, bed elevation on the bank (Figure 5.9a) increased during the summer and decreased during the winter until January 2016. Bed elevation continued to decrease during the rest of the study, but at a slower rate. Wet bulk density (Figure 5.9b) decreased during the summer and increased during the winter, whereas the opposite was measured in the porosity (Figure 5.9d) and chloride concentration (Figure 5.9f). Moisture concentration (Figure 5.9c) initially fluctuated but then continually decreased over the study period and was found to correlate ($r = 0.63$, $P < 0.05$) with the porosity (Table 5.5). Loss on ignition (Figure 5.9e) peaked in May 2015 before decreasing, but steadily increased after reaching a minimum of 3.5 % in August 2015. Grain size initially coarsened (Figure 5.9g-h), but the percentage of fine grained sediment increased from December 2015. The median grain size correlated with the chloride concentration (Table 5.5; $r = -0.67$, $P < 0.05$).

Bed elevation increased by 44 mm in the excavated channel at Site 3 (Figure 5.10a) with rhythmic patterns of accretion and erosion (analysed in Chapter 6). Overall, wet bulk density also increased (Figure 5.10b), but initially decreased during the first seven months of measurements. Moisture concentration (Figure 5.10c), porosity (Figure 5.10d) and loss on ignition (Figure 5.10e) all decreased with periodic fluctuations. Porosity correlated (Table 5.6) with the wet bulk density ($r = -0.78$, $P < 0.05$), moisture concentration ($r = 0.75$, $P < 0.05$) and loss on ignition ($r = 0.68$, $P < 0.05$). Additionally, the moisture concentration correlated with the loss on ignition values (Table 5.6; $r = 0.58$, $P < 0.05$). Porewater chloride concentration (Figure 5.10f) followed a similar pattern to the wet bulk density, but correlated with the porosity of the sediment (Table 5.6; $r = -0.51$, $P < 0.1$). The percentage of fine grained sediments demonstrated evidence of seasonal variability, increasing during the winter and decreasing during summer (Figure 5.10g-h).

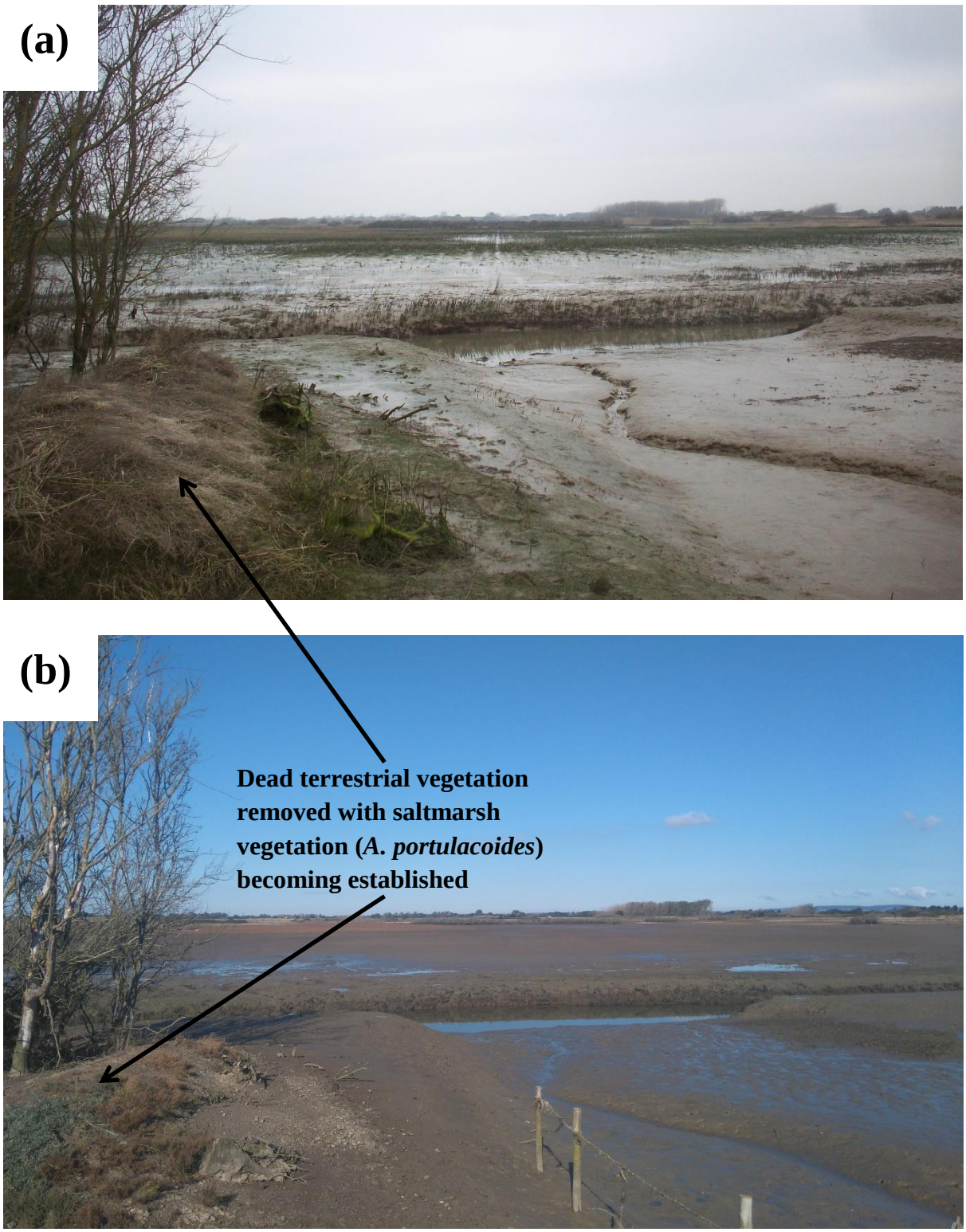

Figure 5.8: The banks and channel at Site 3 (looking north-westwards) in (a) December 2014 and (b) October 2016 (photograph: J.Dale).

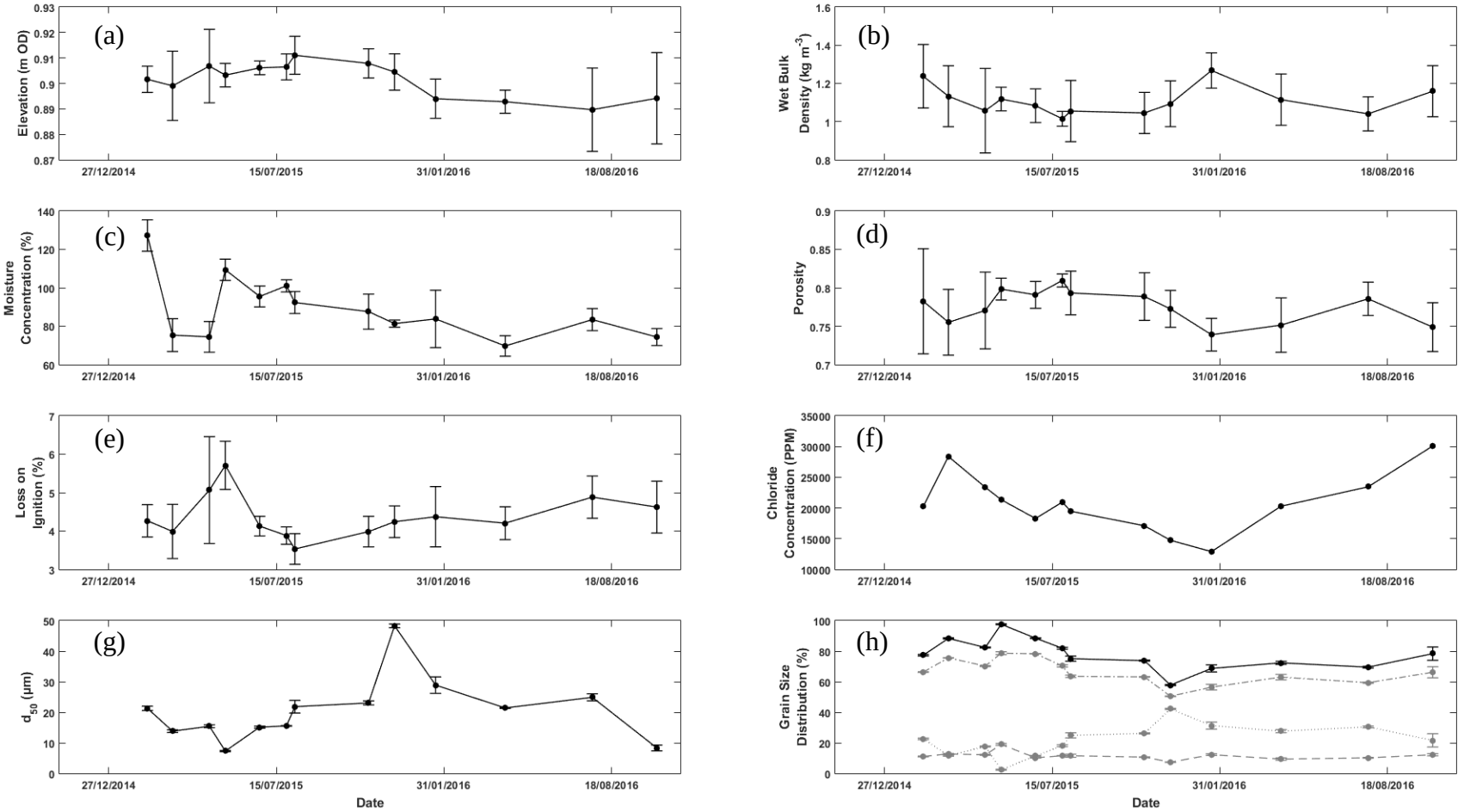

Figure 5.9: Variations (mean ± standard deviation) in surface (a) bed elevation (n = 12), (b) wet bulk density (n = 5), (c) moisture concentration (n = 5), (d) porosity (n = 5), (e) loss on ignition (n = 5), (f) chloride concentration, (g) median grain size (d_{50}) (n = 3) and (h) grain size distribution (clay, grey dashed line; silt, grey dashed-dotted line; sand, grey dotted line; mud, solid black line; n = 3) on the bank at Site 3 at the Medmerry Managed Realignment Site.

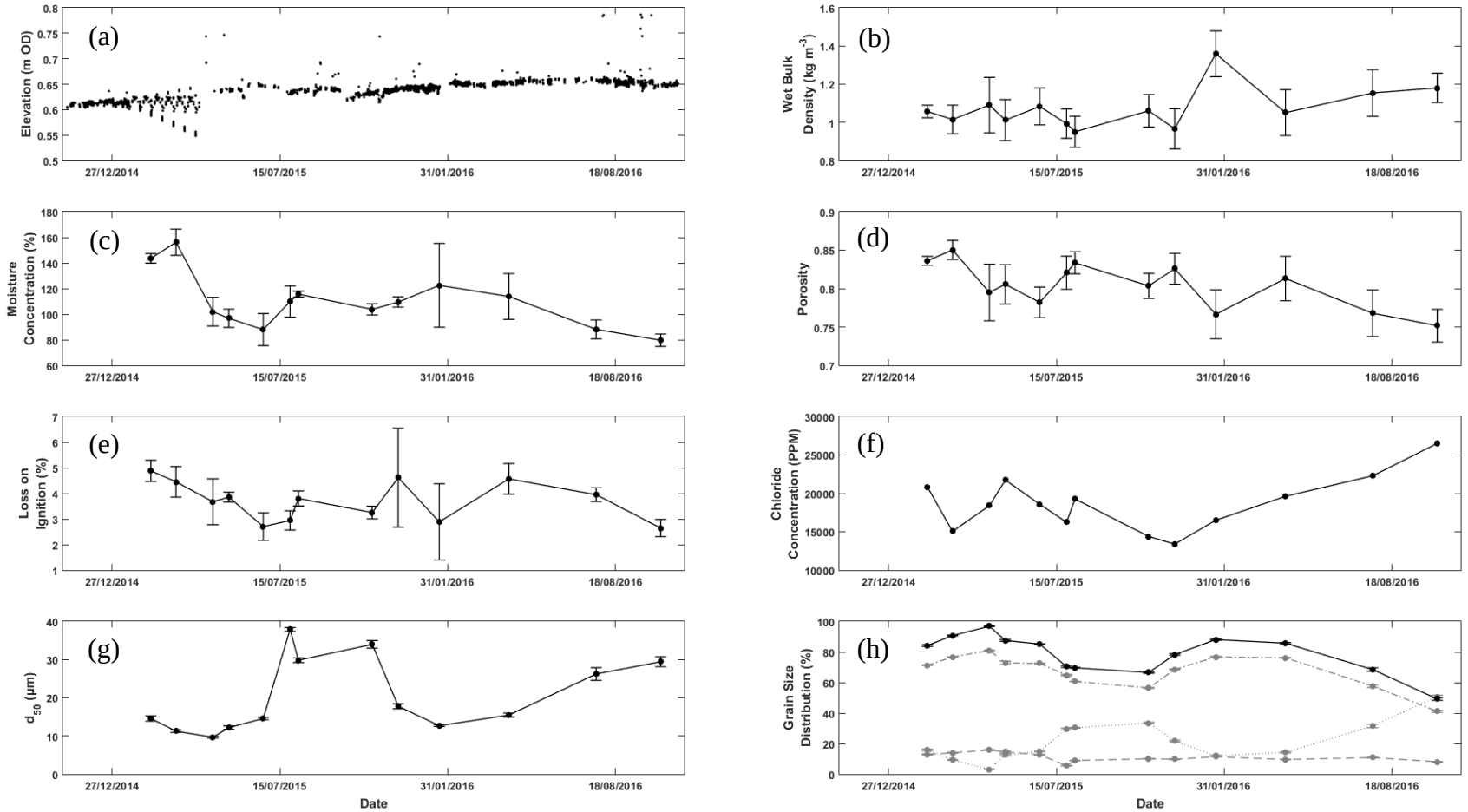

Figure 5.10: Variations (mean ± standard deviation) in surface (a) bed elevation measured using an ALTUS autonomous bed elevation monitor, (b) wet bulk density (n = 5), (c) moisture concentration (n = 5), (d) porosity (n = 5), (e) loss on ignition (n = 5), (f) chloride concentration, (g) median grain size (d_{50}) (n = 3) and (h) grain size distribution (clay, grey dashed line; silt, grey dashed-dotted line; sand, grey dotted line; mud, solid black line; n = 3) in the channel at Site 3 at the Medmerry Managed Realignment Site.

Table 5.5: Pearson correlation coefficients between physical and geochemical surface sediment properties on the bank at Site 3 at the Medmerry Managed Realignment Site. Density, wet bulk density; Moisture, moisture concentration; Porosity; Organic, loss on ignition; Cl^-, chloride concentration; d_{50}, median grain size; Mud, mud concentration (clay + silt). Numbers in bold: statistically significant at ** = $P < 0.05$.

	Density	**Moisture**	**Porosity**	**Organic**	**Cl^-**	**d_{50}**
Moisture	0.20					
Porosity	-0.63	**0.63****				
Organic	0.11	0.06	-0.02			
Cl^-	-0.12	-0.23	-0.13	0.22		
d_{50}	0.05	-0.14	-0.13	-0.30	**-0.67****	
Mud	-0.07	0.32	0.31	0.34	0.46	**-0.87****

Table 5.6: Pearson correlation coefficients between physical and geochemical surface sediment properties and critical erosion shear stress in the channel at Site 3 at the Medmerry Managed Realignment Site. Density, wet bulk density; Moisture, moisture concentration; Porosity; Organic, loss on ignition; Cl^-, chloride concentration; d_{50}, median grain size; Mud, mud concentration (clay + silt). Numbers in bold: statistically significant at * = $P < 0.1$, ** = $P < 0.05$.

	Density	**Moisture**	**Porosity**	**Organic**	**Cl^-**	**d_{50}**
Moisture	-0.17					
Porosity	**-0.78****	**0.75****				
Organic	-0.47	**0.58****	**0.68****			
Cl^-	0.26	-0.46	**-0.51***	-0.16		
d_{50}	-0.18	-0.34	-0.09	-0.40	0.05	
Mud	-0.03	**0.48***	0.35	0.39	-0.39	**-0.84****

5.2.5 Site 4

Site 4 was rarely inundated during the study period and presented little evidence of any marine influence or intertidal forcing due to the high elevation of the site in comparison to the mean high water, and was therefore sampled less frequently than other sites. Moisture concentration at Site 4 was lower than the other sites investigated (Table 5.1) and decreased during the study period (Figure 5.11a). Loss on ignition values (Figure 5.11b) remained relatively constant although a large degree of spatial variability was measured in January 2016, demonstrated by the large standard deviation. Median grain size (Figure 5.11c) and grain size distribution measurements (Figure 5.11d) indicate that the site tended to have a low percentage of clay and high levels of silt and sand, although in October 2016 the distribution of sand increased. With the exception of median grain size and mud concentration (r = -0.99, $P < 0.05$) there was little correlation between surface sediment properties at Site 4 (Table 5.7). Moisture concentration showed a weak and statistically insignificant correlation with the median grain size (r = -0.49, P = 0.41) and the mud concentration (r = 0.46, P = 0.44). Loss on ignition also demonstrated evidence of a relationship with the mud concentration (r = -0.40, P = 0.51).

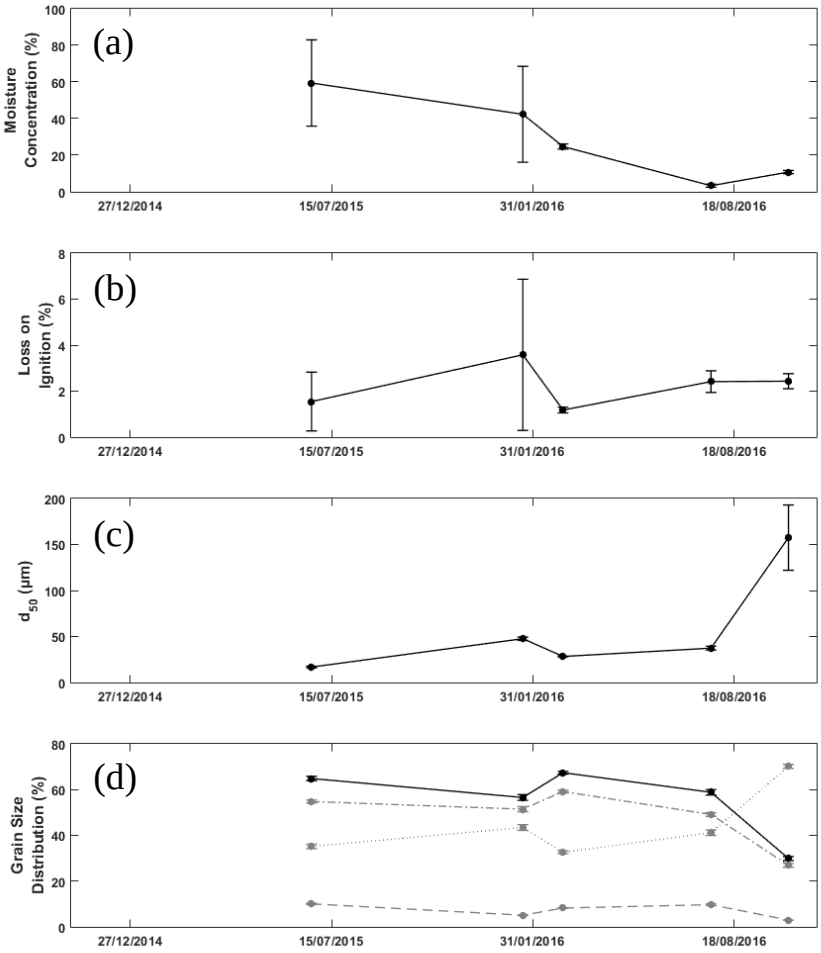

Figure 5.11: Variations (mean ± standard deviation) in surface (c) moisture concentration (n = 5), (e) loss on ignition (n = 5), (g) median grain size (d_{50}) (n = 3) and (h) grain size distribution (clay, grey dashed line; silt, grey dashed-dotted line; sand, grey dotted line; mud, solid black line; n = 3) at Site 4 at the Medmerry Managed Realignment Site.

Table 5.7: Pearson correlation coefficients between physical and geochemical surface sediment properties at Site 4 at the Medmerry Managed Realignment Site. Moisture, moisture concentration; Organic, loss on ignition; d_{50}, median grain size; Mud, mud concentration (clay + silt). Numbers in bold: statistically significant at ** = $P < 0.05$.

	Moisture	**Organic**	**d_{50}**
Organic	-0.08		
d_{50}	-0.49	0.29	
Mud	0.46	-0.40	**-0.99****

5.2.6 Site 5

The change in elevation on the bank at Site 5 differed spatially in response to the site's morphological development; some areas have been eroded as embryonic creek networks have formed, whilst elsewhere a bank of coarse grained sediments has migrated in a west to east direction (discussed in Section 7.3). Sediment pins measured a net accretion of 83 mm on the bank (Figure 5.12a), punctuated by periods of erosion and accretion. Initially, bed elevation decreased from March to May 2015, when elevation increased until December 2015. Elevation subsequently decreased until April 2016, when the bed elevation began increasing again. Wet bulk density (Figure 5.12b), moisture concentration (Figure 5.12c) and porosity (Figure 5.12d) varied throughout, as did loss on ignition (Figure 5.12e), although loss on ignition followed a general trend of decreasing through the summer and increasing to a maximum during the winter. Wet bulk density tended to be greater on the bank of the former arable field compared to other sites (Table 5.1) and strong correlation was found between the bulk density and porosity (Table 5.8; $r = -0.95$, $P < 0.05$).

Chloride concentrations decreased until December 2015, and subsequently increased throughout 2016 (Figure 5.12f), correlating with the wet bulk density ($r = 0.51$, $P < 0.1$) and porosity ($r = -0.55$, $P < 0.05$). The percentage of silt decreased and sand increased, resulting in a coarsening of the median grain size (Figure 5.12g) and a reduction in the overall percentage of the fine grained sediment (Figure 5.12h), until July 2016 when the percentage of silt increased. The distribution of clay remained low throughout. Both median grain size and the mud concentration correlated with the wet bulk density (median grain size, $r = -0.48$, $P < 0.1$; mud concentration, $r = 0.46$, $P < 0.1$), porosity (median grain size, $r = 0.53$, $P < 0.05$; mud concentration, $r = -0.52$, $P < 0.1$) and chloride concentration (median grain size, $r = -0.75$, $P < 0.05$; mud concentration, $r = 0.67$, $P < 0.05$).

In contrast to the bank, bed elevation in the borrow pit increased rapidly (Figure 5.13a) during the study period (analysed in Chapter 6), resulting in significant infill and the loss of the area of lower elevation (Figure 5.14). Bulk density displayed

evidence of seasonal variability, decreasing during the summer and increasing during the winter (Figure 5.13b). The opposite trend was found in the moisture concentration (Figure 5.13c) and porosity measurements (Figure 5.13d), which correlated negatively (Table 5.9) with the wet bulk density of the sediment (r = -0.62, P < 0.05). Loss on ignition (Figure 5.13e) fluctuated throughout, peaking at 3.88 % in July 2016. Porewater chloride concentration decreased until January 2016, reaching a minimum of 11,845 PPM (1.2 %), after which it progressively increased to a maximum of 29,456 PPM (2.9 %). Surface sediments coarsened, decreasing from 88 % to 15 % mud concentration over the measurement period, with the median grain size correlating weakly (Table 5.9) with the chloride concentration (r = -0.52, P < 0.1).

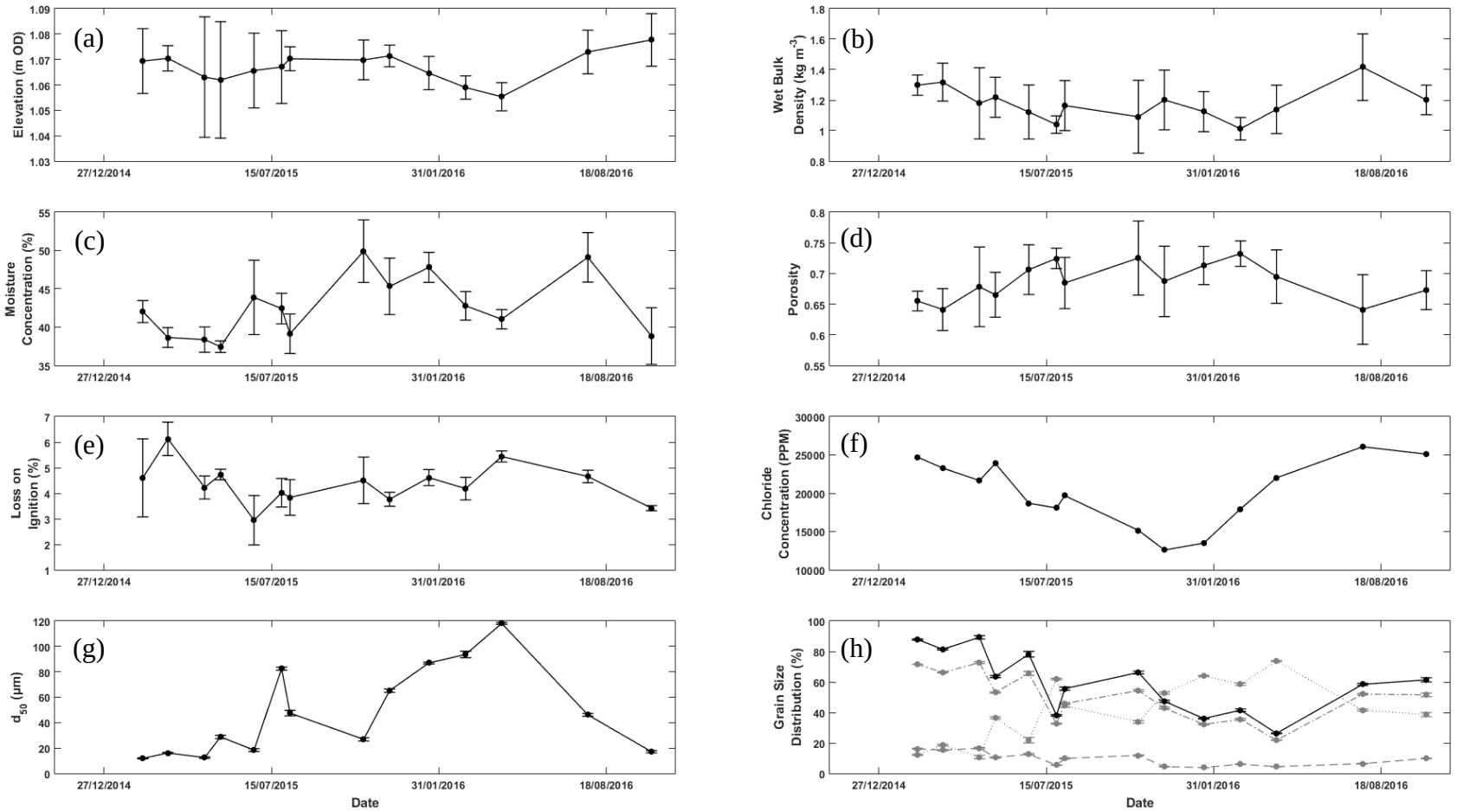

Figure 5.12: Variations (mean ± standard deviation) in surface (a) bed elevation (*n* = 12), (b) wet bulk density (*n* = 5), (c) moisture concentration (*n* = 5), (d) porosity (*n* = 5), (e) loss on ignition (*n* = 5), (f) chloride concentration, (g) median grain size (d_{50}) (*n* = 3) and (h) grain size distribution (clay, grey dashed line; silt, grey dashed-dotted line; sand, grey dotted line; mud, solid black line; *n* = 3)on the bank at Site 5 at the Medmerry Managed Realignment Site.

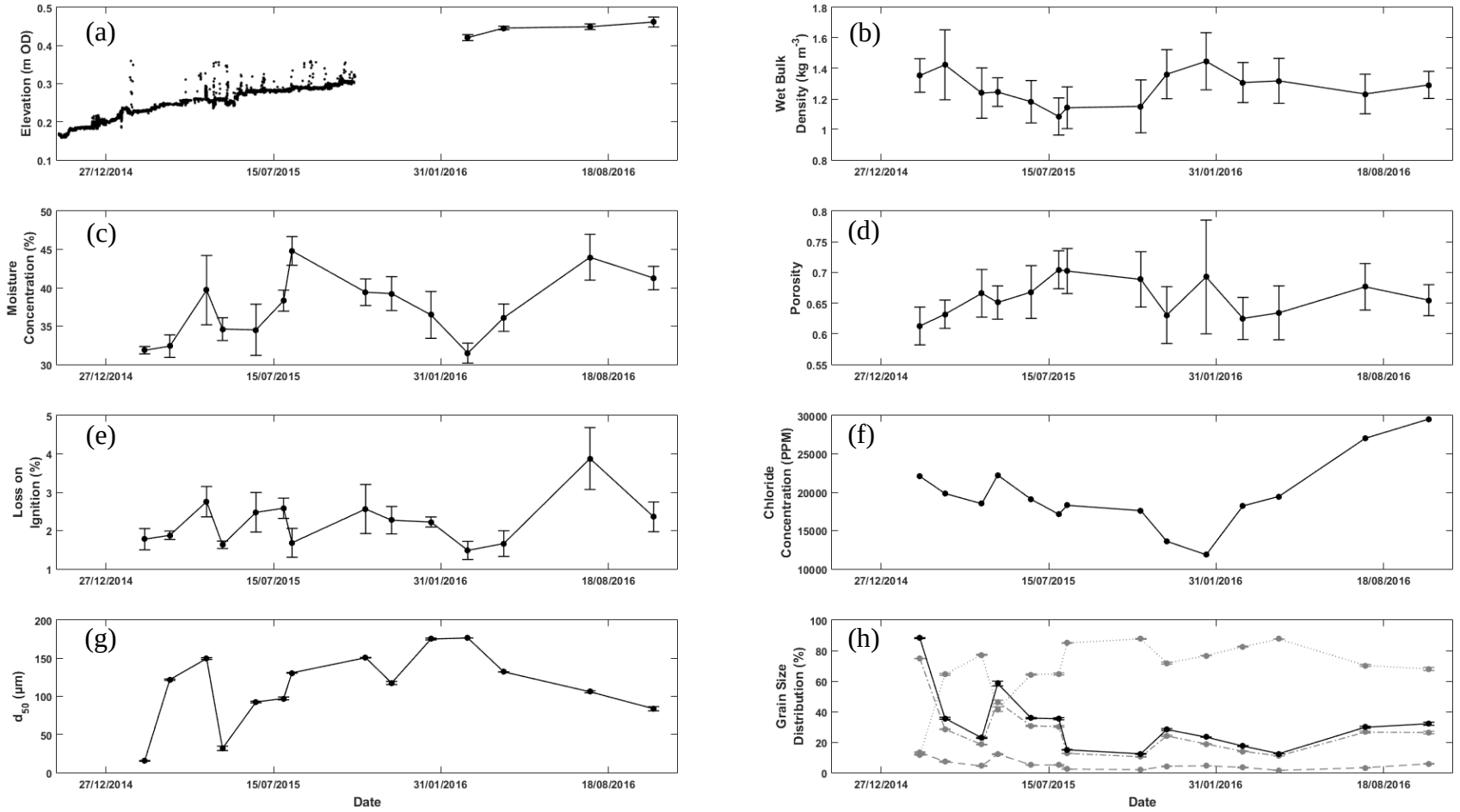

Figure 5.13: Variations (mean ± standard deviation) in surface (a) bed elevation measured using an ALTUS autonomous bed elevation monitor (November 2014 to October 2015) and sediment pins (February to October 2016), (b) wet bulk density (n = 5), (c) moisture concentration (n = 5), (d) porosity (n = 5), (e) loss on ignition (n = 5), (f) chloride concentration, (g) median grain size (d_{50}) (n = 3) and (h) grain size distribution (clay, grey dashed line; silt, grey dashed-dotted line; sand, grey dotted line; mud, solid black line; n = 3) in the borrow pit at Site 5 at the Medmerry Managed Realignment Site.

Table 5.8: Pearson correlation coefficients between physical and geochemical surface sediment properties and critical erosion shear stress on the bank at Site 5 at the Medmerry Managed Realignment Site. Density, wet bulk density; Moisture, moisture concentration; Porosity; Organic, loss on ignition; Cl^-, chloride concentration; d_{50}, median grain size; Mud, mud concentration (clay + silt. Numbers in bold: statistically significant at * = $P < 0.1$, ** = $P < 0.05$.

	Density	**Moisture**	**Porosity**	**Organic**	**Cl^-**	**d_{50}**
Moisture	-0.03					
Porosity	**-0.95****	0.33				
Organic	0.37	-0.09	-0.39			
Cl^-	**0.51***	-0.23	**-0.55****	-0.15		
d_{50}	**-0.48***	0.24	**0.53****	0.15	**-0.75****	
Mud	**0.46***	-0.26	**-0.52***	-0.03	**0.67****	-0.94

Table 5.9: Pearson correlation coefficients between physical and geochemical surface sediment properties and critical erosion shear stress in the borrow pit at Site 5 at the Medmerry Managed Realignment Site. Density, wet bulk density; Moisture, moisture concentration; Porosity; Organic, loss on ignition; Cl^-, chloride concentration; d_{50}, median grain size; Mud, mud concentration (clay + silt). Numbers in bold: statistically significant at * = $P < 0.1$, ** = $P < 0.05$.

	Density	**Moisture**	**Porosity**	**Organic**	**Cl^-**	**d_{50}**
Moisture	-0.07					
Porosity	**-0.62****	0.35				
Organic	-0.30	0.38	0.44			
Cl^-	-0.14	0.20	-0.18	0.27		
d_{50}	0.10	0.20	0.30	0.07	**-0.52***	
Mud	0.18	-0.35	-0.42	-0.15	0.30	-0.88

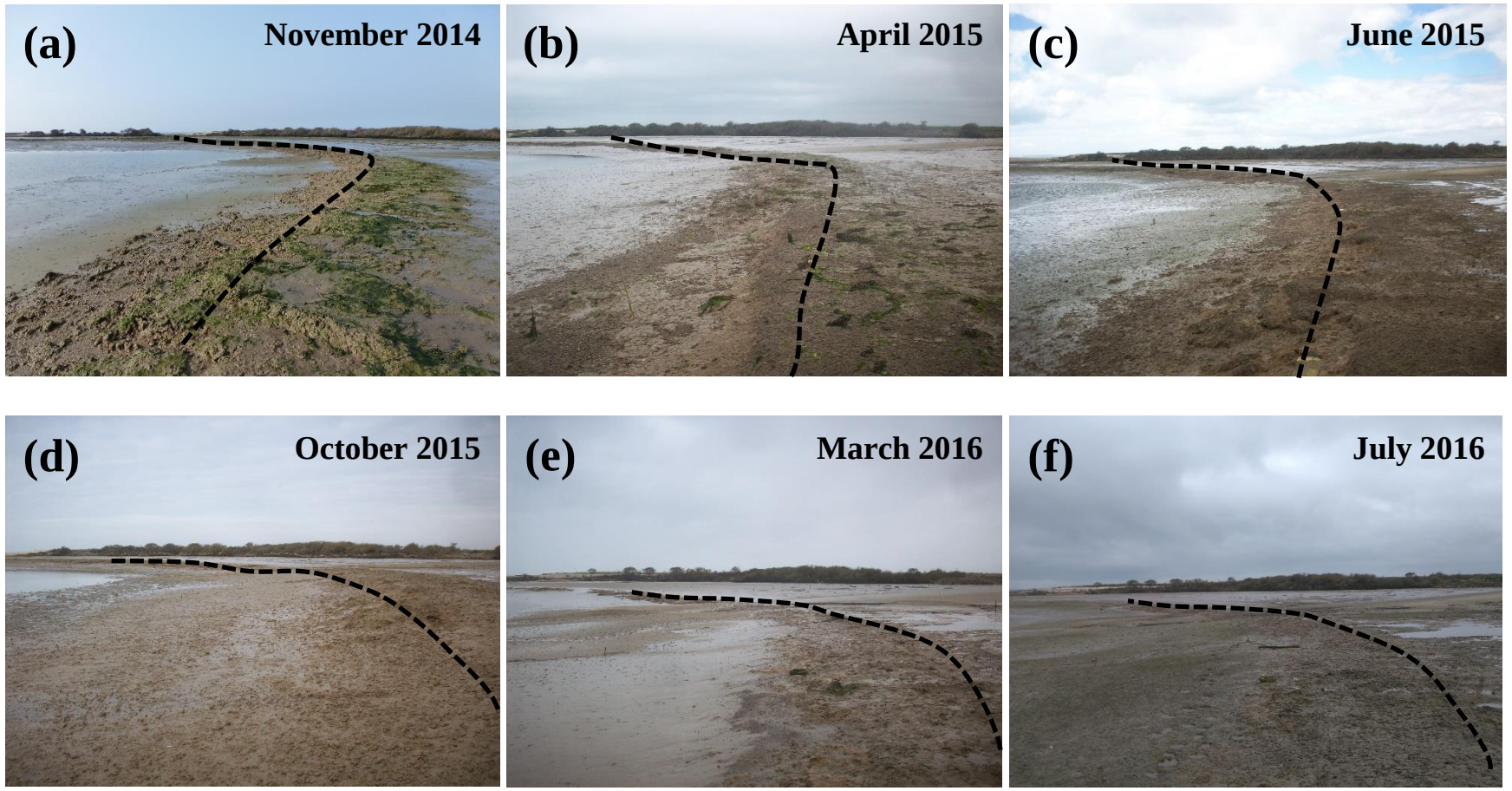

Figure 5.14: The edge of the borrow pit marked by a black dashed line at Site 5 (looking westwards) in (a) November 2014, (b) April 2015, (c) July 2015, (d) October 2015, (e) March 2016 and (f) July 2016. High rates of sedimentation have resulted in the borrow pit filling in and the loss of the area of lower elevation (photograph: J. Dale).

5.3 Spatial Variations in Relationships between Physicochemical Sediment Properties

To assess the within-site spatial variability and local heterogeneity of the relationship between surface sediment properties, measurements were taken from separate plots in transect at Sites 2b, 3 and 5 on three occasions; August 2015, November 2015 and June 2016. In August 2015, at Site 2b (Table 5.10), a strong relationship was found between the bulk sediment properties (wet bulk density, moisture concentration and porosity). Moisture concentration and porosity were both found to relate to the percentage of mud in the sediment (r = 0.83 and 0.82 respectively, $P < 0.05$).

Table 5.10: Pearson correlation coefficients between physical and geochemical surface sediment properties between separate plots at Site 2b at the Medmerry Managed Realignment Site in August 2015. Density, wet bulk density; Moisture, moisture concentration; Porosity; Organic, loss on ignition; Cl^-, chloride concentration; d_{50}, median grain size; Mud, mud concentration (clay + silt). Numbers in bold: statistically significant at * = $P < 0.1$, ** = $P < 0.05$.

	Density	**Moisture**	**Porosity**	**Organic**	**Cl^-**	**d_{50}**
Moisture	**-0.77***					
Porosity	**-0.92****	**0.95****				
Organic	0.08	0.40	0.23			
Cl^-	-0.62	0.50	0.53	0.12		
d_{50}	0.37	-0.47	-0.45	-0.05	-0.51	
Mud	-0.67	**0.83****	**0.82****	0.42	0.60	**-0.80****

A strong relationship was maintained between the bulk sediment properties in November 2015 (Table 5.11). However, in contrast to August, little correlation was found between the moisture concentration and mud concentration (r = 0.36, P = 0.55), but the chloride concentration was found to have a strong relationship with the moisture concentration (r = 0.81, $P < 0.1$). The strength of the relationship between moisture concentration and chloride concentration was weaker and not statistically significant (r = 0.73, P = 0.17) in June 2016 (Table 5.12). The relationships between the bulk sediment properties were also weaker and not of statistical significance, with the exception of moisture concentration and porosity (r = 0.86, $P < 0.1$). Moisture concentration also correlated with the mud concentration (r = 0.82, $P < 0.1$).

Table 5.11: Pearson correlation coefficients between physical and geochemical surface sediment properties between separate plots at Site 2b at the Medmerry Managed Realignment Site in November 2015. Density, wet bulk density; Moisture, moisture concentration; Porosity; Organic, loss on ignition; Cl^-, chloride concentration; d_{50}, median grain size; Mud, mud concentration (clay + silt). Numbers in bold: statistically significant at * = $P < 0.1$, ** = $P < 0.05$.

	Density	**Moisture**	**Porosity**	**Organic**	**Cl^-**	**d_{50}**
Moisture	**-0.96****					
Porosity	**-0.99****	**0.98****				
Organic	-0.18	0.16	0.25			
Cl^-	-0.67	**0.81***	0.69	-0.01		
d_{50}	0.26	-0.13	-0.11	0.72	-0.13	
Mud	-0.48	0.36	0.35	-0.62	0.27	**-0.97****

Table 5.12: Pearson correlation coefficients between physical and geochemical surface sediment properties and critical erosion shear stress between separate plots at Site 2b at the Medmerry Managed Realignment Site in June 2016. Density, wet bulk density; Moisture, moisture concentration; Porosity; Organic, loss on ignition; Cl^-, chloride concentration; d_{50}, median grain size; Mud, mud concentration (clay + silt). Numbers in bold: statistically significant at * = $P < 0.1$.

	Density	**Moisture**	**Porosity**	**Organic**	**Cl^-**	**d_{50}**
Moisture	-0.35					
Porosity	-0.77	**0.86***				
Organic	-0.30	-0.18	-0.01			
Cl^-	-0.40	0.73	0.76	-0.38		
d_{50}	-0.22	-0.46	-0.15	0.35	0.13	
Mud	-0.31	**0.82***	0.71	-0.41	0.43	-0.78

Moisture concentration and porosity were highly correlated ($r = 0.90$, $P < 0.1$) at Site 3 in August 2015 (Table 5.13), as were both the median grain size and mud concentration with the loss on ignition ($r = -0.95$ and 0.96 respectively, $P < 0.05$) and chloride concentration ($r = -0.92$ and 0.91 respectively, $P < 0.1$). The relationship between moisture concentration and porosity was maintained in November 2015 (Table 5.14; $r = 0.92$, $P < 0.1$), although by June 2016 (Table 5.15) the relationship had weakened and was below the 90 % confidence interval ($r = 0.88$, $P = 0.12$). Wet

bulk density and loss on ignition were closely correlated in June 2016 (r = -0.92, P < 0.05).

Table 5.13: Pearson correlation coefficients between physical and geochemical surface sediment properties between separate plots at Site 3 at the Medmerry Managed Realignment Site in August 2015. Density, wet bulk density; Moisture, moisture concentration; Porosity; Organic, loss on ignition; Cl^-, chloride concentration; d_{50}, median grain size; Mud, mud concentration (clay + silt). Numbers in bold: statistically significant at * = P < 0.1, ** = P < 0.05.

	Density	**Moisture**	**Porosity**	**Organic**	**Cl^-**	**d_{50}**
Moisture	0.02					
Porosity	-0.43	**0.90***				
Organic	-0.39	-0.73	-0.49			
Cl^-	0.19	-0.50	-0.54	0.77		
d_{50}	0.18	0.61	0.47	**-0.95****	**-0.92***	
Mud	-0.15	-0.72	-0.58	**0.96****	**0.91***	**-0.99****

Table 5.14: Pearson correlation coefficients between physical and geochemical surface sediment properties between separate plots at Site 3 at the Medmerry Managed Realignment Site in November 2015. Density, wet bulk density; Moisture, moisture concentration; Porosity; Organic, loss on ignition; Cl^-, chloride concentration; d_{50}, median grain size; Mud, mud concentration (clay + silt). Numbers in bold: statistically significant at * = P < 0.1, ** = P < 0.05.

	Density	**Moisture**	**Porosity**	**Organic**	**Cl^-**	**d_{50}**
Moisture	-0.46					
Porosity	-0.78	**0.92***				
Organic	-0.29	-0.18	0.05			
Cl^-	0.39	0.43	0.16	0.19		
d_{50}	-0.49	0.49	0.52	-0.69	-0.49	
Mud	0.44	-0.50	-0.51	0.74	0.45	**-0.99****

Table 5.15: Pearson correlation coefficients between physical and geochemical surface sediment properties and critical erosion shear stress between separate plots at Site 3 at the Medmerry Managed Realignment Site in June 2016. Density, wet bulk density; Moisture, moisture concentration; Porosity; Organic, loss on ignition; Cl^-, chloride concentration; d_{50}, median grain size; Mud, mud concentration (clay + silt). Numbers in bold: statistically significant at ** = $P < 0.05$.

	Density	**Moisture**	**Porosity**	**Organic**	**Cl^-**	**d_{50}**
Moisture	0.36					
Porosity	-0.72	-0.88				
Organic	**-0.97****	-0.26	0.60			
Cl^-	-0.01	0.01	-0.19	0.24		
d_{50}	0.47	0.32	-0.62	-0.25	0.86	
Mud	-0.49	-0.53	0.75	0.27	-0.78	**-0.97****

In August 2015, at Site 5 (Table 5.16), wet bulk density was found to relate to all sediment properties, with the exception of the moisture concentration and chloride concentration. Loss on ignition correlated with both the median grain size and mud concentration (r = -0.98 and 0.96 respectively, $P < 0.05$). This relationship was maintained, although weakened slightly, in November 2015 (Table 5.17; median grain size, r = -0.74, $P < 0.1$; mud concentration, r = 0.76, $P < 0.5$). In contrast, the only relationship with the wet bulk density maintained was with the porosity (r = -0.94, $P < 0.05$).

Table 5.16: Pearson correlation coefficients between physical and geochemical surface sediment properties between separate plots at Site 5 at the Medmerry Managed Realignment Site in August 2015. Density, wet bulk density; Moisture, moisture concentration; Porosity; Organic, loss on ignition; Cl^-, chloride concentration; d_{50}, median grain size; Mud, mud concentration (clay + silt). Numbers in bold: statistically significant at * = $P < 0.1$, ** = $P < 0.05$.

	Density	**Moisture**	**Porosity**	**Organic**	**Cl^-**	**d_{50}**
Moisture	-0.04					
Porosity	**-0.93****	0.41				
Organic	**-0.71***	-0.34	0.52			
Cl^-	0.33	-0.33	-0.44	-0.18		
d_{50}	**0.70***	0.28	-0.53	**-0.98****	0.02	
Mud	**-0.72***	-0.21	0.57	**0.96****	-0.01	**-0.99****

Table 5.17: Pearson correlation coefficients between physical and geochemical surface sediment properties between separate plots at Site 5 at the Medmerry Managed Realignment Site in November 2015. Density, wet bulk density; Moisture, moisture concentration; Porosity; Organic, loss on ignition; Cl^-, chloride concentration; d_{50}, median grain size; Mud, mud concentration (clay + silt). Numbers in bold: statistically significant at * = $P < 0.1$, ** = $P < 0.05$.

	Density	**Moisture**	**Porosity**	**Organic**	**Cl^-**	**d_{50}**
Moisture	0.50					
Porosity	**-0.94****	-0.19				
Organic	-0.31	0.17	0.42			
Cl^-	0.15	-0.33	-0.30	0.43		
d_{50}	-0.25	-0.35	0.15	**-0.74***	-0.46	
Mud	0.19	0.37	-0.08	**0.76****	0.37	**-0.99****

Wet bulk density and moisture concentration were both found to correlate strongly with the porosity, loss on ignition and chloride concentration at Site 5 in June 2016 (Table 5.18), although only moderate correlation was found between the bulk density and the moisture concentration which was slightly above the 90 % confidence interval (r = -0.65, P = 0.11). High correlation coefficients were calculated between the porosity, loss on ignition and chloride concentration. The loss on ignition was found to correlate with the mud concentration (r = 0.70, $P < 0.1$).

Table 5.18: Pearson correlation coefficients between physical and geochemical surface sediment properties between separate plots at Site 2b at the Medmerry Managed Realignment Site in June 2016. Density, wet bulk density; Moisture, moisture concentration; Porosity; Organic, loss on ignition; Cl^-, chloride concentration; d_{50}, median grain size; Mud, mud concentration (clay + silt). Numbers in bold: statistically significant at * = $P < 0.1$, ** = $P < 0.05$.

	Density	**Moisture**	**Porosity**	**Organic**	**Cl^-**	**d_{50}**
Moisture	-0.65					
Porosity	**-0.89****	**0.92****				
Organic	**-0.88****	**0.74***	**0.84****			
Cl^-	**0.77****	**-0.83****	**-0.84****	**-0.93****		
d_{50}	0.17	0.29	0.04	0.15	-0.08	
Mud	-0.56	0.56	0.58	**0.70***	-0.50	**0.69***

5.4 Temporal Variation in Surface Sediment Cohesive Strength and the Relationship with the Surface Sediment Properties

Measurements of sediment cohesive strength, taken since March 2015 using the Sand 1 test on a Mark IV Cohesive Strength Meter (CSM) (see Section 4.4.2 for description), at each site are shown in Figure 5.15 and reported as the stagnation pressure (P_{stag}) of the critical erosion threshold. At Site 1 mean critical shear stress values were greater during the summer and lower during the winter. During the summer P_{stag} values were also more variable, with complete tests being run without detecting an erosion event during the last two measurement time points. No statistically significant correlation coefficients were found between the critical shear stress and the sediment parameters (Table 5.19), although a weak relationship was found with the loss on ignition measurements ($r = 0.41$, $P = 0.22$).

During the first year of measurements at Site 2a, mean P_{stag} values were variable but increased during the spring and summer, decreasing after a peak in June 2015. The critical erosion threshold increased again in January 2016, subsequently decreasing whilst maintaining a degree of variability. No relationship was found between the critical shear stress and the physical or geochemical sediment properties (Table 5.19), as with Site 1, but a weak relationship was found with the wet bulk density ($r = 0.48$, $P = 0.16$) and to a lesser extent the loss on ignition ($r = 0.35$, $P < 0.33$). At Site 2b, mean values varied throughout, with the critical shear stress being above the detection limit of the CSM device on five occasions. Median grain size did, however, correlate with the critical shear stress measurements ($r = -0.62$, $P < 0.05$).

In the centre of the Medmerry site, at Site 3, mean critical shear stress values also demonstrated evidence of seasonal variability, peaking in April and June 2015 before decreasing until April 2016 when the critical shear stress increased and became more variable. A weak relationship (Table 5.19) was found between the critical shear stress and the wet bulk density ($r = -0.41$), chloride concentration ($r = 0.50$) and median grain size ($r = -0.42$) but none were found to be statistically significant. A similar pattern was observed in the channel at Site 3, although the mean critical shear stress

tended to be lower than on the bank. Critical shear stress did not correlate significantly with any variable (Table 5.19), but weak relationships were found with wet bulk density (r = -0.34, P = 0.31), moisture concentration (r = -0.38, P = 0.24), loss on ignition (r = -0.32, P = 0.33), and chloride concentration (r = 0.42, P = 0.20).

On the bank at Site 5, mean P_{stag} decreased until January 2016 when, after some initial variability, critical shear stress increased above the limit of the CSM. Critical shear stress correlated (Table 5.19) with the chloride concentration (r = 0.75, $P < 0.05$), the median grain size (r = -0.62, $P < 0.1$) and the mud concentration (r = 0.55, $P < 0.1$). Measurements in the borrow pit at Site 5 followed a similar trend to those at Site 1, peaking with high variability in June and July 2015 and again in July and October 2016. The critical shear stress was found to relate to the wet bulk density (r = -0.52, $P < 0.1$) and the chloride concentration (r = 0.53, $P < 0.1$), although both were only statistically significant at the 90 % confidence interval (Table 5.19).

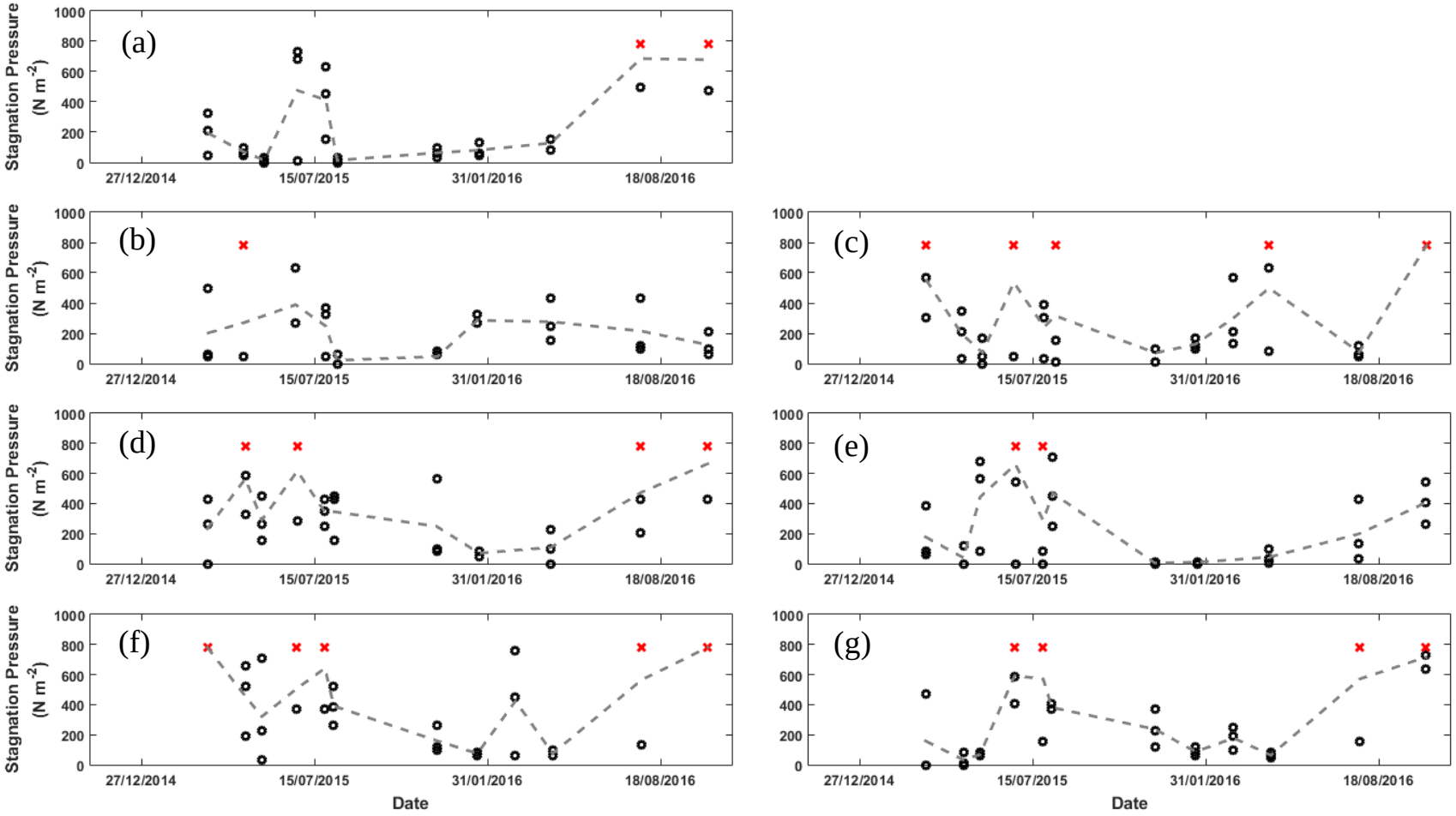

Figure 5.15: Measurements of the critical erosion shear stress taken using the Sand 1 test on a Mark IV Cohesive Strength Meter (CSM), reported as the equivalent P_{stag} value for (a) Site 1, (b) Site 2a, (c) Site 2b, (d) Site 3 Bank, (e) Site 3 Channel, (f) Site 5 Bank, (g) Site 5 Borrow Pit at the Medmerry Managed Realignment Site. Grey dashed line denotes the mean, black open circles the measurement and red crosses the cases where the critical erosion shear was beyond the limit of the CSM.

Table 5.19: Pearson correlation coefficients between physical and geochemical surface sediment properties and critical erosion shear stress at the Medmerry Managed Realignment Site. Density, wet bulk density; Moisture, moisture concentration; Porosity; Organic, loss on ignition; Cl^-, chloride concentration; d_{50}, median grain size; Mud, mud concentration (clay + silt). Numbers in bold: statistically significant at * = $P < 0.1$, ** = $P < 0.05$.

	Density	**Moisture**	**Porosity**	**Organic**	**Cl^-**	**d_{50}**	**Mud**
Site 1	-0.14	0.21	0.20	0.41	0.18	-0.26	0.02
Site 2a	0.48	-0.10	-0.37	0.35	-0.02	-0.31	0.16
Site 2b	-0.14	-0.09	0.38	-0.11	0.34	**-0.62****	0.10
Site 3 Bank	-0.41	0.03	0.28	0.20	0.50	-0.42	0.29
Site 3 Channel	-0.34	-0.38	-0.03	-0.32	0.42	0.10	-0.24
Site 5 Bank	0.27	-0.31	-0.35	-0.08	**0.75****	**-0.62***	**0.55***
Site 5 Borrow Pit	**-0.52***	0.24	0.39	0.49	**0.53***	-0.37	0.14

5.5 Spatial Variations in the Relationship between the Surface Sediment Properties and the Cohesive Strength

Critical shear stress measurements were taken from separate plots at Sites 2b, 3 and 5 in August 2015 and June 2016 to assess the spatial variability and heterogeneity of the relationship between surface sediment properties measurements and the erodibility of the sediment. Table 5.20 presents Pearson correlation coefficients (r) of the relationship between the mean critical shear stress measured by the CSM and the physicochemical surface sediment variables. At Site 2b no statistically significant relationship was found between the critical shear stress and the measured surface sediment parameters on either occasion. Correlation coefficients did suggest a weak relationship between the critical shear stress and the percentage lost on ignition (r = -0.47, P = 0.34) in August 2015 which strengthened in June 2016 (r = -0.79, P = 0.11).

At Site 3 a strong negative correlation was found between the critical shear stress and the porosity (r = 0.99, P < 0.05) in August 2015. In contrast, the critical shear stress closely followed the chloride concentration (r = 0.93, P < 0.1) in June 2016. At Site 5 wet bulk density and the critical shear stress were correlated in August 2015 (r = 0.71, P < 0.1), whereas in June 2016 a relationship was found between the critical shear stress and the chloride concentration (r = -0.67, P < 0.1).

Table 5.20: Pearson correlation coefficients between physical and geochemical surface sediment properties and critical erosion shear stress at the Medmerry Managed Realignment Site from separate plots at three locations. Density, wet bulk density; Moisture, moisture concentration; Porosity; Organic, loss on ignition; Cl^-, chloride concentration; d_{50}, median grain size; Mud, mud concentration (clay + silt). Numbers in bold: statistically significant at * = $P < 0.1$, ** = $P < 0.05$.

		Density	Moisture	Porosity	Organic	Cl^-	d_{50}	Mud
Site 2b	**August 2015**	0.14	-0.19	-0.28	-0.47	0.24	0.14	-0.42
	June 2016	0.10	-0.27	-0.20	-0.79	-0.01	-0.18	0.17
Site 3	**August 2015**	0.47	-0.86	**-0.99****	0.53	0.65	-0.55	0.65
	June 2016	-0.32	0.05	-0.07	0.54	**0.93***	0.68	-0.64
Site 5	**August 2015**	**0.71***	0.30	-0.53	-0.40	0.08	0.34	-0.37
	June 2016	-0.08	0.46	0.25	0.49	**-0.67***	0.33	0.22

5.6 Discussion

Analysis of the physicochemical surface sediment properties at the Medmerry Managed Realignment Site (Table 5.21) suggests seasonal variations in the measured parameters. Indications of seasonality in surface sediment properties were also observed by Kadiri et al. (2011) at the Wallasea Island Managed Realignment Site (United Kingdom), 18 months after site inundation. However, these authors found noticeable differences between the sediments in the restored site compared to the surrounding natural saltmarsh, which they associated with differences in vegetation abundance and organic matter content. A degree of temporal and spatial association was found between the measured parameters in this study, evidenced by statistically significant correlation coefficients, although the relationship between sediment property parameters varied between sites. Additionally, the cohesive strength of the sediment, represented by measurements of the critical erosion shear stress, demonstrated signs of seasonal variability, with sediments becoming more resistant to erosion (but also more variable) during the summer. However, few physicochemical parameters were found to correlate with critical shear stress measurements. Given the complexity of the relationship between sediment properties and the erodibility of cohesive sediments (Grabowski et al., 2011), particularly with in situ field measurements, such small scale internal variability is not unexpected.

The percentage variability between the separate plots measured in transect at Site 2b, Site 3, Site 5 and the three sites collectively is presented in Table 5.22**.** Analysis of the percentage variance indicates that, although in some cases substantial within site spatial variability occurred (such as the chloride concentration), greater variance was found between sites. The exception to this is the mud concentration at Site 5, although this is probably due to increased variability caused by the coarse grained sediment that has been deposited within the borrow pit (see Section 5.2.6). This provides confidence that inter-site differences observed are demonstrative of spatial variability across Medmerry, and are not a product of random within-site variability. This spatial variability confirms that analysis of one or two sites within Medmerry would not give an appropriate representation of the evolution of the sediment regime across the MR site, and multiple monitoring sites are needed.

Table 5.21: Summary of analysis of bed elevation, relationship between physical and geochemical surface sediment properties and cohesive strength measurements from the Medmerry Managed Realignment Site.

Site	Former Land Use / Site Design	Bed Elevation	Sediment Properties	Cohesive Strength
Site 1	Pastoral grassland used to store excavated material during site construction. Cleared and levelled prior to site inundation.	Overall 12 mm increase. Decreased during summer and increased during winter.	Fluctuated initially then demonstrated seasonal variability in all properties.	Higher in the summer
Site 2a	Freshwater drainage channel (Grange Rife) cut and re-profiled during site construction.	Increased by 42 mm.	Evidence of seasonal variability observed in all properties apart from grain size.	Increased during summer
Site 2b	Low quality arable / pastoral land.	6.5 mm decrease.	Values varied throughout. Evidence of seasonality in chloride concentration.	Varied throughout
Site 3 Bank	Vegetated pastoral land.	19 mm decrease with evidence of seasonal variability.	Moisture concentration decreased during the study period, fluctuations in wet bulk density, porosity and chloride concentration suggest evidence of seasonality.	Possible seasonal variability peaking in spring / summer.

Site 3 Channel	Channel excavated during site construction.	44 mm increase with periodic rhythms of accretion and erosion (analysed in Chapter 6).	Variable throughout. Possible seasonality in grain size measurements.	Similar pattern to on the bank observed but generally lower.
Site 4	Large borrow pit created during site construction. Rarely inundated due to relatively high elevation compared to the tidal frame.	N/A	Moisture concentration decreased. Grain size increased in final measurements.	N/A
Site 5 Bank	Intensive arable site, used for growing barley. Last harvested two weeks prior to site inundation.	83 mm increase.	No clear trends but possible seasonality in loss on ignition values.	Initially decreased, but then increased beyond the detection limit.
Site 5 Borrow Pit	Near breach borrow pit excavated during site construction.	Almost 30 cm increase (analysed in Chapter 6).	Seasonal variability in bulk density, moisture concentration and porosity measurements.	Evidence of seasonality, peaking during the mid to late summer.

Table 5.22: Percentage variance (%) between plots taken in transect at Site 2b, Site 3, Site 5 and collectively. Density, wet bulk density; Moisture, moisture concentration; Porosity; Organic, loss on ignition; Cl^-, chloride concentration; d_{50}, median grain size; Mud, mud concentration (clay + silt); P_{stag}, cohesive strength meter measured critical erosion shear stress (stagnation pressure).

		Density	**Moisture**	**Porosity**	**Organic**	**Cl^-**	**d_{50}**	**Mud**	**P_{stag}**
August 2015	**Site 2b**	28.56	102.82	17.73	24.64	46.66	37.13	13.30	211.83
	Site 3	13.90	58.80	7.17	17.33	43.93	80.59	16.47	128.18
	Site 5	23.54	34.93	12.30	132.85	51.88	140.52	157.27	155.61
	Collectively	40.23	189.05	31.58	142.31	59.81	310.11	133.96	597.03
November 2015	**Site 2b**	51.24	78.30	22.81	79.97	48.62	21.47	3.81	
	Site 3	12.53	40.96	7.15	197.17	13.17	92.15	20.64	
	Site 5	50.11	53.29	18.01	86.81	29.45	120.96	117.23	
	Collectively	69.29	117.78	32.51	224.44	63.68	261.08	102.33	
June 2016	**Site 2b**	26.65	74.15	12.12	28.64	68.12	179.26	27.83	166.03
	Site 3	10.43	49.68	7.91	21.24	17.91	48.78	23.31	209.08
	Site 5	35.26	113.76	34.42	113.17	71.59	36.80	162.98	186.15
	Collectively	52.27	170.46	44.69	161.83	132.98	207.69	172.12	280.70

5.6.1 The Legacies of the Former Land Use and Site Construction

Bed elevation is considered to be the critical parameter in the design of MR sites (Howe et al., 2010), as elevation controls the hydroperiod which has a direct control on the colonisation of vegetation. However, this is an oversimplification, with changes in the sediment structure, geochemical and physical characteristics, including compaction and the collapse of pore space, resulting from the former land use and site construction processes needing to be considered (Spencer et al., 2017). Wet bulk density and moisture concentration both relate to the percentage of mud in natural intertidal cohesive sediment environments (e.g. Flemming and Delafontaine, 2000). Figure 5.16 presents the relationship between these parameters from the temporal and spatial measurements taken at Site 2b, the bank and channel at Site 3 and across Site 5.

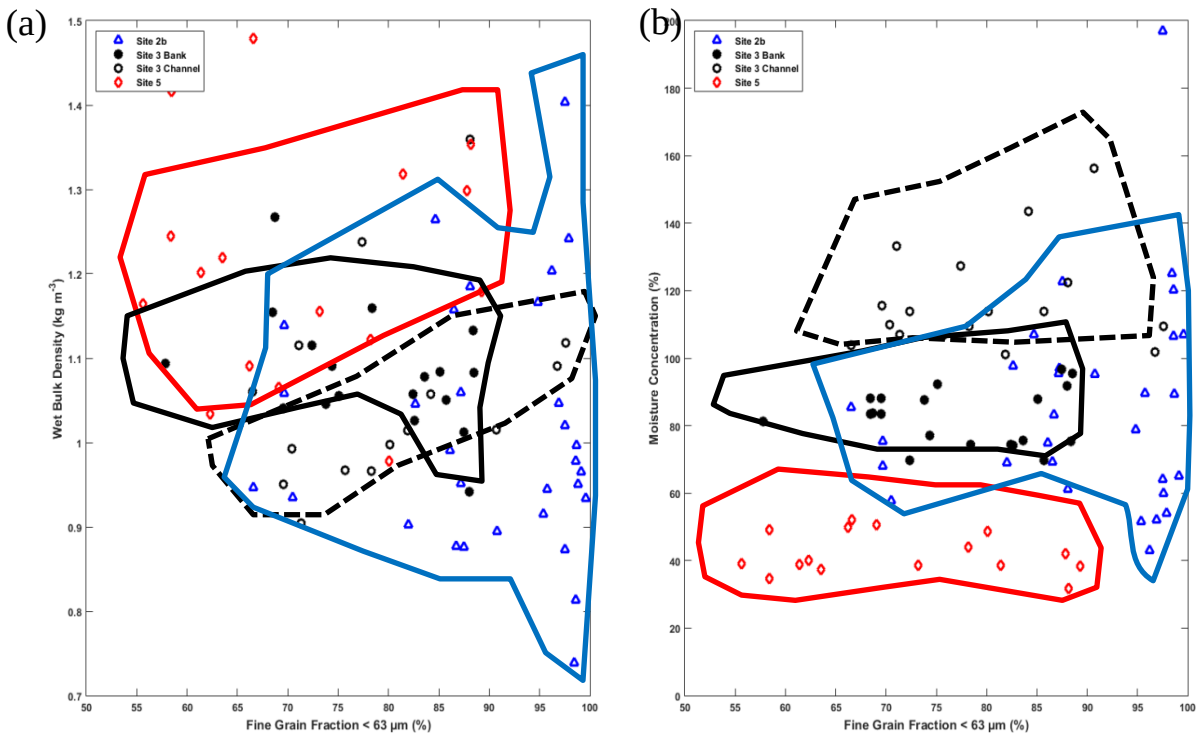

Figure 5.16: (a) Wet bulk density and (b) moisture concentration against the fine grained fraction < 63 µm (mud concentration) in the surface sediment at Site 2b, Site 3 (Bank and Channel) and Site 5 at the Medmerry Managed Realignment Site between March 2015 and October 2016. Only measurements with > 50 % mud (clay + silt) concentration are shown.

At Site 5, which had previously been used for intensive agricultural activity and had material extracted during site construction, there was a higher wet bulk density and lower moisture concentration compared to the other sites. Site 2b was used occasionally, and usually unsuccessfully, for agriculture, and the bank at Site 3 remained pastoral land. Both of these sites had similar moisture concentrations, although there was a greater range in wet bulk density measurements at Site 2b. Up to 1.5 m of soil were excavated to construct the channel at Site 3. The influence of the compaction caused by the heavy plant used to extract this material, and by the overburden of the removed material itself, has resulted in the sediment being unable to drain efficiently and becoming waterlogged, demonstrated in Figure 5.16 by the lower bulk density and high moisture concentration.

5.7 Summary

This chapter demonstrates that the bed elevation and sediment properties in the Medmerry Managed Realignment Site had begun to show indications of seasonal variations in the second and third year of tidal inundation. Analysis of sediment bulk density and moisture concentration across similar distributions of fine grained sediments demonstrate clear differences associated with compaction caused by the former land use and site construction. These results provide a new insight into the temporal and spatial changes in the sedimentary processes in terms of changes in bed elevation, surface physicochemical properties and the erodibility in a recently inundated MR site. However, further research is required to assess the lasting influence of disturbances caused by the former land use and site construction on the evolution of the sediment regime.

The results presented in this chapter will now be used to inform and support analysis of: hydrodynamics influencing the supply and removal of sediment and the rhythms of sedimentation (Chapter 6), the morphogenesis and evolution of embryonic creek networks (Chapter 7), and the evolution of the sub-surface sediment environment (Chapter 8). Analysis of these areas will provide further insight into changes in sediment drainage, cycling of sediment and the influence, and preservation, of the

sub-surface terrestrial soil horizon, which in turn influence the ecosystem function and structure, and therefore the ecosystem services and the success of the scheme.

6 Hydrodynamics and sedimentary processes

6.1 Introduction

The influence of physical disturbances, resulting from the former land use, site design and construction, on the evolution of the sediment regime at the Medmerry Managed Realignment Site have so far been investigated in terms of changes to the surface bed elevation, sediment physical and geochemical properties and cohesive strength (Chapter 5). This chapter presents an evaluation of the evolution of the sediment regime at Medmerry (Figure 6.1) through measurements of the rhythmic sedimentation patterns or rhythmites (Dale et al., 2017) taken using NKE ALTUS altimeter systems (see Section 4.2.1) at Site 3 and Site 5. The hydrodynamics (salinity, temperature depth) and variations in suspended sediment concentration (SSC) at Site 2b, Site 3, Site 5 and the breach, were also measured using YSI EXO2 Sondes (see Section 4.5.1).

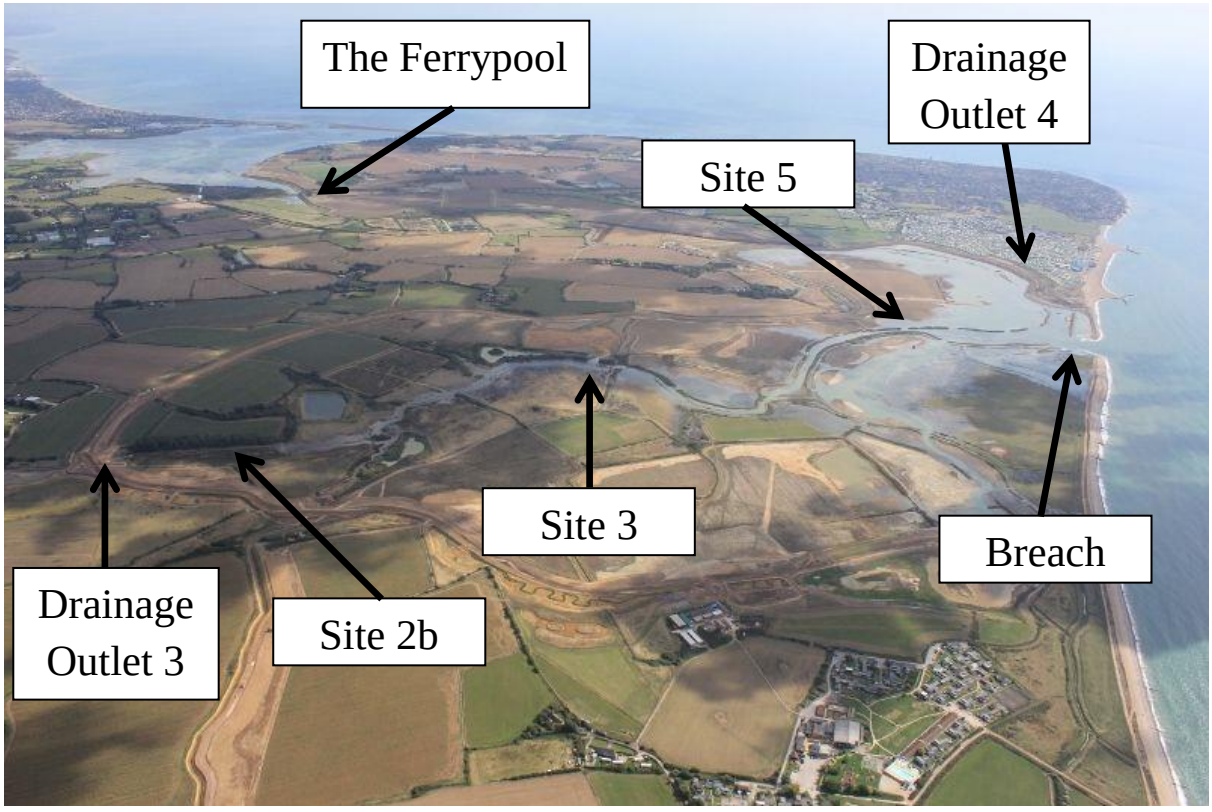

Figure 6.1: Sites analysed and discussed in Chapter 6 (looking south-eastwards, photograph: John Akerman).

6.2 Comparison between Two Heavily Engineered Environments

High frequency bed elevation and near-bed hydrodynamic and SSC measurements were taken from the excavated channel at Site 3 (Section 3.3.4), in the centre of the Medmerry site, and the near-breach borrow pit at Site 5 (Section 3.3.6). Measurements were taken for a one year period, from 1st November 2014 to 31st October 2015, and evaluated to assess: (i) the local hydrodynamics and its influence on sediment supply and erosion / accretion, and (ii) differences in the rates of sedimentation and erosion, patterns of sediment accumulation, and sediment supply and sources at the two sites on short (tidal), medium (lunar) and longer (annual) time scales.

6.2.1 Hydrodynamic Analysis

To quantify temporal variations in the hydrodynamics at different time scales, data were classified into:

1. Spring and neap tidal data, divided using the mean tidal range at each site during the measurement period. Tides where the change in water level (low to high) was greater than the average tidal range were classified as spring tides, whereas tides with a change in water level less than the average range were classified as neap tides. At Site 3 the average tidal range was 1.92 m, whereas at Site 5 the range was 1.50 m. This classification divided the measurements into two, approximately equal, groups, which were visually examined against the predicted semi-lunar and observed high water variability.
2. Summer and winter periods. Winter measurements were defined as the period between November and April and summer measurements as the period May to October (e.g. Fettweis et al., 1998).

To quantitatively assess temporal differences in the driving mechanism of variations in SSC over a tidal cycle, Pearson's Linear Correlation Coefficients were calculated between each variable and the level of suspended sediment for each point in the tide,

relative to high water. After checking the normality of the data, correlation coefficients (*r*) were calculated, with statistical significance (*P*) measured to the 95 % confidence interval throughout.

6.2.1.1 Site 3

Tidal averaged (12 hour running mean) hydrodynamic measurements for Site 3 are presented in Figure 6.2. Missing data are due to equipment failure or have been considered to be an anomaly (e.g. weed wrapped around sensor). At Site 3, the maximum high water depth measured was 3.57 mOD in October 2015 and the minimum recorded low water was 0.49 mOD in June 2015. The average tidal ranges for different time periods are displayed in Table 6.1. Differences in the tidal range were predominantly controlled by the semi-lunar tidal cycle, with spring tidal ranges being around 14 % larger than neap tidal ranges.

A maximum salinity value of 38.03 PSU was measured in August 2015 and a minimum value of 6.28 PSU in January 2015. Salinities were almost 30 % higher during the summer than the winter, whilst spring tides tended to be 15 % more saline than neap tides (Table 6.2). Water temperatures decreased during the winter and increased during the summer before beginning to decrease again during September and October, and showed very little semi-diurnal or semi-lunar variance (Table 6.3).

Initially, the average SSC per tide at Site 3 was highly variable before remaining relatively constant from February until October, when concentrations became variable again (Figure 6.2d). Overall, no clear relationship between SSC and tidal range (spring or neap tides) was observed over the measurement period (Table 6.4). During winter, SSCs were over 21 % greater than those in summer with levels of suspended sediment greater during neap tide, whereas the average SSC was greater during spring tides in the summer.

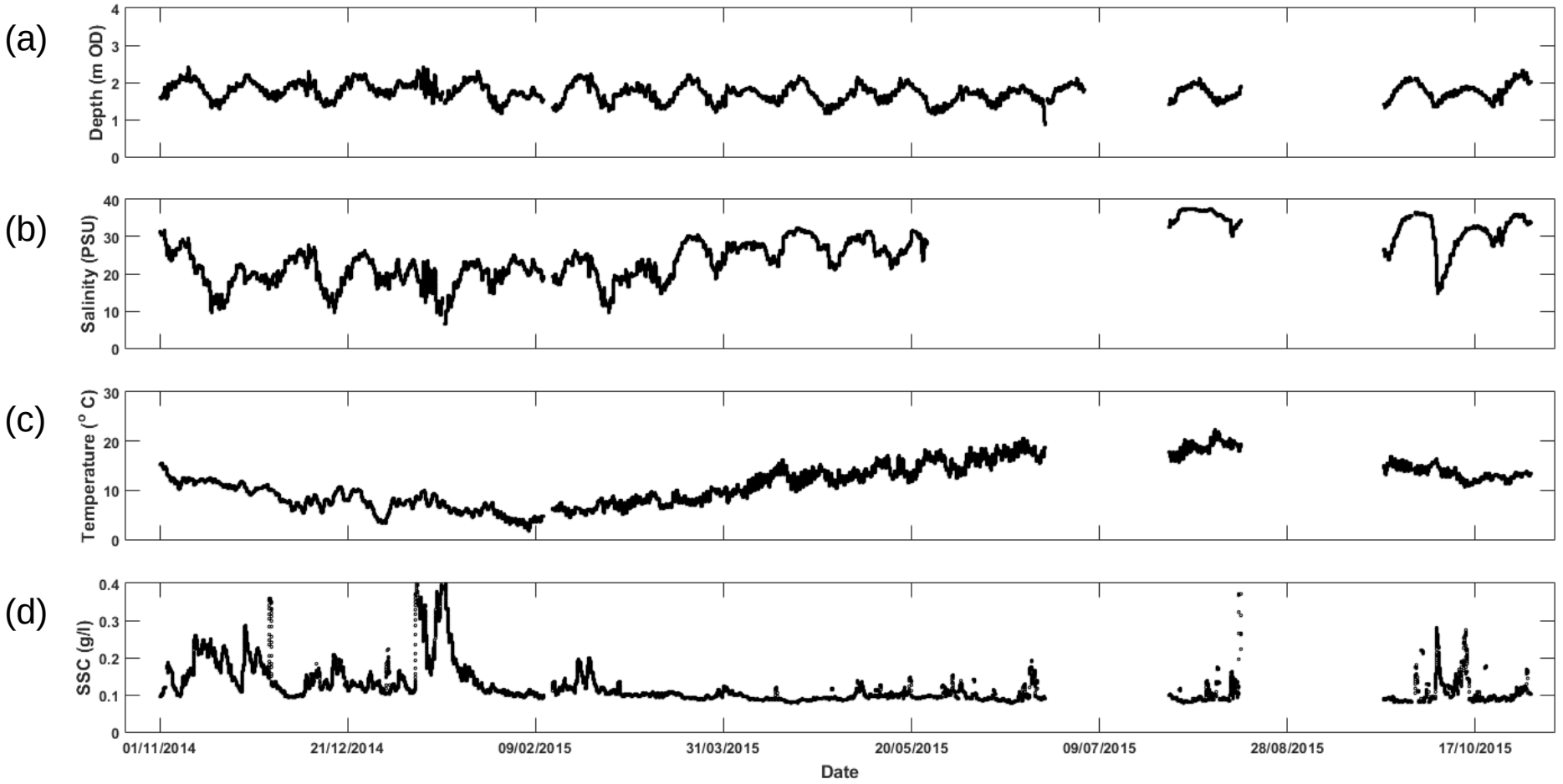

Figure 6.2: Tidal averaged (a) depth, (b) salinity, (c) temperature and (d) suspended sediment concentration (SSC) November 2014 to October 2015, Site 3, Medmerry Managed Realignment Site.

Table 6.1: Average tidal range (maximum-minimum depth during each tidal cycle) and standard deviation in metres for different tidal conditions over a one year period, winter and summer, Site 3, Medmerry Managed Realignment Site..

	All Tides	Spring Tide	Neap Tide
Year	1.92 ± 0.32	2.03 ± 0.31	1.74 ± 0.25
Winter	1.89 ± 0.33	2.00 ± 0.31	1.74 ± 0.26
Summer	1.96 ± 0.32	2.07 ± 0.29	1.71 ± 0.27

Table 6.2: Average salinity (PSU) and standard deviation for different tidal conditions over a one year period, winter and summer, Site 3, Medmerry Managed Realignment Site.

	All Tides	Spring Tide	Neap Tide
Year	24.58 ± 6.56	26.18 ± 10.81	22.25 ± 11.49
Winter	21.66 ± 4.82	22.41 ± 11.71	19.44 ± 11.47
Summer	30.95 ± 4.82	31.89 ± 5.67	29.37 ± 7.92

Table 6.3: Average temperature (°C) values and standard deviation for different tidal conditions over a one year period, winter and summer, Site 3, Medmerry Managed Realignment Site.

	All Tides	Spring Tide	Neap Tide
Year	11.19 ± 4.39	10.90 ± 4.15	11.05 ± 4.44
Winter	8.55 ± 2.96	8.27 ± 2.63	8.61 ± 2.98
Summer	15.37 ± 2.71	14.86 ± 2.57	15.67 ± 2.77

Table 6.4: Average suspended sediment concentration (g/l) and standard deviation for different tidal conditions over a one year period, winter and summer, Site 3, Medmerry Managed Realignment Site.

	All Tides	Spring Tide	Neap Tide
Year	0.12 ± 0.06	0.12 ± 0.06	0.12 ± 0.06
Winter	0.14 ± 0.07	0.10 ± 0.05	0.14 ± 0.07
Summer	0.11 ± 0.05	0.14 ± 0.06	0.11 ± 0.09

SSC had the highest correlation with water depth during winter spring tides, when positive correlations were found during the flood tide and negative correlations during the ebb, with statistically nonsignificant relationships two hours either side of high water (Figure 6.3). Generally, a negative relationship was found between salinity and SSC with statistically significant correlation coefficients tending to occur either side of high water (Figure 6.4). The relationship between salinity and SSC was most prominent during winter ebb neap tides (Figure 6.4f) and was usually stronger during neap tides compared to springs. The relationship between spring tide salinities and SSCs was weaker during the summer months (Figure 6.4h).

6.2.1.2 Site 5

Tidal averaged (12 hour running mean) hydrodynamic measurements for Site 5 are presented in Figure 6.5. The maximum depth measured at Site 5 was 2.23 mOD, recorded in October 2015. During large tides the site drained below the position of the depth sensor. Average tidal range varied on both a seasonal and semi-lunar scale (Table 6.5); on average spring tides had a 23 % greater range than neaps, whereas during the summer the tidal range was on average 32 % the tidal range during the winter. At Site 5 the maximum measured salinity was 37.33 PSU in September 2015, whereas the lowest recorded salinity was 4.64 PSU in December 2014. Averaged salinity values showed a small amount of seasonal and semi-lunar variation (Table 6.6). In contrast to Site 3, variations in salinity were minimal over a tidal cycle. Temperature variations matched those at Site 3 (Table 6.7).

SSCs varied throughout the measurement period at Site 5 (Figure 6.5), although SSCs were 25 % greater during spring than neap tides (Table 6.8). Unlike Site 3, no overall relationships between depth and SSC were detected on a semi-diurnal scale. Low correlation coefficients were found between salinity and SSC at Site 5 during the 12 month measurement period, which were not significant at the 95 % confidence level (Figure 6.7), with the exception of during winter spring tides (Figure 6.7e). During these tides statistically significant negative correlations were found between salinity and SSC during the tidal cycle.

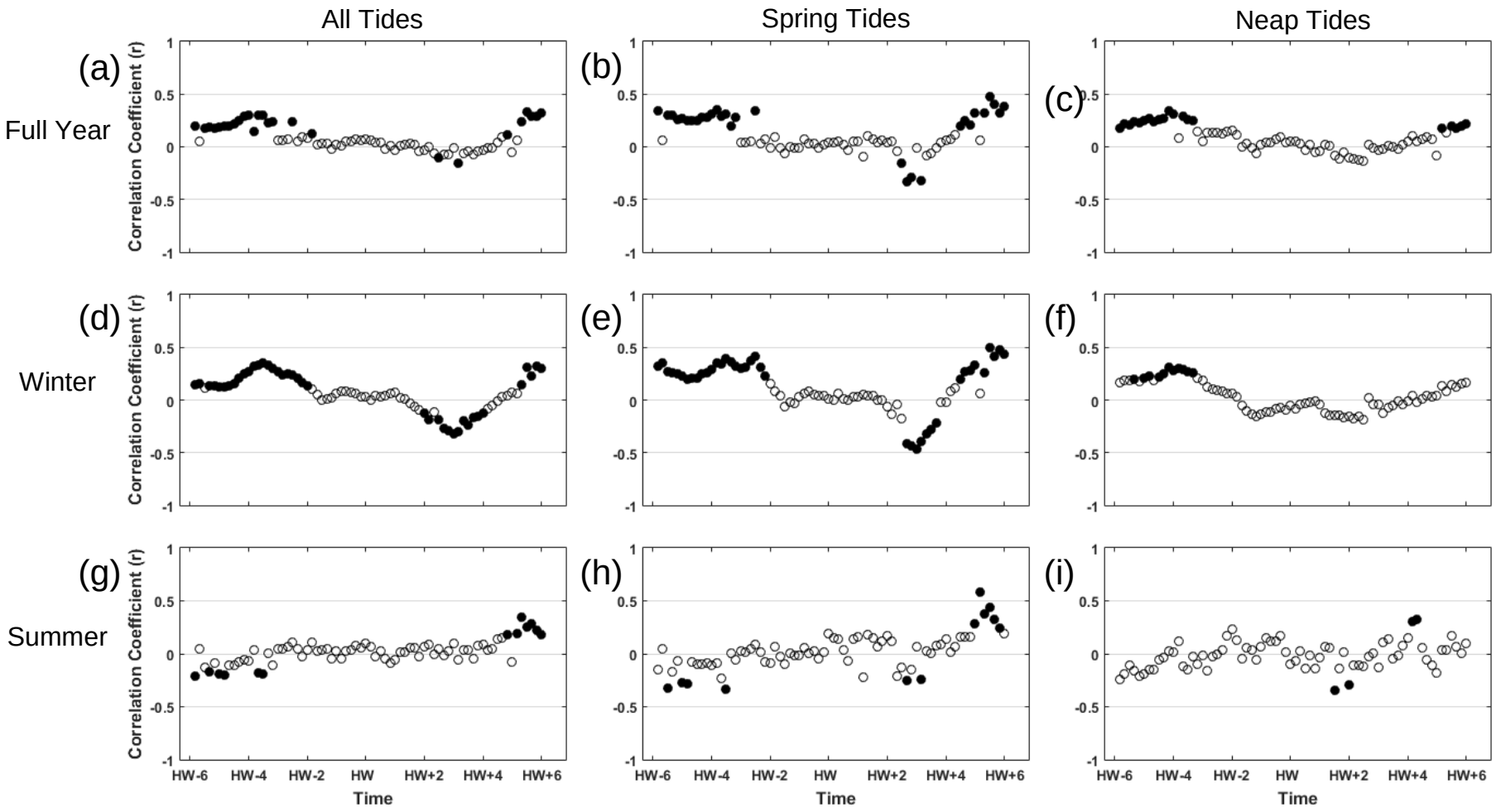

Figure 6.3: Pearson's Correlation Coefficients for the relationship between depth and suspended sediment concentration for each point in the tidal cycle during (a) all tides over a year, (b) all spring tides over a year, (c) all neap tides over a year, (d) all winter tides, (e) winter spring tides, (f) winter neap tides, (g) all summer tides, (h) summer spring tides, (i) summer neap tides at Site 3, Medmerry Managed Realignment Site. Filled circles are statistically significant at the 95 % confidence interval.

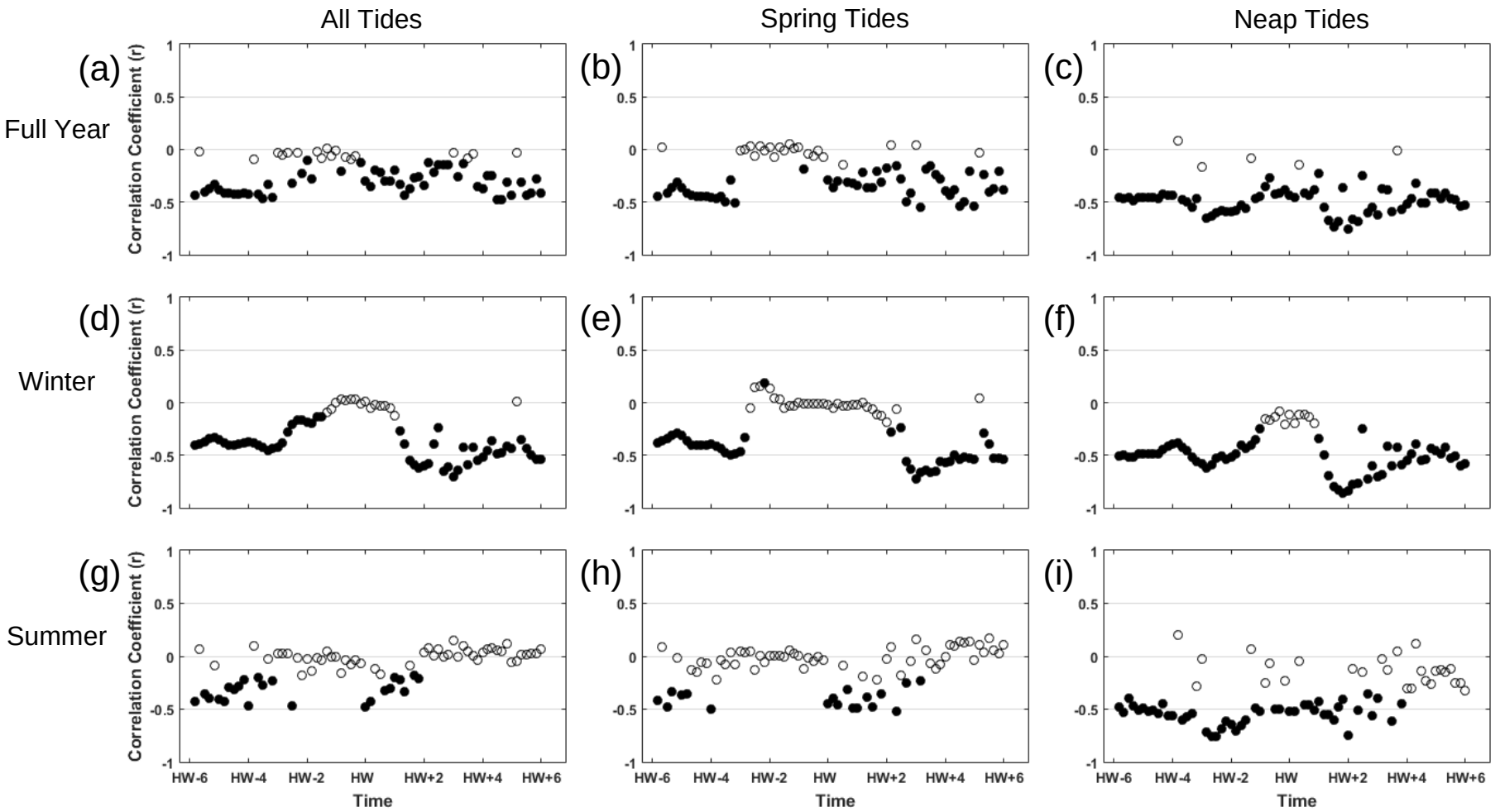

Figure 6.4: Pearson's Correlation Coefficients for the relationship between salinity and suspended sediment concentration for each point in the tidal cycle during (a) all tides over a year, (b) all spring tides over a year, (c) all neap tides over a year, (d) all winter tides, (e) winter spring tides, (f) winter neap tides, (g) all summer tides, (h) summer spring tides, (i) summer neap tides at Site 3, Medmerry Managed Realignment Site. Filled circles are statistically significant at the 95 % confidence interval.

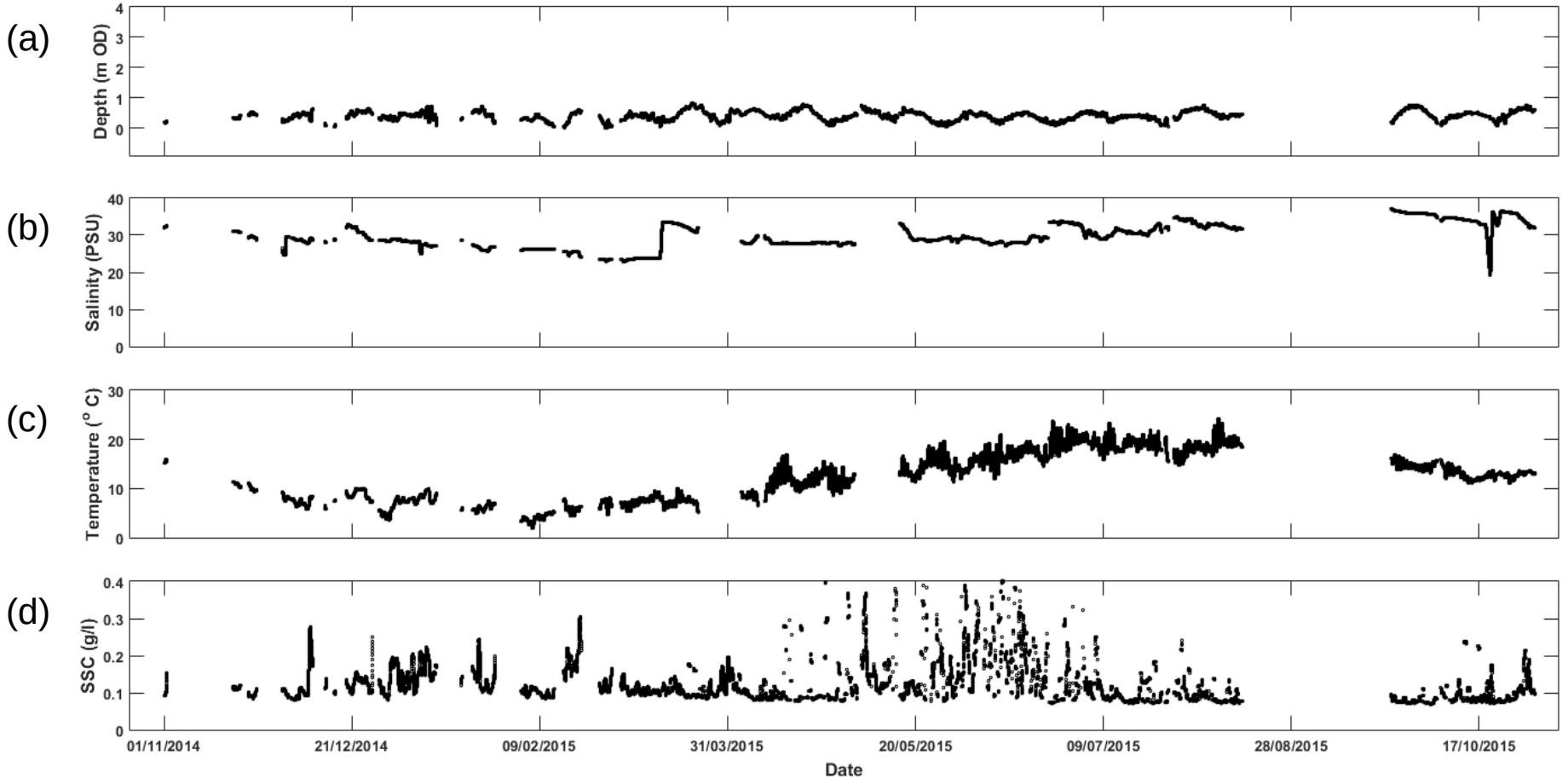

Figure 6.5: Tidal averaged (a) depth, (b) salinity, (c) temperature and (d) suspended sediment concentration (SSC) November 2014 to October 2015, Site 5, Medmerry Managed Realignment Site.

Table 6.5: Average tidal range (maximum-minimum depth during each tidal cycle) and standard deviation in metres for different tidal conditions over a one year period, winter and summer, Site 5, Medmerry Managed Realignment Site.

	All Tides	Spring Tide	Neap Tide
Year	1.60 ± 0.35	1.75 ± 0.28	1.34 ± 0.31
Winter	2.00 ± 0.31	2.09 ± 0.25	1.56 ± 0.26
Summer	1.36 ± 0.22	1.50 ± 0.21	1.13 ± 0.22

Table 6.6: Average salinity (PSU) and standard deviation for different tidal conditions over a one year period, winter and summer, Site 5, Medmerry Managed Realignment Site.

	All Tides	Spring Tide	Neap Tide
Year	29.76 ± 3.38	30.23 ± 3.34	29.48 ± 3.49
Winter	27.98 ± 2.75	28.34 ± 2.43	27.66 + 2.96
Summer	31.70 ± 2.89	32.05 ± 3.07	31.50 ± 2.86

Table 6.7: Average temperature (°C) and standard deviation for different tidal conditions over a one year period, winter and summer, Site 5, Medmerry Managed Realignment Site.

	All Tides	Spring Tide	Neap Tide
Year	12.12 ± 5.06	12.26 ± 4.85	12.19 ± 5.39
Winter	8.32 ± 2.93	8.34 ± 2.72	8.13 ± 3.03
Summer	16.26 ± 3.34	16.03 ± 3.16	16.71 ± 3.52

Table 6.8: Average suspended sediment concentration (g/l) and standard deviation for different tidal conditions over a one year period, winter and summer, Site 5, Medmerry Managed Realignment Site.

	All Tides	Spring Tide	Neap Tide
Year	0.15 ± 0.11	0.16 ± 0.14	0.12 ± 0.07
Winter	0.16 ± 0.14	0.16 ± 0.14	0.16 ± 0.15
Summer	0.14 ± 0.14	0.16 ± 0.14	0.11 ± 0.06

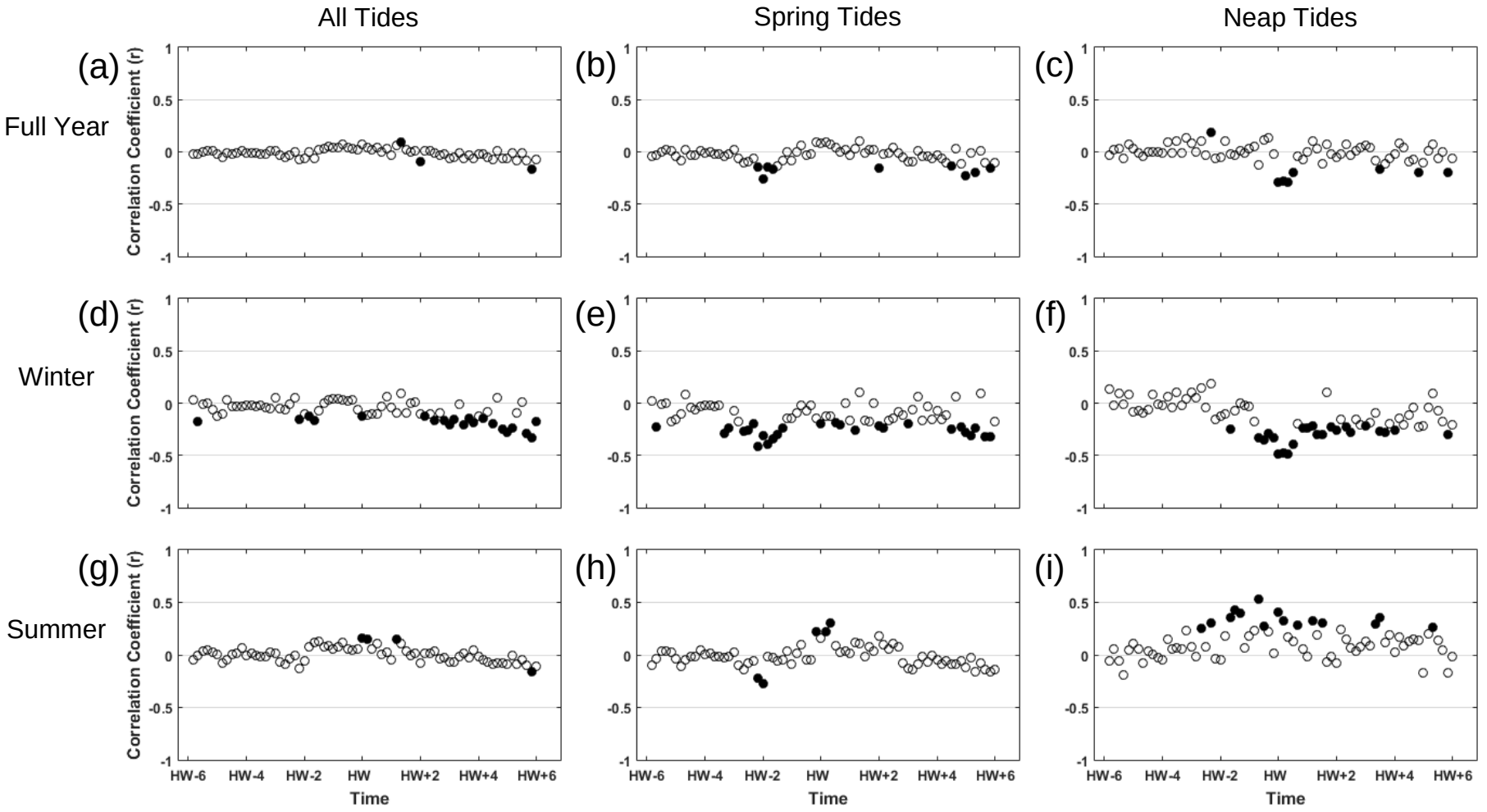

Figure 6.6: Pearson's Correlation Coefficients for the relationship between depth and suspended sediment concentration for each point in the tidal cycle during (a) all tides over a year, (b) all spring tides over a year, (c) all neap tides over a year, (d) all winter tides, (e) winter spring tides, (f) winter neap tides, (g) all summer tides, (h) summer spring tides, (i) summer neap tides at Site 5, Medmerry Managed Realignment Site. Filled circles are statistically significant at the 95 % confidence interval.

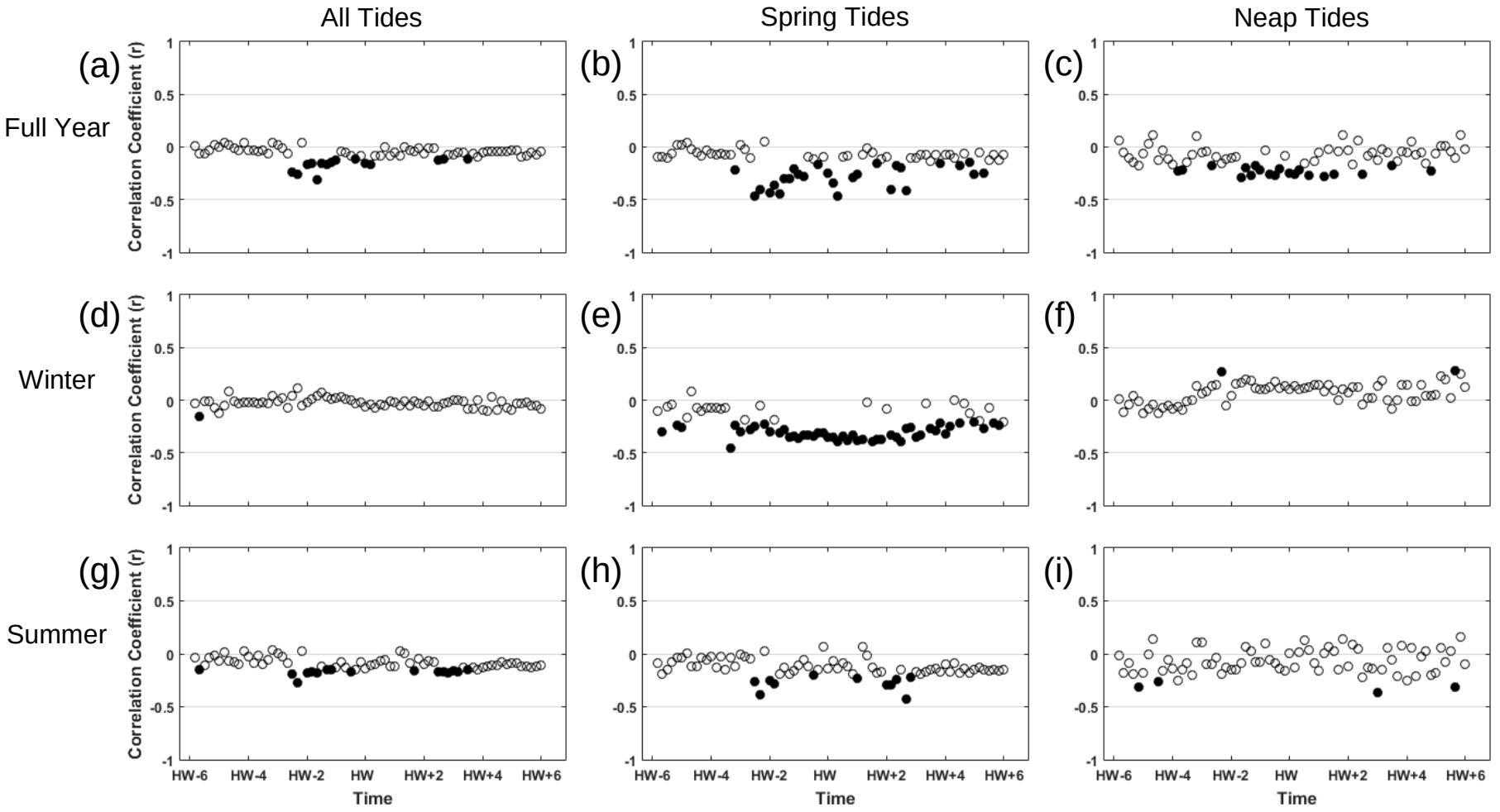

Figure 6.7: Pearson's Correlation Coefficients for the relationship between salinity and suspended sediment concentration for each point in the tidal cycle during (a) all tides over a year, (b) all spring tides over a year, (c) all neap tides over a year, (d) all winter tides, (e) winter spring tides, (f) winter neap tides, (g) all summer tides, (h) summer spring tides, (i) summer neap tides at Site 5, Medmerry Managed Realignment Site. Filled circles are statistically significant at the 95 % confidence interval.

6.2.2 Sedimentation Rhythms and Mechanisms

Bed elevation measurements were taken to assess sedimentation rhythms and evaluate rates of bed elevation change using an ALTUS altimeter at each site (previously reported in Chapter 5). Measurements were plotted on annual, monthly and tidal scales to identify any possible relationships between changes in the bed elevation and the hydrodynamics. A comparison of the annual bed level measurements at the two locations is presented in Figure 6.8.

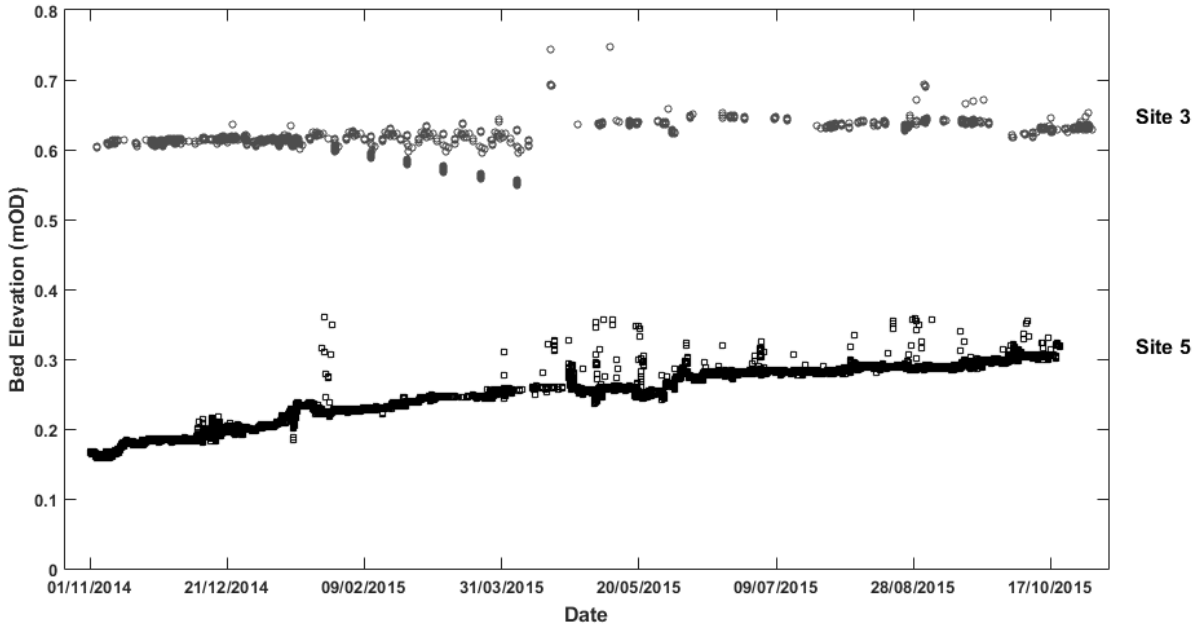

Figure 6.8: Bed elevation over 12 months at two sites at Medmerry Managed Realignment Site.

6.2.2.1 Site 3

A net increase in bed elevation of 2.7 cm over the 12 month period was measured at Site 3, with sedimentation controlled by the semi-lunar tidal cycle. On an annual scale, semi-lunar changes were slight in comparison to the net elevation change, with the exception of a period between January and March 2015 (Figure 6.8). On a monthly scale (Figure 6.9), however, a pattern of bed level increasing during the spring tide and decreasing or stabilising during neap tides was identified. Nonetheless, there was some disturbance to this pattern during high SSC events, during which bed elevation initially lowered and then increased for a number of tides, with SSC following a similar pattern.

A similar pattern was observed on a semi-diurnal scale (Figure 6.10), with particles settling during the flood tide and experiencing resuspension during the ebb tide. Deposition continued during high tide slack water, reaching a maximum approximately one hour after high water. Bed elevation then decreased as sediment was eroded by the outgoing tide. This is reflected in the SSC, with low levels of suspended sediment corresponding with the high bed elevations.

6.2.2.2 Site 5

During the measurement period, Site 5 received a net deposition of 15.2 cm (Figure 6.8). Near-constant sediment deposition was observed, with enhanced rates of deposition associated with higher levels of suspended sediment and deceleration in the rate of deposition related to lower SSCs. However, in contrast to Site 3, there was very little relationship between the semi-lunar tidal cycle and bed elevation (Figure 6.11). On a semi-diurnal scale, deposition of sediment occurred during the flood tide with most sediment deposited by high tide slack water (Figure 6.12), with further deposition occurring once water level had decreased. In the case of Figure 6.12, this resulted in a 0.5 cm thick sediment deposit. SSC showed some relation to bed elevation changes, decreasing as sedimentation occurred and remaining relatively stable once sediment had been deposited.

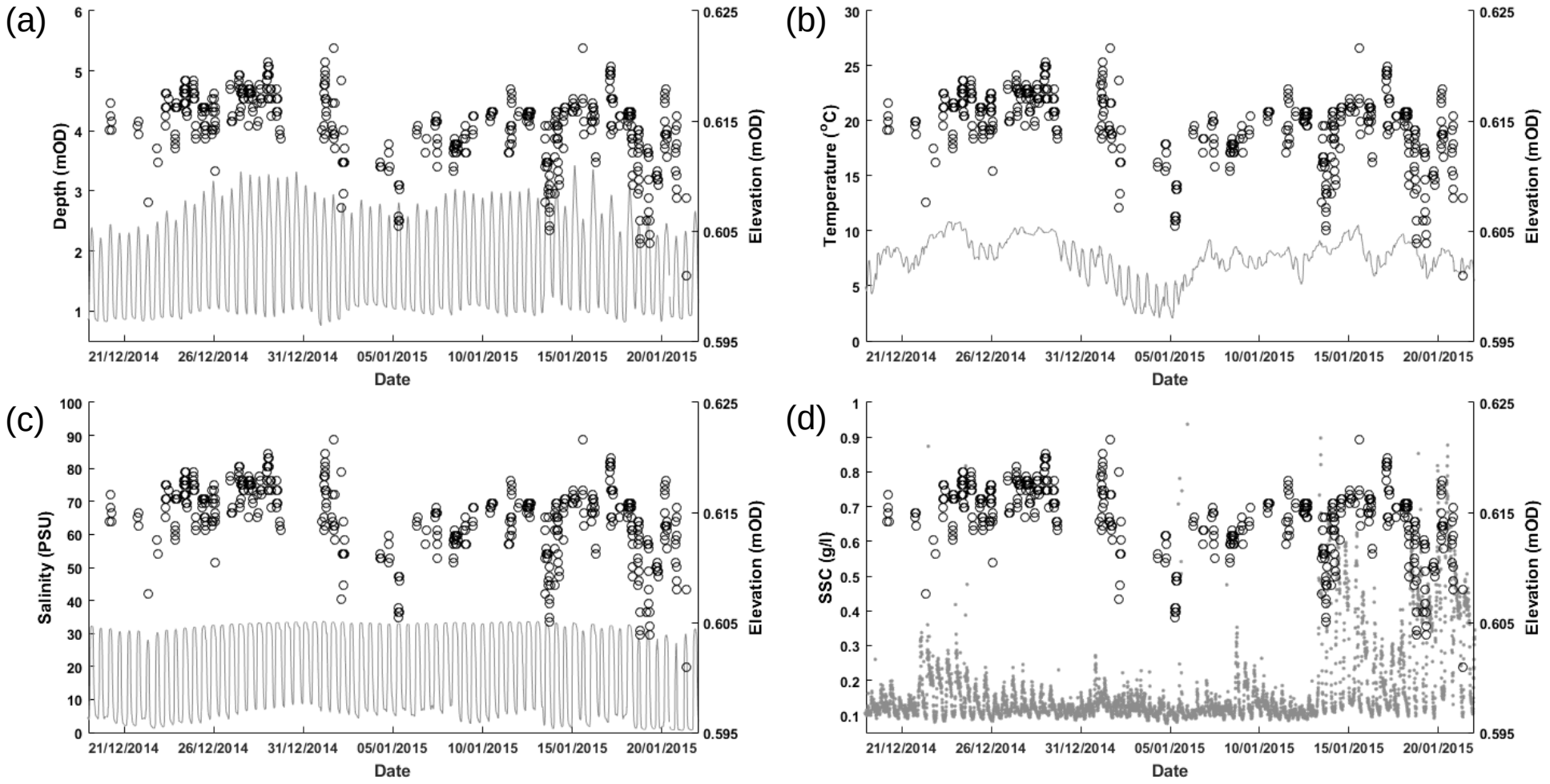

Figure 6.9: Comparisons between monthly sedimentation rhythms (circles) and (a) depth, (b) temperature, (c) salinity and (d) suspended sediment concentration (SSC) at Site 3, Medmerry Managed Realignment Site.

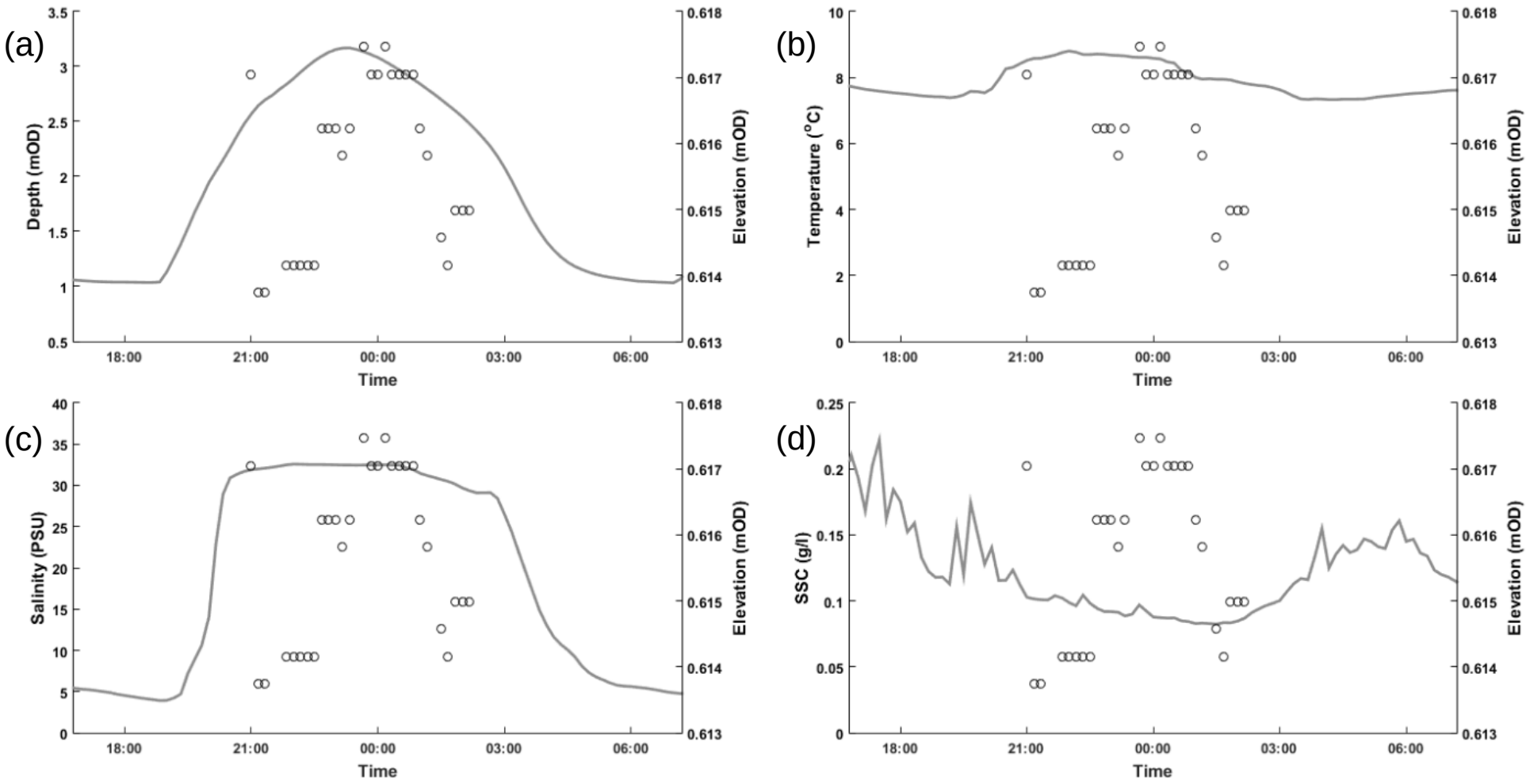

Figure 6.10: Comparisons between semi-diurnal bed elevation changes (circles) and (a) depth, (b) temperature, (c) salinity and (d) suspended sediment concentration (SSC) at Site 3, Medmerry Managed Realignment Site on 20th and 21st December 2014 representative of a typical flood-ebb tidal cycle.

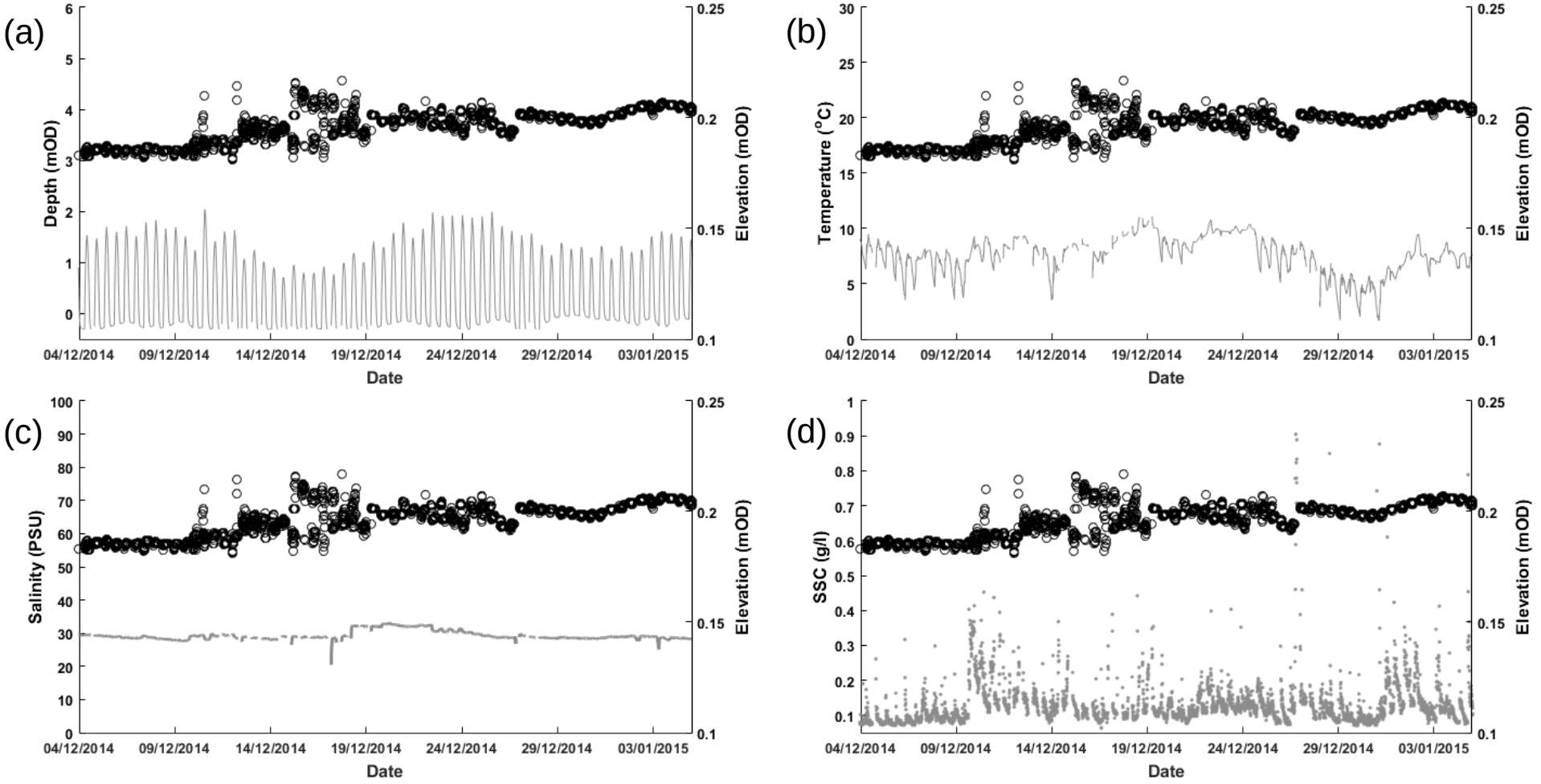

Figure 6.11: Comparisons between monthly sedimentation rhythms (circles) and (a) depth, (b) temperature, (c) salinity and (d) suspended sediment concentration (SSC) at Site 5, Medmerry Managed Realignment Site.

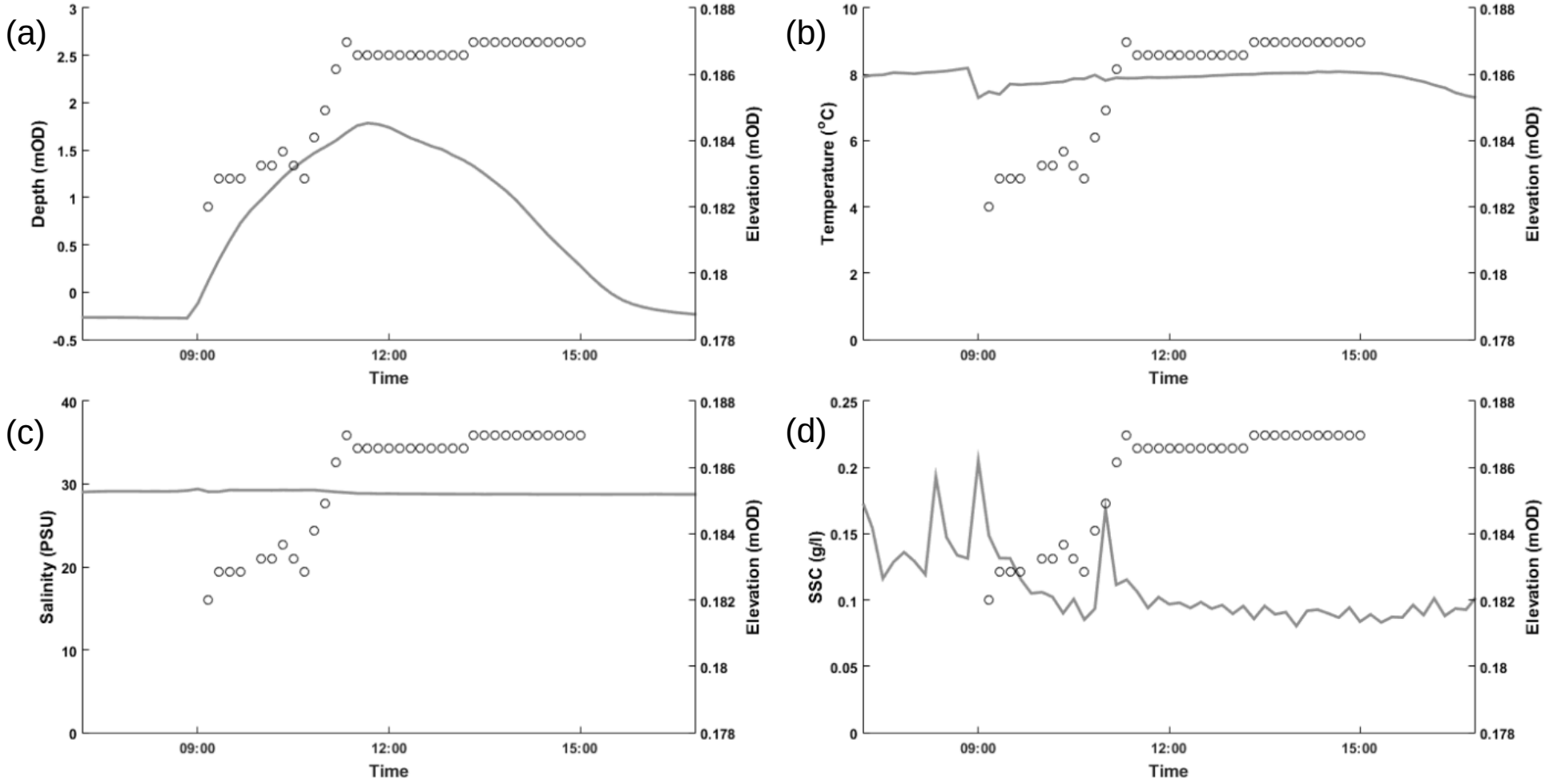

Figure 6.12: Comparisons between semi-diurnal bed elevation changes (circles) and (a) depth, (b) temperature, (c) salinity and (d) suspended sediment concentration (SSC) at Site 5, Medmerry Managed Realignment Site on 7th December 2014 representative of a typical flood-ebb tidal cycle.

6.3 Hydrodynamic and Sedimentary Processes in the Main Drainage Channel

Near-bed measurements of the hydrodynamics and SSC were taken the following year from November 2015 to October 2016 at three sites along Easton Rife (see Section 4.5.2 for method); the breach, Site 3 and Site 2b (see Figure 6.1 for locations). These sites were selected to assess the fluxes of sediment transported from the wider terrestrial catchment (Site 2b) and levels of suspended sediment imported from and exported to the surrounding coastal environment (the breach). Repeated measurements at Site 3 provided a comparison between years and the SSC in the centre of the site, in comparison to the extremities of the site, leading to analysis of the internal redistribution of sediment. Temporal and spatial measurements of the water column were collected via static and longitudinal profiling (see Section 4.5.3 for method) to evaluate the level of stratification and the position of the turbidity maximum in the site.

6.3.1 Variations in Hydrodynamics and Sedimentation

6.3.1.1 Temporal Variability

Tidal averaged data (12 hour running mean) are presented for the breach (Figure 6.13), Site 3 (Figure 6.14) and Site 2b (Figure 6.15). The maximum recorded depth in the breach was 2.75 mOD in December 2015 whereas the lowest water depth, -0.61 mOD, occurred in October 2016. The highest and lowest salinities measured were 37.7 PSU and 0.48 PSU respectively, both occurring in October 2016. Measurements taken from a nearby weather station at the Ferrypool (see Figure 6.1 for location and Section 6.5.2 for discussion) suggests this low salinity value was caused by localised dilution as a result of rainfall during low water. Generally, salinity values rarely fell below 20 PSU at the breach. The SSC varied throughout with no clear trends or patterns showing in the data.

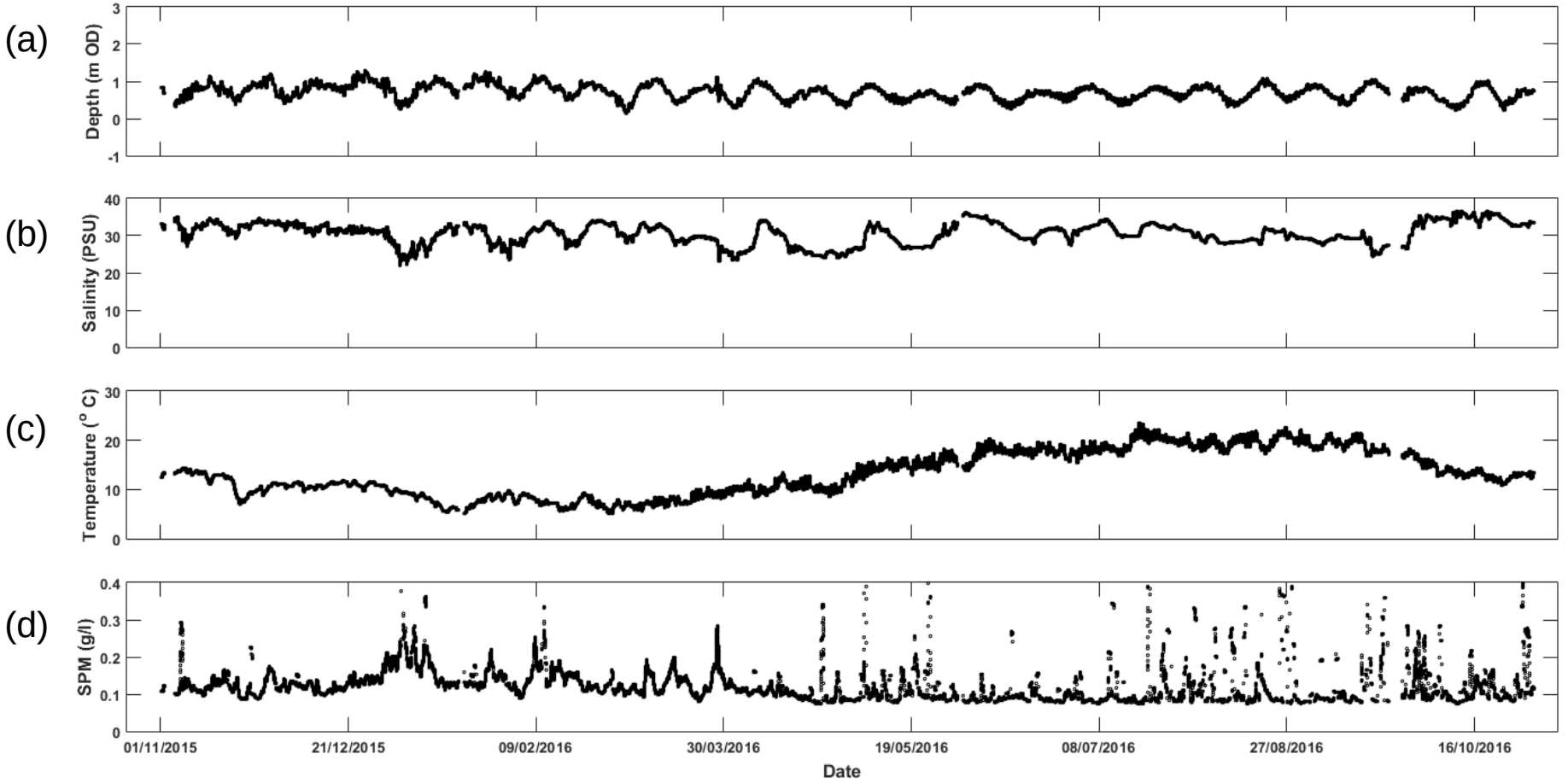

Figure 6.13: Tidal averaged (a) depth, (b) salinity, (c) temperature and (d) suspended sediment concentration (SSC) November 2015 to October 2016, the breach, Medmerry Managed Realignment Site.

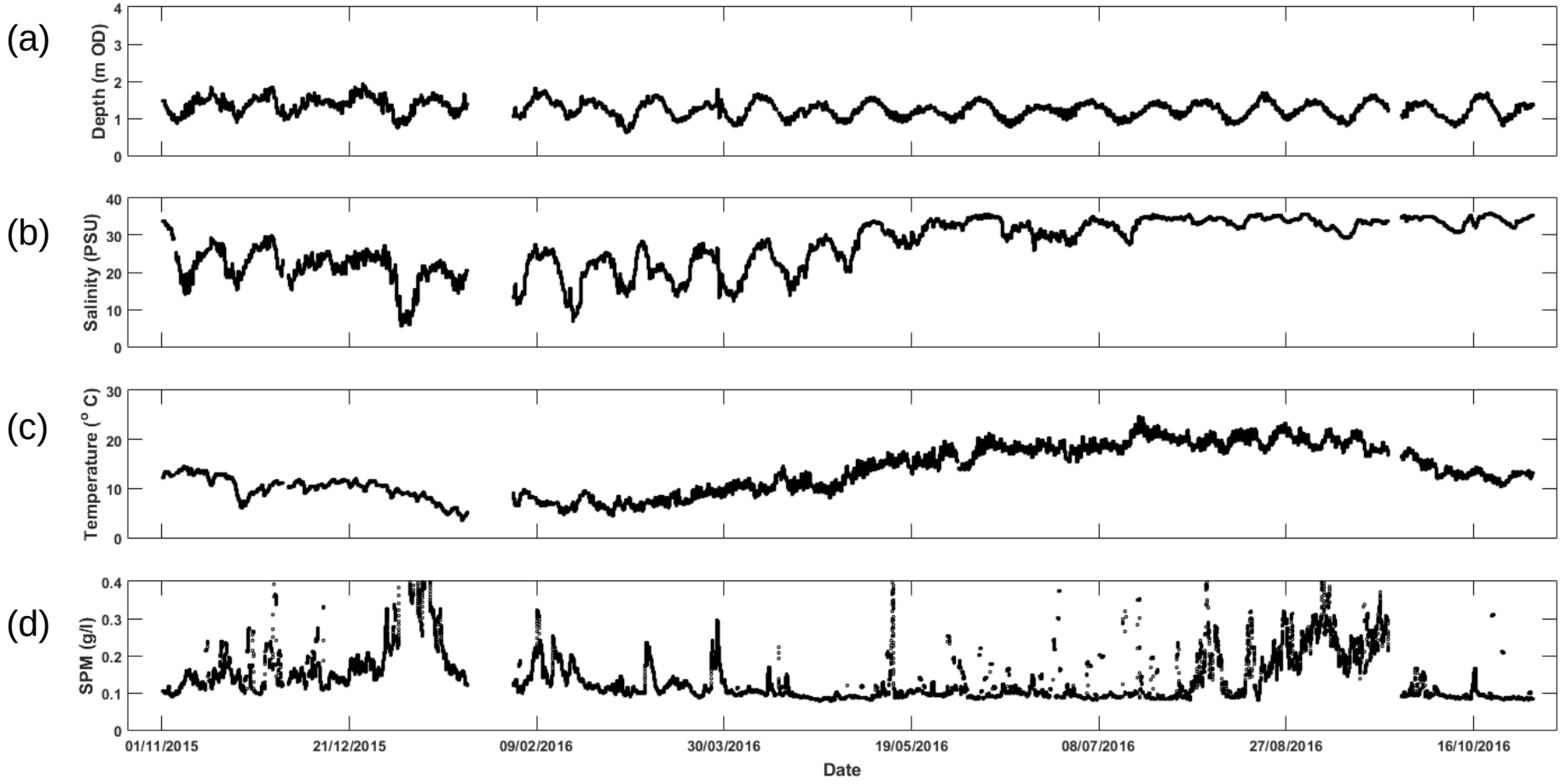

Figure 6.14: Tidal averaged (a) depth, (b) salinity, (c) temperature and (d) suspended sediment concentration (SSC) November 2015 to October 2016, Site 3, Medmerry Managed Realignment Site.

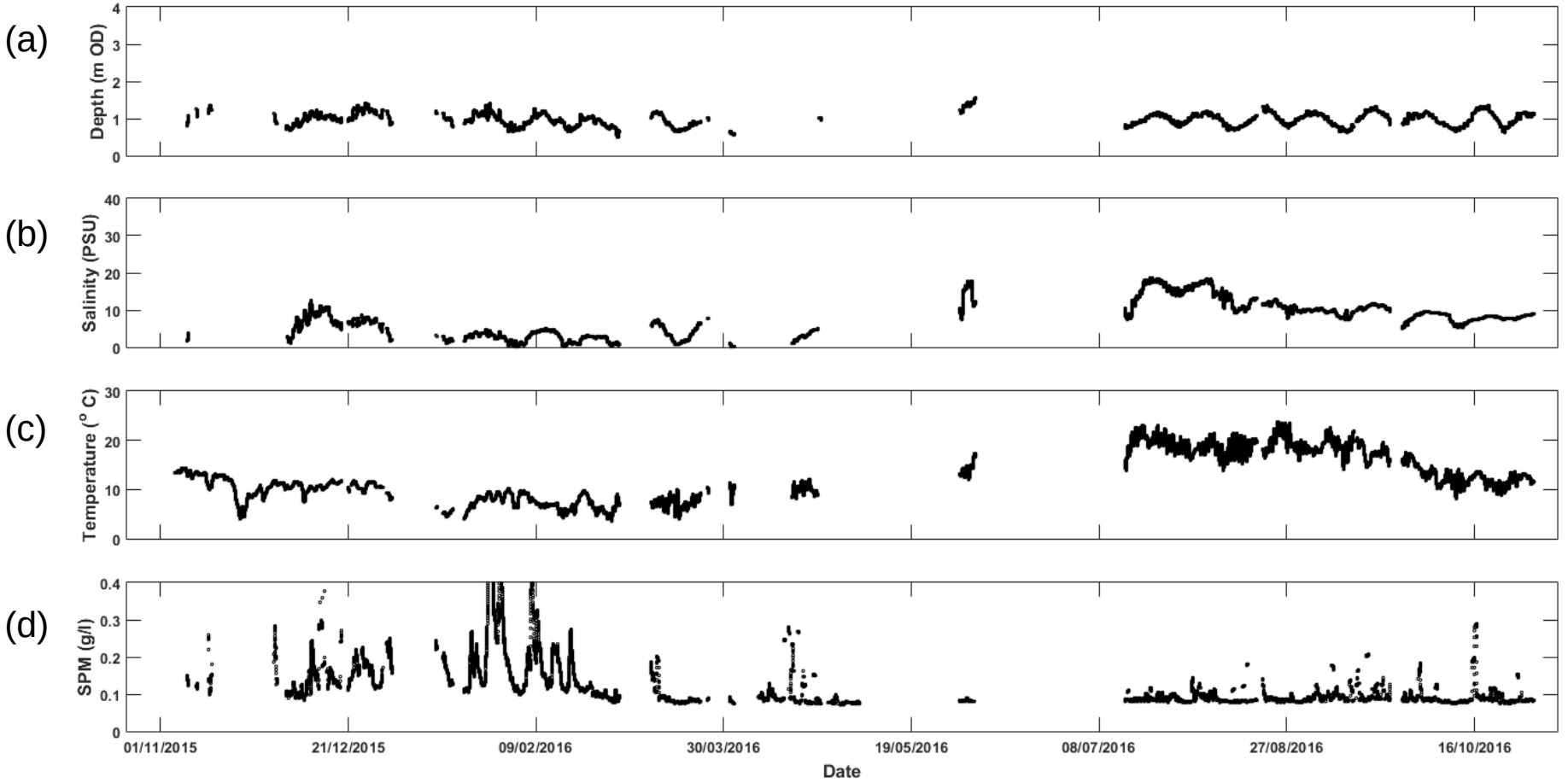

Figure 6.15: Tidal averaged (a) depth, (b) salinity, (c) temperature and (d) suspended sediment concentration (SSC) November 2015 to October 2016, Site 2b, Medmerry Managed Realignment Site.

Inland, at Site 3, the maximum depth recorded was 3.09 mOD in December 2015, almost half a metre lower than the maximum high water measured in the previous year (Section 6.2.1.1). The lowest water depth, 0.12 mOD, was measured in March 2016. High water at Site 3 occurs approximately 60 minutes after high water at the breach. Salinity values followed a similar trend to the previous year (see Section 6.2.1.1) with a maximum of 37.83 PSU recorded in May 2016 and a minimum of 0.88 PSU in January 2016, 5.4 PSU lower than the previous year. More variability in SSC was measured during the winter, and during August and September. Levels of suspended sediment tended to be higher at Site 3 in comparison to the breach.

In the excavated entrance of the borrow pit at Site 3, 1.7 cm of net accretion was measured (Figure 6.16); 1 cm less net accretion than measured during the previous year (Section 6.2.2.1). Rhythmic semi-lunar and semi-diurnal sedimentation patterns continued to be observed but additional evidence of seasonal variability was detected, with accretion during the winter and erosion during the summer. This pattern was periodically broken by larger erosion and accretion events, which appeared to be driven by additional variability separate from the seasonal, semi-lunar and semi-diurnal change.

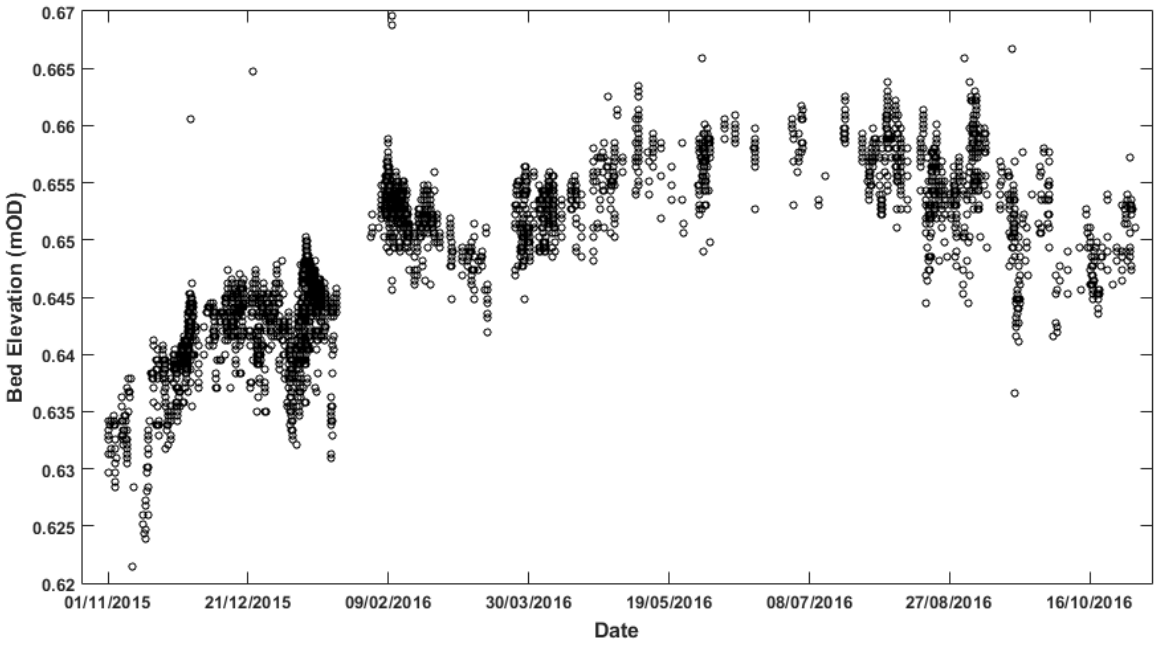

Figure 6.16: Bed elevation over 12 months (November 2015 – October 2016) at Site 3 at the Medmerry Managed Realignment Site.

At the landwards extremity of the site, Site 2b, a maximum measured water depth of 2.58 mOD occurred in June 2016. High water at this site occurs approximately 20 minutes after high water at Site 3, and 80 minutes after high water at the breach. During some low tides the channel drained below a measurable water depth (< 1 cm). The salinity at Site 2b remained relatively low (< 20 PSU) during the study period, although a maximum salinity of 32.9 PSU was measured in June 2016. The SSC initially demonstrated a high degree of variability until March 2016, when the magnitude of fluctuations in the concentration of suspended sediment decreased.

6.3.1.2 Spatial Variability

Monthly comparisons between depth, salinity and SSC for March and August 2016 are presented in Figure 6.17 for the breach, Figure 6.18 for Site 3 and Figure 6.19 for Site 2b. Examples of single spring and neap tidal events during both these months are presented in Figure 6.20 for the breach, Figure 6.21 for Site 3 and Figure 6.22 for Site 2b. During March differences in salinity between high and low water are observed in the breach (Figure 6.17) and at Site 3 (Figure 6.18), although the variability was greater at Site 3. This difference between high and low water is also seen on a semi-diurnal scale at Site 3 (Figure 6.21), although salinity values in the breach demonstrated little semi-diurnal variability during spring tides but fluctuated during neap tides. At Site 2b semi-diurnal changes in salinity (Figure 6.22) varied according to the semi-lunar tidal cycle (Figure 6.19), with a greater variability in salinity occurring during spring tides as a result of larger inputs of saline water to the site. During neap tides salinity values remained low with less variability due to reduced saline water incursion.

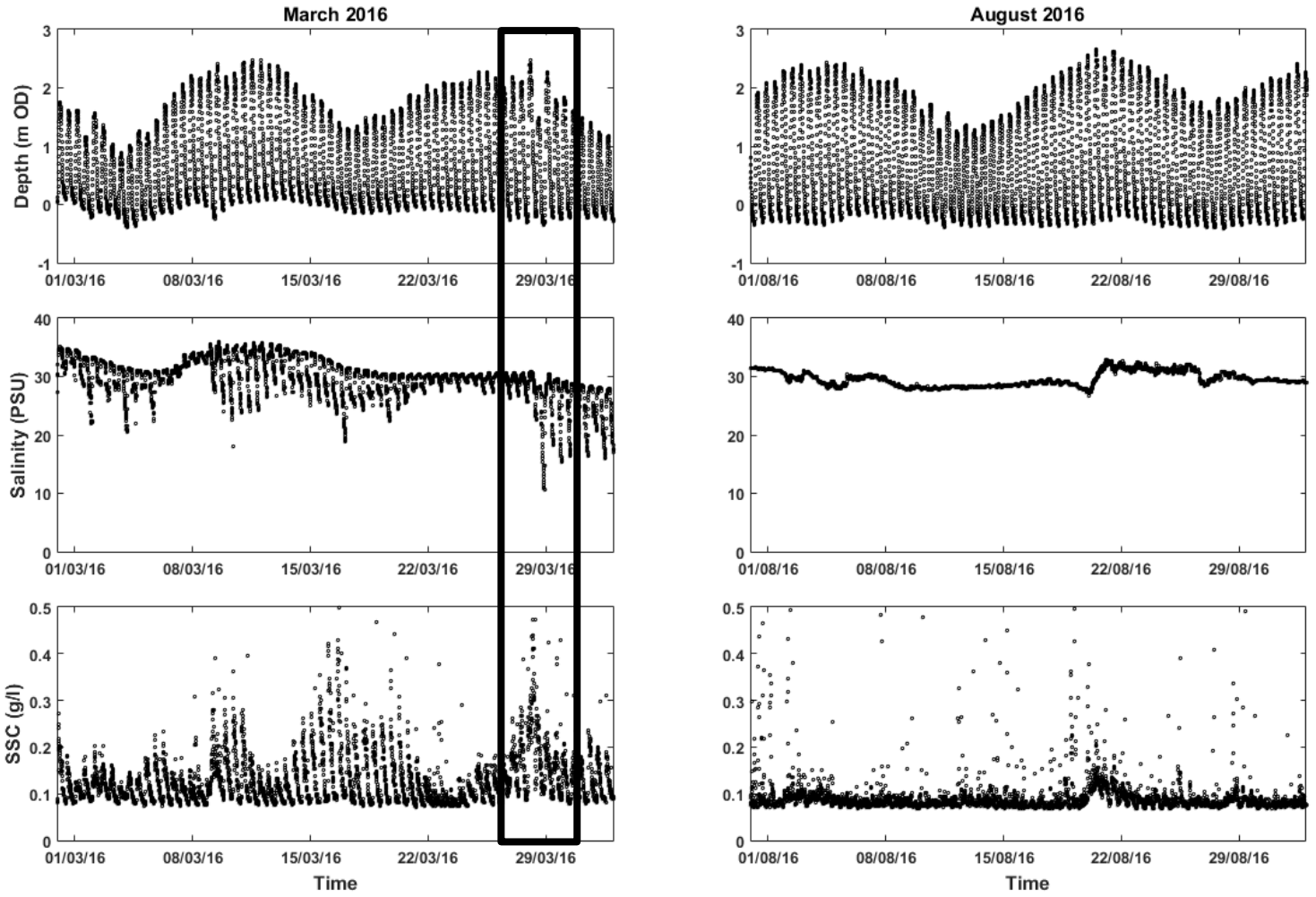

Figure 6.17: Comparison of depth, salinity and suspended sediment concentration (SSC) for the breach for March 2016 and August 2016. The black box marks the occurrences of a storm event (Storm Katie – see text for discussion).

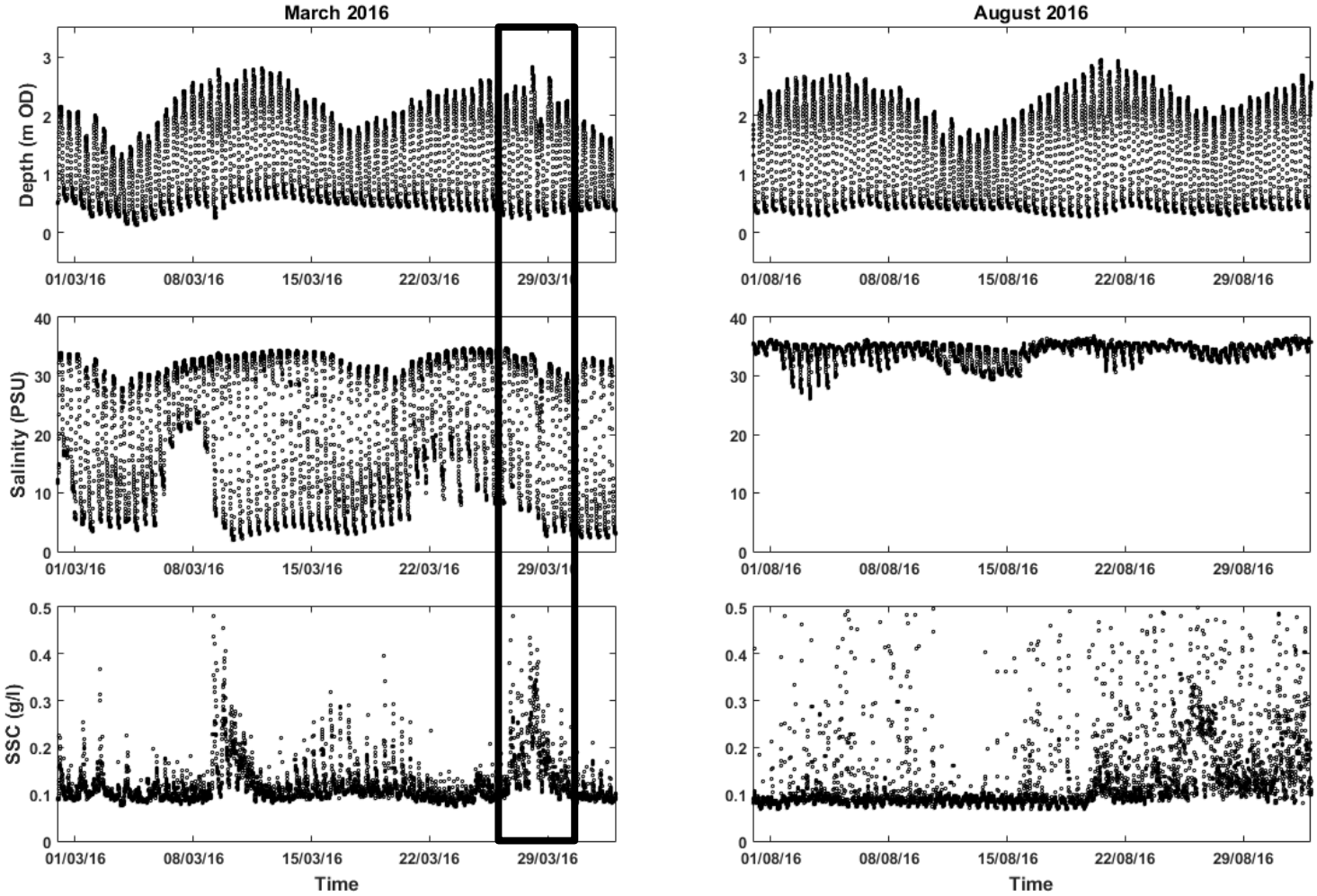

Figure 6.18: Comparison of depth, salinity and suspended sediment concentration (SSC) for Site 3 for March 2016 and August 2016. The black box marks the occurrences of a storm event (Storm Katie – see text for discussion).

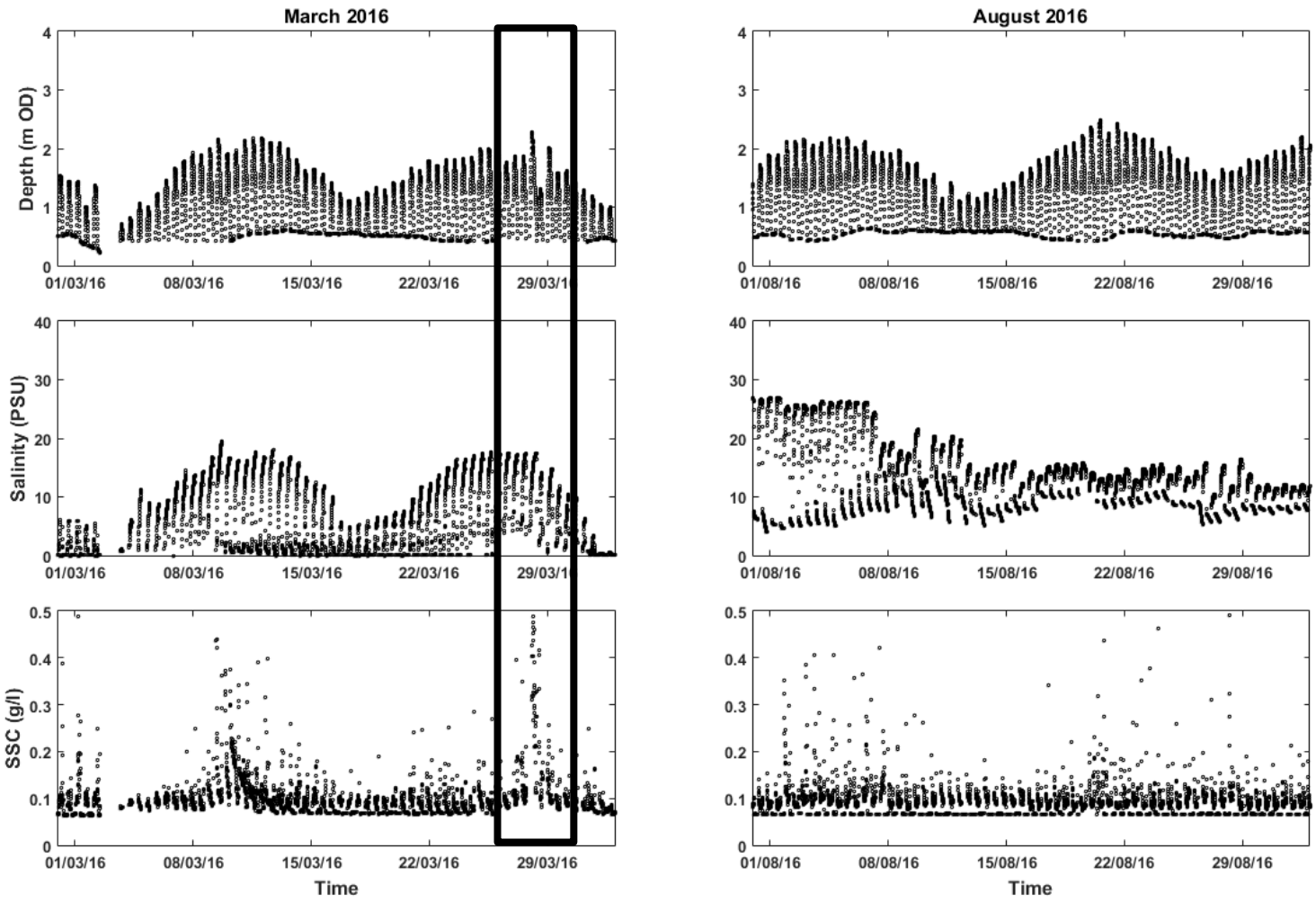

Figure 6.19: Comparison of depth, salinity and suspended sediment concentration (SSC) for Site 2b for March 2016 and August 2016. The black box marks the occurrences of a storm event (Storm Katie – see text for discussion).

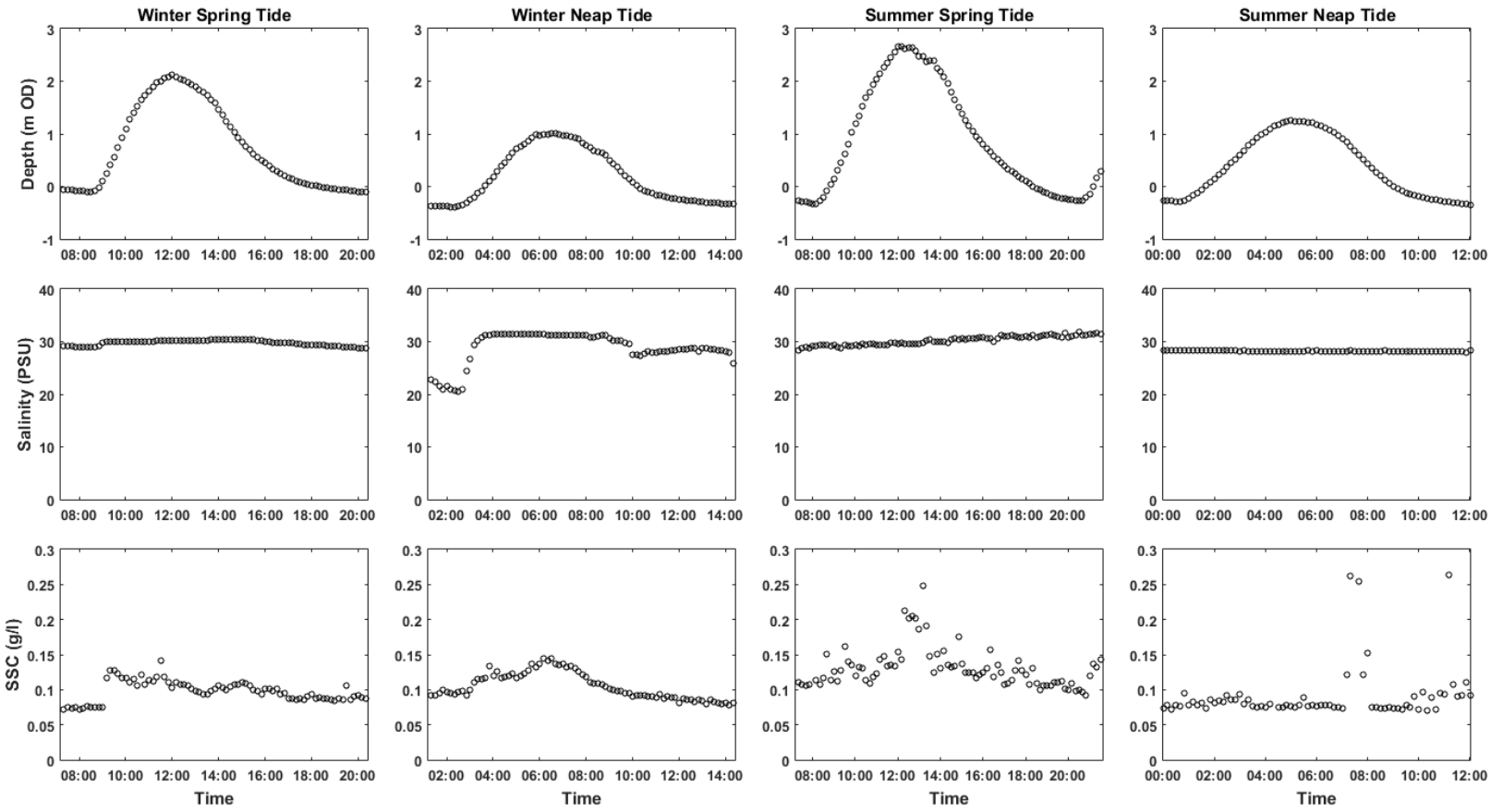

Figure 6.20: Comparison of depth, salinity and suspended sediment concentration (SSC) over a tidal cycle for the breach for a winter spring tide (24/3/2016), a winter neap tide (2/3/2016), a summer spring tide (20/8/2016) and a summer neap tide (12/8/2016).

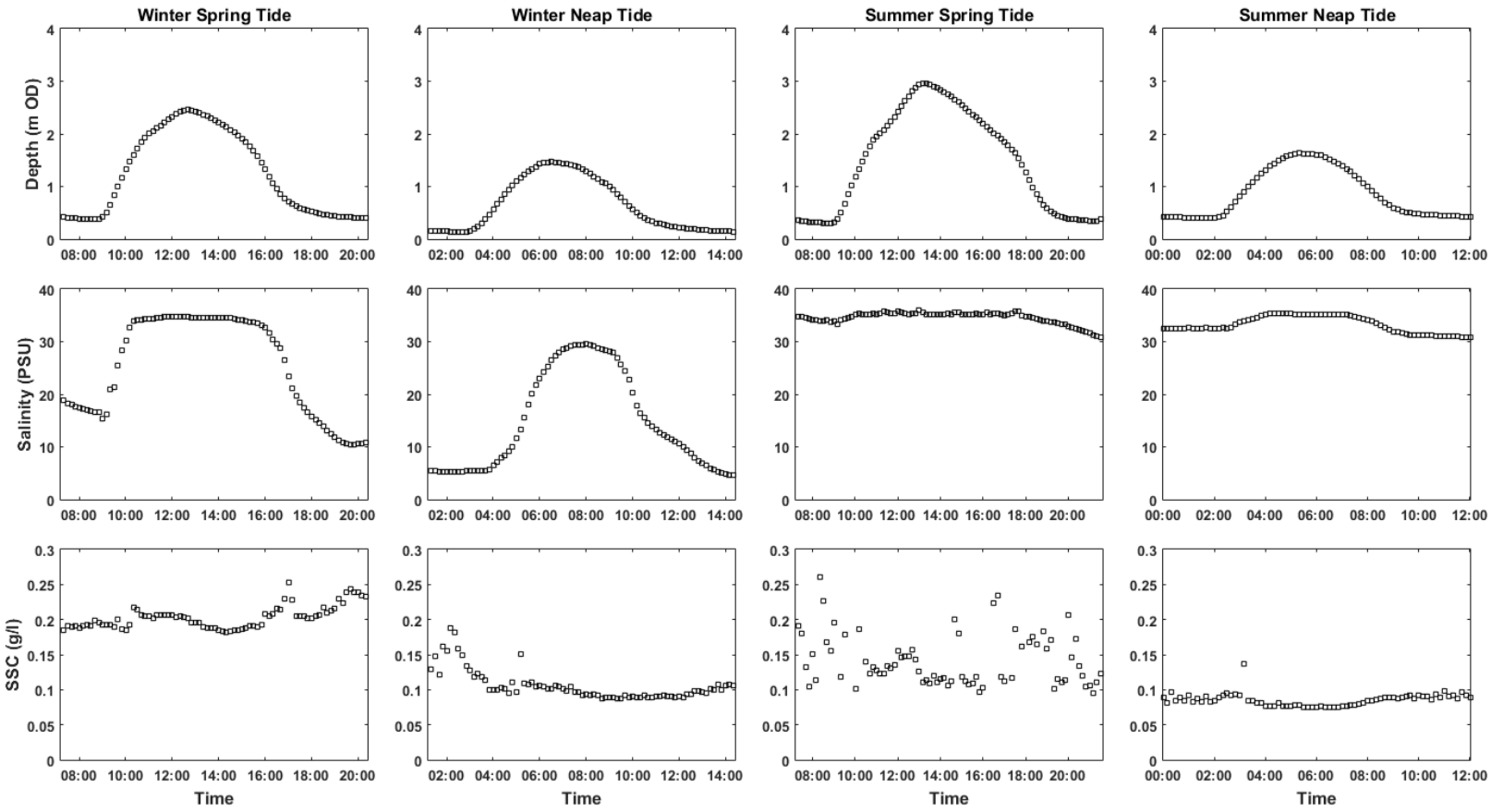

Figure 6.21: Comparison of depth, salinity and suspended sediment concentration (SSC) over a tidal cycle for Site 3 for a winter spring tide (24/3/2016), a winter neap tide (2/3/2016), a summer spring tide (20/8/2016) and a summer neap tide (12/8/2016).

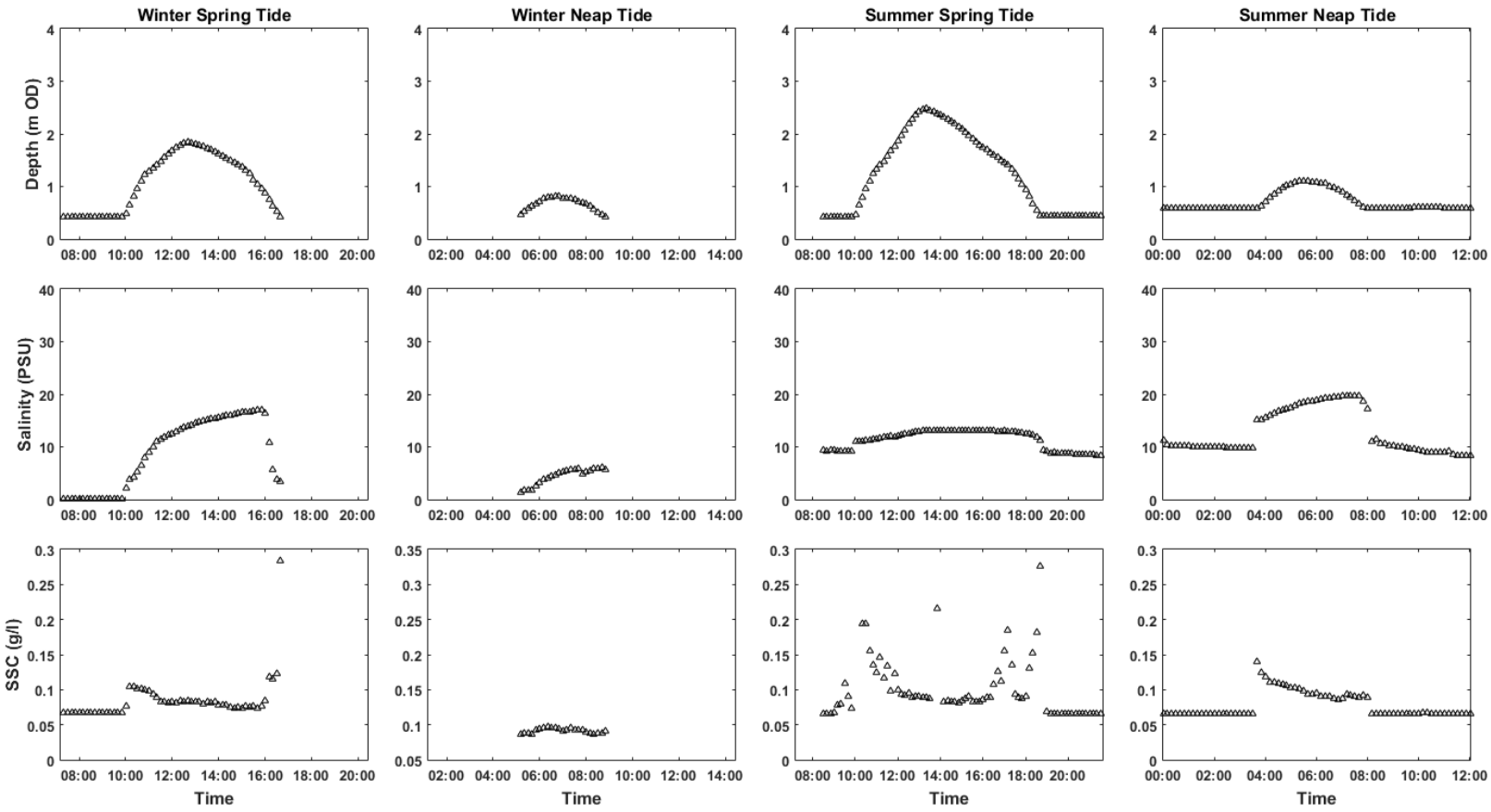

Figure 6.22: Comparison of depth, salinity and suspended sediment concentration (SSC) over a tidal cycle for Site 2b for a winter spring tide (24/3/2016), a winter neap tide (2/3/2016), a summer spring tide (20/8/2016) and a summer neap tide (12/8/2016).

Variability in SSC was observed at all three sites. In the breach, peak SSC occurred during the flood tide (Figure 6.20), suggesting the site is a net importer of sediment, whereas a small peak occurred during the flood phases and larger peaks were measured during the ebb tide at Sites 3 (Figure 6.21) and 2b (Figure 6.22). A peak in SSC was also detected at low water at Site 3. During neap tides, Site 2b did not share the same variability in SSC fluxes, as demonstrated by the peak in SSC seen during the middle of March in the breach (Figure 6.17) and at Site 3 (Figure 6.18), but not at Site 2b (Figure 6.19). The increased levels of suspended sediment, matched by a high freshwater discharge event from the breach (Figure 6.17), seen towards the end of the month (highlighted), are the result of a storm surge, Storm Katie, which occurred at this time (see Section 6.4 for discussion). In contrast, during August, salinity values remained relatively constant in the breach (Figure 6.17). Measurements at Site 3 (Figure 6.18) indicated a small amount of tidal variability in the salinity, with a similar amount of variability occurring at Site 2b (Figure 6.19) during the spring tides at the start of August. However, this variability is not repeated during the spring tides later in the month.

6.3.2 Water Column Profiling

Although near-bed measurements provide an insight into hydrodynamic processes at various temporal and spatial scales, they do not provide data on vertical changes in salinity and SSC within the water column. Static vertical profile measurements of the water column were taken over a tidal cycle at Sites 2b and 3 on 6th June 2016 and longitudinal surveys were taken along Easton Rife on 7th June 2016 on the flood (from one hour before high water) and ebb (up to one hour after high water) tides. Measurements were averaged every 10 minutes into 5 cm bins.

6.3.2.1 Static Tidal Cycle Profiling

Vertical measurements at Site 3 demonstrated that the water column was fully saline (Figure 6.23a) and well mixed with very little variability throughout the tidal cycle. SSC measurements (Figure 6.23b) indicated an initial increase in suspended sediment at the

start of the flood tide. A larger increase in SSC occurred during the ebb tide, corresponding to the peaks in SSC observed in the near-bed measurements. Further inland, at Site 2b, salinity measurements (Figure 6.24a) suggest evidence of some stratification during the mid-part of the flood and ebb tidal phases. During high water the water column was fully saline. Lower salinities measured during the latter stages of the ebb tide corresponded with the opening of the tidal gates within the upstream culvert at Drainage Outlet 3 (DO3, see Section 3.3.3). Measurements of SSC at Site 2b (Figure 6.24b) indicated initial high levels of suspended sediment, re-suspended by the incoming tide. Levels of suspended sediment then decreased, originally in the lower part of the water column with higher SSCs measured nearer the surface. During the ebb tide the SSC increased, initially in just the upper part of the water column, before becoming more turbid. The concentration of suspended sediment then decreased at depth with higher concentrations continuing to be measured in the surface waters.

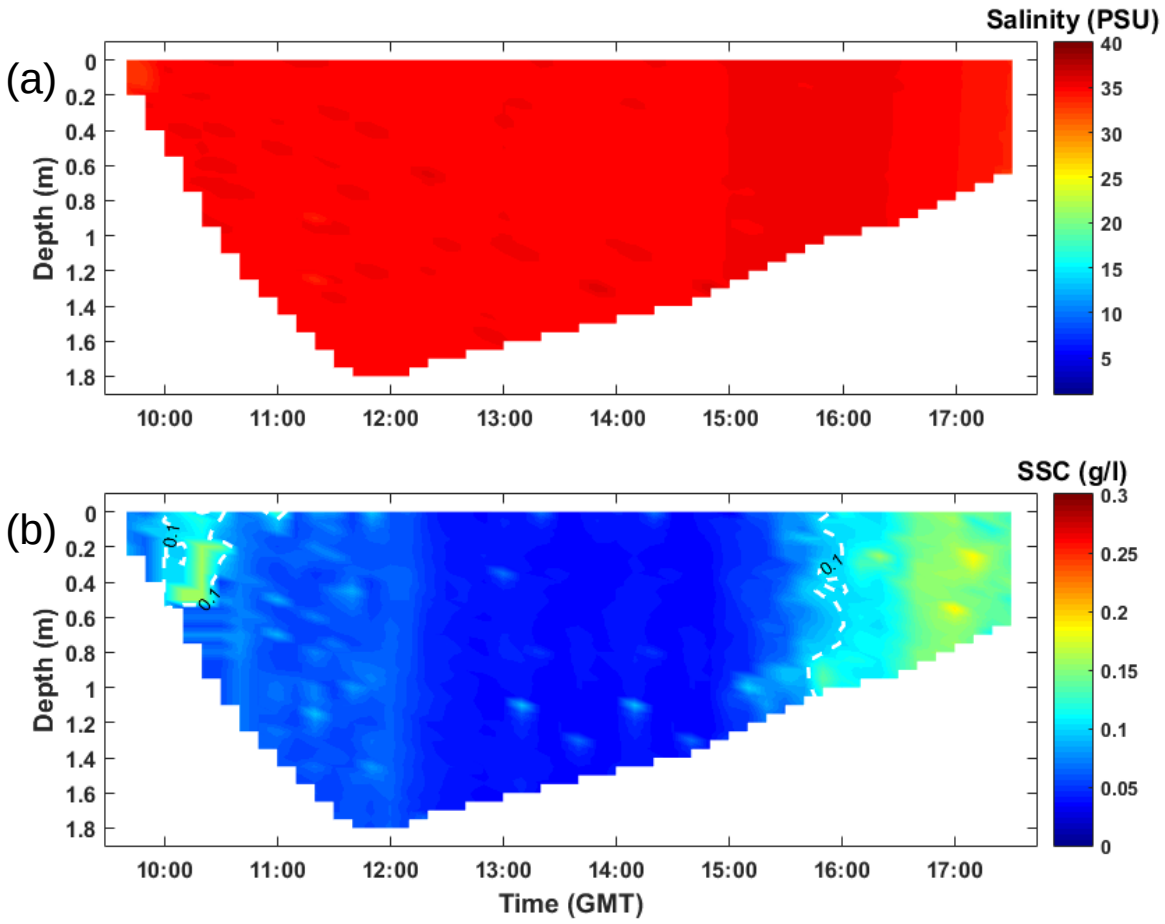

Figure 6.23: Vertical (a) salinity and (b) suspended sediment concentration (SSC) measurements taken at Site 3 on 6th June 2016. Vertical profiling data interpolated and plotted using Matlab (R2010a).

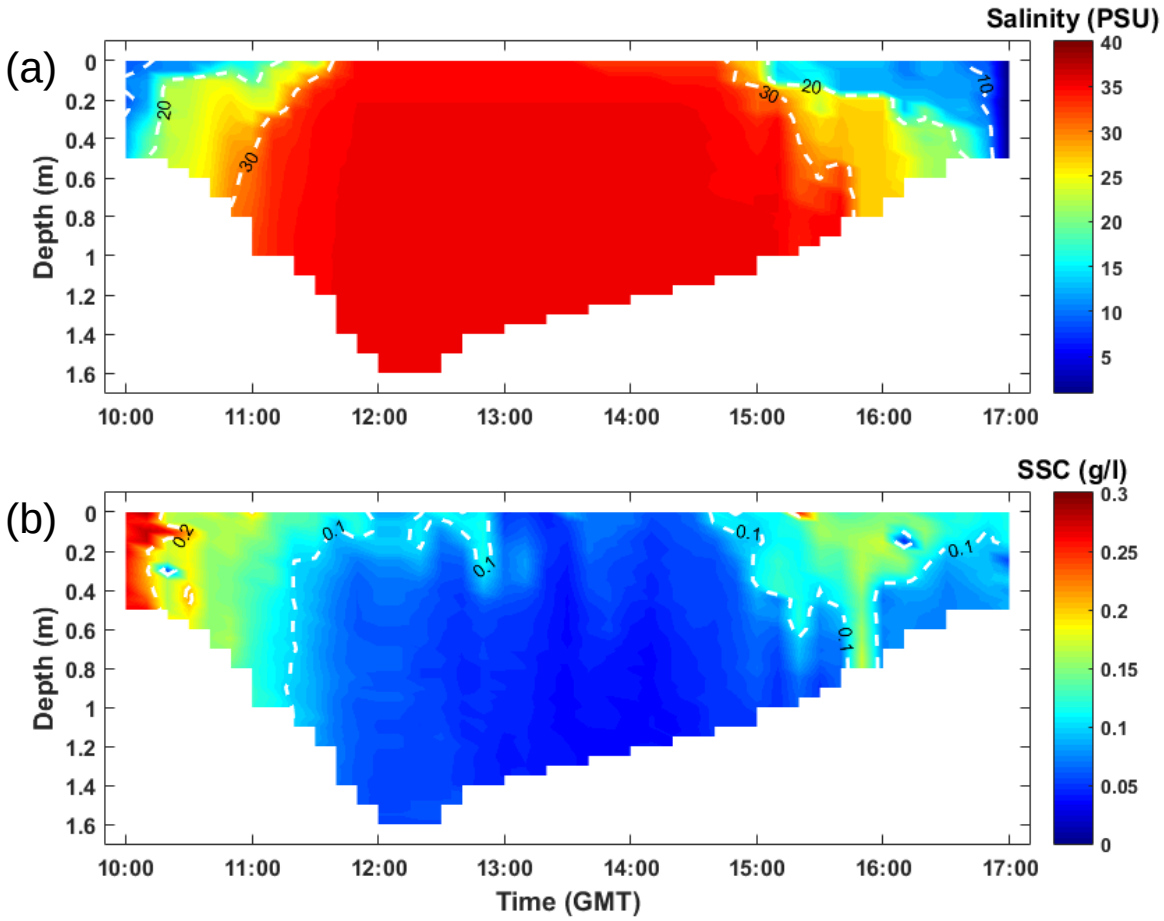

Figure 6.24: Vertical (a) salinity and (b) suspended sediment concentration (SSC) measurements taken at Site 2b on 6th June 2016. Vertical profiling data interpolated and plotted using Matlab (R2010a).

6.3.2.2 Longitudinal Profiling

During the end of the flood tide, waters within the Medmerry site were in the most part saline (Figure 6.25a). Salinity decreased within the vicinity of the tidal gates in the culvert at DO3 with evidence of stratification. SSC measurements (Figure 6.25b) exhibited a peak near the bed 2 km from the breach, corresponding to a location between Site 3 and the confluence of Easton Rife (leading up to Site 2b) and Grange Rife (to Site 2a). The amount of suspended sediment within the water column increased towards the drainage outlet. In contrast, the halocline during the ebbing tide was located further seawards with the rest of the system containing saline water (Figure 6.26a). A strong turbidity maximum was detected at the landwards extremity (Figure 6.26b), indicative of sediment which had been resuspended during the flood tide and had accumulated in front of the closed tidal gates.

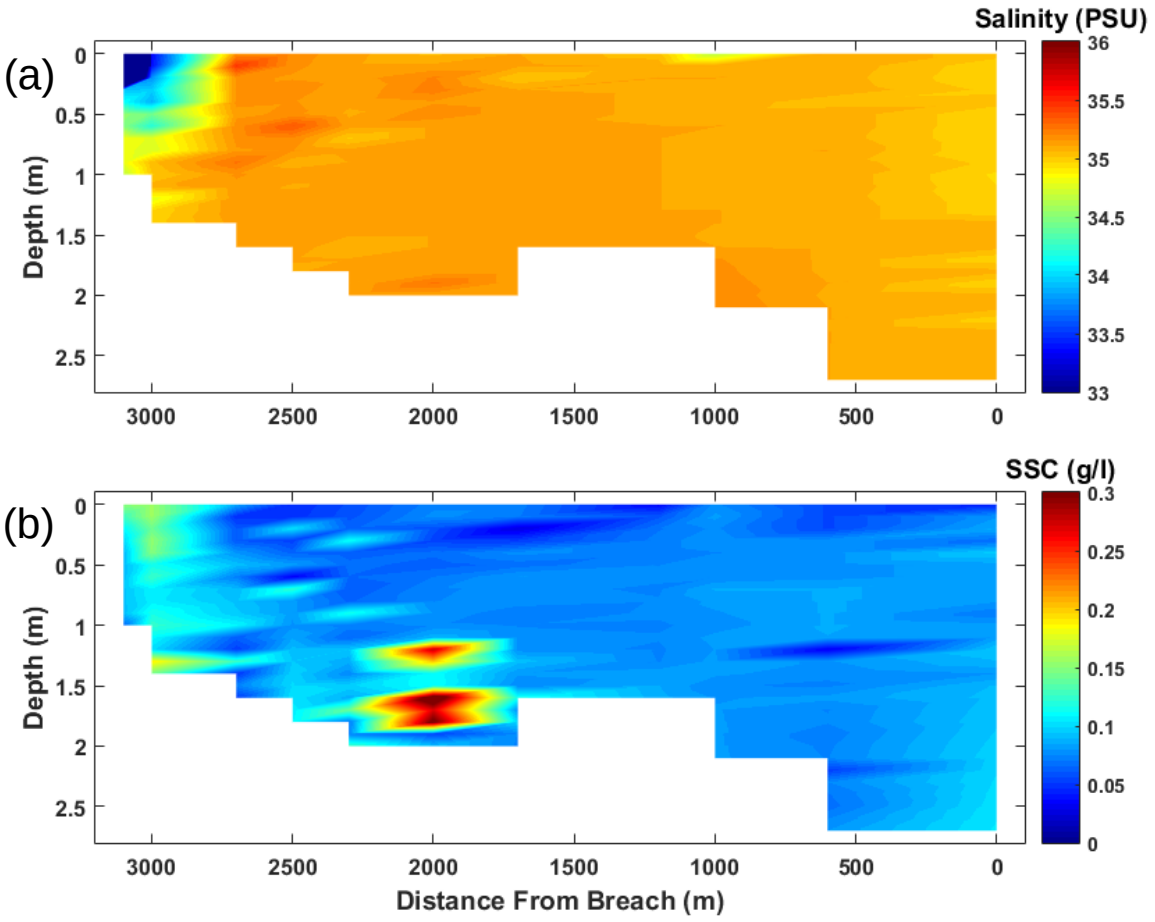

Figure 6.25: Longitudinal vertical (a) salinity and (b) suspended sediment concentration (SSC) measurements during the flood tide (from one hour before high water until high water) on 7th June 2016 along Easton Rife, Medmerry Managed Realignment Site. Vertical profiling data interpolated and plotted using Matlab (R2010a).

6.3.3 High Suspended Sediment Events

Occasions when high SSCs were measured in the breach and at Site 2b were analysed to assess the upstream and downstream suspended sediment fluxes and sediment sources to the excavated channel entrance at Site 3. Two types of high SSC events are presented in Figure 6.27: high SSCs repeated for a number of tides; and single tides with high SSCs. Although the SSC was recognised to generally increase in the breach during flood tides, during multiple tides with high levels of suspended sediment the maximum SSC tended to occur during the ebb tide and at low water. During these events high SSCs were measured during the ebb tides and during low water at Site 3, rapidly falling during the flood tides. At Site 2b, peaks in SSC were measured during the early flood and late ebb tides, decreasing during the period of tidal inundation. Throughout the

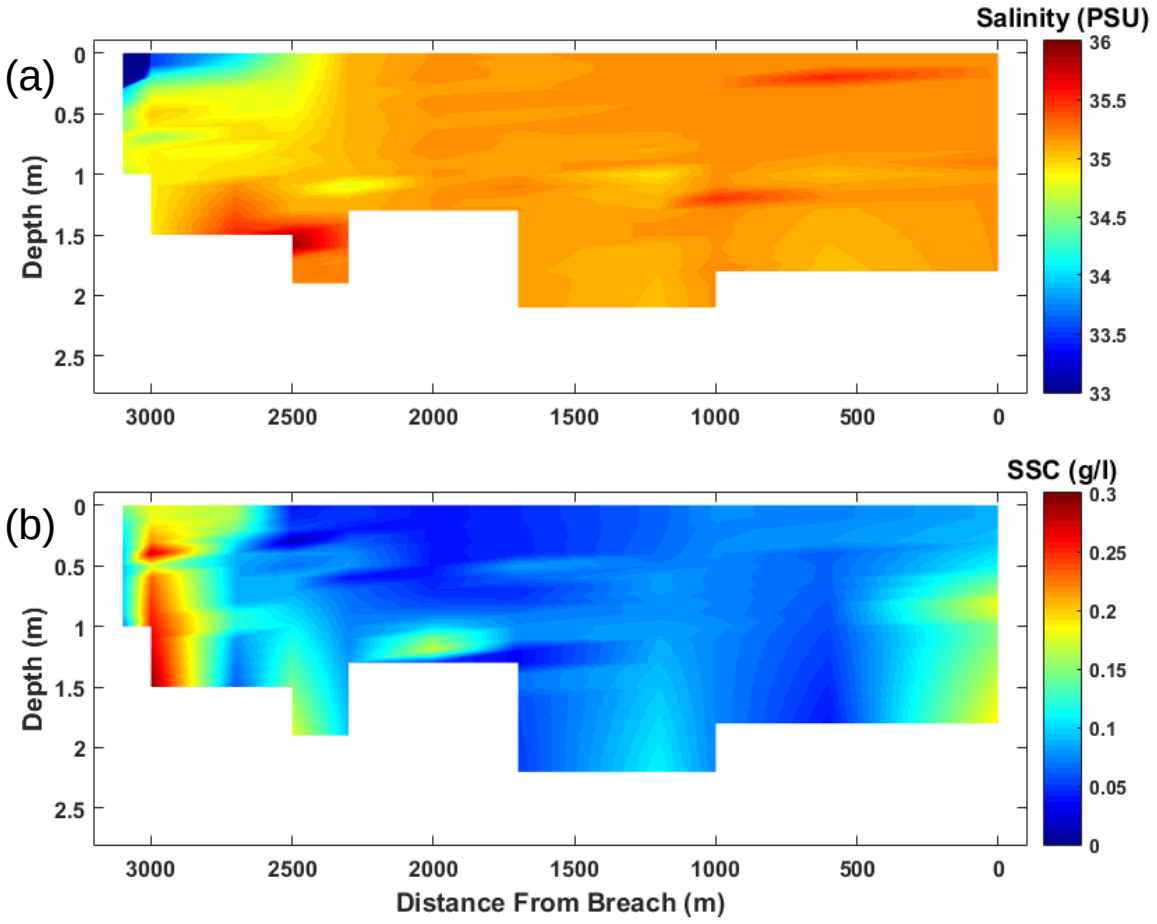

Figure 6.26: Longitudinal vertical (a) salinity and (b) suspended sediment concentration (SSC) measurements during the ebb tide (from high water until one hour after high water) on 7th June 2016 along Easton Rife, Medmerry Managed Realignment Site. Vertical profiling data interpolated and plotted using Matlab (R2010a).

example illustrated in Figure 6.27, bed elevation measurements indicated that around 5 mm of sediment were accreted following inundation on the flood tide. Bed elevation peaked at high water and decreased sharply during the ebb tide. By the start of the succeeding flood tide, bed elevation had fallen to a similar level to that of the previous tide. When levels of SSC within the breach decreased, the sedimentation rhythms returned to the typical more symmetrical pattern of accretion during the flood and erosion during the tides as described in Section 6.2.2.1.

During the single high SSC event shown in Figure 6.27, levels of suspended sediment at Site 2b peaked at low water with smaller increases occurring during the following two low waters. SSCs at Site 3 also peaked at low water, and decreased until halfway

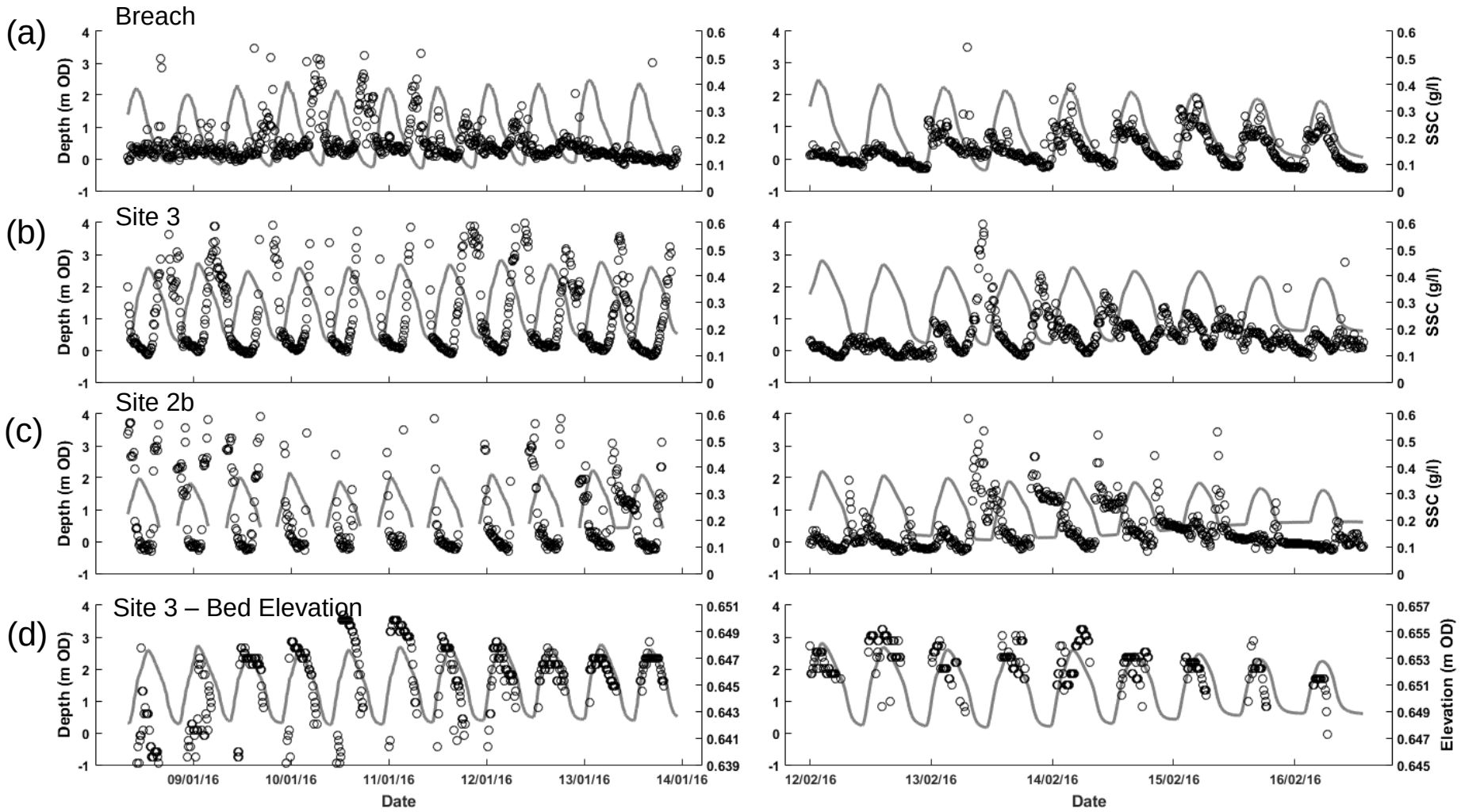

Figure 6.27: Depth against suspended sediment concentration (SSC) at (a) the breach, (b) Site 3 and (c) Site 2b, and (d) depth against bed elevation at Site 3 for multiple tides (*left*) and a single tide (*right*) with high SSC.

through the following ebb tide. In the breach, SSCs continued to display a trend of importing sediment. Bed elevation at Site 3 decreased during the tides directly preceding and succeeding the peak in SSC, but from approximately the same starting bed elevation each time, suggesting sediment was accreted whilst the sensor (but not the bed) was exposed. Sediment was then accreted during the following tide, before returning to a pattern of rhythmic depositions and erosion.

6.4 Response to Storm Events

In addition to being a restoration and habitat loss compensation scheme, the site was constructed to improve coastal flood defence in the Medmerry region. During the winter of 2015-16 a series of storms hit the United Kingdom, the first year they were assigned names by the Meteorological Office (United Kingdom). The sedimentary response to three of these storms, Storms Eva, Imogen and Katie (outlined in Table 6.9), are assessed here in terms of the SSC (Figure 6.28) and bed elevation (Figure 6.29) measured at the breach, Site 3 and Site 2b.

Table 6.9: Three of the 2015-16 winter storms selected to assess the response of the Medmerry Managed Realignment Site to storm events. Rainfall data were provided by the Environment Agency (United Kingdom) from the Ferrypool, Pagham Harbour.

Storm Name	Date	Duration	Total Precipitation (mm)	Maximum Precipitation (mm/hr)	Maximum Wind Speed (m/s)
Eva	24th December 2015	15 hours	4.27	1.74	11
Imogen	7th – 8th February 2016	43 hours	5.6	0.78	18.75
Katie	27th – 28th March 2016	42 hours	12.2	2.14	24.15

During Storm Eva, the SSC at the breach increased during the flood tide and continued to increase during the start of the ebb, decreasing during the latter part of the outgoing tide. At Site 3, the ebbing tide had a higher concentration of suspended sediment than had previously been the case before the storm. Afterwards, the SSC decreased at Site 3 to a similar concentration as before the storm. SSCs at Site 2b peaked on both the flood and ebb tides, decreasing during both high and low waters with the exception of the low water after the storm when SSCs remained high. Bed elevation measurements were patchy during this period, but suggest that sediment accreted during the storm and the tide the following day before eroding.

Storm Imogen, during which the entire beach front was overtopped (Figure 6.30), had a similar effect as Storm Eva on SSCs in the breach, although concentrations of sediment were greater and remained higher after the storm. SSC peaked at low water at Site 3, decreasing during the flood and increasing again during the ebb tide. At Site 2b, SSCs were more variable than during Storm Eva demonstrating a pattern of increasing during the ebb and decreasing during the flood. Bed elevation at Site 3 increased during the storm and remained relatively constant during the following tidal cycle. However, at the start of the next tide, bed elevation was 2 mm lower than before the storm and increased again during the tidal cycle. Sedimentation then reversed back to its rhythmic pattern of accretion and erosion.

The SSC also increased in the breach and at Site 3 during Storm Katie, peaking during the ebbing tide and then rapidly decreasing. At Site 2b SSCs were high, decreasing during the ebb tide and remaining low during the following tides. Bed elevation increased during the storm and, although no data were collected during the subsequent tide (presumed to be due to the smaller amplitude of this tide and therefore the sensor not being sufficiently inundated), bed elevation decreased during the tide on the following day.

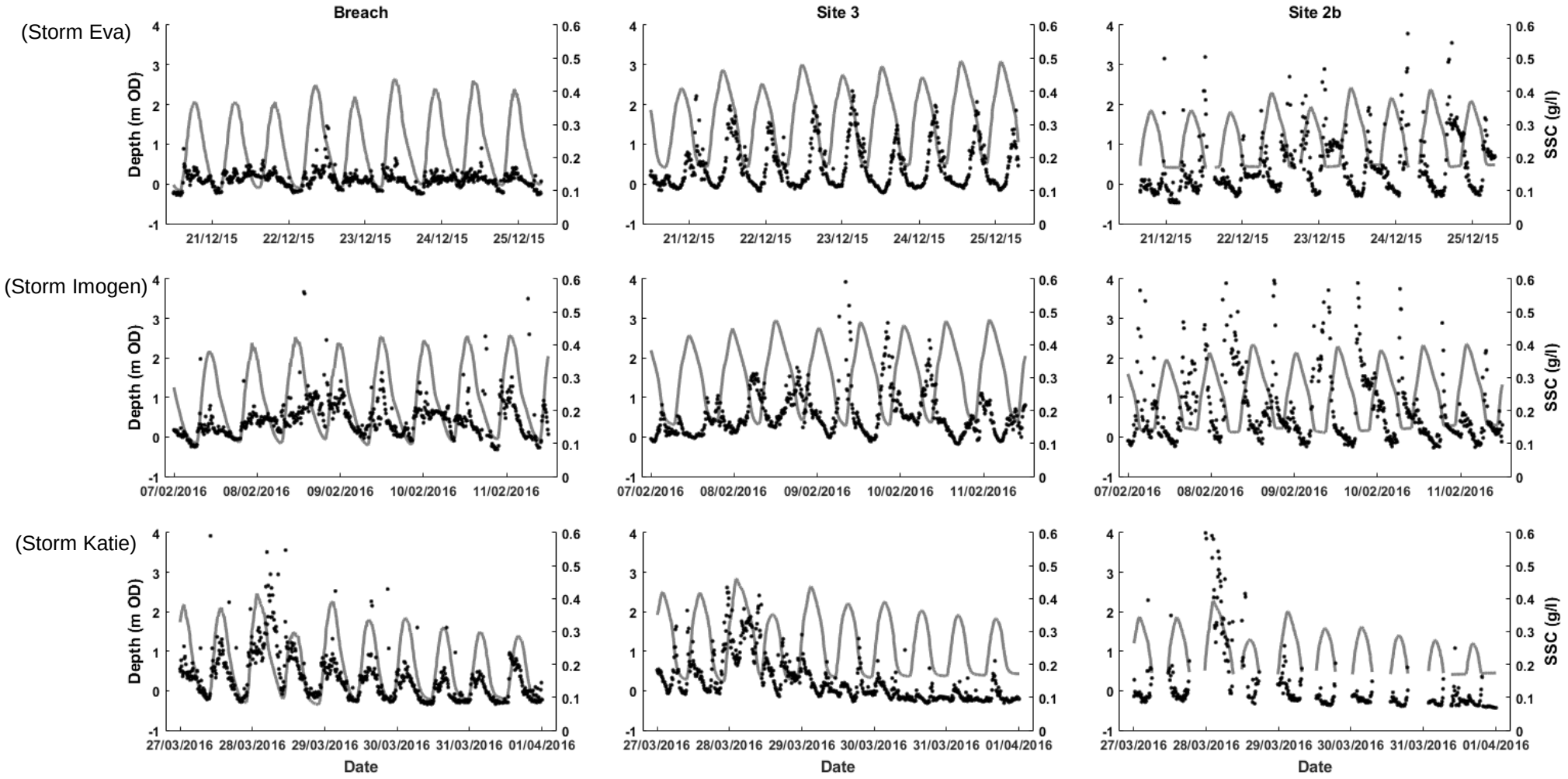

Figure 6.28: Depth against suspended sediment concentration (SSC) for the breach, Site 3 and Site 2b during Storms Eva (24th December), Imogen (7h – 8th February) and Katie (27th-28th March).

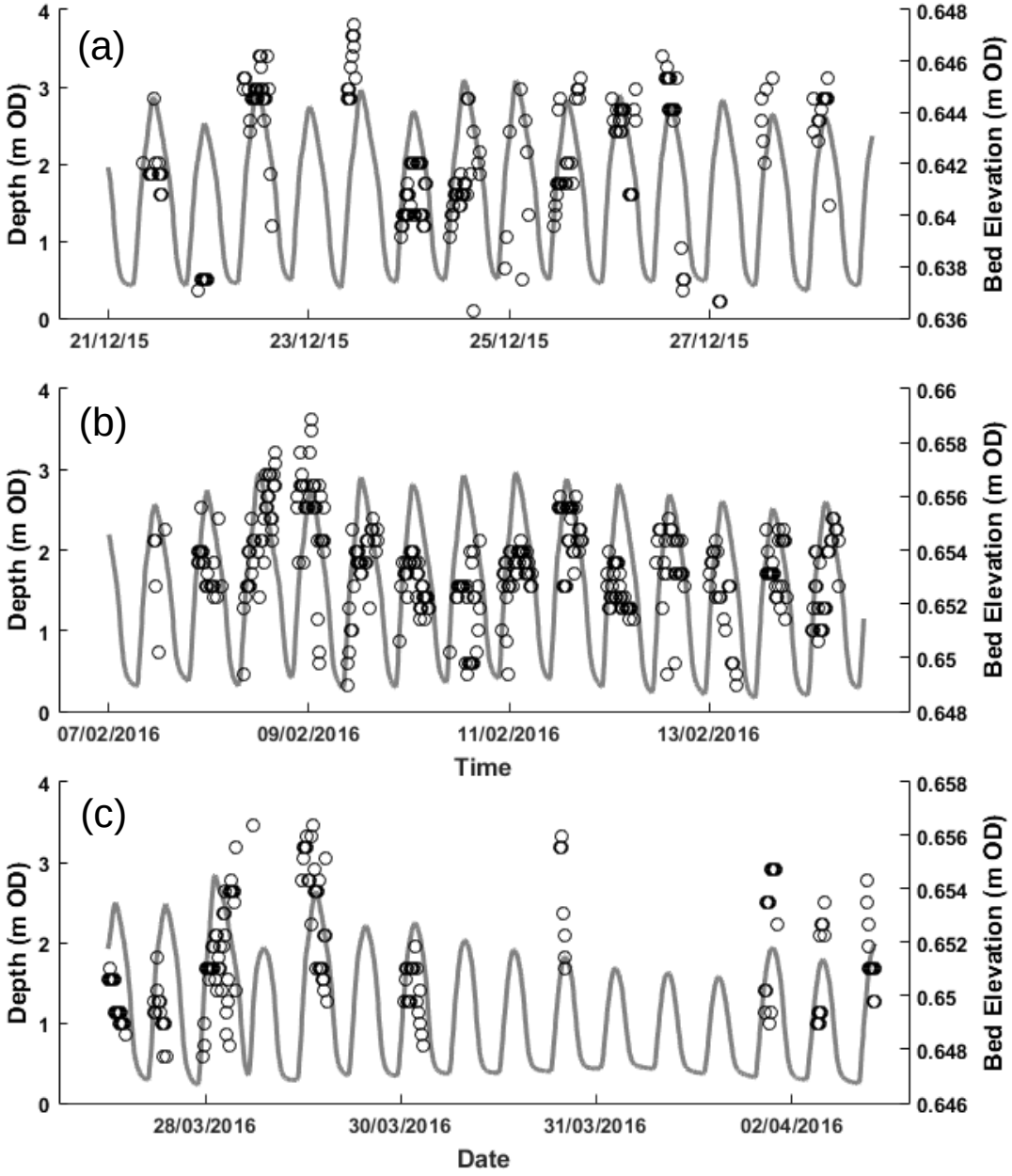

Figure 6.29: Changes in bed elevation at Site 3 during (a) Storm Eva, (b) Storm Imogen and (c) Storm Katie.

Figure 6.30: The beachfront at Medmerry (taken from the same location looking westwards) during (a) ambient conditions at high water (photograph: J. Dale) and (b) Storm Imogen (photograph: Peter Hughes, RSPB). Signpost circled for reference.

6.5 Discussion

High resolution data of site hydrodynamics along the main drainage channel, and the preservation and occurrence of sedimentation rhythms for two infilling sites (Sites 3 and 5) heavily altered during site construction, are provided in this chapter. At Site 3, SSCs related to salinity and, to some extent, depth, whereas at Site 5 the SCCs had some relation to salinity during low water. Sediment altimeter data highlighted different sedimentation patterns at the two sites; near constant deposition of sediment occurred at Site 5 resulting in 15.2 cm of sediment being accreted over the one year monitoring period, whereas periodic accretion and erosion of sediment occurred inland, at Site 3, leading to 4.4 cm of net accretion (2.7 cm from November 2014 to October 2015 and 1.7 cm during the same period the following year).

6.5.1 Sedimentary Rhythmites

Although altimetry measurements indicated net accretion at the two engineered sites, different sediment rhythms were detected. The different sedimentation rhythms are a product of spatial and temporal variations in sedimentary processes resulting from the complex relationship between the hydrodynamics and SSCs measured and the surface sediment properties (and site morphological characteristics). The preservation of sedimentary rhythmites can be calculated from the altimetry measurements as a percentage of the sediment preserved from each depositional event (after Deloffre et al., 2007):

Preservation rate (%)=(Σ(thickness of deposit episodes during one year)(cm))/(Annual Sedimentation rate (cm))

The preservation rate was 28 % during the first year (November 2014 to October 2015) at Site 3, and 16 % during the second (November 2015 to October 2016), owing to the periodic accretion and subsequent erosion of sediment, whereas at Site 5 the preservation rate was much higher at 65 % (November 2014 to October 2015) due to

less significant periods of erosion. However, preservation rate at both these sites were lower than the values reported by Deloffre et al. (2007) for the Authie and Seine estuaries (Table 6.10).

Table 6.10: Annual accretion rate, semi-diurnal rhythm type and preservation rate reported for Site 3 and Site 5 at the Medmerry Managed Realignment Site in this study compared to the values and sedimentary rhythmites reported by Deloffre et al. (2007) for the Authie and Seine estuaries.

	Medmerry Managed Realignment Site		**Authie**	**Seine**
	Site 3	Site 5		
Annual Accretion (cm)	2.7 (first year) 1.7 (second year)	15.2	15	18
Semi-diurnal Rhythm Type	Sedimentation during flood, erosion during ebb	Sedimentation during flood, consolidation during ebb	Sedimentation during flood, consolidation during ebb	Stability followed by sedimentation on flood, erosion and dewatering during ebb
Preservation Rate (%)	28 (first year) 16 (second year)	65	90	50

At Site 3, which consists of waterlogged sediment in a sheltered central site area (see Chapter 5), sedimentation corresponded to a semi-lunar rhythm typical of a sheltered natural mudflat (Deloffre et al., 2007) with a superimposed rhythm of deposition during the flood tide and resuspension during the ebb. Deposition of sediment matched a decrease in near-bed SSC and, following erosion, the SSC increased. Rates of sedimentation were greater at the more exposed and lower elevation Site 5, where generally 1 to 2 mm of coarse grained sediment (see Chapter 5) were accreted regardless of the hydrodynamic conditions during each tidal cycle, predominantly during the flood tidal phase. The main period of sedimentation on the flood tide matched a decrease in SSC and decelerated rates of sedimentation occurred during

periods of low SSC. However, rates of accretion overall showed no evidence of deceleration during the measurement period.

Medmerry is a large open coast managed realignment (MR) site, and is exposed to a range of forces and processes resulting in different sedimentation patterns in different parts of the site. At present, there is no evidence of hydro-geomorphic equilibrium having been attained, with sediment remaining to be redistributed around the site. It remains to be seen how the sediment regime will evolve as the site approaches a state of quasi-equilibrium and all sediment has been redistributed, particularly in response to rising sea levels, at a site where (in contrast to many previous MR sites) there are no surrounding intertidal saltmarsh or mudflat habitats to act as a potential fine sediment source (discussed further below).

6.5.2 Sources of Suspended Sediment

Measurements of the SSC taken from within the breach indicate that the Medmerry site, under typical conditions, imports sediment. The SSC peaked during the flooding tide and decreased during high water, remaining low during the ebb tide. Previous studies have suggested that material transported and accreting in estuarine MR sites has come from externally eroding saltmarshes (e.g. Symonds and Collins, 2005). For example, Rotman et al. (2008) calculated that 54 % of the material accreting within the Freiston Shore Managed Realignment Site, Lincolnshire, United Kingdom, originated from eroding saltmarshes outside of the site. However, the Medmerry site is located on the open coast, a considerable distance from any external pre-existing saltmarshes (approximately 7.5 km eastwards from Chichester Harbour entrance and on the opposite side of the peninsular from Pagham Harbour), and is banked by a shingle beach. The external sources of sediment to the Medmerry site remain unknown, but may well originate from former, relict, intertidal saltmarsh deposits exposed within the breach area (Section 3.2.4) or from the eroding Hound Bank offshore. Nonetheless, the wider impact on the coastal system of this import of sediment, particularly to the west in the direction of littoral drift, remains unclear and requires further investigation.

Larger concentrations of suspended sediment were measured within the site than in the breach, despite the site being recognised to import sediment. Peaks in SSC were measured during both the flood and ebb tidal phases at Sites 2b and 3, indicating the resuspension, redistribution and recycling of sediment around the site during both stages of the tidal cycle. Similar observations were made by Mitchell et al. (2006) at neighbouring Pagham Harbour, which naturally breached during a storm in 1910 AD, where sediment is transported from seaward locations or is resuspended locally (or both) and builds up at the landward extremities of the site.

SSCs were found to relate to differences in water depth on a semi-diurnal scale at Site 3, and at both sites lower salinities were related to high levels of suspended sediment. A higher input of freshwater is often associated with transporting greater levels of eroded sediment from elsewhere in the catchment and influencing the position of the turbidity maximum, whilst the transport of eroded terrestrial sediment from runoff within the site may also occur (e.g. Fettweis et al., 1998). Analysis of consecutive tides with elevated concentrations of suspended sediment in this chapter indicated that during these events material is flushed completely from the system and discharged to the open coast during low water. During these events, SSCs increase during the flood and ebb tides at both internal sites, but decrease over high water. An increase in bed elevation was observed at Site 3 during the early flood tide, followed by a rapid decrease during the ebb. Rainfall measurements (provided by the Environment Agency, United Kingdom) from the Ferrypool (see Figure 6.1 for location), where prior to being reclaimed the Medmerry site used to connect and drain through Pagham Harbour (e.g. Bone, 1996), indicate that the peaks in SSC illustrated in Figure 6.27 were observed two days after 8.6 mm of rain fell within a 7 hour period (Figure 6.31).

Freshwater levels on the landwards side of the site, recorded at Drainage Outlet 4 (also provided by the Environment Agency, United Kingdom) indicate that two days following this intensive rainfall event freshwater input increased and match the period of consecutive elevated high SSC (Figure 6.31). Freshwater levels decreased on the ebb tide and during low water (whilst the tidal gates were open), but built back up again during the flood tide and high water (whilst the tidal gates were closed). This suggests that the relationship between SSC and salinity resulted from terrestrial input external to

the site, as has been proposed elsewhere (e.g. Fettweis et al., 1998), given the multiple tides with elevated SSCs which match the time taken for freshwater levels on the terrestrial side of the site to decrease. A similar trend has been observed in Pagham Harbour (Burgess, *personal communication*, 2017) which also has similar tidal gates located in a sea wall constructed in the 18th century (Mitchell et al., 2008).

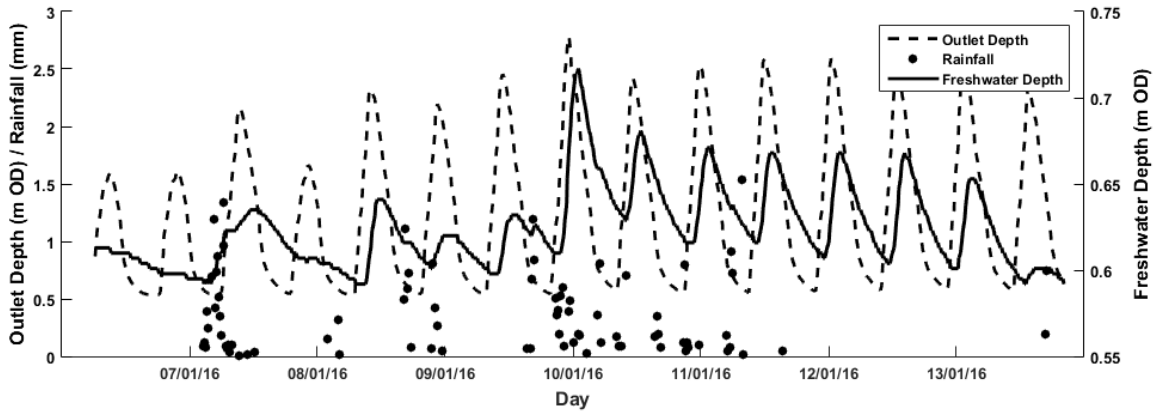

Figure 6.31: Water depth on the outlet (seaward) and freshwater (terrestrial) sides of Drainage Outlet 4 at the Medmerry Managed Realignment Site and rainfall (dots) from the Ferrypool (see **Figure 6.1** for location) for the period of multiple tides with high SSC shown in **Figure 6.27**. Data provided by the Environment Agency, United Kingdom (contains Environment Agency information © Environment Agency and database right).

Single high SSC events have also been observed at Sites 2b and 3. During these events, SSCs in the breach continued to peak on the flood tide and decrease during the ebb. Individual high suspended sediment events occurred during low water but, when compared to changes in the freshwater input to the site, peaks occurred during the subsequent low water. An alternative explanation for the negative relationship between SSC and salinity is internal erosion caused by run off during rainfall events. Rainfall data from the Ferrypool site suggest that 7.11 mm of rainfall occurred over 7 hours during the period of exposure (Figure 6.32) for the occasion exemplified in Figure 6.27. Visual observations of pluvial water draining, not only over the terrestrial land within the site but the forming saltmarsh and mudflat exposed at low water, indicate an increase in suspended sediment caused by a decrease in the cohesive strength of the sediment (Tolhurst et al., 2006c).

The impact of rainfall on the erosion of cohesive sediments requires much further investigation including the impact of the rain droplets themselves and the spatial and

temporal variability associated with events of different magnitude. Comparisons between events of different frequency and magnitude, at varying temporal scales to allow for day-night variations (Friend et al., 2003) and different stages of the tidal cycle (i.e. different durations of exposure to tidal and subaerial processes and time since immersion by tidal waters) is also required (Tolhurst et al., 2006a). This is particularly important in newly inundated MR sites undergoing the transition from terrestrial soil to intertidal sediment and may well have a significant impact on the evolution of the sediment regime within these environments.

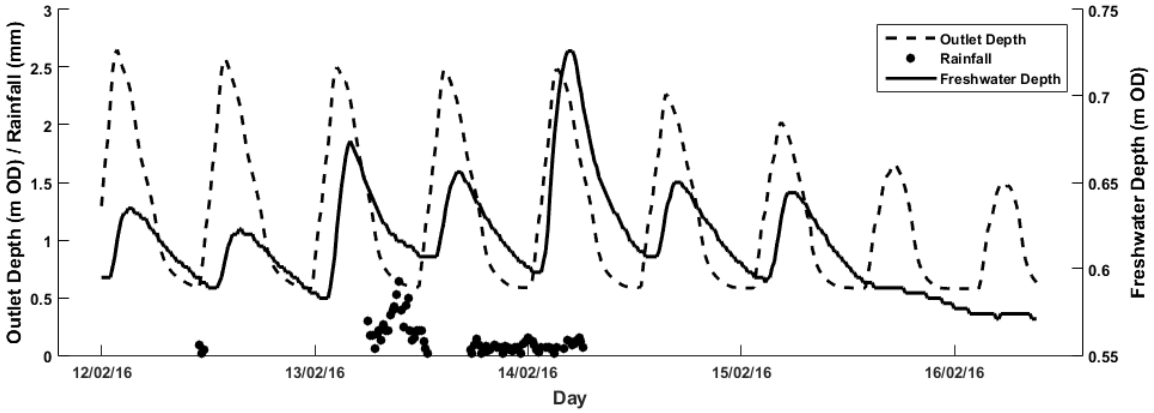

Figure 6.32: Water depth on the outlet (seaward) and freshwater (terrestrial) sides of Drainage Outlet 4 at the Medmerry Managed Realignment Site and rainfall (dots) from the Ferrypool (see **Figure 6.1** for location) for the single tide with high SSC exemplified in **Figure 6.27**. Data provided by the Environment Agency, United Kingdom (contains Environment Agency information © Environment Agency and database right).

Under ambient conditions, long-term near-bed measurements and vertical water column measurements taken over individual tides indicate that during the flood tide sediment is resuspended within the main drainage channel, with a turbidity maximum located between Sites 2b and 3. Evidence of stratification was recorded at Site 2b during both the flood and ebb tides, with the freshwater and a peak in SSC becoming trapped in front of the tidal gates at the landward extremity of the site. The position and gradient of any halocline and stratification that may be preserved over a tidal cycle will depend on the amount of freshwater trapped between the incoming tide and the tidal gates (Mitchell et al., 2008). This may also affect the magnitude of the flux of suspended sediment along the main drainage channel driven by vertical salinity induced density gradients, seen elsewhere including Pagham Harbour (e.g. Mitchell et al., 2006).

Vertical profiling measurements were, however, taken in June, when reduced freshwater input would typically be expected, with near-bed measurements indicate that fully saline conditions only occur at Site 2b during high water in the summer months. Therefore, further consideration of the level of stratification and the influence on the transportation of sediment during periods of high freshwater input is required to provide a better insight into the hydrodynamics, the position and gradient of any stratification or turbidity maximum and the level of mixing within the water column. This will enhance the understanding of the cycling of sediment and the evolution of the sediment regime within the Medmerry site.

At Site 5, sedimentation showed a less clear relationship with hydrodynamic differences, and high accretion rates of typically sandy sediment (see Section 5.2.6). The sediment source at this site originates from sand deposits in local collapsed banks and former hedgerows and is washed landward by locally induced wind waves. Relic banks and hedgerows are positioned seaward of Site 5, orientated in line with the prevailing wind from the south-west, and are the only features which remain exposed during high water, but are gradually diminishing in extent over time (Dale et al., 2017). Some sediment has also been provided from the surrounding intertidal floodplain, a former barley field prior to site inundation, which has been experiencing erosion via embryonic creek formation (see Chapter 7). This has implications for future site design, in that account has to be taken of the availability of large local sediment sources which may erode or reprofile and cause rapid infilling, impacting the type of intertidal environment which develops.

6.5.3 Rates of Sedimentation

Predictive models (e.g. Allen, 2000) and measurements (e.g. Clapp, 2009; Dixon et al., 2008) of the evolution of intertidal environments suggest high sedimentation rates would initially be expected following inundation, particularly in areas of lower elevation. Lower rates of accretion were measured at Site 3, which could be due to the site being positioned towards the lower energy centre of the MR site away from a readily available source of sediment. Furthermore, lower rates of accretion at Site 3 may

be caused by the relatively high elevation of the site at the time of initial inundation compared with areas nearer the breach, a reason given for the relatively low rates of sedimentation observed by Cundy et al. (2002) at neighbouring Pagham Harbour following its natural breaching in 1910. Cundy et al. (2002) presented evidence of a near-constant sediment accretion rate of approximately 5 mm/year since breaching, significantly lower than those measured at either site at Medmerry, although these authors note that the calculated errors on the historic (i.e. immediate post-breaching) sedimentation rates were greater than in more recent sediments. Despite sedimentary rhythmites at Site 3 being more typical of a natural intertidal mudflat, compared to Site 5, the sediment remains heavily waterlogged (see Section 5.2.4) due to the high levels of sub-surface sediment compaction generated during site construction. Compact sediment reduces the efficiency of sediment drainage in frequently inundated areas due to poor vertical hydrological connectivity. Poor drainage could, in turn, hinder the physical, chemical and ecological development of the site.

Rapid, near-constant accretion was observed at Site 5 throughout the measurement period. This site is located nearer the breach, at lower elevation in a borrow pit, and is exposed to the prevailing wind from the south-west and therefore locally induced wind waves. Despite the pattern of sedimentation matching the models of sediment accretion (e.g. Allen, 2000), the rates of sedimentation measured at Site 5 were half those reported by Dixon et al. (2008) at the Wallasea Managed Realignment Site, an estuarine based scheme that is also considerably smaller than Medmerry. It remains to be seen whether these high sedimentation rates will be maintained, presuming there is a sufficient sediment supply. This is particularly the case now bed elevation in the borrow pit has reached the level of the surrounding bank and intertidal floodplain (Chapter 5). It is likely that the rates of sedimentation will decrease as the site elevation increases relative to the tidal frame, but further monitoring is required in order to evaluate whether this will be the case. Nonetheless, the high rate of accretion observed at Site 5 could have significant consequences for the ecological development of this site due to the loss of the lower elevation intertidal habitat.

The sedimentation patterns at other realignment sites show varying levels and styles of accretion. Some sites, such as Tollesbury in Essex (United Kingdom), have maintained

high levels of accretion following site inundation (e.g. Chang et al., 2001). Other sites, for example the abandoned and subsequently inundated reclaimed agricultural land on the Blyth estuary in Suffolk (also United Kingdom), failed to accrete sufficient levels of sediment to form saltmarsh and remained as mudflat habitat (French et al., 2000). In sediment-rich estuarine MR sites, rapid rates of accretion have resulted in the establishment of extensive saltmarsh at the expense of mudflat as elevation has increased relative to the tidal frame (e.g. Pontee, 2014).

Differences in accretion rates between Medmerry and other MR sites highlight the site specific nature of the cycling of sediment in these environments, whilst the results presented here demonstrate additional internal spatial complexity within MR sites. This is demonstrated by the different patterns and rates of sedimentation which have evolved following site inundation at Sites 3 and 5, despite both experiencing similar disturbances and engineering during site construction. This generates difficulty in designing and engineering MR schemes. Analysis of the mechanisms and rates of sedimentation and erosion presented in this chapter provides new insights into the preservation of deposited sediment and therefore the rate of accretion in a recently inundated intertidal environment, and enhances the understanding of the evolution of the sediment regime. Although the long term influence of these initial (post-inundation) sedimentation patterns on habitat creation at Medmerry remains to be seen, this allows greater consideration of the role of sedimentary processes in the development and likely success (in terms of habitat creation and coastal protection goals) of MR sites and other newly inundated intertidal environments.

6.5.4 Sedimentary Processes during Storm Events

Not only are MR schemes implemented to restore and compensate for habitat loss and degradation, but to improve coastal flood defence. Analysis of three storms revealed that despite variations in suspended sediment and bed elevation during the storm, the system recovered relatively quickly (within two to three tidal cycles). Mitchell et al. (2006) suggested that the main input of coastal sediment to the adjacent Pagham Harbour occurred during storm events. However, SSC measurements at Medmerry

suggest that sediment is both imported and exported from the system during high energy storm events.

Whilst recent research (e.g. Moller, 2006; Moller et al., 2014) has focused on the effect saltmarsh vegetation has as a form of natural coastal flood defences, through dampening and dissipating wave energy, little attention has been given to the influence (and response) of intertidal fine grained sediments. Whilst the analysis presented here provides an insight into the sedimentary processes during storm events, further investigation is required of the resilience of MR sites during extreme events. Consideration is required of site design, including the use of areas of lower elevation and drainage networks, to maximise the defence provided by these environments. These findings need to be contextualised with baseline measurements of the sedimentary processes during the evolution of these sites from a terrestrial to intertidal system. Further long term data of multiple storm events will allow for consideration of the impact storms have on the cycling of sediment, changes in bed elevation, and the wider sustainability of creating new areas of intertidal mudflat as a method of coastal flood defence.

6.6 Summary

High resolution data of site hydrodynamics and sedimentation rhythms at the Medmerry Managed Realignment Site are provided in this chapter, enhancing the understanding of the evolution of the sediment regime in newly inundated intertidal environments. Sediment is imported to the Medmerry site from the wider coastal environment and is only exported during repeated periods of high SSC. Greater levels of suspended sediment were cycled and redistributed around the site during ambient conditions. Higher concentrations of suspended sediment were found to relate to external freshwater input and internal erosion caused by rainfall.

Different rhythms of sedimentation were observed at two spatially contrasting sites, both heavily altered during site construction and designed to support a range of

intertidal habitat. Further monitoring is required to identify whether sedimentation continues at the measured rates, but differences between the two sites has long term implications for the evolution of the sediment regime at the Medmerry site. There is a need for wider consideration of the hydrodynamics and sedimentation rhythms in the construction of future MR schemes to ensure they are a success, especially as restoration techniques become an increasingly significant component in coastal management strategies. Further field measurements and knowledge are required to support theoretical and numerical models for these environments, which can only be accomplished through consistent, long term post-breach monitoring of the sedimentation rhythms and hydrodynamic controls.

7 Morphogenesis and Evolution of Embryonic Creek Networks

7.1 Introduction

In the previous chapters, the evolution of the sediment regime at the Medmerry Managed Realignment Site has been investigated through measurements of variations in surface sediment elevation, physicochemical properties, and cohesive strength (Chapter 5). The rhythms of sedimentation in relation to the hydrodynamics and the different sources, and mechanisms of suspended sediment input, removal and internal redistribution were assessed in Chapter 6. This chapter reviews the formation and development of embryonic creek networks within the Medmerry site (Figure 7.1), discounting the main drainage (rife) network, which incorporated pre-existing former terrestrial drainage channels.

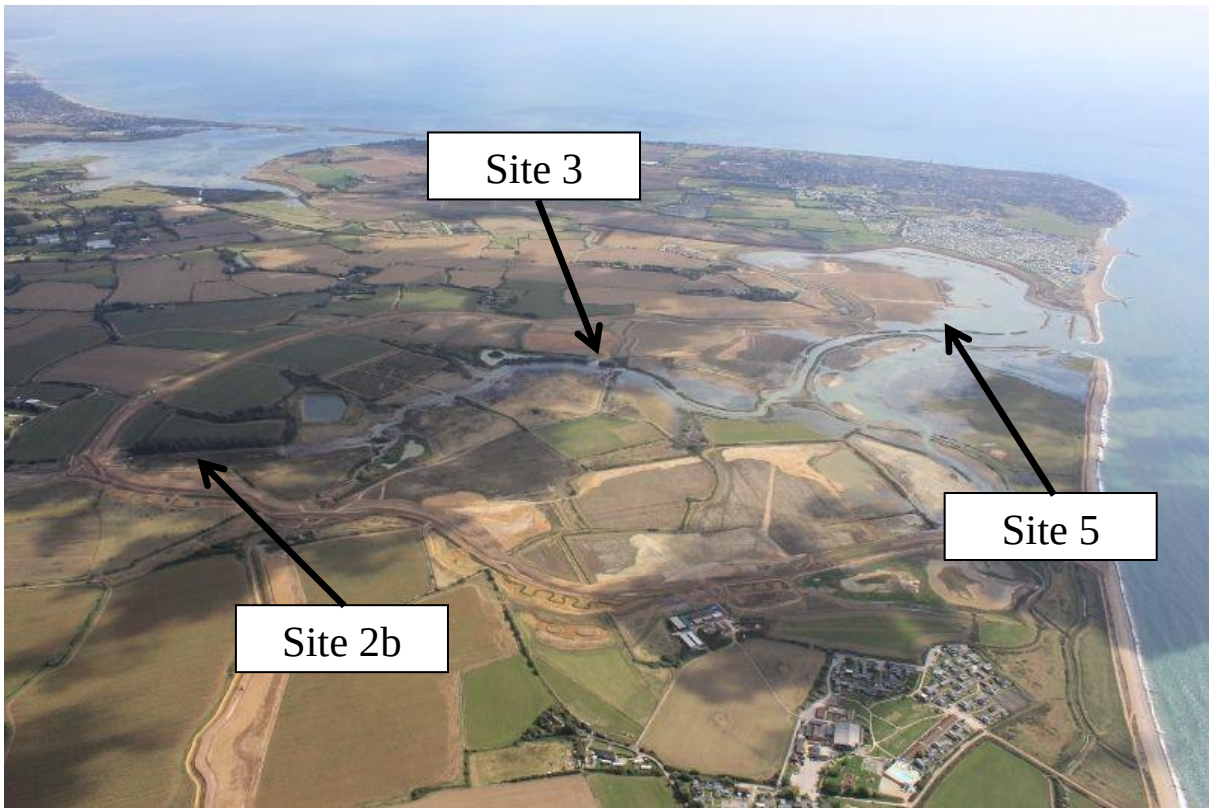

Figure 7.1: Sites analysed and discussed in Chapter 7 (looking south-eastwards, photograph: John Akerman).

The evolution of creeks at Site 3 (Section 3.3.4) and Site 5 (Section 3.3.6), which formed during the first year of site inundation (i.e. before the time period investigated in this thesis), are examined here, as are a series of smaller creeks which formed at Site 2b during the study period. Differential global positioning system (dGPS) measurements of the embryonic creek development were taken at Site 5. Measurements were supported by a novel use of a high resolution orthomosaic and digital surface model (DSM), constructed using Structure-from-Motion (SfM) analysis of images taken using an Unmanned Aerial Vehicle (UAV) (Section 4.6.2).

The influence of surface and sub-surface sediment characteristics, resulting from different pre- and post-breach sediment conditions and physical disturbances, on the creek development were investigated. Sediment samples were taken for analysis of the moisture concentration, organic concentration via a loss on ignition proxy, median grain size and mud (clay + silt) concentration, as outlined in Section 4.3, to evaluate any differences in these physical sediment properties. These parameters were investigated to characterise any sub-surface differences and, therefore, assess the influence of different sub-surface sediment zones on creek development. Samples were taken in July 2016 from the surface of the bank, close (< 1 m) to where the creeks were forming, and from the bed of the creeks themselves.

7.2 Embryonic Creek Development

7.2.1 Evolution of the Pluvial Creek at Site 3

The pluvial creek at Site 3 (see Section 3.4.3 for description) was formed by runoff during a series of storms in early 2014 (Burgess et al., 2016). During this study, visual observations of the creek suggest it has incised deeper through the waterlogged fine-grained sediment exposing a lower layer of coarse sediment with low loss on ignition and moisture concentration (Table 7.1). Since reaching this layer, first observed in April 2014, the creek has appeared to stabilise and has remained at a relatively constant depth. Fine sediment accumulates during the summer in the lower part of the creek, which is

inundated during all tides, but is then flushed out during winter pluvial events and larger spring tides.

Table 7.1: Average (mean ± standard deviation) physical sediment parameters (n = 3) for the bank surface and bed of the pluvial creek at Site 3 at the Medmerry Managed Realignment Site.

	Moisture Concentration (%)	**Loss on Ignition (%)**	**d_{50} (µm)**	**Mud (Clay + Silt) Concentration (%)**
Bank Surface	84.62 ± 4.64	3.38 ± 0.20	8.35 ± 0.31	75.80 ± 0.96
Creek Bed	38.45 ± 2.99	1.39 ± 0.23	56.06 ± 0.83	38.04 ± 0.60

7.2.2 Evolution of Creeks at Site 5

During the first year of site inundation, two embryonic creek networks (Figure 7.2) developed in the bank of the borrow pit at Site 5 (see Section 3.3.6). Repeated dGPS positional measurements illustrate that as the creeks develop they became more complex and dendritic, eroding both landwards and seawards, and eventually joining at the edge of the borrow pit (Figure 7.3). Minimal landward erosion occurred in the eastern creek network following the second survey in October 2015, whereas the western creek continued to develop multiple branches and networks.

Elevation measurements taken in cross-section (see Figure 7.3 for locations) demonstrate that around the edge of the borrow pit, T1, the position and elevation of the bed of the western creek remained relatively constant, with sediment accreting on the banks (Figure 7.4a). In contrast, the elevation of the eastern creek fluctuated at the edge of the borrow pit, initially eroding then increasing in elevation, with the channel migrating in a westerly direction. Analysis of this sediment within the embryonic creeks and on the surrounding bank, presented in Table 7.2, indicate that the banks were coarse

with a much lower mud concentration and percentage lost on ignition compared to the sediments found at the bottom of the creeks.

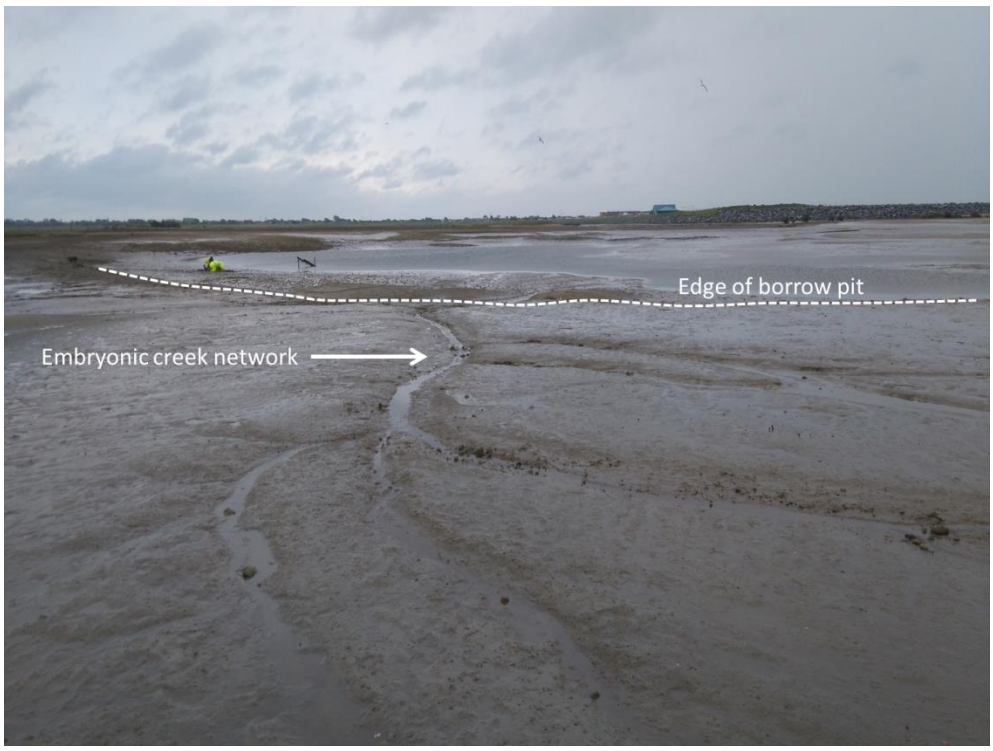

Figure 7.2: The western embryonic creek network, looking towards the south-east, at Site 5 at the Medmerry Managed Realignment Site in May 2016, one of two embryonic creeks which have formed at this site.

Across the middle transect, T2, the position of the western creek network fluctuated and varied in depth and width, although it constantly increased in elevation (Figure 7.4b). In the most recent survey (June 2016), a decrease in elevation to the west of the main network was detected due to the headward erosion of a sub-channel (Figure 7.3d). The depth of the eastern creek network increased across the middle transect, with the channel incision creating a broader channel, and accretion occurring on the surrounding banks.

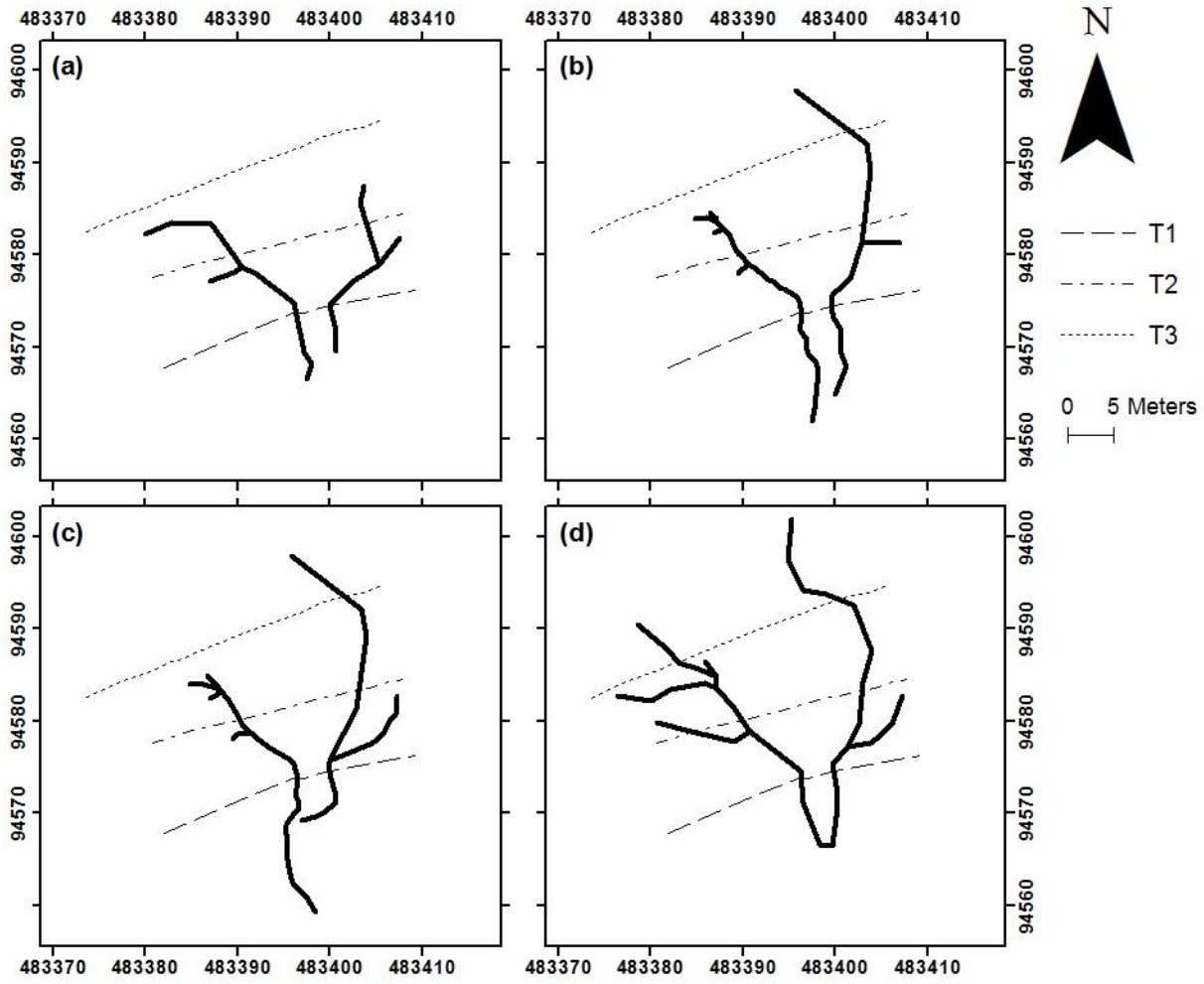

Figure 7.3: Differential global positioning system (dGPS) measurements of the position of the embryonic creek networks at Site 5 at the Medmerry Managed Realignment Site on (a) 8th August 2015, (b) 22nd October 2015, (c) 3rd March 2016 and (d) 10th June 2016. Measurements were taken from within the borrow pit to the nickpoint; the abrupt break in the longitudinal profile. Positions of transects (T1, T2 and T3) are marked by dashed lines (see Figure 7.4).

At T3, the landwards extremity of the developing creek network (Figure 7.4c), the eastern creek eroded and incised significantly resulting in a wide channel with steep banks. The western channel, which had only reached the third transect (T3) in the most recent survey, was not detected in elevation measurements.

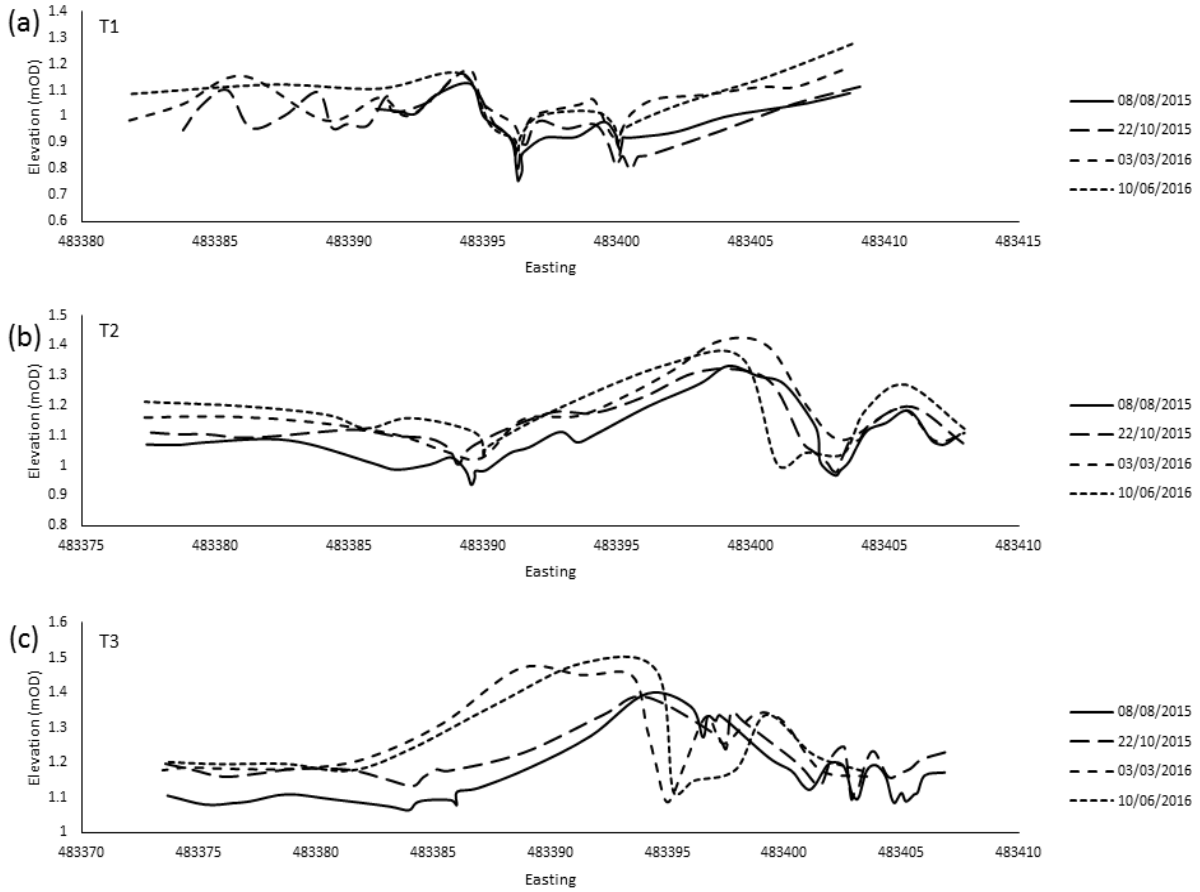

Figure 7.4: Elevation changes across the bank taken from (a) T1 at the edge of the borrow pit, (b) T2 inland and (c) T3 at top of the embryonic creek system on the 8th August 2015, 22nd October 2015, 3rd March 2016 and 10th June 2016 (see Figure 7.3 for location).

Table 7.2: Average (mean ± standard deviation) physical sediment parameters (n = 3) for the bank surface and bed of the embryonic creek network which has formed following pipe collapse at Site 5 at the Medmerry Managed Realignment Site.

	Moisture Concentration (%)	**Loss on Ignition (%)**	**d_{50} (µm)**	**Mud (Clay + Silt) Concentration (%)**
Bank Surface	31.05 ± 1.03	0.87 ± 0.28	177.15 ± 0.20	4.46 ± 0.11
Creek Bed	39.13 ± 2.95	2.80 ± 1.00	22.50 ± 1.22	54.59 ± 1.08

7.3 Topographic Model of Site 5

A high resolution orthomosaic (Figure 7.5) and DSM (Figure 7.6) of Site 5 was produced following an aerial survey with a small UAV on 13th July 2016 (Section 4.6.2). The orthomosaic produced from the UAV images shows the two creek systems and a sand bar, which has migrated from the south-west (Section 5.2.6), between the two creeks. Bedforms, in the form of ripples, are present on this sand bar and indicate a wave direction from the south-west matching the orientation of the prevailing wind. The DSM produced following SfM analysis (Figure 7.6) presents evidence of dendritic and complex creek networks, beyond that measured in Section 7.2.2 using dGPS. In addition, a series of equally spaced parallel lines are present in the north-east of the DSM and are probably the remnants of plough lines from the site's arable former land use; the stalks from the barley crop harvested the week before site inundation are still present in the area around these lines.

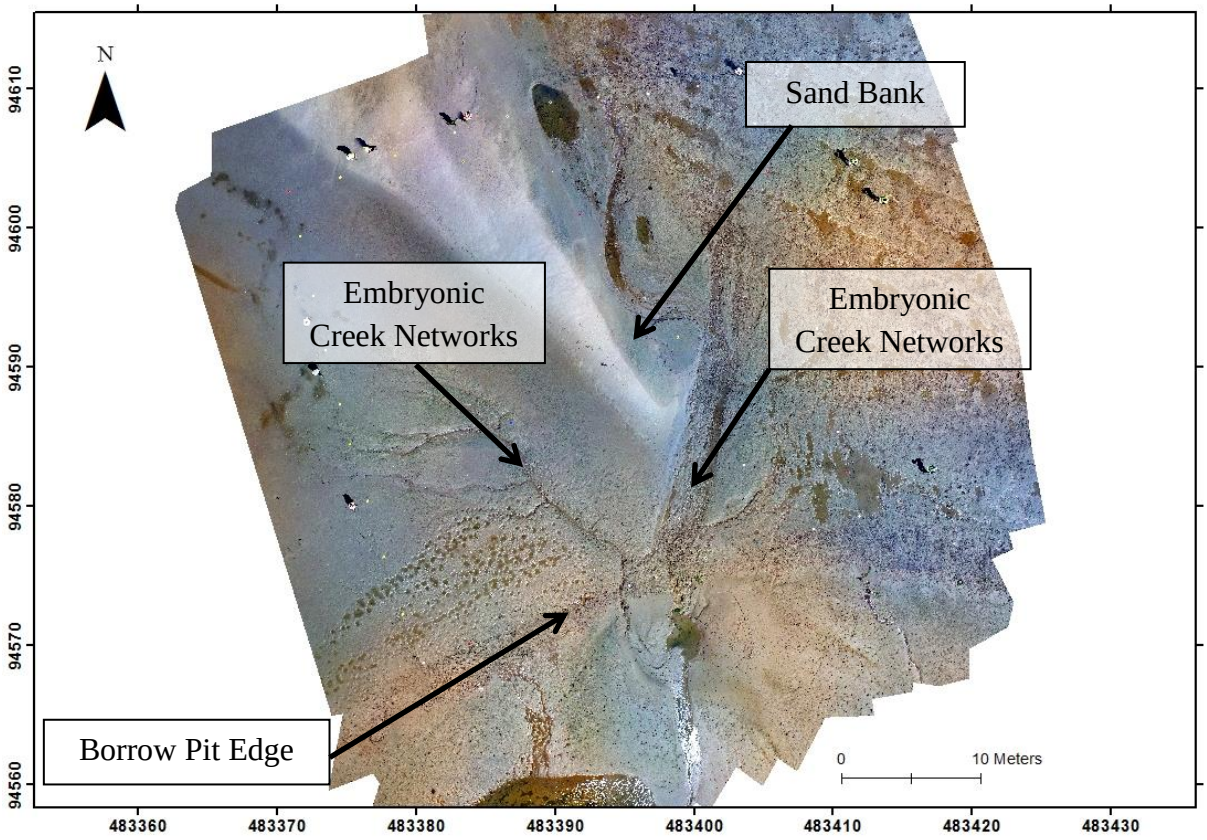

Figure 7.5: Orthomosaic of the surveyed area on 13th July 2016 at Site 5 at the Medmerry Managed Realignment Site annotated to show the main morphological features (see text for discussion).

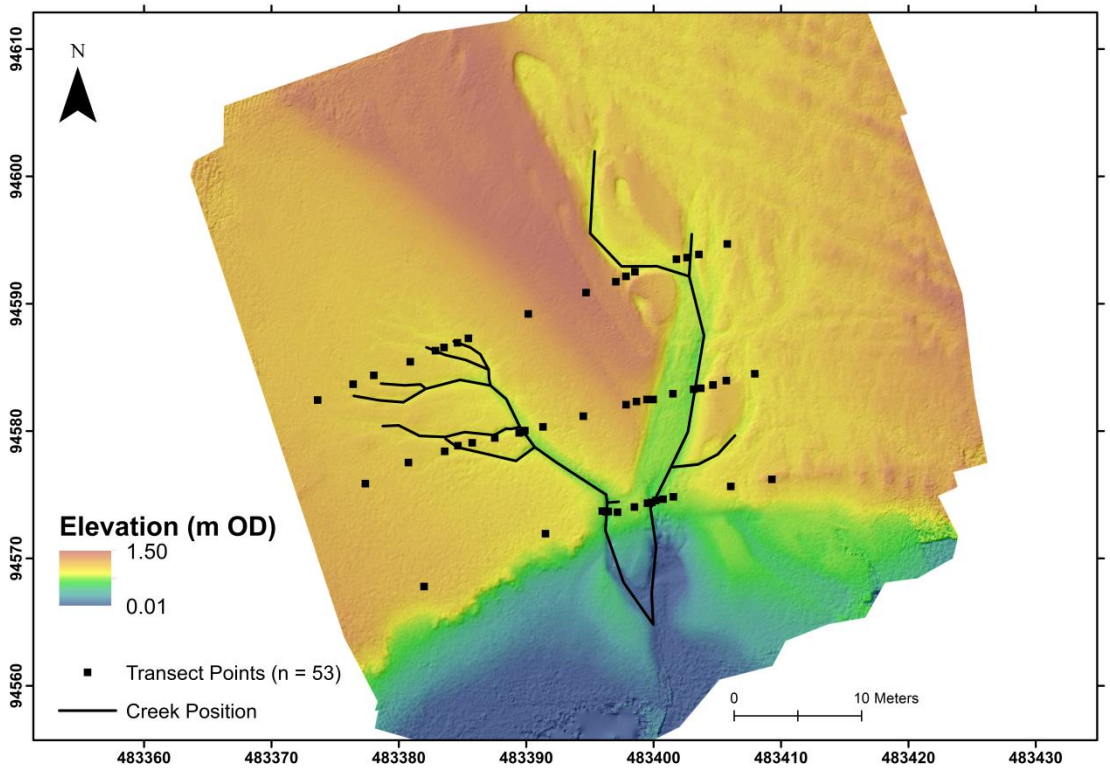

Figure 7.6: The digital surface model (taken on 17th July 2016) of Site 5 produced following Structure-from-Motion (SfM) analysis of images taken using an Unmanned Aerial Vehicle (UAV) and a comparison between differential global positioning system (dGPS) measurements of creek position and elevation transections (taken on 27th July 2016) at the Medmerry Managed Realignment Site.

7.3.1 The Effectiveness of UAV Surveys for Assessing Morphological Development

Figure 7.6 presents a comparison between the DSM, derived from SfM analysis of the UAV images, and measurements of creek position taken using dGPS. Both dGPS and UAV measurements appear to be in agreement of the creek position within the main central part of the network, although increased spatial complexity was detected by the UAV survey at the margins of these features. Analysis of the DSM also provides a comparison of differences in creek width, although these changes have been captured in measurements of elevation taken in transect by dGPS. The mean vertical difference (DSM – dGPS measurements) between the DSM and the dGPS transects (see Figure 7.6 for locations) was small (0.009 m) with a maximum and minimum vertical difference of 0.085 m and -0.056 m respectively. Overall, the vertical root-mean-square-error (RMSE) was 0.032 m and the mean-absolute error (MAE) was 0.025 m, both below the

upper range of acceptable values for reasonable surface reconstruction reported by Tonkin and Midgley (2016). These low error values indicate high confidence in the model's ability to represent morphological development, but at higher resolution than is possible using traditional dGPS techniques, demonstrating the suitability of using UAV surveying to assess morphological development within managed realignment (MR) sites.

7.4 Proposed Mechanism of Creek Formation

Following observations and measurements of creek formation and development at Site 5, it is proposed that these creeks formed as a result of the collapse of sub-surface tunnels, created via a phenomenon known as piping. The occurrence of piping has commonly been documented in arid and semi-arid regions with occasional very high rainfall events (e.g. Gutierrez et al., 1997), within the engineering literature regarding dam failure (e.g. Liu, 2012), and was first observed in saltmarsh environments at Nigg Bay, Scotland (United Kingdom) by Kesel and Smith (1978). Piping occurs when there is a subsurface flow of water through pores, cracks, root channels and other subsurface (high permeability) features, which flushes out the fine sediment forming a pipe below the surface. Pipe formation has also been associated with burrows created by crabs (Van Huissteden and Van de Plassche, 1998), although no evidence of this was found at the Medmerry site.

Observations from the Medmerry site suggest that piping forms as a result of the sudden exposure of the previously free draining terrestrial environment to tidal cyclicity and saturation twice a day. As tidal waters recede faster than the soil can drain a differential hydraulic head forms at the edges of the banks and main drainage features (channels and borrow pits). During periods of bank exposure (i.e. low water), water flows through the bank towards the lower hydraulic head due to the difference in hydrostatic pressure. The flow of water flushes fine sediments from the bank, increasing the diameter of the subsurface pipe, with entrances forming at the top of the banks due to focussed surface collapse. Eventually, the subsurface pipes collapse along their length, forming

embryonic creeks. To the author's knowledge this is the first reporting of piping in a newly inundated intertidal environment.

The first evidence of piping at Site 5 (Figure 7.7) was observed in June 2014 (Burgess, *personal communication*, 2014), and has been examined *in situ* through reconstruction of draining tidal waters (Appendix 6). Analysis of the UAV derived orthomosaic evidences two locations where additional pipes emerge from the bank (Figure 7.8). One of the pipe systems, to the west of the embryonic creek networks (Figure 7.8a), appears to be fed by a series of small pipe tops running parallel to the borrow pit edge. A larger, more irregularly shaped, pipe top feeds the second of these creek systems to the east of the creek network (Figure 7.8b).

Figure 7.7: Water flowing from the bottom of a pipe (insert) through the bank of the borrow pit (looking north-eastwards) in June 2014 (photograph: H. Burgess).

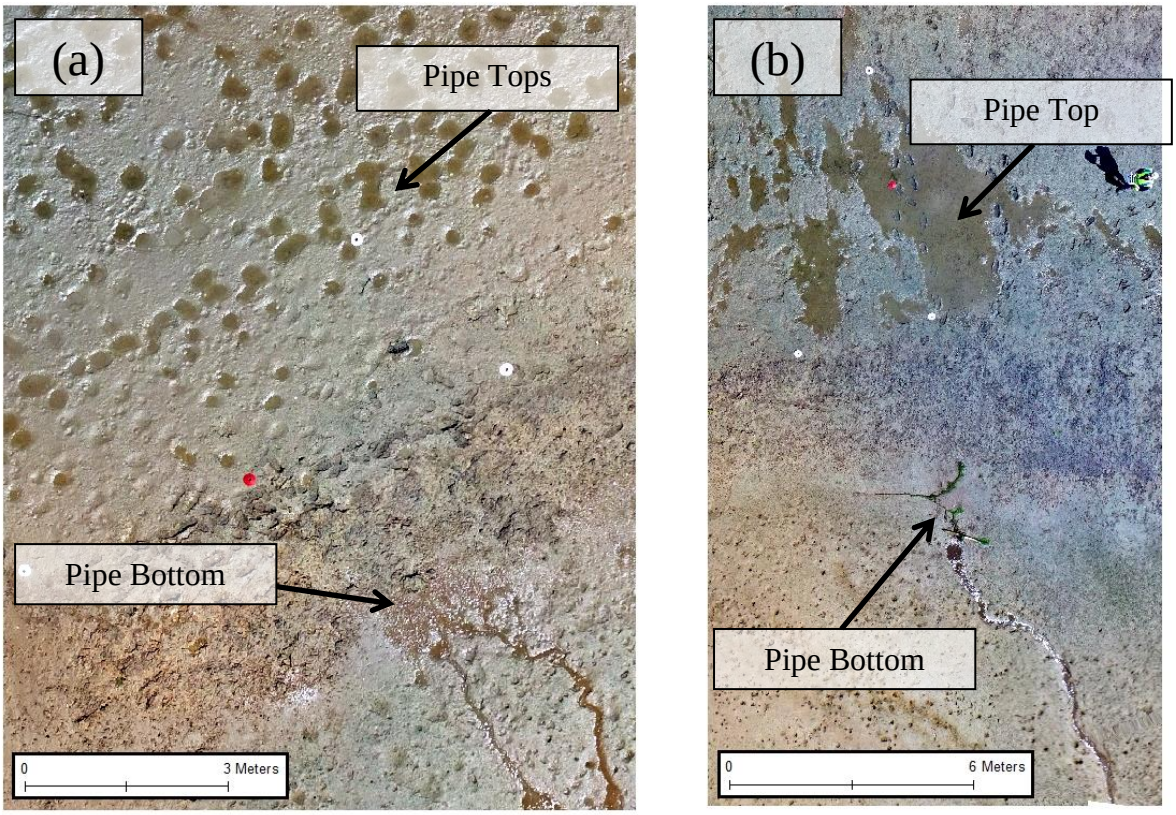

Figure 7.8: Evidence of piping (a) to the west and (b) to the east of the embryonic creek networks at Site 5 at the Medmerry Managed Realignment Site.

7.4.1 Piping at Site 2b

A large number of small pipes, similar to those found at Site 5, were identified in the bank at Site 2b in August 2015. Pipe entrances have formed in the bank surface at Site 2b, with water emerging at the interface between two separate and discrete sediment units exposed along the bank of the main drainage channel (Figure 7.9); the draining water flows along the top of this boundary sloping towards the channel at an angle of 30°. This process has resulted in the flushing of sediment from within the upper sediment unit, the collapse of the sediment structure, and either bank collapse or the formation of embryonic drainage creeks. Table 7.3 presents the principal physical sediment parameters measured for the two sediment units exposed along the bank where piping has occurred. The lower sediment unit had high moisture concentration and mud concentration. In comparison, the upper sediment unit, in which the piping had occurred, was more organic (higher percentage lost on ignition) and had a lower

proportion of fine grained sediments. On visual inspection this unit also appeared unconsolidated and more friable in comparison to the lower sediment unit.

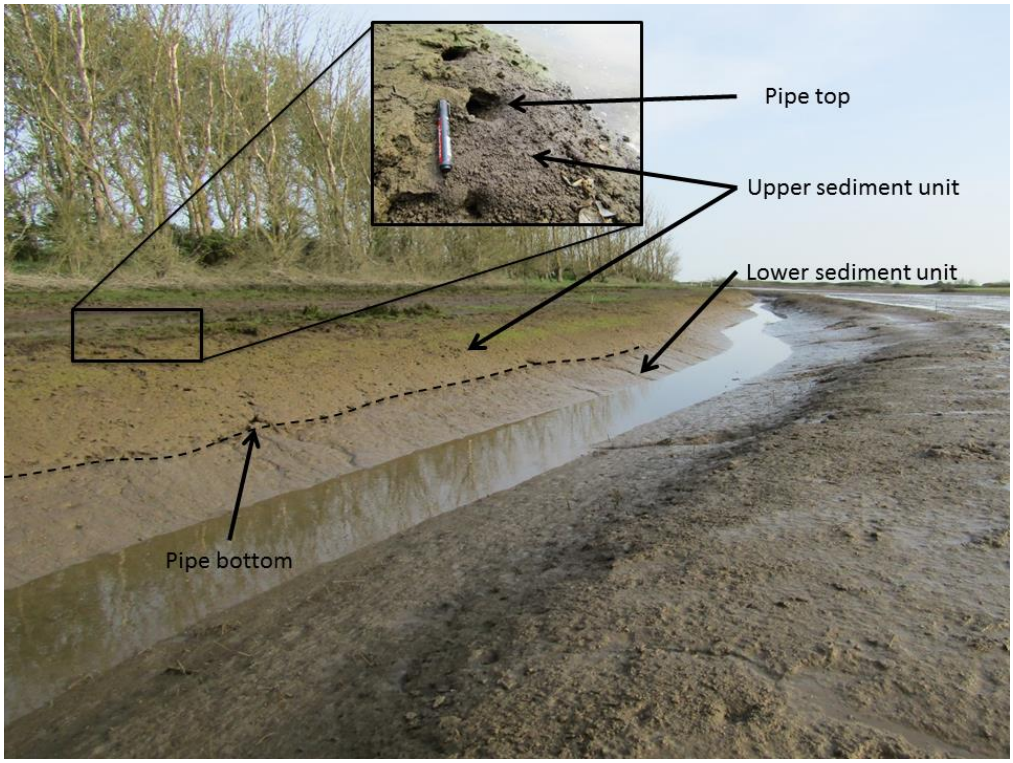

Figure 7.9: Sediment units (boundary marked by dashed line), the pipe top (insert, pen for scale) and bottom of the pipes which have formed in the bank at Site 2b, (looking southwards) in June 2016 (photograph: J.Dale).

Table 7.3: Average (mean ± standard deviation) physical sediment parameters (n = 3) for the upper and lower sediment units at Site 2b at the Medmerry Managed Realignment Site.

	Moisture Concentration (%)	**Loss on Ignition (%)**	**d_{50} (µm)**	**Mud (Clay + Silt) Concentration (%)**
Upper Sediment Unit	61.62 ± 1.18	10.43 ± 0.13	107.66 ± 11.37	33.80 ± 1.61
Lower Sediment Unit	91.45 ± 5.62	8.16 ± 0.48	5.92 ± 0.20	91.22 ± 0.55

7.5 Discussion

7.5.1 Influences and Mechanisms of Embryonic Creek Morphogenesis

Two main processes of creek morphogenesis have been observed at the Medmerry Managed Realignment Site. In the centre of the site, at Site 3, a creek formed during a period of intense rainfall in January 2014. Despite the main cut channel being a sink for sediment (see Section 5.2.4 and Chapter 6), the pluvial creek at Site 3 has continued to incise and deepen since it formed. The bed of the pluvial creek incised down to a coarse (cherts and sand) inorganic sediment layer (Table 7.1) which appears to act as a physical barrier preventing further incision or erosion within the creek. It is probable that this layer constitutes a marine terrace similar to those found across the Sussex coastal plain; raised intertidal deposits have been reported at similar elevations at locations (Pagham and Earnley) neighbouring (Bates et al., 1997) and within the Medmerry site (Krawiec, in press).

Creek networks have also formed through the transfer of water through subsurface pipes which have subsequently collapsed. Piping has occurred in the banks surrounding the main drainage channel at Site 2b (Figure 7.9), and around the borrow pit at Site 5. Following pipe collapse, at Site 5 (Figure 7.8), a series of embryonic creek networks have formed, which have become more complex and dendritic with time. At Site 2b, the piping has occurred in a friable soil-like layer with a higher organic (loss on ignition) concentration, lower moisture concentration and coarser grain size than the sediments found in the lower portion of the bank. This upper unit is regarded to be the former terrestrial (reclaimed) soil and the lower unit is the older, pre-reclamation, intertidal sediment, similar to the stratigraphy exposed within the breach area (Section 3.2.4). Whilst the functioning of the pipe networks has been evaluated at Site 2b (Appendix 6), further work is required to assess the connectivity and the subsurface movement of water, which may be possible utilising techniques used elsewhere such as ground-penetrating radar (e.g. Holden et al., 2002).

Following pipe collapse at Site 5 coarse inorganic sediment has been deposited (Section 7.2.2), with creeks developing on top of a bed consisting of the former terrestrial surface. Mapping the detailed development of embryonic creeks is, however, difficult as surface elevation measurements taken by dGPS are both spatially limited and open to user bias (in terms of selection of measurement point location). Measuring the evolution of creek development is essential for evaluating the factors controlling their development, yet many of these embryonic features are small and difficult to detect. There is a need to collect high-frequency, high-resolution, measurements beyond the capabilities of standard remote sensing techniques (such as LiDAR and aerial photography analysis), but without the limitations of dGPS measurements, over a sufficient area in order to capture the onset of embryonic creek development. The use of repeated terrestrial laser scanner or UAV surveys may be appropriate here; these technologies have already proven to be effective in mapping bedforms, erosion and geomorphic features in various alternative settings including wetlands (e.g. Castillo et al., 2012; Friess et al., 2014; Long et al., 2016; Cook, 2017; Masselink et al., 2017), and was demonstrated to be successful at the Medmerry site in Section 7.3.

7.5.2 Influence of Former Land Use and Site Design

Watts et al. (2003), based on analysis of the Tollesbury Managed Realignment Site, Essex, United Kingdom, proposed that creeks would only form in soft accreted sediments exceeding a critical depth of 20 to 30 cm. There has been a large amount of accretion in the vicinity of the forming creek networks at Site 5 (see Section 5.2.6). However, creek formation at Medmerry occurred prior to the level of accretion exceeding the depth suggested (albeit site specifically) by Watts et al. (2003), with creeks forming at Medmerry through (i.e. eroding into) the terrestrial soil surface exposed at the time of site inundation.

Evidence of the creek evolution at Medmerry suggests that the development of these features is influenced by the difference in subsurface sediment conditions. Similar observations were reported by Vandenbruwaene et al. (2012), who found creek formation was hindered by a compact clay layer in controlled reduced tides schemes on

the Scheldt (Belgium). It is widely considered that MR should be carried out on areas previously reclaimed for agricultural use (French, 2006); this inevitably means that most sites will have a complex subsurface stratigraphy. Cundy et al. (2002), for example, found evidence that the terrestrial soil horizon could still be detected at nearby Pagham Harbour almost a hundred years after natural site inundation during a storm event, whilst Tempest et al. (2015) demonstrated that the former terrestrial horizon significantly restricted sub-surface hydrological connectivity at the Orplands Farm Managed Realignment Site (Essex, United Kingdom). Visual observations of the creek networks at Orplands Farm, where a number of creeks were constructed prior to site inundation, suggest that creeks formed after site inundation will not incise below the level of the terrestrial sediment layer (Spencer, *personal communication* 2016). Furthermore, the creeks which have developed at Orplands Farm tend to run parallel and do not flow in a seawards direction. This is likely to be the result of physical disturbance to the sediment related to either farming practices prior to site inundation, or site construction methods.

Creek development in MR sites is essential for site, and sediment, drainage and the evolution of the sediment regime (Leggett et al., 2004) and the provision of ecosystem services, due to the interaction between the developing creek networks and the wider morphological and ecological progression (e.g. D'Alpaos et al., 2007b; Kirwan and Murray, 2007; Temmerman et al., 2007). Yet, analysis of drainage networks here and in in other MR sites has suggested that creek development is influenced by differences in subsurface sediment structure (Vandenbruwaene et al., 2012; Tempest et al., 2015). Given that the majority of MR sites are constructed on areas of the coastal hinterland that have been used for arable agriculture, it is likely that sediment has been compacted and structurally altered (Dent et al., 1976; Spencer et al., 2017). Consequently, there is a need to reduce the influence of the underlying terrestrial soil or to engineer sites to encourage creek development and growth. Sites could be ploughed or engineered in order to expose uncompacted soils that are more susceptible to creek formation, or dredged material could be distributed over the terrestrial soil prior to site inundation; D'Alpaos et al. (2007a), for example, reported rapid creek evolution in a reconstructed saltmarsh in Venice Lagoon, where dredged material had been used in site regeneration.

The design of drainage networks and borrow pits in MR sites could also be enhanced to encourage the formation of a difference in hydraulic head to accelerate piping, and therefore creek development. Additionally, it might be possible to landscape sites during the construction phase to direct drainage via relatively small and shallow ditches, no more than a couple of centimetres deep (Boorman and Hazelden, 1995). This could also incorporate pre-existing drainage features such as soakaways and drainage pipes; features that have received little consideration in the design of MR sites to date. However, further work is required to quantify and model the process of creek morphogenesis observed at Medmerry and assess whether these processes can be replicated in the design of future saltmarsh restoration schemes.

Identification of the processes and analysis of the parameters influencing embryonic creek development within other MR sites is required to assess the similarity between sites. Sub-surface pipes are transient features, limiting the timeframe available for capturing their influence on embryonic creek development. Further work, through experimental laboratory or numerical modelling studies may, therefore, be necessary to analyse the influence of different sub-surface sedimentological conditions on creek formation in an intertidal setting, as have previously been carried out for alternative environments (e.g. Wang et al., 2016). This would improve the design of MR sites and encourage creek development following site inundation, thereby increasing the level of coastal flood defence, providing compensation for habitat losses and degradation, and enhancing the ecosystem services provided.

7.6 Summary

Measurements and observations of embryonic creek formation and growth at the Medmerry Managed Realignment Site indicate that creeks will develop relatively quickly (within a couple of years), but are influenced by different sub-surface sedimentological conditions (such as sediment compaction and consolidation), which relate to historic environmental change and the former land use. Higher resolution measurements of embryonic creek growth are required following site inundation to capture the onset of creek development and to provide further insight into the factors

controlling creek evolution in newly inundated MR sites. It is also necessary to consider different site construction processes, including accidentally breached and historically flooded sites with no engineering prior to site inundation (i.e. non-managed realignment). The use of dredged material and site landscaping to accelerate creek growth post-site inundation also requires wider consideration.

Results in this chapter provide a new insight into the influence of surface and sub-surface sedimentological conditions, in relation to the former land use and site design, on the morphogenesis of embryonic creek networks. Creeks play a crucial role in the delivery of ecosystem services provided by intertidal saltmarsh and mudflat environments. Ensuring the rapid development of these features will enhance the success of MR schemes in terms of habitat loss compensation and wave and tidal energy dissipation, and therefore level of coastal flood defence provided.

8 Sediment Structure and Subsurface Physicochemical Evolution

8.1 Introduction

In previous chapters, the evolution of the sediment regime has been evaluated at the Medmerry Managed Realignment Site through measurements of the change in surface sediment properties (Chapter 5). The rhythms of sedimentation and the sources, and fluxes, of suspended sediment in response to site hydrodynamics have been analysed (Chapter 6), as has the creek formation and development processes (Chapter 7). This chapter examines the subsurface sediment evolution at Medmerry, in terms of the physical structure of the sediment and its physical and geochemical characteristics. The restored and constructed saltmarshes in managed realignment (MR) sites elsewhere have been demonstrated to differ structurally, physically and geochemically from natural saltmarshes (Spencer et al., 2017; Spencer et al., 2008; Tempest et al., 2015). Here, the differences in sedimentary structure and (physical and geochemical) subsurface composition are analysed, in comparison to the different former land uses and construction processes, to assess the preservation of the pre-breach terrestrial surface and the evolution of subsurface physicochemical properties.

To identify differences and changes in the subsurface physicochemical and structural evolution, sediment cores were collected in parallel in January and February 2015 (16 to 17 months after site inundation) from Sites 1, 2a, 2b, 3 and 5 (Figure 8.1, Table 8.1). Core depths varied between 20 and 49 cm, although parallel cores were not always taken to the same depth. At Site 3, samples were collected from a lower elevation, non-vegetated area and a higher elevation, vegetated area. These samples were analysed for broad scale (centimetre to decimetre) physical changes. Following this analysis core samples from Site 2b, both coring locations at Site 3, and Site 5 were selected for geochemical analysis for a range of major elements using inductively coupled plasma optical emission spectrometry (ICP-OES), after extraction via acid digestion. These locations were selected to compare sites of different former land use, evaluating sites

used for low and high intensity arable agriculture (Sites 2b and 5 respectively), and no arable agriculture (Site 3). These four locations were re-sampled in September 2016 (36 months after site inundation) for comparison of the subsurface physicochemical development. Sites 2b and 5 were also selected for high resolution sediment structure and geochemical analysis, with shorter (10 cm long) cores taken in July 2015 and September 2016 for a novel combination of X-Ray microtomography (µCT) and non-destructive X-ray fluorescence (ITRAX) analysis.

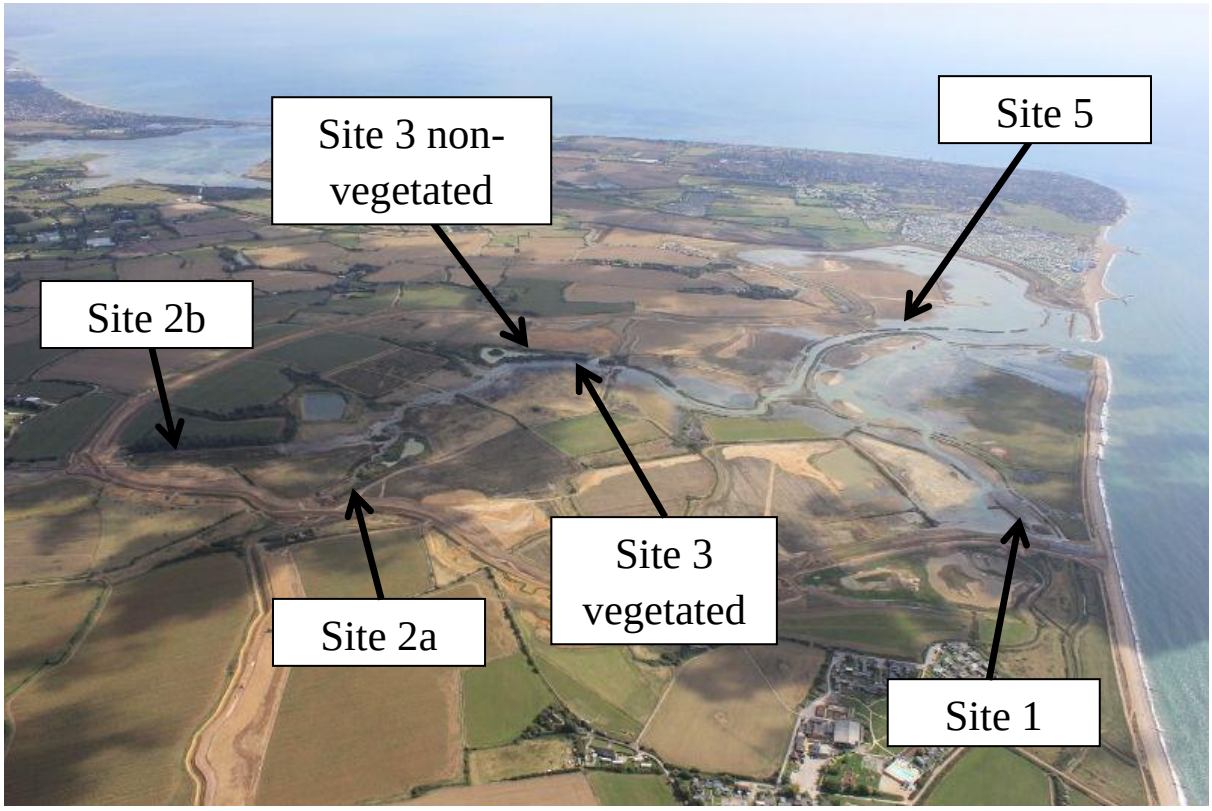

Figure 8.1: Sites analysed and discussed in Chapter 8 (looking south-eastwards, photograph: John Akerman).

Table 8.1: Summary of sites sampled, former land use and the dates sampled for broad and intensive scale analysis in Chapter 8

Site	Former Land Use	Broad Scale Analysis (2015)	Broad Scale Analysis (2016)	Intensive Scale Analysis (2015)	Intensive Scale Analysis (2016)
Site 1	Pastoral grassland flattened during site construction	February 2015			
Site 2a	Freshwater drainage channel	February 2015			
Site 2b	Low quality arable / pastoral land	January 2015	September 2016	July 2015	September 2016
Site 3	Pastoral land	January 2015	September 2016		
Site 5	Intensive arable field	January 2015	September 2016	July 2015	September 2016

8.2 Broad Scale (centimetre to decimetre) Physicochemical Changes in the Subsurface

Typically, the sediment cores exhibited clear vertical zonation (Figure 8.2) and can be divided into three units (from core surface to core base): (i) a post-breach intertidal unit dating from the period following site inundation in September 2013, (ii) a terrestrial boundary and unit formed since site reclamation in 1810, and (iii) below the reclamation boundary an older pre-reclamation intertidal unit. The depth, composition and structure of the three units varied between sites.

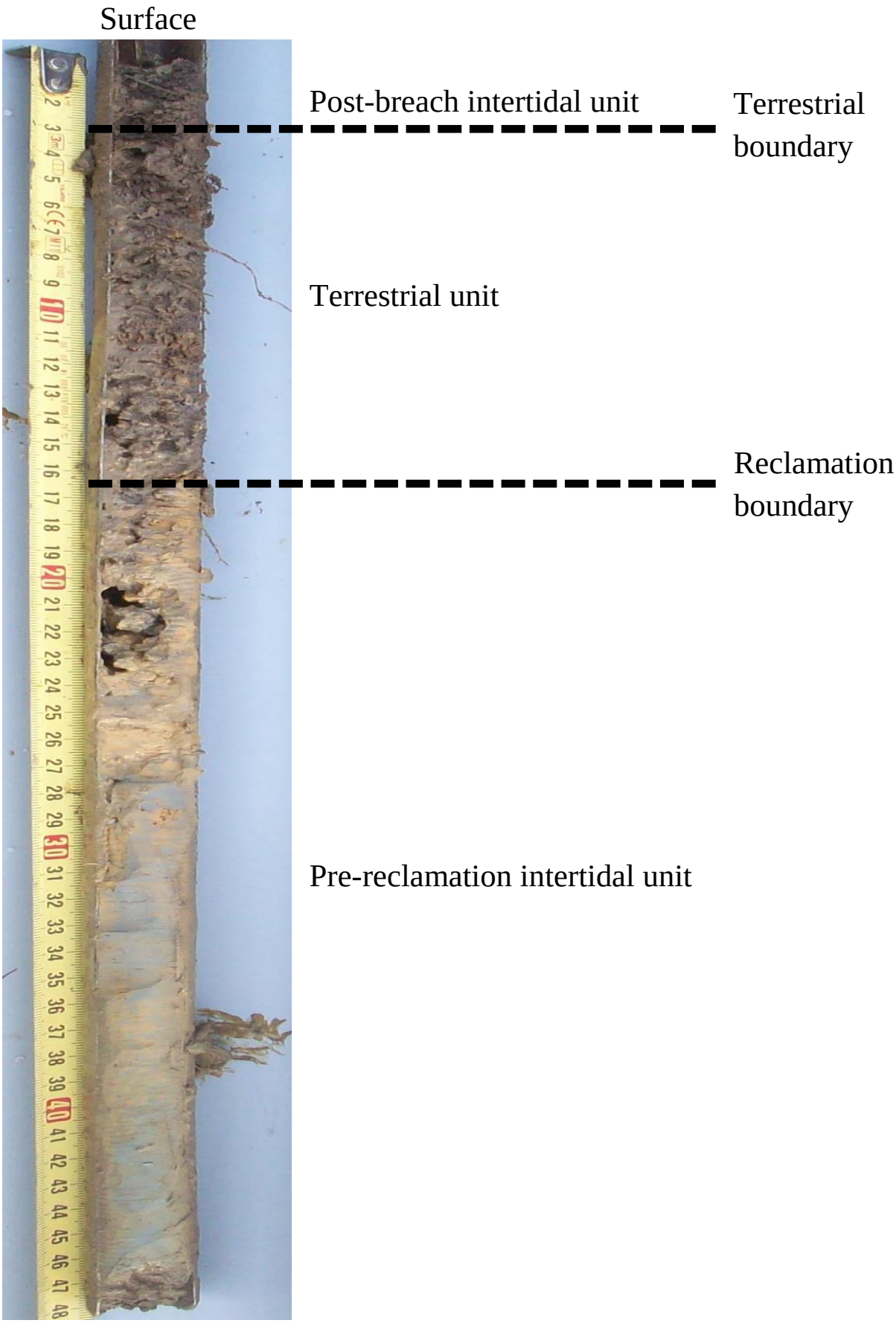

Figure 8.2: Typical vertical zonation exhibited in sediment cores taken from the Medmerry Managed Realignment Site, exemplified by one of the cores taken from the vegetated surface at Site 3 in September 2016. Three separate units were identified (labelled); a post-breach intertidal unit, a terrestrial soil unit, and an older pre-reclamation intertidal unit. The divisions between these units, marking the terrestrial (upper) and reclamation (lower) boundaries are marked by the dashed horizontal lines. Depth is indicated by the tape measure.

8.2.1 Site 1

A 20 cm core was taken from Site 1, which showed the typical zonation displayed in Figure 8.2. The post-breach intertidal unit was found in the top 5 cm (Figure 8.3), and consisted of a uniform grey clay unit with occasional organic fragments and no apparent sediment structure. The terrestrial unit, from 6 to 12 cm, was brown, friable, and poorly consolidated with a lower clay content. A sharp terrestrial boundary, marked by a large amount of root and plant litter (although this was not detected in loss on ignition measurements), divided the terrestrial unit from the lower pre-reclamation intertidal unit (13 to 20 cm) which contained dark brown, compact clay rich sediment.

The bulk density and porosity generally match the visual observations described above, increasing in the lower unit. A peak in moisture content was observed above the interface between the post-breach intertidal and terrestrial units, implying pooling and poor hydrological connectivity through the terrestrial boundary into terrestrial unit. Median grain size was higher in the terrestrial unit, which also showed a reduced mud (clay + silt) content.

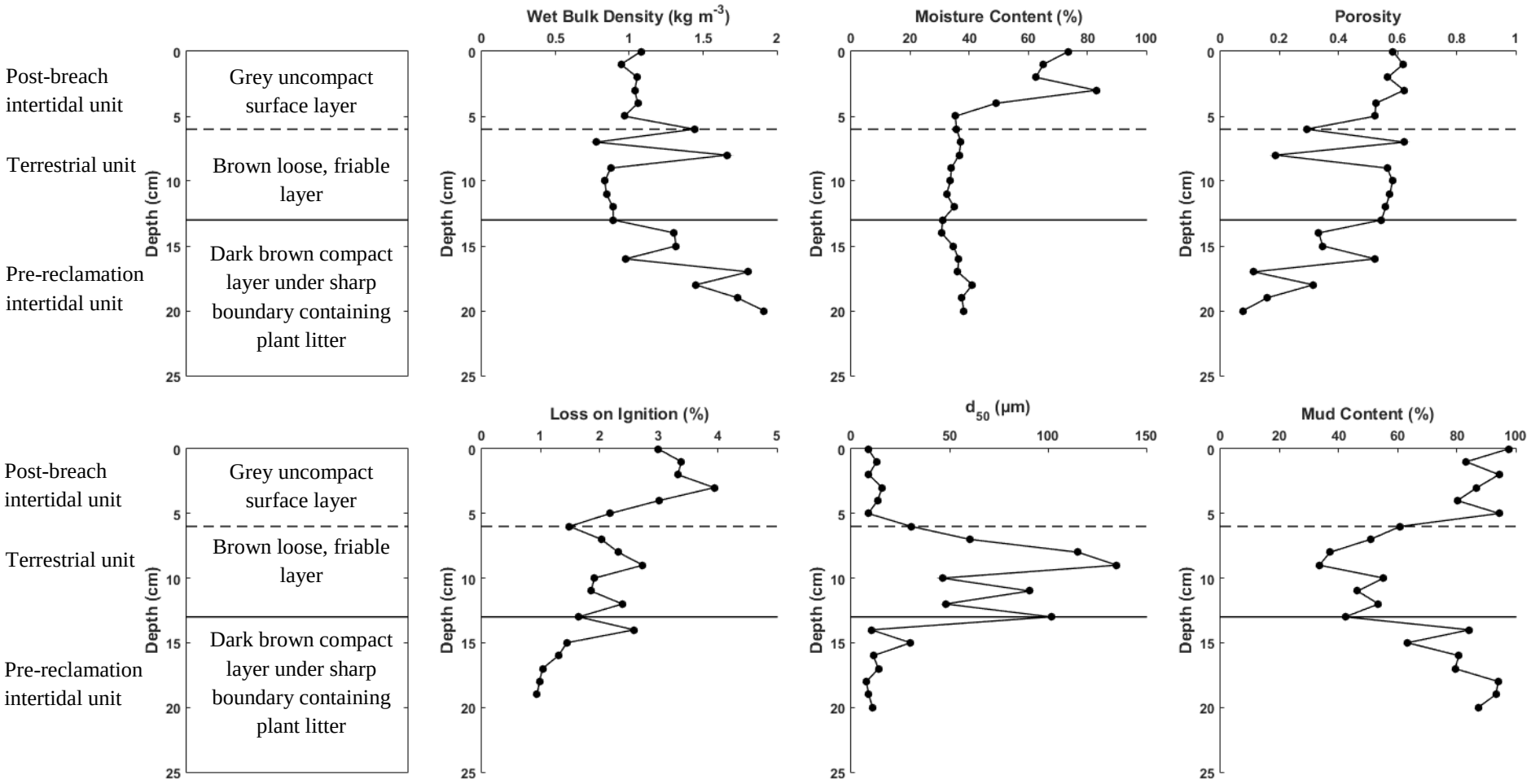

Figure 8.3: Comparison of the sediment log with wet bulk density, moisture content, porosity, loss on ignition, median grain size (d_{50}) and mud content (clay + silt) measured in parallel cores at Site 1. On the sedimentary logs dashed lines represent a gradational boundary and a solid line represents a sharp boundary between sediment units.

8.2.2 Site 2a

A 35 cm core showing the typical zonation presented in Figure 8.2 was taken from Site 2a. The post-site inundation intertidal unit was found in the surface and first centimetre of the core (Figure 8.4) and consisted of a thin, light brown, oxic, clay rich layer 2 mm thick underlain by a black uniform anoxic layer with no apparent sediment structure. A sharp boundary divided the post-site inundation intertidal unit and the terrestrial unit, which was from 2 to 10 cm, light brown, and partially friable, with small (< 2 mm) angular clasts and long (~ 2 cm) fragments of organic matter. From 11 to 35 cm, below the terrestrial unit, was the former intertidal unit, which consisted of light grey clay rich sediment with strands of organic matter. This unit became more compact from 15 cm and contained a number of small angular flint clasts from 25 to 35 cm depth, especially at 34 cm.

Wet bulk density increased, and moisture content and porosity decreased, with depth. Loss on ignition decreased in the post-site inundation intertidal unit but increased near the top of the terrestrial unit. Loss on ignition then decreased through the rest of the sample, with a large decrease occurring 10 cm into the pre-reclamation intertidal unit. A peak in the median grain size occurred at the reclamation boundary (between the terrestrial and pre-reclamation units), and increased in the lower section of the pre-reclamation intertidal unit.

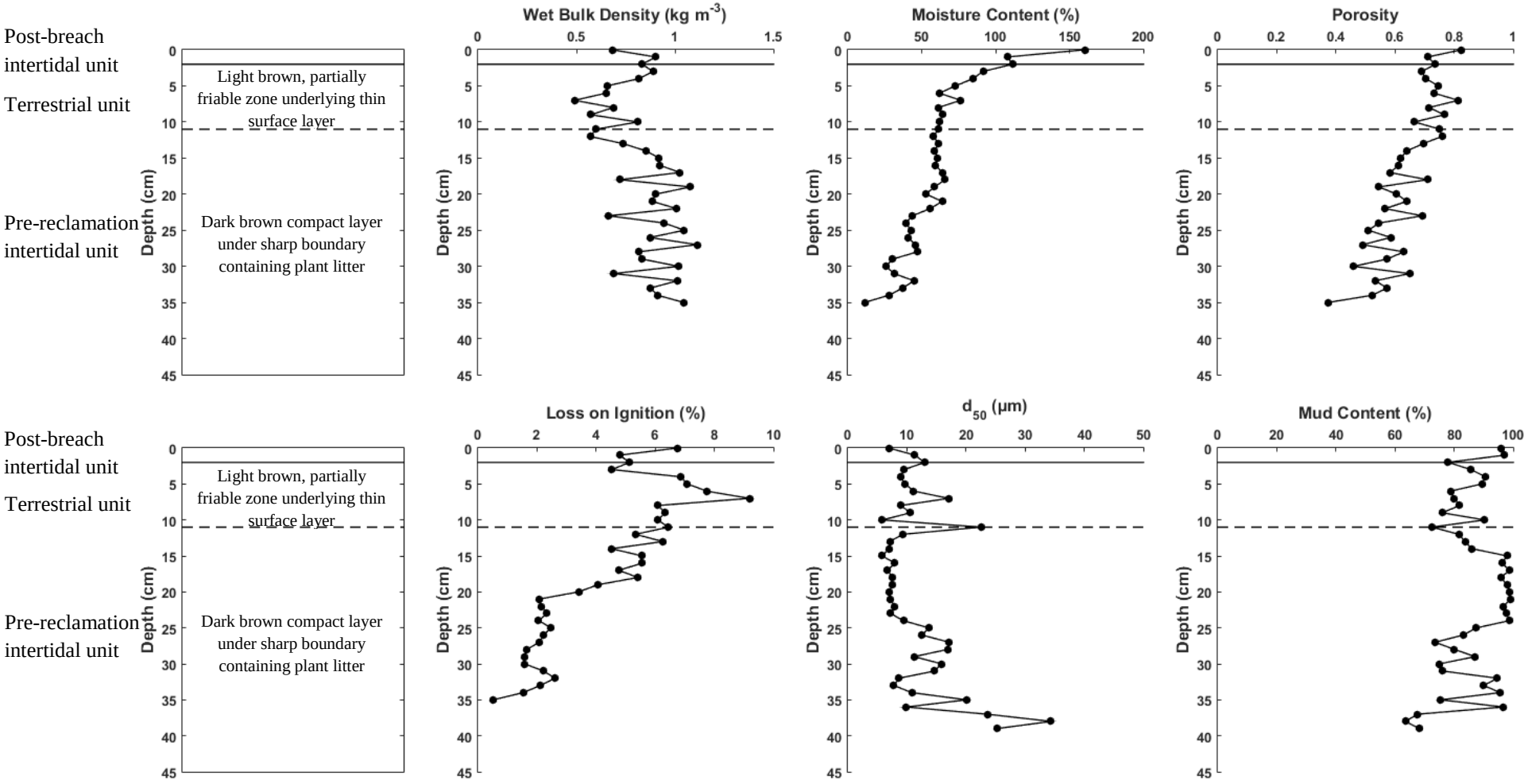

Figure 8.4: Comparison of the sediment log with wet bulk density, moisture content, porosity, loss on ignition, median grain size (d_{50}) and mud content (clay + silt) measured in parallel cores at Site 2a. On the sedimentary logs dashed lines represent a gradational boundary and a solid line represents a sharp boundary between sediment units.

8.2.3 Site 2b

8.2.3.1 2015

An algal mat covered the top of the 37 cm core taken from Site 2b in 2015 (Figure 8.5), which showed the vertical zonation displayed in Figure 8.2. Below this mat was the post-breach intertidal unit consisting of 2 cm of soft brown clay rich sediment with black staining. After a sharp boundary, the terrestrial unit (from 2 to 29 cm) consisted of grey / red mottled sediment caused by the presence of (partly-reduced) Fe and Mn oxides and oxyhydroxides. This reflects a sediment zone subject to a fluctuating water table and periodic shifts from oxidising to reducing conditions during tidal inundation (Cundy and Croudace, 1995; Zwolsman et al., 1993). Plant matter was found towards the top of this zone, with poorly decomposed root material and small angular clasts (< 5 mm) found through the unit. Beneath this unit was a compact, grey, silty clay rich pre-reclamation intertidal unit, marked by a sharp contact between the two units. The lower pre-reclamation unit was present from 30 cm for the rest of the sample.

Minimum wet bulk density, and maximum moisture content and porosity were measured at the boundary between the post-breach and terrestrial units. A similar peak was observed in the loss on ignition values with a second, larger, percentage loss being observed at the reclamation boundary. Below the reclamation interface, median grain size increased, although the mud content remained relatively constant indicating the change in median grain size was caused by a shift in the clay to silt ratio.

Major element data (Al, Ca, Fe, Mn, S, Na) are presented in Figure 8.6. To account for variations in grain size, data have been geochemically normalised to Al (after Spencer et al., 2008). Ca decreased through the upper centimetre of the sample, and then increased in concentration towards the bottom (last 3 cm). This may be the result of decalcification, typical of oxic saltmarsh sediments as a result of a lowering of the pH caused by nitrification and decomposition of organic matter (Luther and Church, 1988; Vranken et al., 1990), and then re-precipitation at depth. However the decrease, and subsequent increase, in Ca concentration occurs at the post-breach and reclamation

boundaries, indicative of finely comminuted shell debris being present in the pre-reclamation and newly deposited intertidal sediments.

The diagenetic cycles of Fe and Mn have been well documented for oxic saltmarsh sediments (e.g. Spencer et al., 2003; Zwolsman et al., 1993). A peak in Fe or Mn could indicate redox mobilisation of Fe and Mn, whereas an increase in S may represent bacterial reduction of sulphate (Cundy and Croudace, 1995). Mn, which is more sensitive to redox changes, and to a lesser extent Fe decreased through the near-surface sediment and showed some enrichment in middle terrestrial unit, although without any consistent or clear peaks. This is suggestive of a fluctuating water table, consistent with the visual observations of Fe-stained mottled sediment in this zone, as a result of tidal variability causing fluctuations in the redox boundary, preventing the formation of a stable redox zone and a strong Fe and Mn peak (Cundy and Croudace, 1995; Zwolsman et al., 1993). S decreased through the surface sediment. A similar trend was observed in Na, indicative of introduction through tidal waters with higher concentrations in the surface sediment caused by evaporation of seawater. PCA allowed for grouping of different depths based on their physicochemical variability, revealing for Site 2b (Figure 8.7) that the surface sediment differed from the rest of the sample and a separate group containing the lower, pre-reclamation intertidal sediments.

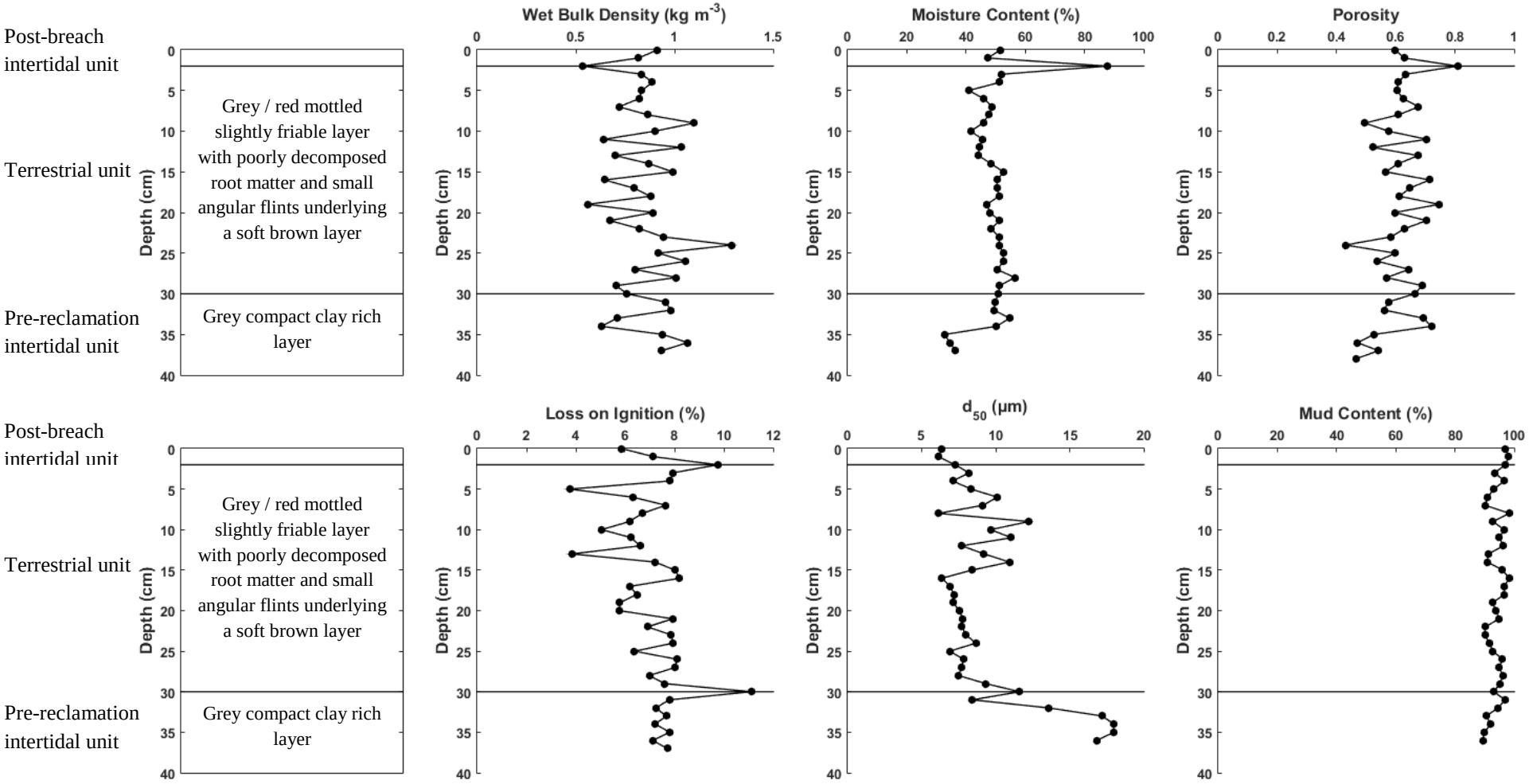

Figure 8.5: Comparison of the sediment log with wet bulk density, moisture content, porosity, loss on ignition, median grain size (d_{50}) and mud content (clay + silt) measured in parallel cores at Site 2b in 2015. On the sedimentary logs the solid lines represent the sharp boundaries between sediment units.

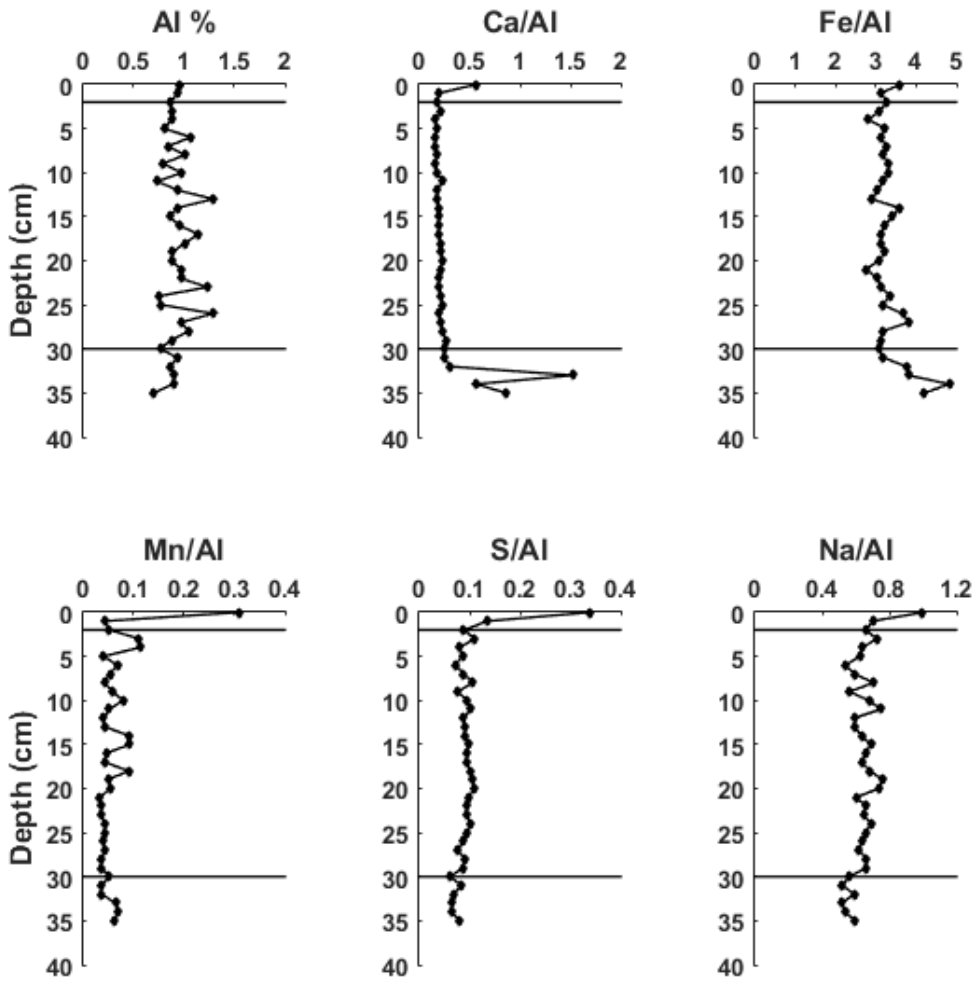

Figure 8.6: Variation in Al, Ca, Fe, Mn, S and Na with depth at Site 2b in 2015. The solid lines represent the sharp boundaries between sediment units.

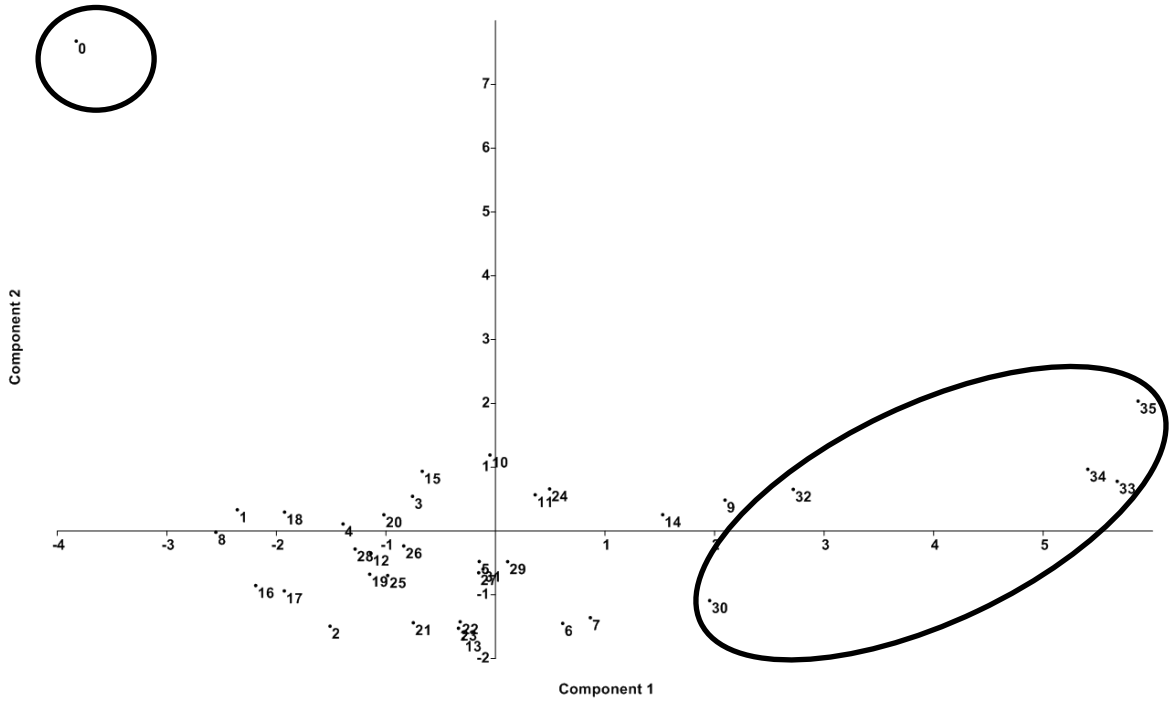

Figure 8.7: Principal component analysis (PCA) of different depths (numbered) for the Site 2b 2015 core plotted as Principal Component 1 vs. Principal Component 2. Components 1 and 2 explained 48.96 % of the variance. Circles highlight groups of depths with similar physicochemical variability (see text for discussion).

8.2.3.2 2016

The algal mat was no longer present when Site 2b was re-sampled in September 2016 (Figure 8.8), with the 31 cm core exhibiting the same post-breach intertidal, terrestrial, pre-reclamation intertidal vertical zonation. The top 2 cm consisted of the post-breach intertidal unit, a soft, light brown, silty clay layer underlain by a grey / red, mottled, partially friable terrestrial unit, from 2 to 28 cm, with small organic fragments, although the terrestrial boundary had become more gradual. The terrestrial unit then transitioned into the pre-reclamation intertidal unit, which consisted of compact grey sediment. The sample had become more compact and had lower moisture content, although this is likely to reflect the influence of seasonality; the site was first sampled in January when a higher moisture content would be expected than in September, when the site was re-sampled, due to increased levels of evaporation during the summer. Median grain size demonstrated a similar pattern between the 2015 and 2016 samples, although slightly coarser sediments were detected at the surface and no increase was found at depth, either due to local variability or the core not reaching that specific depth.

The concentration of Al, Ca and Mn were lower and relatively homogenous down core (Figure 8.9). Fe showed some variations with a small peak, matched by a decrease in S, at the reclamation boundary, potentially evidence of a redox-cline. Na increased in the near-surface sediment but decreased after the terrestrial boundary. PCA gives a less clear discrimination between sedimentary units, apart from the lower pre-reclamation intertidal sediment (Figure 8.10).

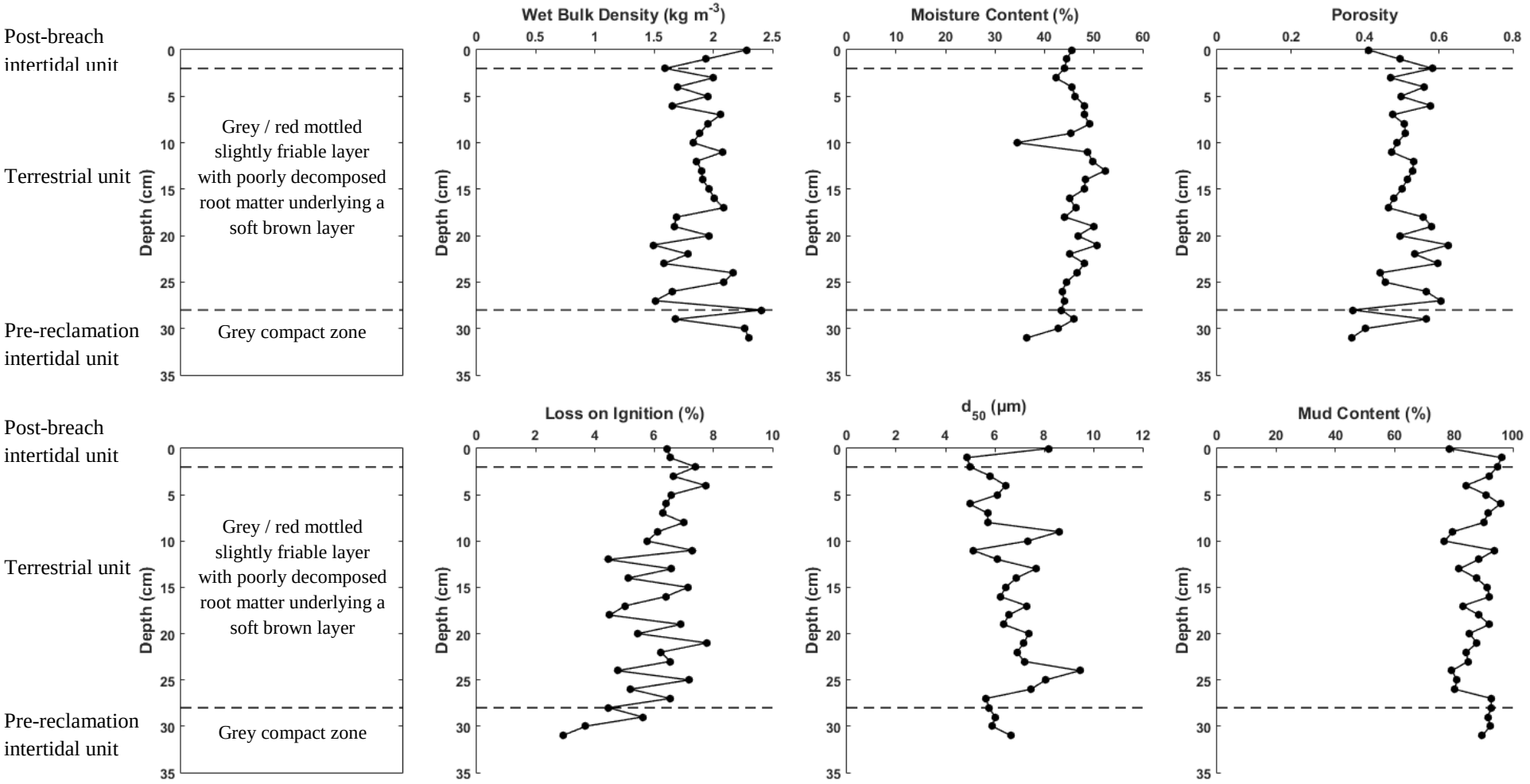

Figure 8.8: Comparison of the sediment log with wet bulk density, moisture content, porosity, loss on ignition, median grain size (d_{50}) and mud content (clay + silt) measured in parallel cores at Site 2b in 2016. On the sedimentary logs dashed lines represent the gradational boundaries between sediment units.

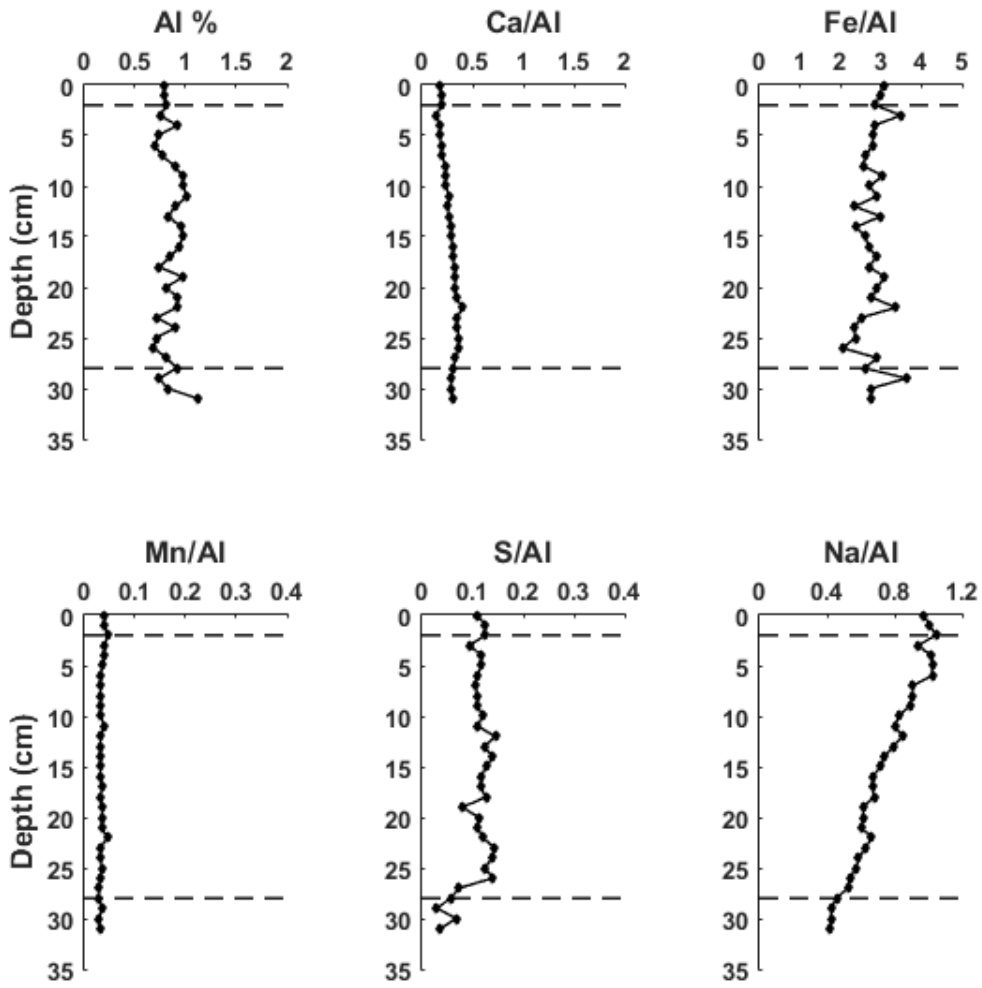

Figure 8.9: Variation in Al, Ca, Fe, Mn, S and Na with depth at Site 2b in 2016. The dashed lines represent the gradational boundaries between sediment units.

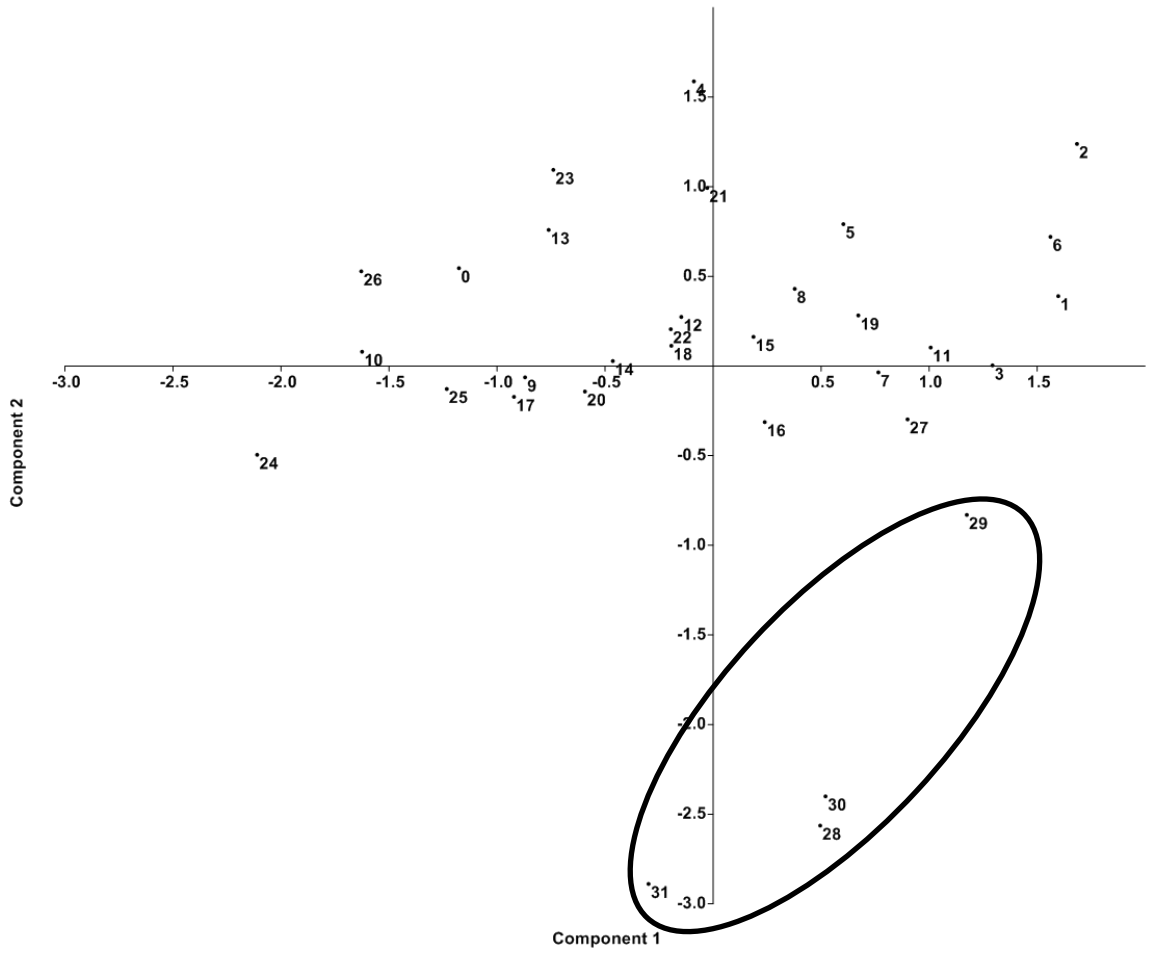

Figure 8.10: Principal component analysis (PCA) of different depths (numbered) for the Site 2b 2016 core plotted as Principal Component 1 vs. Principal Component 2. Components 1 and 2 explained 51.78 % of the variance. Circles highlight groups of depths with similar physicochemical variability (see text for discussion).

8.2.4 Site 3 Non-Vegetated

8.2.4.1 2015

The core taken from the non-vegetated surface at Site 3 (Figure 8.11) demonstrated the same vertical zonation presented in Figure 8.2. The top 5 cm of the 35 cm core consisted of the post-breach intertidal unit, which contained brown uniform clay rich sediment with some small strands of organic matter. Beneath this, there was a sharp boundary leading into a dark brown, crumbly, friable uncompact terrestrial unit with no clear structure, long interconnected root systems and red mottling towards the bottom. This zone graded into a grey pre-reclamation intertidal unit with red mottling, suggesting tidally induced fluctuations in the water table throughout the sampled sub-surface. Within the pre-reclamation zone, large strands of organic matter were found, including some large wood fragments in the bottom 3 cm, and a number of large (2 – 4 cm) rounded flint clasts.

The Ca concentration decreased in the post-breach intertidal unit and through the terrestrial boundary (Figure 8.12), remaining low throughout the rest of the sample, either as a result of a decreases in finely comminuted shell debris or decalcification. Fe and Mn concentrations decreased down core, most distinctly for Mn, with temporary increases at the boundary between the post-breach intertidal and terrestrial unit indicative of an oxic / suboxic boundary. S also decreased after the terrestrial boundary, although these trends corresponded to variations in Na and are likely to be derived from saltwater input, rather than redox (specifically, microbially mediated sulphate reduction) processes. PCA identified a group consisting of the upper 7 cm (the post-breach intertidal sediment) and a group just below the reclamation boundary in the pre-reclamation intertidal sediments (Figure 8.13).

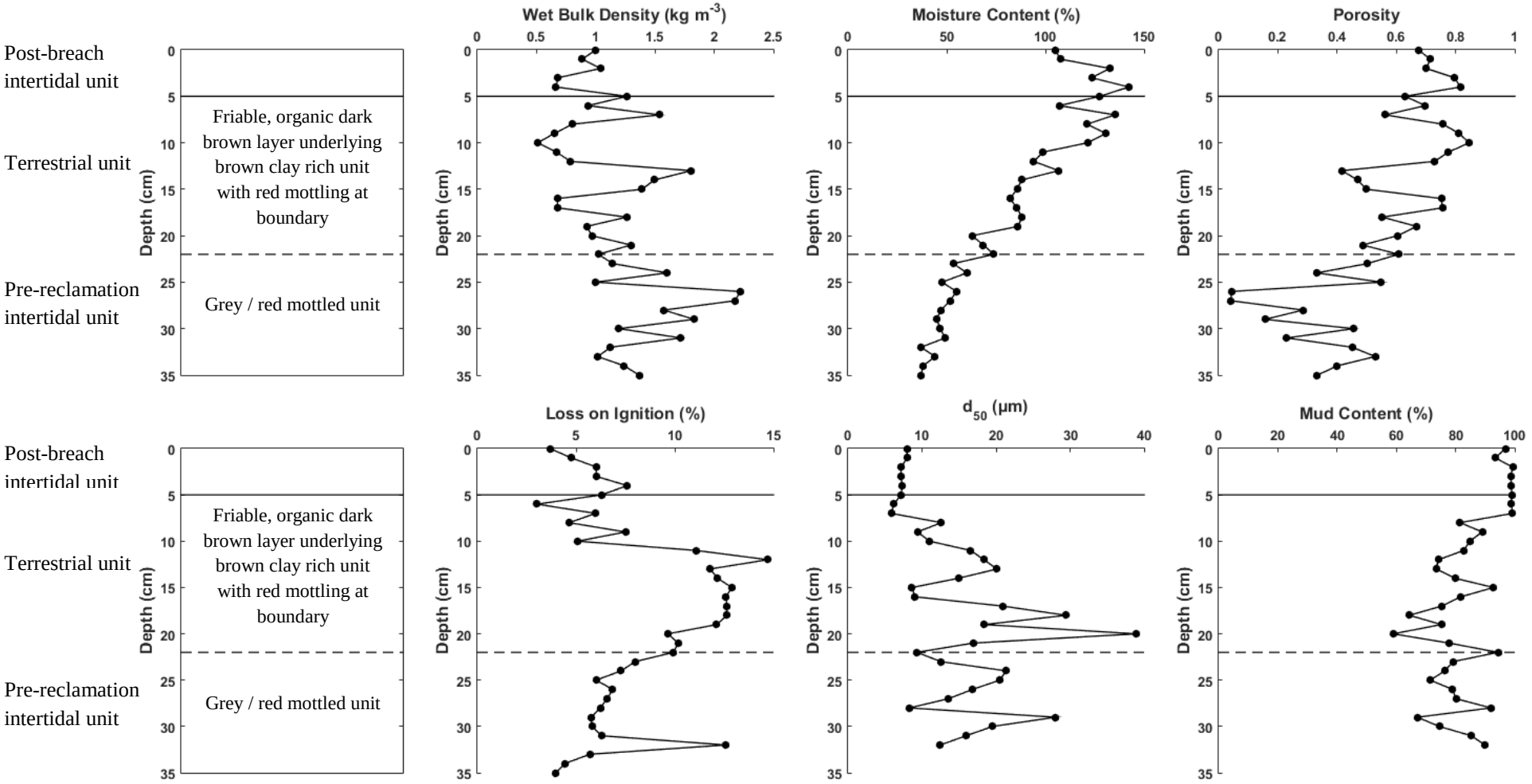

Figure 8.11: Comparison of the sediment log with wet bulk density, moisture content, porosity, loss on ignition, median grain size (d_{50}) and mud content (clay + silt) measured in parallel cores at Site 3 non-vegetated in 2015. On the sedimentary logs dashed lines represent a gradational boundary and a solid line represents a sharp boundary between sediment units.

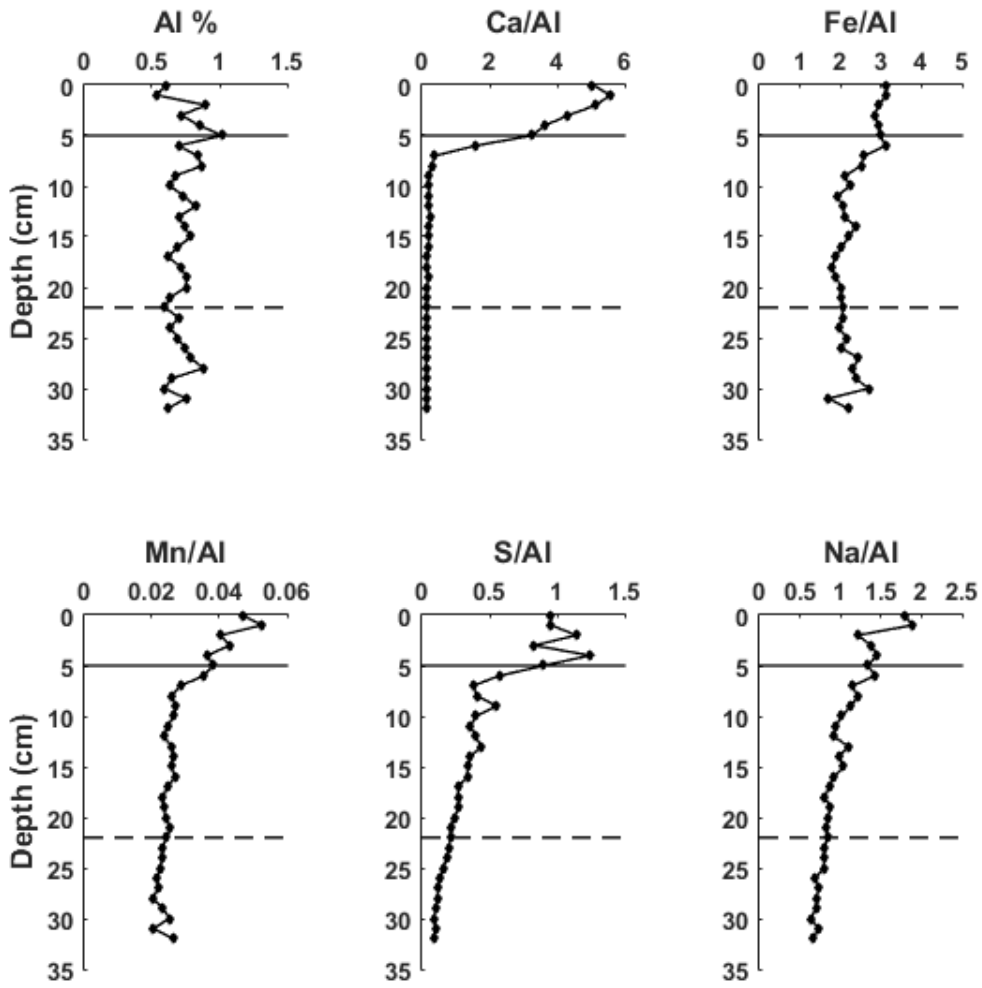

Figure 8.12: Variation in Al, Ca, Fe, Mn, S and Na with depth at Site 3 non-vegetated in 2015. The dashed lines represent a gradational boundary and the solid line represents a sharp boundary between sediment units.

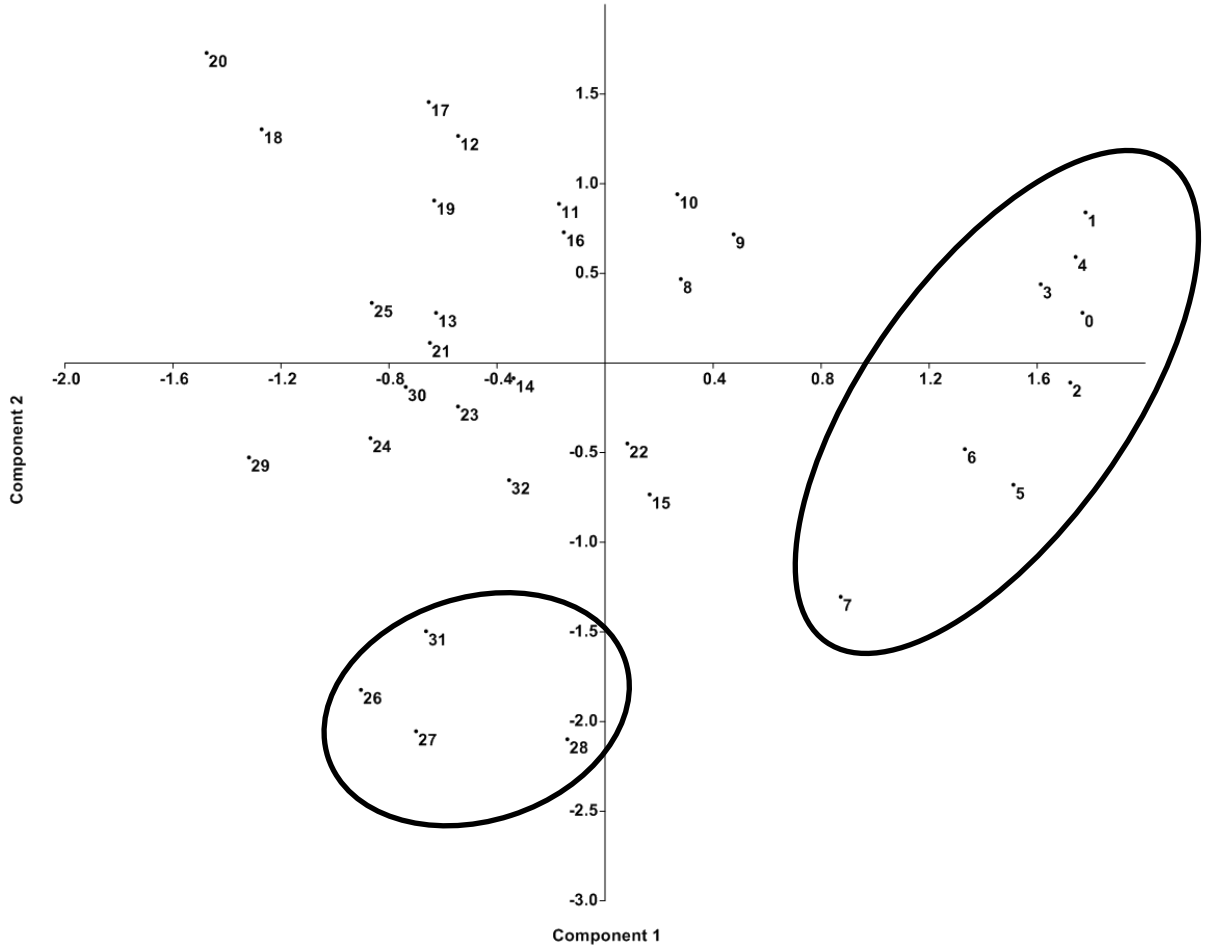

Figure 8.13: Principal component analysis (PCA) of different depths (numbered) for the Site 3 non-vegetated 2015 core plotted as Principal Component 1 vs. Principal Component 2. Components 1 and 2 explained 71.92 % of the variance. Circles highlight groups of depths with similar physicochemical variability (see text for discussion).

8.2.4.2 2016

Following re-coring at the non-vegetated location at Site 3, the same three units (post-breach intertidal, terrestrial and pre-reclamation intertidal) was revealed in a 41 cm core (Figure 8.14). However, the post-breach intertidal unit was larger, from 0 to 6 cm, and consisted of grey / black anoxic clays and silts, with a thin (1 mm) light brown oxic layer. A sharp boundary divided the post-breach intertidal unit from a grey / black friable terrestrial unit, from 7 to 29 cm with common root and organic matter. Sediment became more compact towards the bottom of the core. The basal 30 to 41 cm consisted of the pre-reclamation unit, which was grey and compact with red mottling, less organic

matter and an increase in coarse grained sediment. Moisture content peaked just below the terrestrial boundary. Loss on ignition peaked in the terrestrial unit as a result of the large amounts of root material. Median grain size increased and mud content decreased in the pre-reclamation intertidal unit, matching the observations made in the sedimentary log and in the sample taken in the previous year (Figure 8.11).

The increase in grain size in the pre-reclamation intertidal unit of the sample was reflected in a reduction in the Al concentration at the same depth (Figure 8.15). Ca decreased at the terrestrial boundary and below, as had previously been observed. Concentrations of Fe and Mn also decreased at the terrestrial boundary, and increased after the reclamation boundary, although Fe fluctuated at the lower boundary indicating that a stable redox zone had not developed. Furthermore, Fe peaked at the terrestrial boundary, which was observed visually in the sediment log, implying localised diagenetic enhancement at the interface of the two sediment units. S remained relatively high beyond the terrestrial boundary, decreasing through the terrestrial unit. Na decreased down core with peaks in the upper and lower parts of the post-breach intertidal sediment unit. PCA showed clear grouping of the three sediment units (Figure 8.16).

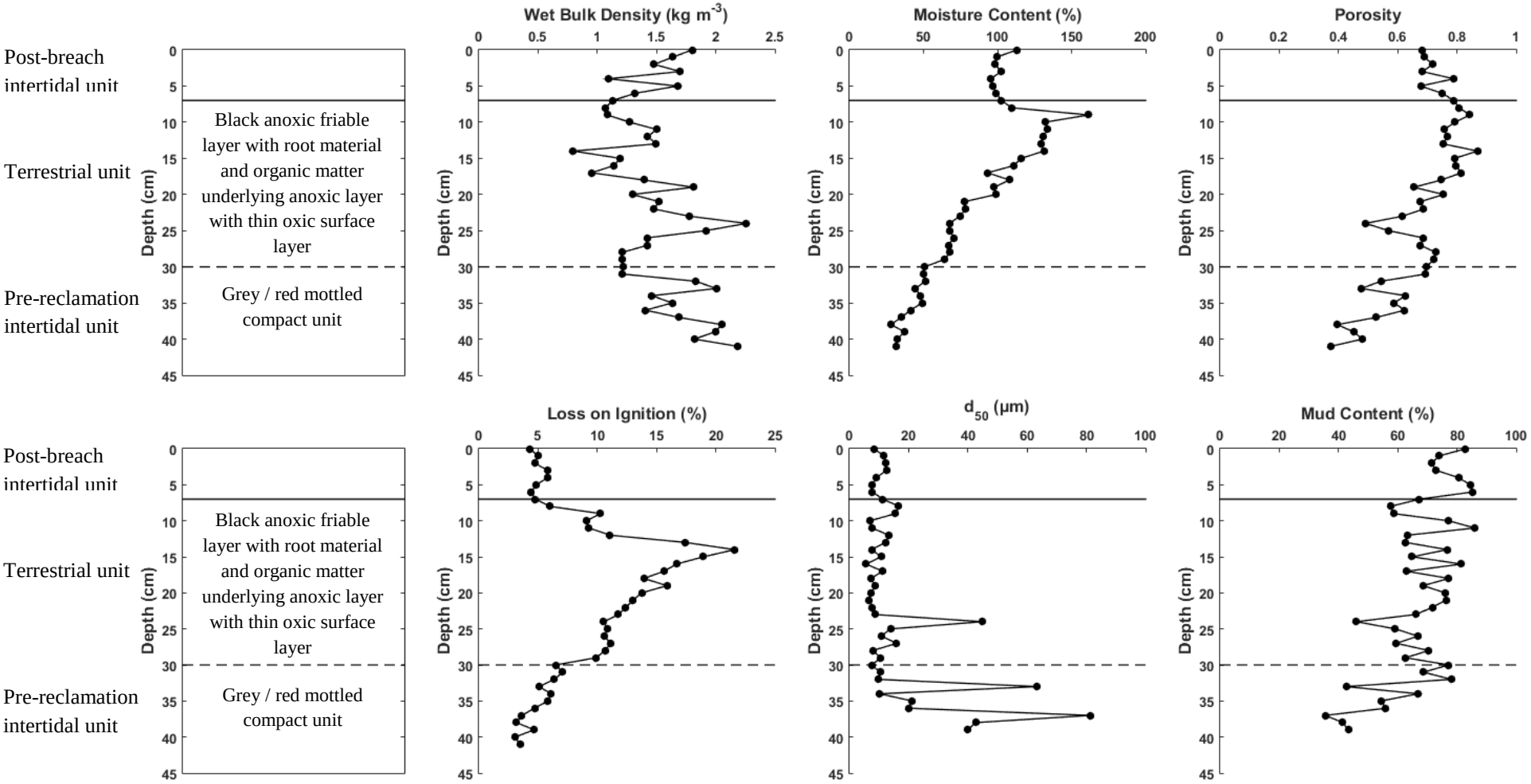

Figure 8.14: Comparison of the sediment log with wet bulk density, moisture content, porosity, loss on ignition, median grain size (d_{50}) and mud content (clay + silt) measured in parallel cores at Site 3 non-vegetated in 2016. On the sedimentary logs dashed lines represent a gradational boundary and a solid line represents a sharp boundary between sediment units.

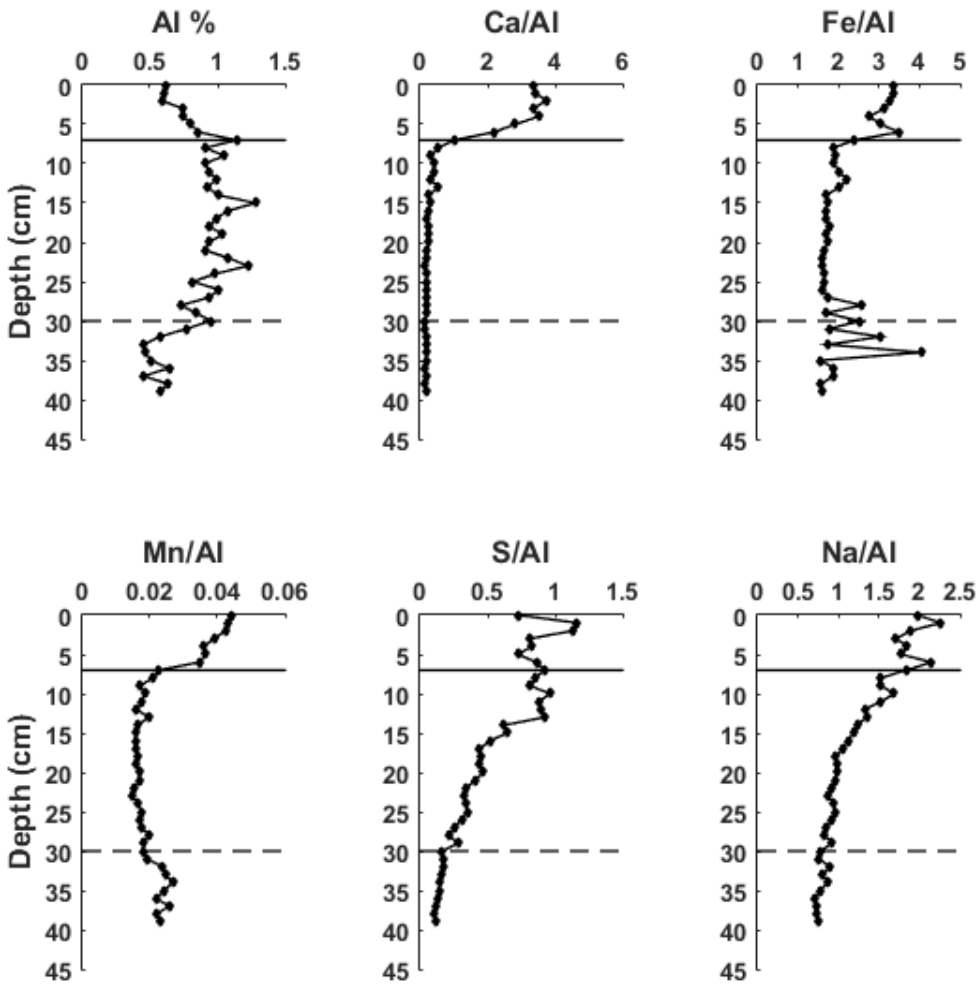

Figure 8.15: Variation in Al, Ca, Fe, Mn, S and Na with depth at Site 3 non-vegetated in 2016. The dashed lines represent a gradational boundary and the solid line represents a sharp boundary between sediment units.

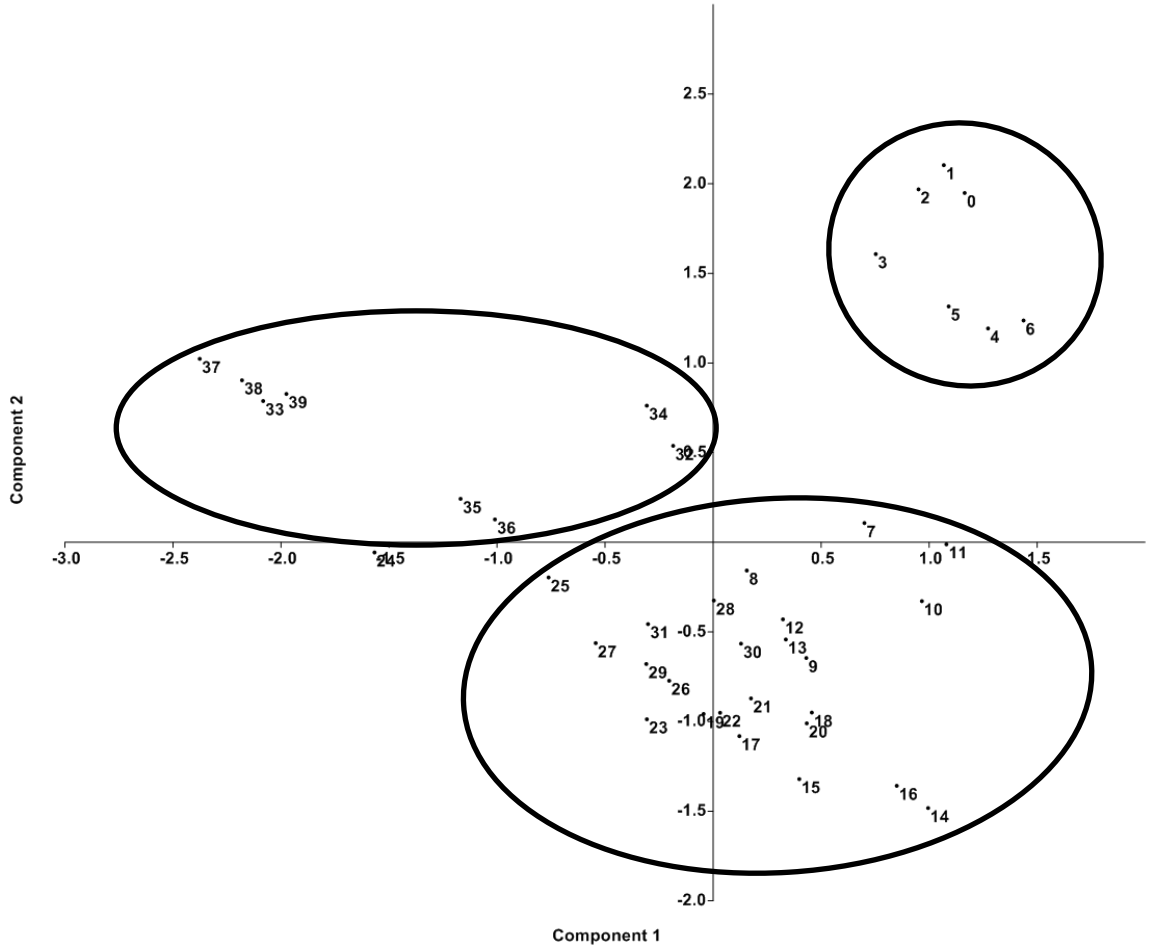

Figure 8.16: Principal component analysis (PCA) of different depths (numbered) for the Site 3 non-vegetated 2016 core plotted as Principal Component 1 vs. Principal Component 2. Components 1 and 2 explained 74.77 % of the variance. Circles highlight groups of depths with similar physicochemical variability (see text for discussion).

8.2.5 Site 3 Vegetated

8.2.5.1 2015

Vertical zonation in the 33 cm core taken from the vegetated surface at Site 3 in 2015 matched observations made elsewhere, presented in Figure 8.2. The post-breach intertidal unit consisted of a thin, 1 cm, dark brown clay rich zone present in the surface of the sample (Figure 8.17). Below this unit were a sharp (terrestrial) boundary and a friable, light brown / red mottled terrestrial unit, between 2 and 15 cm, bound by interconnected root networks. The lower part of the sample, from 16 cm, consisted of the pre-reclamation unit which was more compact, less friable and light grey in colour with red mottling, indicative of a fluctuating water table throughout the section sampled. Moisture content decreased through the sample, as did loss on ignition after a peak at the terrestrial boundary.

A slight enrichment of Fe was observed in the middle of the terrestrial unit (Figure 8.18), although Fe concentrations fluctuated within the pre-reclamation intertidal unit suggesting no stable redox zone had been established due to a variable water table. S and Na concentrations remained relatively constant through the sample. The three units were identified through PCA (Figure 8.19), matching the sediment log.

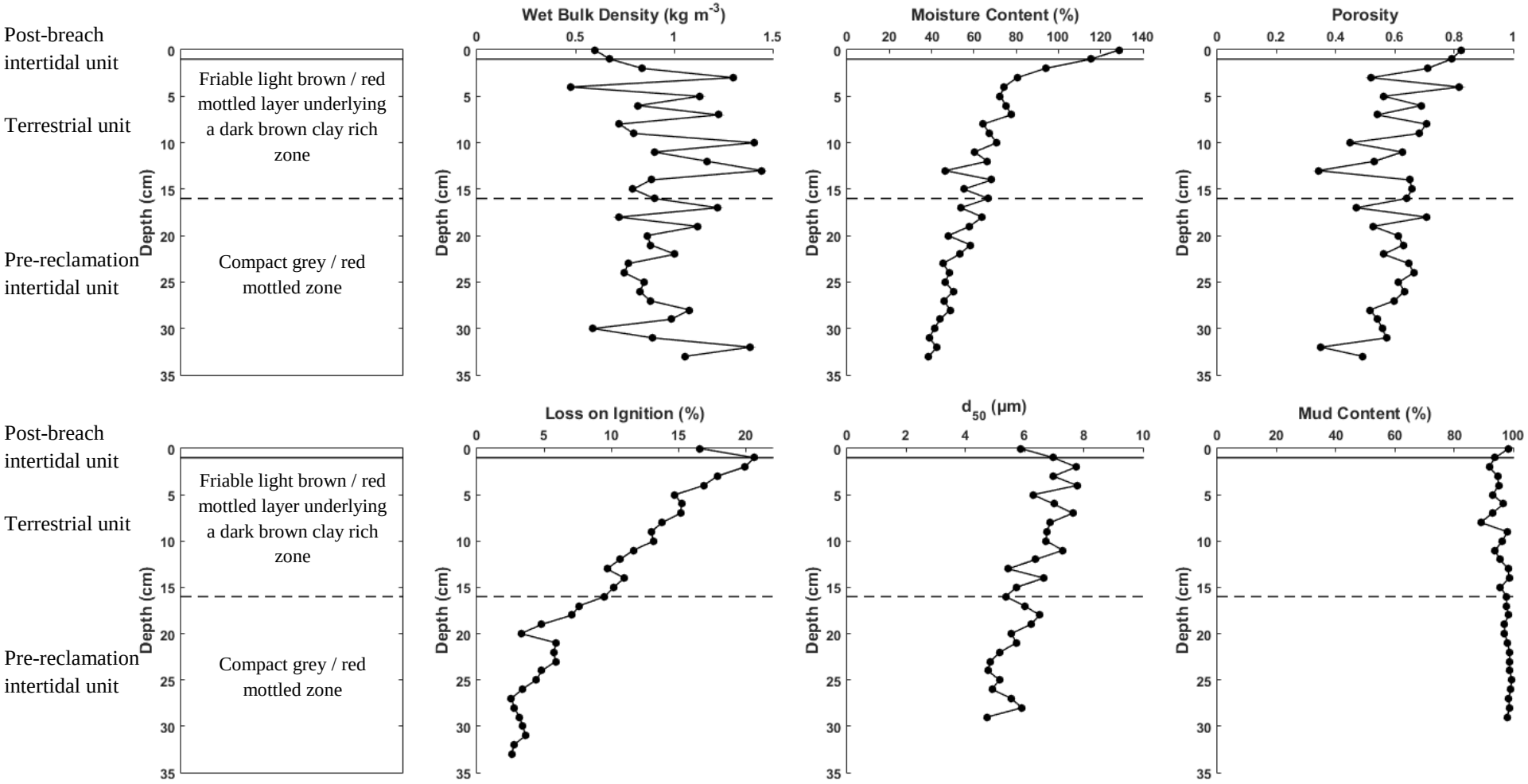

Figure 8.17: Comparison of the sediment log with wet bulk density, moisture content, porosity, loss on ignition, median grain size (d_{50}) and mud content (clay + silt) measured in parallel cores at Site 3 vegetated in 2015. On the sedimentary logs dashed lines represent a gradational boundary and a solid line represents a sharp boundary between sediment units.

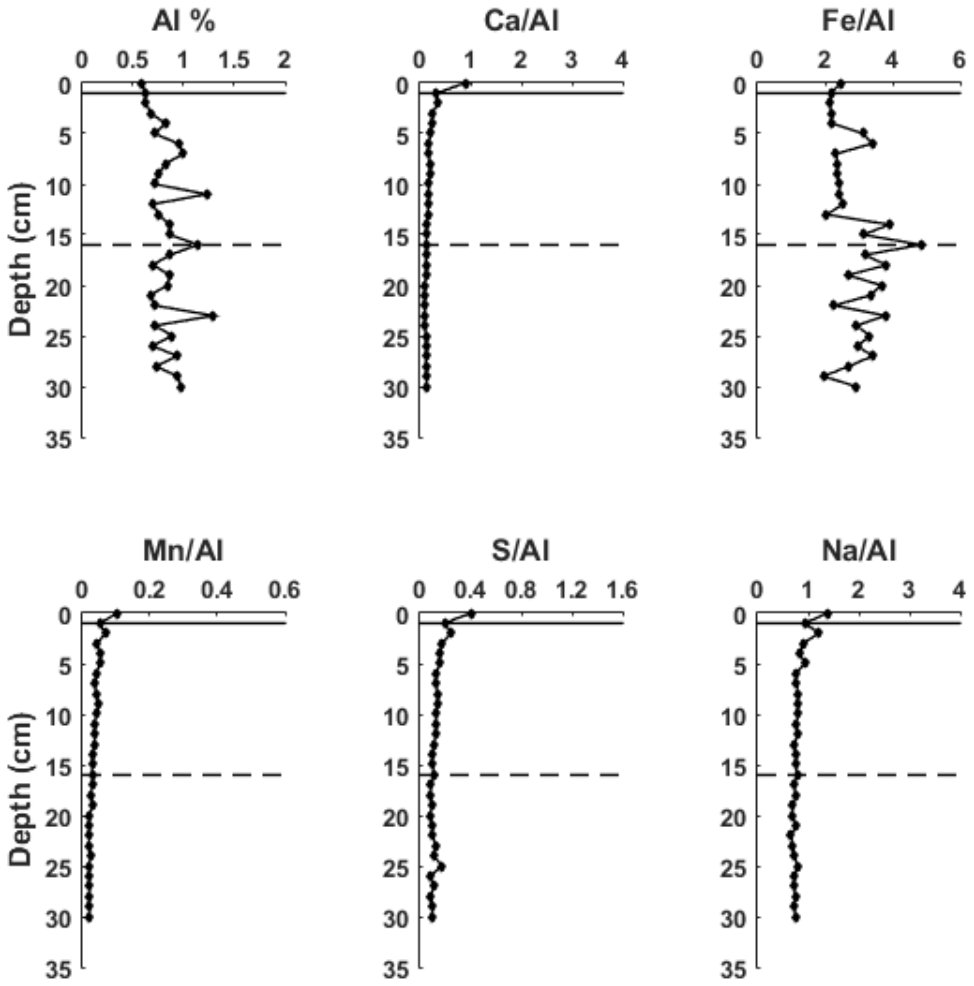

Figure 8.18: Variation in Al, Ca, Fe, Mn, S and Na with depth at Site 3 vegetated in 2015. The dashed lines represent a gradational boundary and the solid line represents a sharp boundary between sediment units.

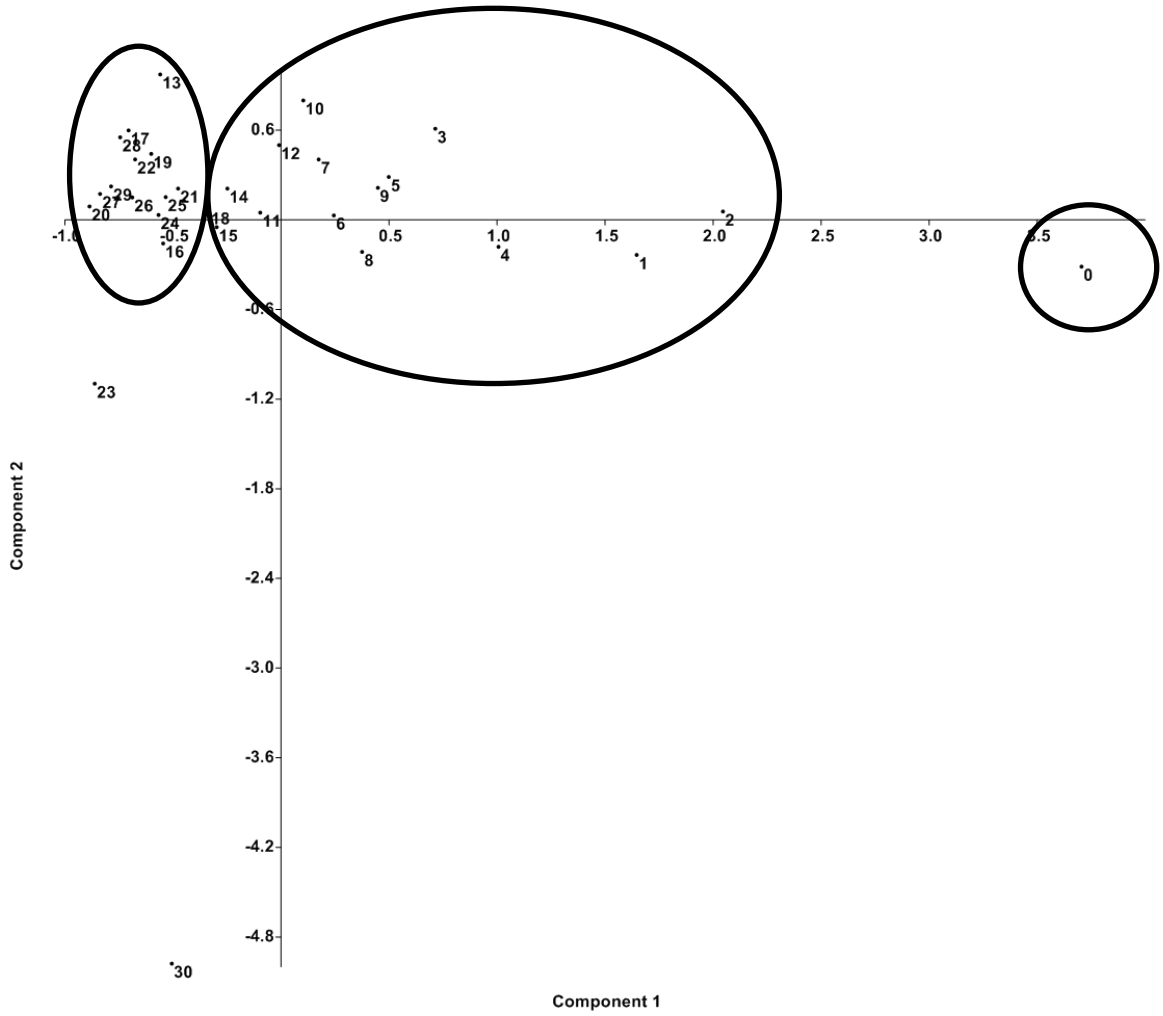

Figure 8.19: Principal component analysis (PCA) of different depths (numbered) for the Site 3vegetated 2015 core plotted as Principal Component 1 vs. Principal Component 2. Components 1 and 2 explained 65.11 % of the variance. Circles highlight groups of depths with similar physicochemical variability (see text for discussion).

8.2.5.2 2016

Figure 8.2 presents the core, and vertical zonation found elsewhere, from the vegetated surface in 2016. The top 3 cm consisted of dark brown silty post-breach intertidal sediment (Figure 8.20). As found previously, a sharp boundary divided this zone and a lower light brown with red mottling, friable, terrestrial unit from 3 to 17 cm. The lower grey pre-reclamation unit maintained a higher level of compaction and red mottling. A large decrease in moisture content was observed in the top centimetre of the sample, with this parameter becoming more constant through the pre-reclamation intertidal unit. Similarly, loss on ignition decreased through the top part of the sample and also became more constant in the pre-reclamation intertidal unit. Unlike the previous sample, the grain size coarsened in the near-surface and lower parts of the sample, reflecting local spatial variability.

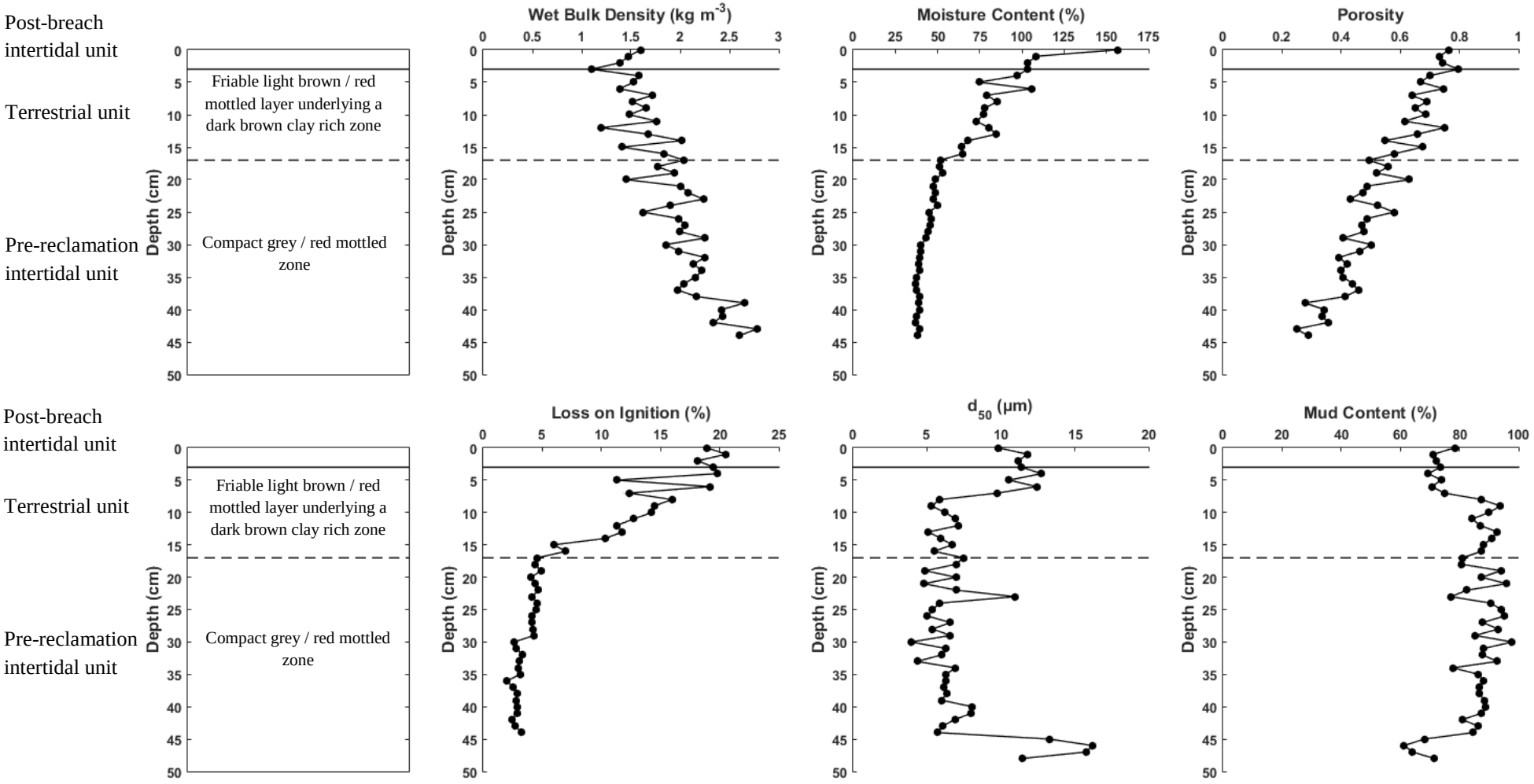

Figure 8.20: Comparison of the sediment log with wet bulk density, moisture content, porosity, loss on ignition, median grain size (d_{50}) and mud content (clay + silt) measured in parallel cores at Site 3 vegetated in 2016. On the sedimentary logs dashed lines represent a gradational boundary and a solid line represents a sharp boundary between sediment units.

High concentrations of Ca were measured in the surface sediment and then decreased through the top 3 cm (Figure 8.21), either due to the presence of finally comminuted shell debris or a sub-surface change in pH resulting in decalcification. Fe fluctuated throughout the record, peaking in the middle terrestrial zone. A clearer trend was observed in the concentration of Mn, which peaked at the boundary between the post-breach intertidal and terrestrial unit, suggesting possible diagenetic enrichment of Mn, which is more sensitive to changes in redox status. S concentration decreased with depth, matching the changes in Na concentration, and therefore implying variations in S are driven by the introduction and evaporation of sea water. Na, and to a lesser extent S, increased at the terrestrial boundary. PCA indicated that the surface sediment differed to the rest of the post-breach sediment unit (Figure 8.22). Below the sediment surface, the top 1 to 7 cm were found to group together, as were the terrestrial and pre-reclamation intertidal unit.

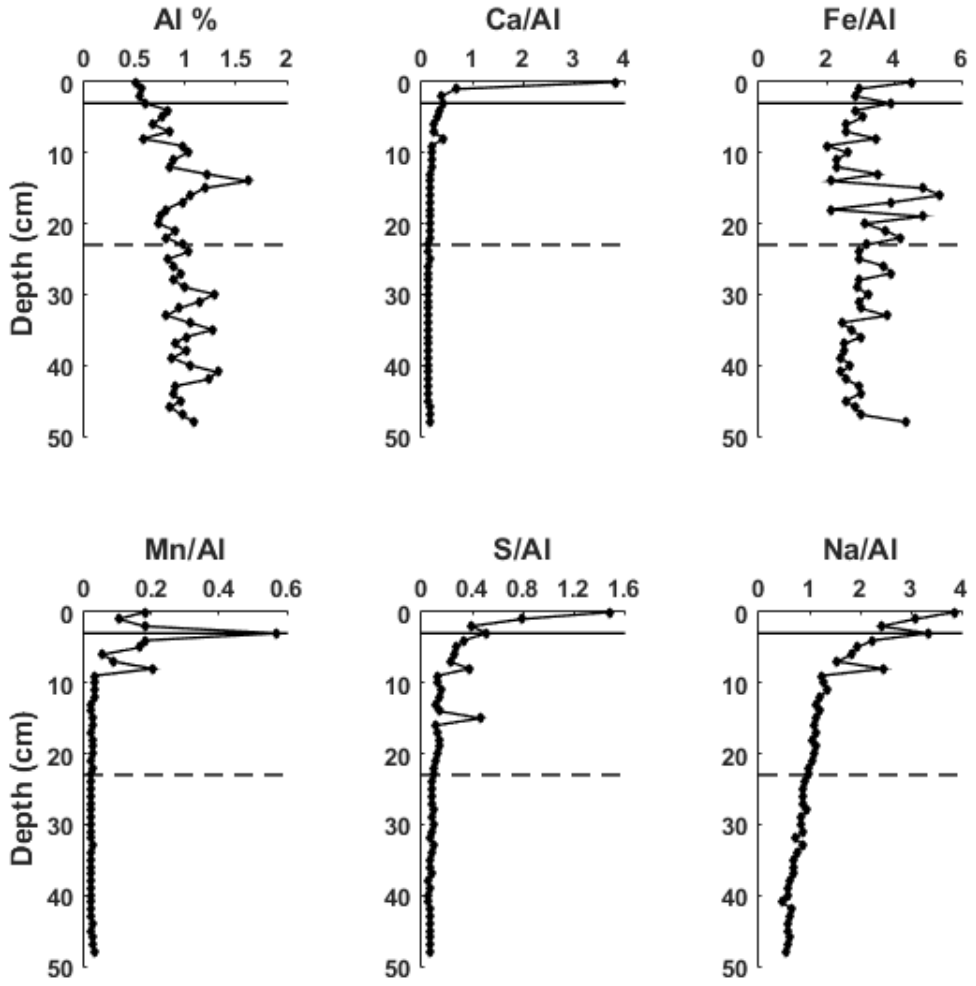

Figure 8.21: Variation in Al, Ca, Fe, Mn, S and Na with depth at Site 3 vegetated in 2016. The dashed lines represent a gradational boundary and the solid line represents a sharp boundary between sediment units.

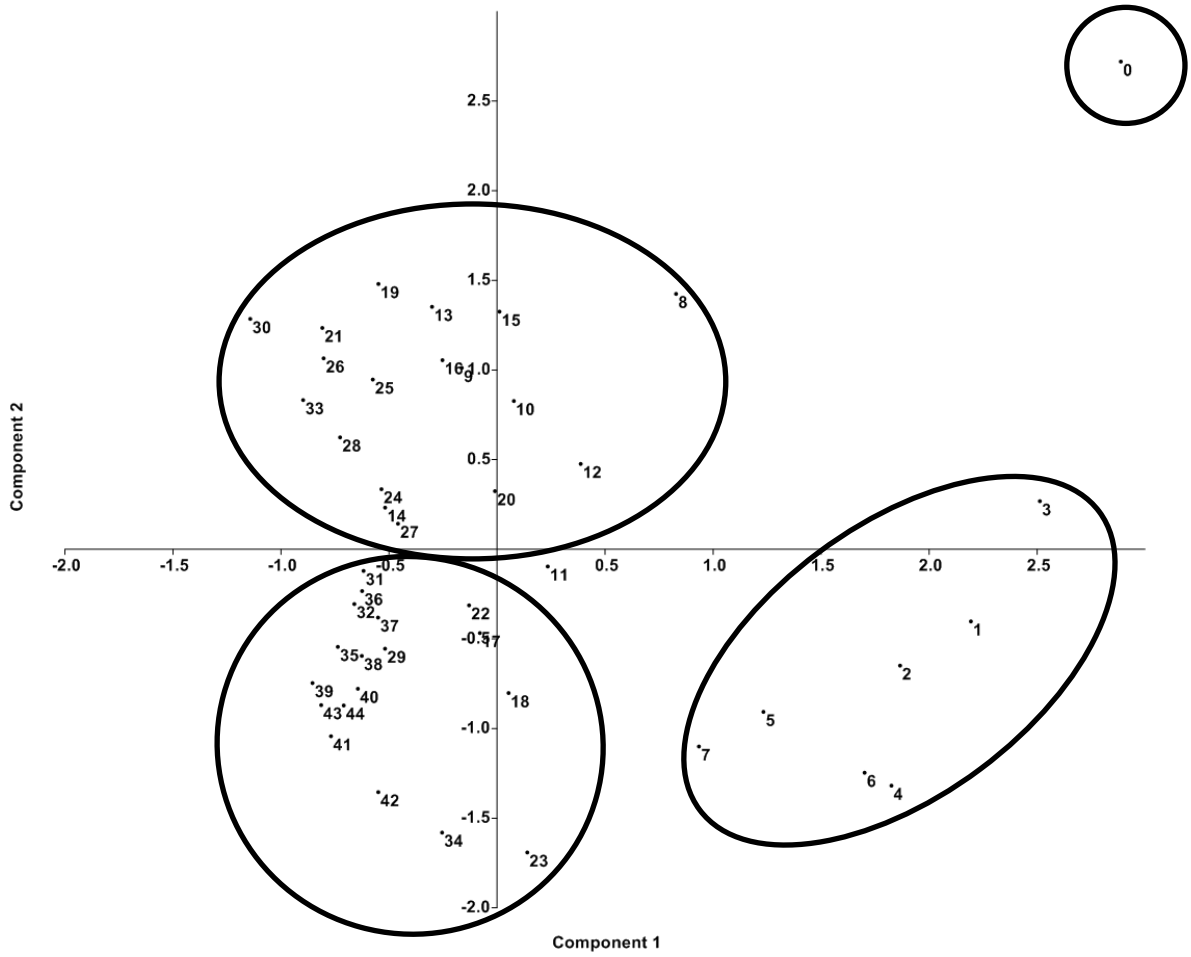

Figure 8.22: Principal component analysis (PCA) of different depths (numbered) for the Site 3 vegetated 2016 core plotted as Principal Component 1 vs. Principal Component 2. Components 1 and 2 explained 71.5 % of the variance. Circles highlight groups of depths with similar physicochemical variability (see text for discussion).

8.2.6 Site 5

8.2.6.1 2015

The 30 cm core taken from Site 5 in 2015 had the same post-breach intertidal, terrestrial, pre-reclamation intertidal zonation observed elsewhere (Figure 8.2). The top 3 cm of the sample, the post-breach intertidal unit, consisted of sandy sediment overlying a dark brown / red mottled terrestrial unit from 3 to 17 cm, with occasional angular clasts (< 5 mm) and poorly decomposed organic matter, and a pre-reclamition intertidal unit consisting of grey compact silt rich sediment (Figure 8.23). Loss on ignition fluctuated in the lower part of the terrestrial unit before rapidly decreasing below the reclamation boundary. Coarser sediments were measured in the post-breach intertidal unit (median grain size and percentage mud content data, Figure 8.23), decreasing at the terrestrial boundary and matching the observations made in the sedimentary log.

The increase in grain size in the top 3 cm was reflected in a decrease in Al concentration (Figure 8.24). Ca decreased through the post-breach intertidal unit, remained relatively constant through the terrestrial unit, and increased again in the pre-reclamation intertidal unit, indicating the presence of finely comminuted shell debris in the two zones of intertidal sediment. Both Fe and Mn decreased through the post-breach intertidal zone before increasing through the rest of the sample. S and Na followed a similar pattern, decreasing through the sample especially in the post-breach intertidal sediments. PCA revealed that the top of the sample differed from the underlying stratigraphy, with the transition at the reclamation boundary also differing from the rest of the sample (Figure 8.25).

.

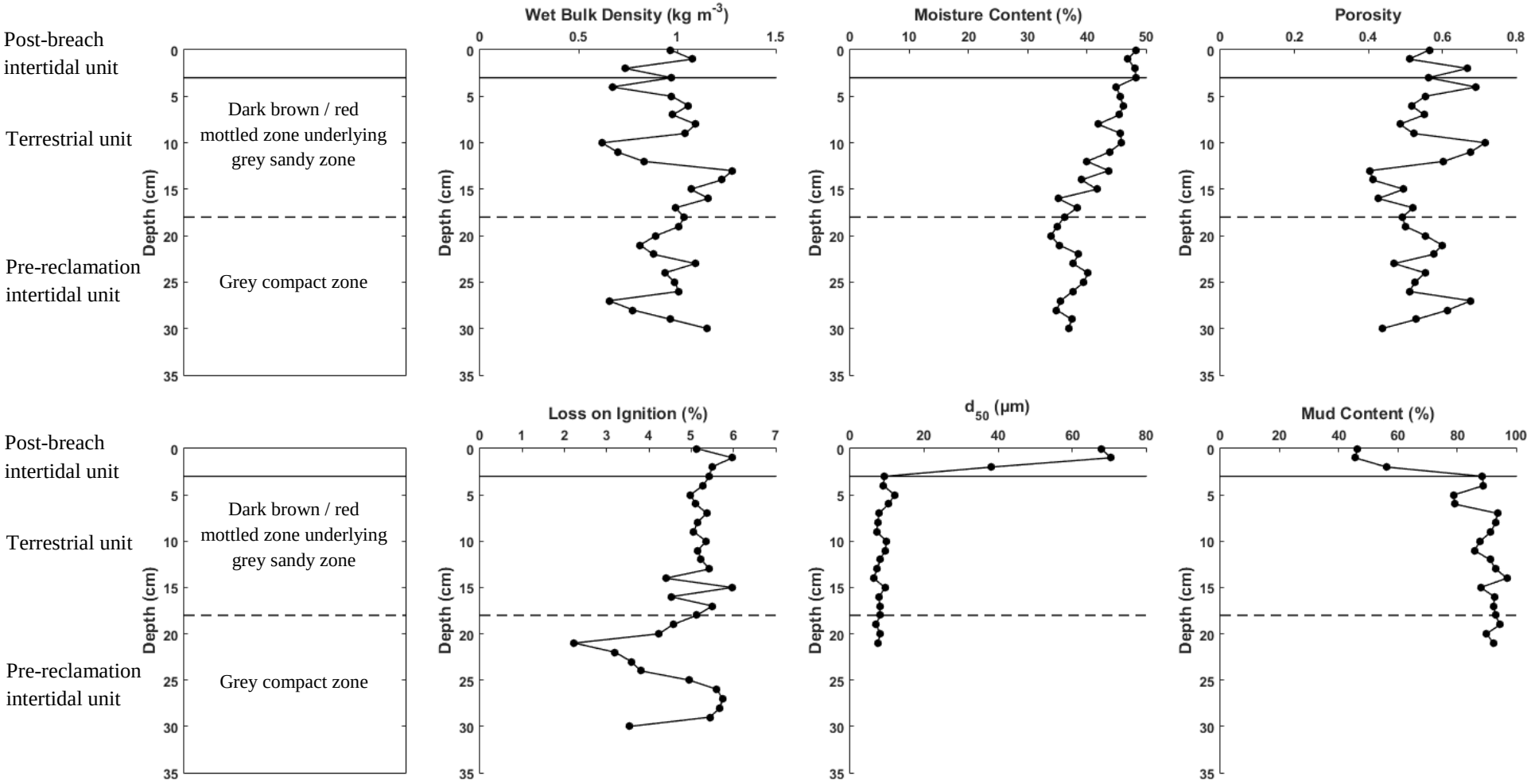

Figure 8.23: Comparison of the sediment log with wet bulk density, moisture content, porosity, loss on ignition, median grain size (d_{50}) and mud content (clay + silt) measured in parallel cores at Site 5 in 2015. On the sedimentary logs dashed lines represent a gradational boundary and a solid line represents a sharp boundary between sediment units.

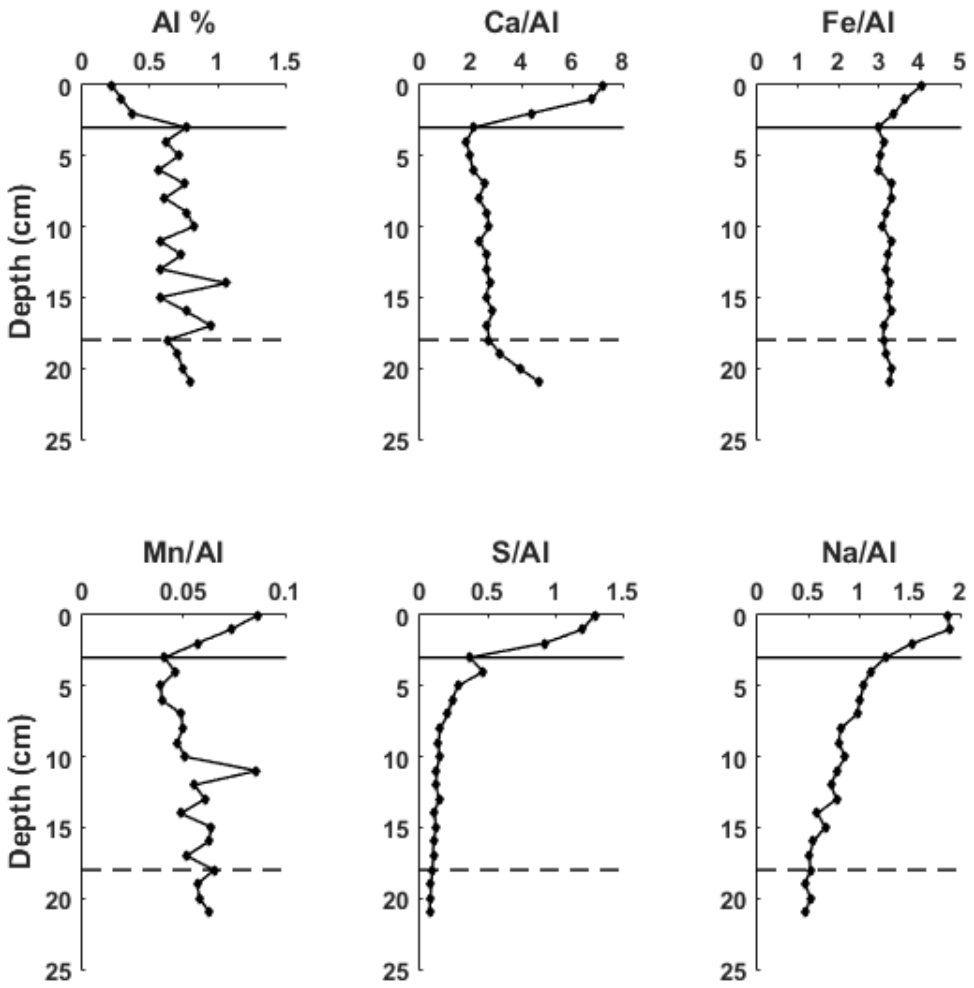

Figure 8.24: Variation in Al, Ca, Fe, Mn, S and Na with depth at Site 5 in 2015. The dashed lines represent a gradational boundary and the solid line represents a sharp boundary between sediment units.

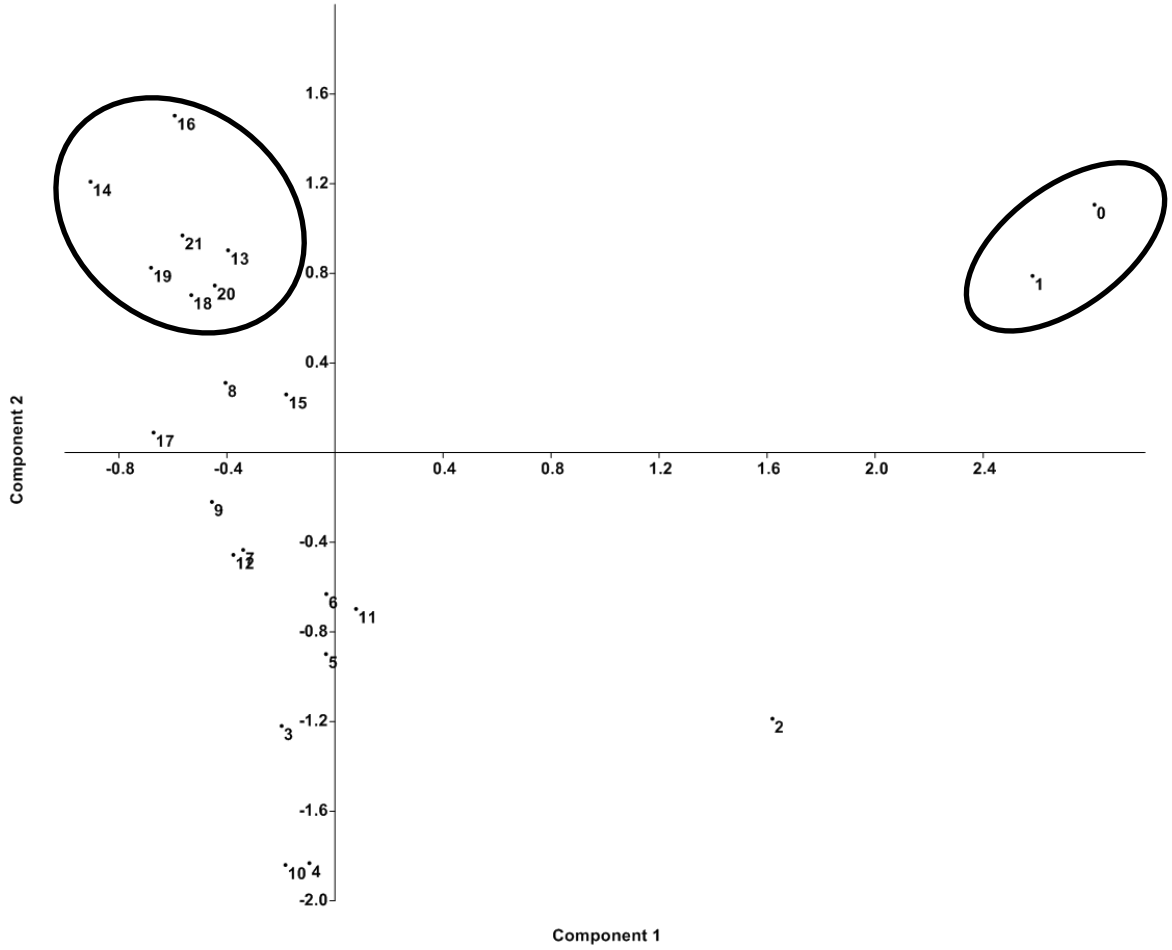

Figure 8.25: Principal component analysis (PCA) of different depths (numbered) for the Site 5 2015 core plotted as Principal Component 1 vs. Principal Component 2. Components 1 and 2 explained 77.33 % of the variance. Circles highlight groups of depths with similar physicochemical variability (see text for discussion).

8.2.6.2 2016

The sample from Site 5 taken in 2016 was compact and dark brown throughout (Figure 8.26), without the zonation seen elsewhere. Median grain size and percentage mud content indicated that coarse sediment was only identified at the surface, although this increase was not evident in the geochemical data. A sub-surface maximum in Ca and Mn was observed at 19 cm depth, possibly the legacy of the reclamation boundary previously identified. PCA showed little grouping, although the surface was found to differ from the rest of the sample.

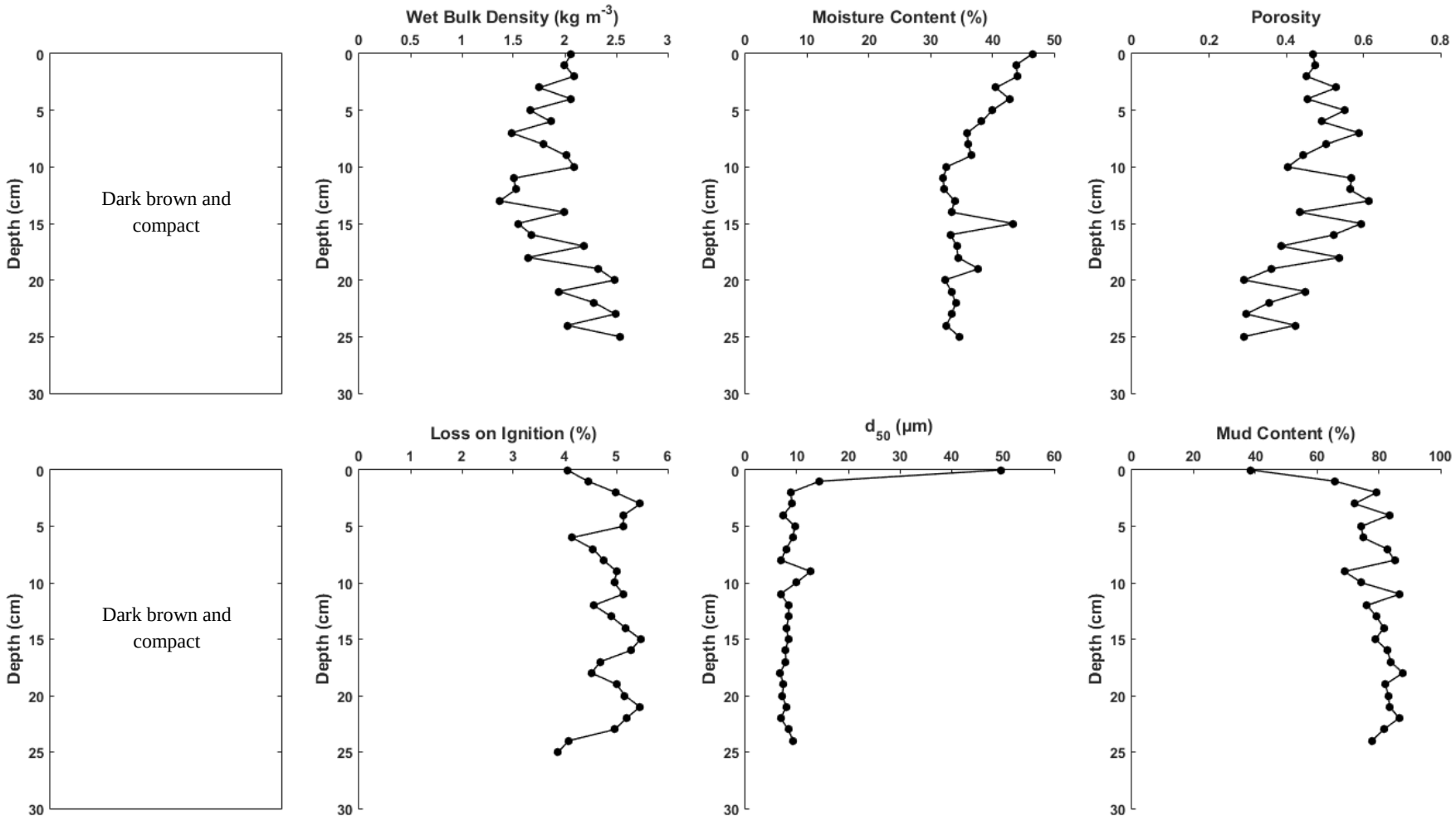

Figure 8.26: Comparison of the sediment log with wet bulk density, moisture content, porosity, loss on ignition, median grain size (d_{50}) and mud content (clay + silt) measured in parallel cores at Site 5 in 2016.

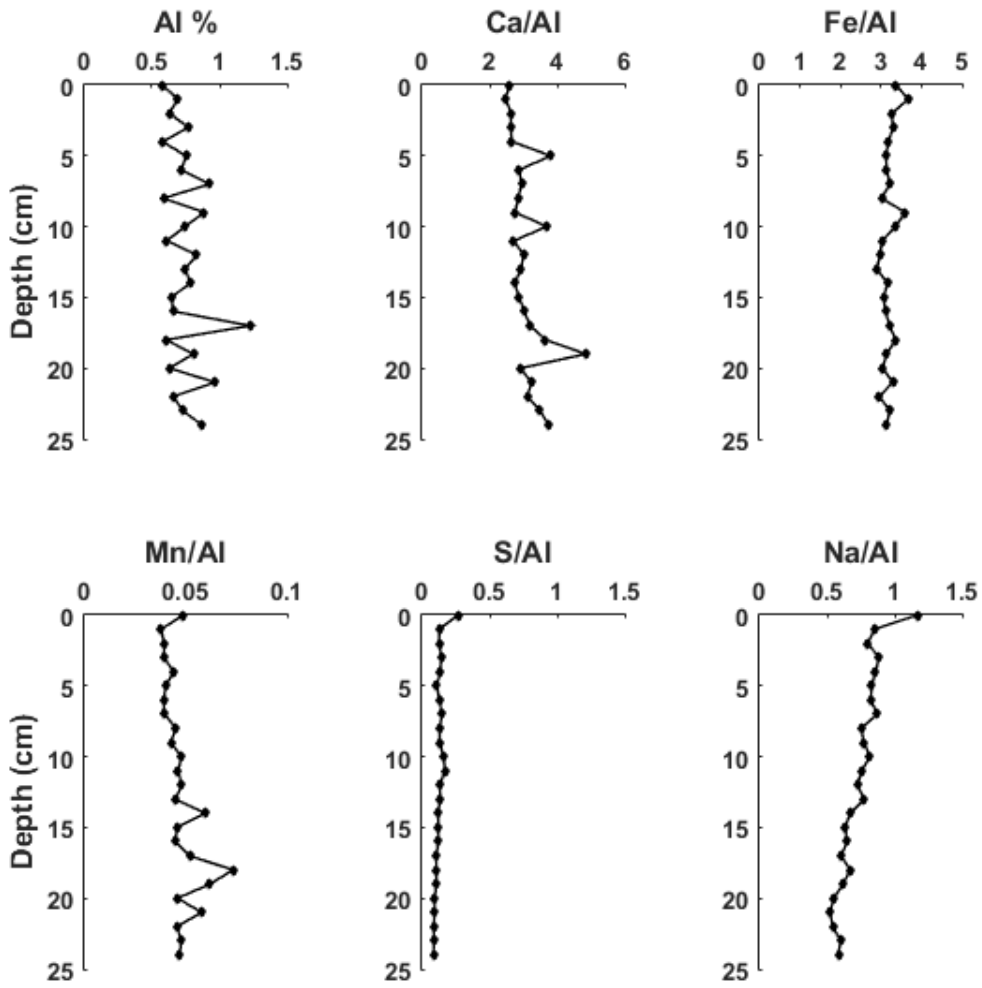

Figure 8.27: Variation in Al, Ca, Fe, Mn, S and Na with depth at Site 5 in 2016.

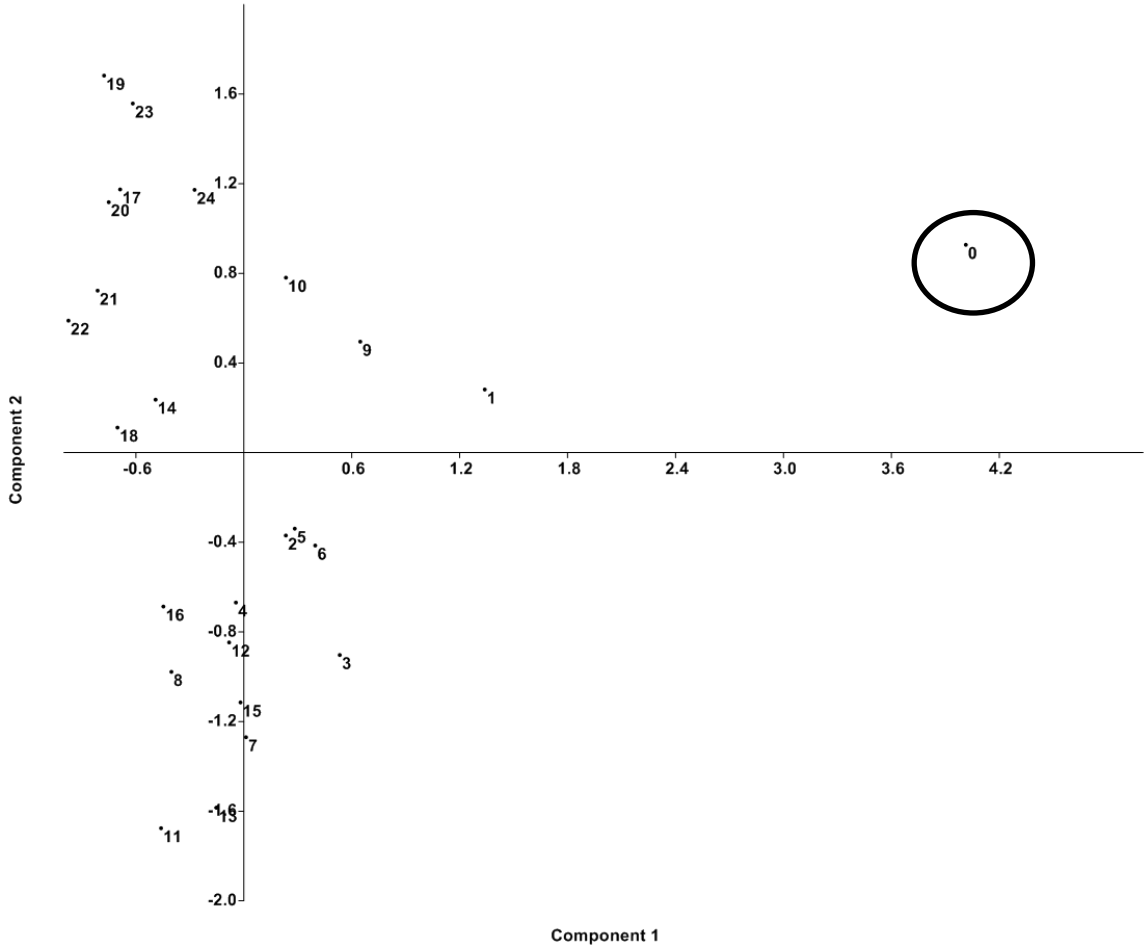

Figure 8.28: Principal component analysis (PCA) of different depths (numbered) for the Site 5 2016 core plotted as Principal Component 1 vs. Principal Component 2. Components 1 and 2 explained 62.88 % of the variance. Circles highlight groups of depths with similar physicochemical variability (see text for discussion).

8.3 Intensive scale (sub-millimetre) Subsurface Structure Physicochemical Characteristics

8.3.1 Sediment Structure

Representative reconstructions of sediment structure, produced using µCT analysis at a voxel resolution of 65 microns, are presented for Site 2b (Figure 8.29) and Site 5 (Figure 8.30). Bulk mineralogical composition of the sediment is likely to be broadly similar, given the sampling locations are within the same site, with the same underlying geology. Therefore, differences in X-ray attenuation will primarily (to a first approximation) reflect differences in the sediment structure and porosity at the sub-voxel scale (Cnudde and Boone, 2013).

Segregation of the sample taken at Site 2b in 2015 indicated a relatively consistent solid matrix phase with the exception of the lowest part of the sample where lower attenuation (suggesting lower sediment density) was measured, indicated by the lighter brown in Figure 8.29. Analysis of the lowest attenuating phase, representative of the macro-porosity, shows a tortuous, interconnected, pore network running throughout the sample, occupying 14 % of the sample. In the sample taken from Site 2b, in 2016, more consistent attenuation was measured throughout the solid matrix phase. The pore network consisted of horizontal elongated networks with apparent reduced connectivity, occupying 7 % of the sample.

Structural differences were clearly visible in the sample taken from Site 5 in 2015 (Figure 8.30). The bulk sediment matrix phase and macro-porosity indicate two distinct sediment units; an upper post-breach intertidal unit and a lower terrestrial unit. A sheet like macro-pore was detected across the division between the units, although it is likely that this an artificial feature caused by the coring process (which resulted in sediment cracking along this interface). Laminations were present in a compact upper sediment unit, consisting of sediment deposited post-site inundation. The lower unit was dominated by a large horizontal macro-pore, with low interconnectivity to the rest of the

sample. A number of smaller macro-pores were located under the large horizontal pore, but generally a low abundance of macro-pores was found throughout the rest of this lower unit. Overall, 7 % of the core from Site 5 taken in 2015 consisted of macro-pore space.

In the second sample from Site 5, taken in 2016, no evidence of the laminated sediments or separate sediment units, identified in the sample taken in 2015, were found. There was also no evidence of the vertical pore system with few macro-pores found; only 3 % of the volume of the sample was classified as pore space. The pore network was dominated by a vertical pore (on the left of the 2016 macro-pore phase in Figure 8.30) and areas of isolated, flattened macro-pore space.

8.3.2 Sediment Geochemistry

ITRAX scanning was employed to examine the variability of nine elements at high spatial resolution (200 microns) over the upper 10 cm of the sediment column at Sites 2b and 5. The ITRAX produces elemental data in counts but previous studies (e.g. Miller et al., 2014) have shown that these data correlate well with quantitative analytical data (e.g., ICP-OES or Wave Dispersive X-ray Fluorescence). Furthermore, the high frequency compositional changes identified using the ITRAX are often missed when analysing lower resolution bulk sub-samples using more traditional, destructive analytical methods.

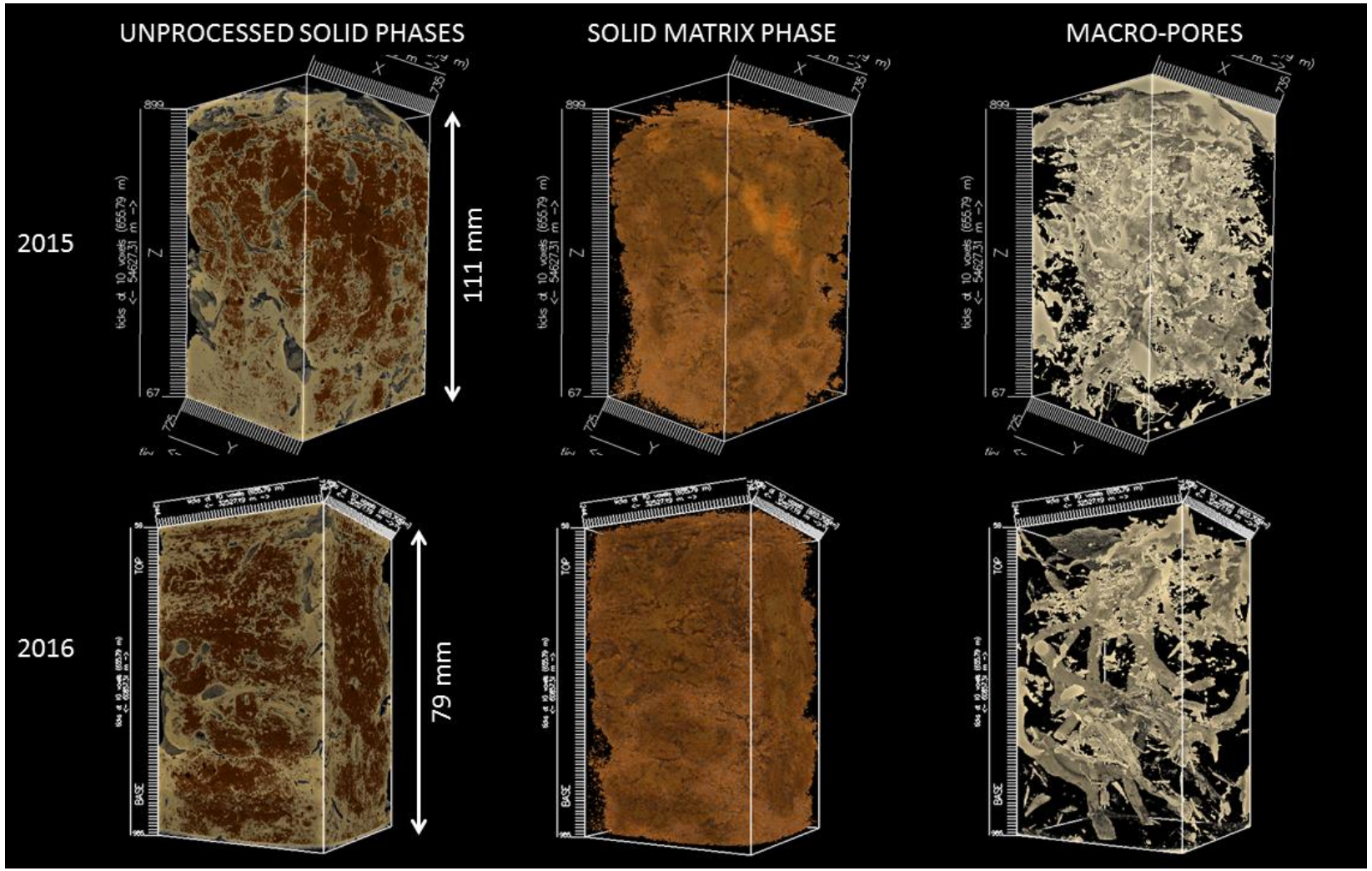

Figure 8.29: Reconstructions of sediment phases, imagined used µCT analysis, at Site 2b in 2015 and 2016.

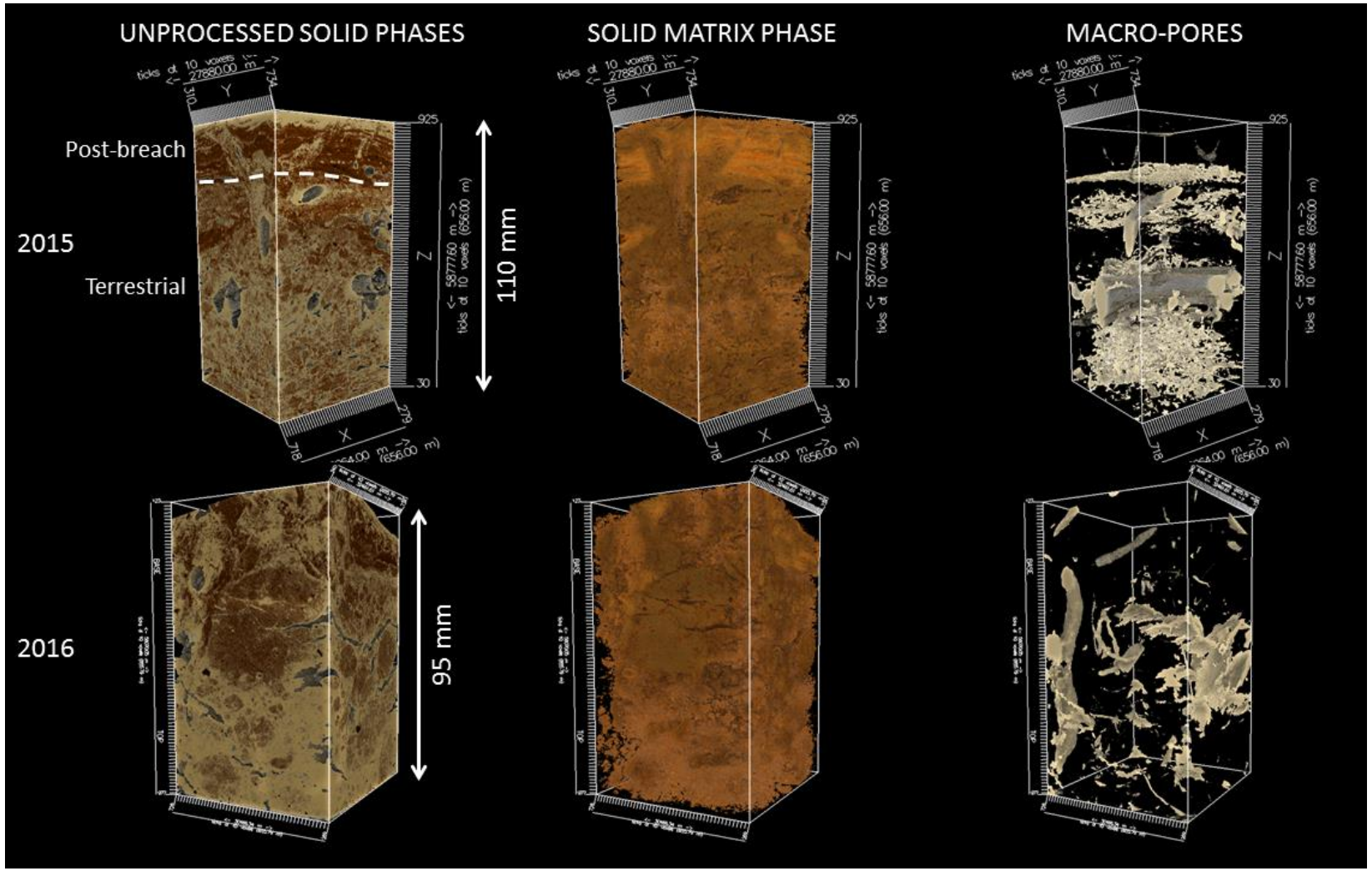

Figure 8.30: Reconstructions of sediment phases, imagined used µCT analysis, at Site 5 in 2015 and 2016.

The concentration of coarse grained sediment, indicated by the Zr and Cr intensity, remained relatively constant at Site 2b in the 2015 sample (Figure 8.31). Two major peaks were observed in the Cr intensity, although the second of these peaks corresponded with an area of high intensity measured on the radiograph, likely to be a clast. Measurements of the K intensity indicate that the fine grained fraction decreased in the middle section of the sample, increasing again deeper in the sample, which is also reflected in Si and the bulk µCT attenuation measurements (Figure 8.29). Similar trends were observed in the Cl and Ca intensity. Black sediment, low Fe and Mn, and a peak in S, indicate possible bacterial reduction of sulphate within the cracked and desiccated near-surface sediments (Figure 8.29), although broadly coincident peaks in Cl and Ca may indicate that the peak in S is a function of increased porewater sulphate, rather than sulphate reduction processes. Fe and Mn increased below this unit and remained constant throughout the rest of the sample, with a couple of large peaks. However, these peaks corresponded with peaks in the kcps data and are likely to be the product of X-ray response rather than increases in concentration. After peaking in the near-surface sediment, S followed a similar pattern to Si, K, Cl and Ca.

No major vertical changes in bulk sediment composition were detected in the second sample taken at Site 2b (Figure 8.32), demonstrated by the relatively constant distribution of Si with the major peaks corresponding to variability in the X-ray response. These observations were supported by similar trends in Zr and Cr intensities, although peaks were also observed in these elements corresponding to the presence of high density material (clasts, evident in the X-radiograph image). The distribution of K indicated constant clay content within the sample. Cl decreased slightly through the sample, whereas Ca decreased in the lower section of the sample, indicative of decalcification. In contrast to the other elements, Mn showed a strong increase in intensity in the middle part of the core, possibly reflecting early diagenetic enrichment, although this observation was not supported by change in the Fe intensity. However, analysis of the Mn / Fe ratio (Figure 8.33) indicated higher concentrations of Mn to Fe in the middle of the core, suggesting mildly reducing conditions and early diagenetic mobilisation of Mn. No evidence of the bacterial reduction of sulphate, present in the near-surface of the previous sample, was found, although trends in S generally coincided with peaks in Cl and Ca so may be caused by increased porewater sulphate rather than microbial reduction.

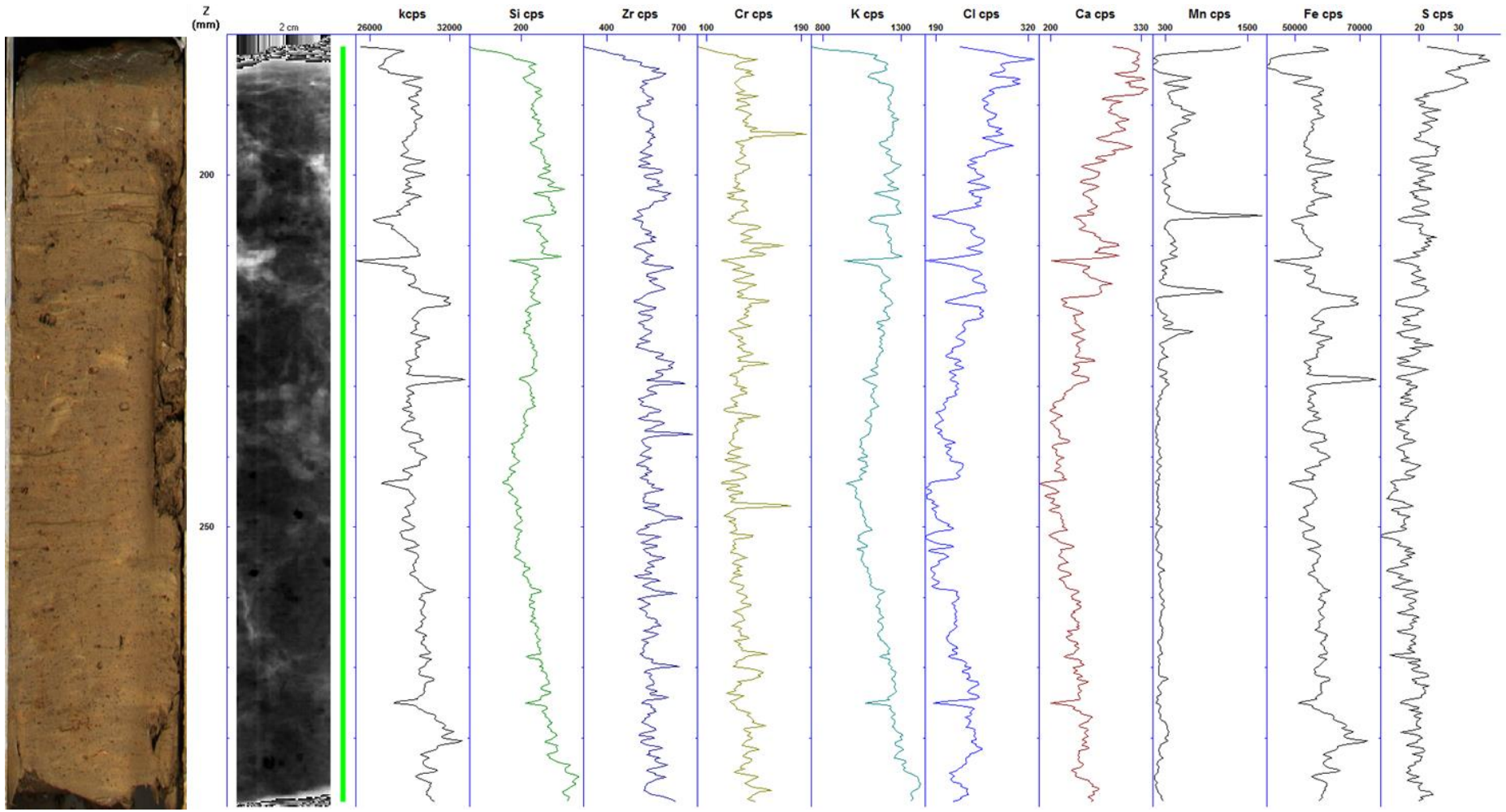

Figure 8.31: Si, Zr, Cr, K, Cl, Ca, Mn, Fe and S distribution, X-radiograph and photograph of core from Site 2b in 2015. Data are from ITRAX scanning: X-axis shows X-ray response, y-axis represents depth.

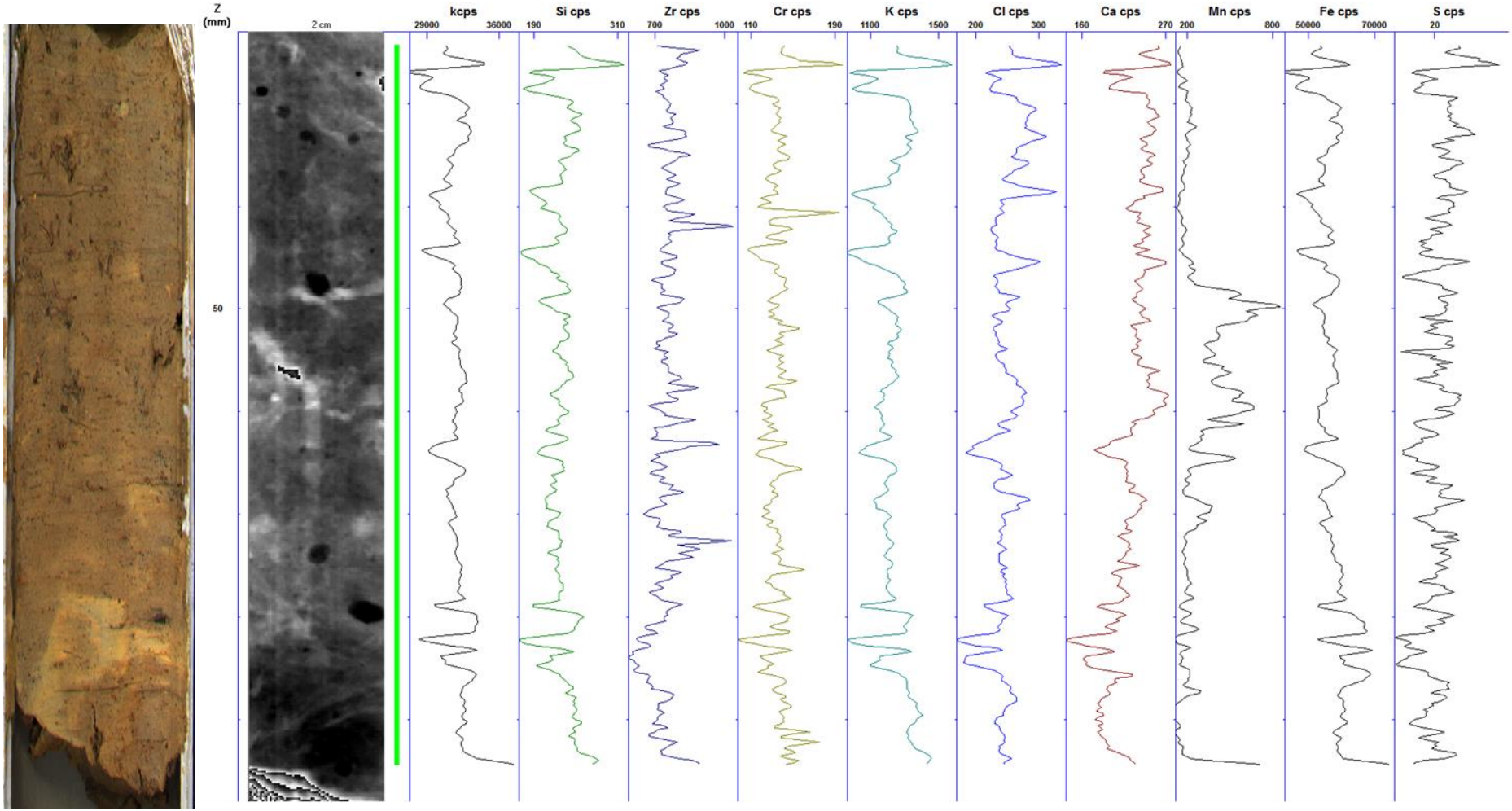

Figure 8.32: Si, Zr, Cr, K, Cl, Ca, Mn, Fe and S distribution, X-radiograph and photograph of core from Site 2b in 2016. Data are from ITRAX scanning: X-axis shows X-ray response, y-axis represents depth.

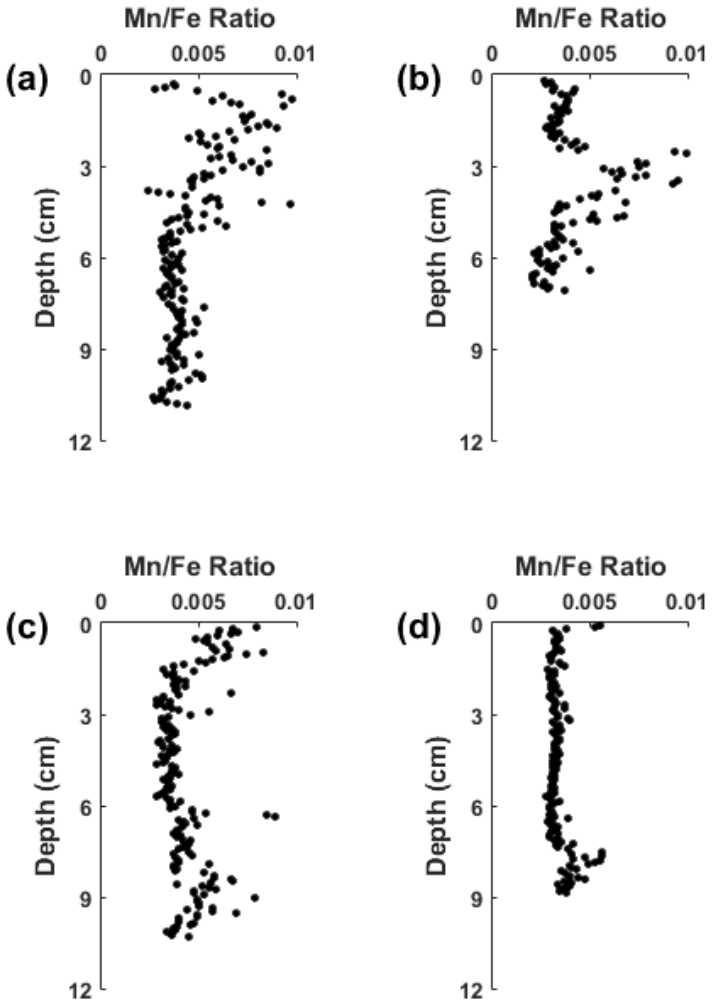

Figure 8.33: Mn / Fe ratio for (a) Site 2b 2015, (b) Site 2b 2016, (c) Site 5 2015 and (d) Site 5 2016 derived from ITRAX geochemical data.

Coarse grained sediments dominated the near-surface sediment of the sample taken at Site 5 in 2015 (Figure 8.34), visible in the photographic image and indicated by the high intensity of Zr. Several peaks in Cr were detected in the upper part of the pore, likely to be the laminations observed in the µCT scan. At the boundary between the post-breach and terrestrial sediment units Cr peaked below a unit of low density detected by the radiograph, matching the sheet like pore space present in the µCT scan (Figure 8.30). Below this unconformity, K intensity increased, and Zr / Cr decreased, indicating an increase in fine grained sediment. Cl generally decreased through the sample, whereas Ca decreased and then increased again. Evidence of sub-surface diagenetic enrichment of Mn was provided by an increase, and peak, in intensity in the lower third of the core. The peak in Mn corresponded to an area of low density measured by the radiograph,

although this is not visible on the photography. It is possible that this area is the large horizontal macro-pore feature present in the µCT analysis. The distribution of Fe also increased through the sample, with areas of enrichment corresponding to red mottling on the sample. The Mn / Fe ratio decreased through the upper 2 cm of the sample (Figure 8.33), but increased again at a similar depth to the large horizontal macro-pore. After the terrestrial boundary, S intensity decreased through the sample. Small scale increases in S intensity occurred in areas where red mottling of the sediment was not present.

In the second sample from Site 5 (Figure 8.35) coarser grained sediments were only found in the surface sediment, indicated by the surface peak in Zr, consistent with the findings from the broad scale and µCT analysis. Trends in K suggested increased clay content was present in the middle of the sample. A peak in Cl occurred within the upper sub-surface, corresponding to a peak in S, which could indicate the depth of saline intrusion to the sediment. Fe and Mn decreased through the top of the red mottled surface sediment. Fe, and to a lesser extent Mn, increased through the middle of the sample, supporting visual observations of red mottling, with an additional increase present in the deeper parts of the sample.

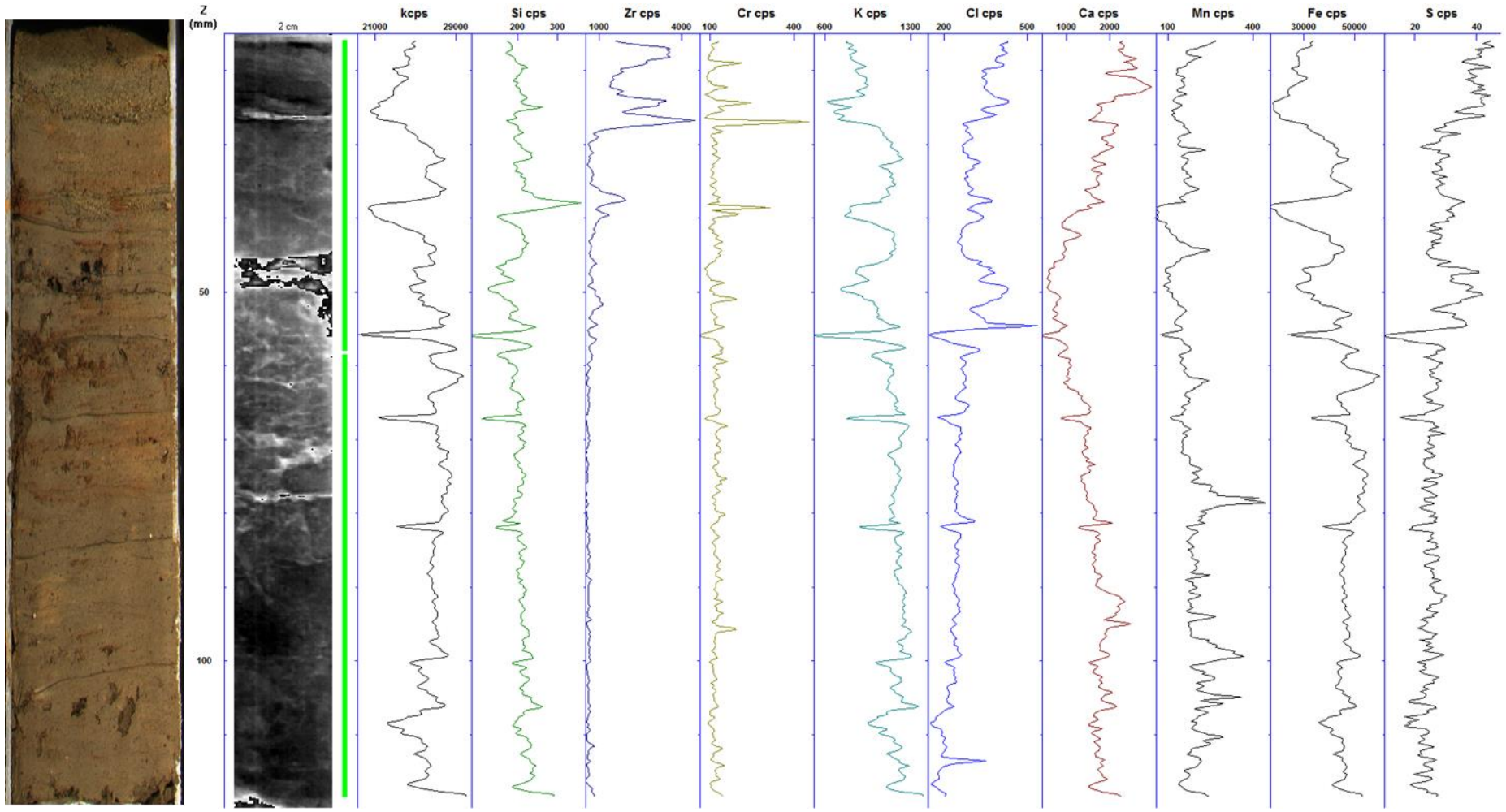

Figure 8.34: Si, Zr, Cr, K, Cl, Ca, Mn, Fe and S distribution, X-radiograph and photograph of core from Site 5 in 2015. Data are from ITRAX scanning: X-axis shows X-ray response, y-axis represents depth.

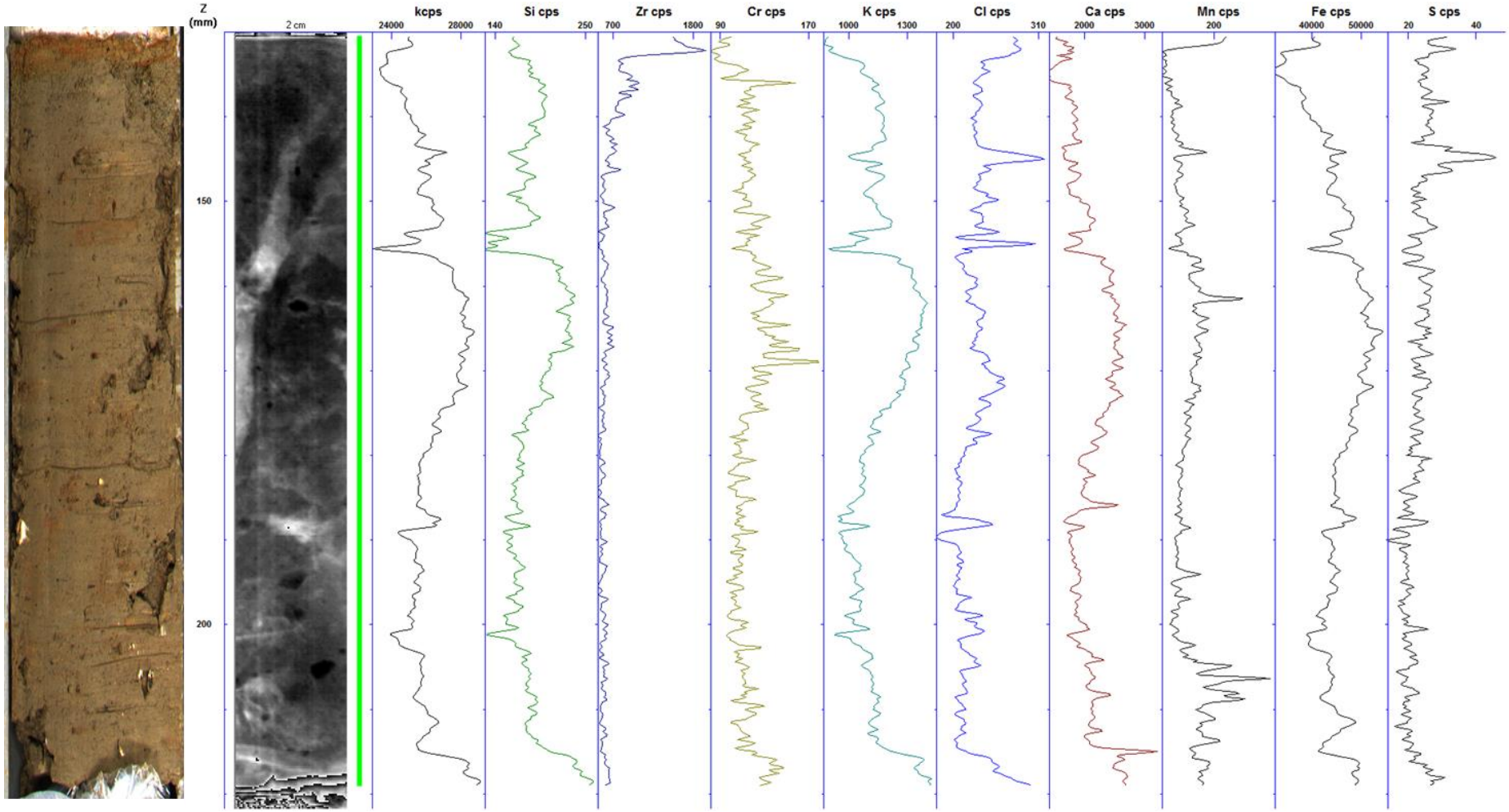

Figure 8.35: Si, Zr, Cr, K, Cl, Ca, Mn, Fe and S distribution, X-radiograph and photograph of core from Site 5 in 2016. Data are from ITRAX scanning: X-axis shows X-ray response, y-axis represents depth.

8.4 Discussion

8.4.1 Preservation of the Pre-Breach Terrestrial Surface

Observations made at other, older, MR sites suggest that visual changes in the sediment characteristics associated with a terrestrial boundary would no longer be present within a number of years; Spencer et al. (2008) found no visual evidence of the terrestrial unit at Orplands Farm Managed Realignment Site 8 years after site inundation. Broad scale analysis from six sites at the Medmerry Managed Realignment Site provided visual evidence of three sub-surface units (post-breach intertidal, terrestrial and pre-reclamation intertidal, e.g. Figure 8.2) at all sites except the second sample taken at Site 5, the nearest site to the breach (in a significantly higher energy environment than the other sites sampled). However, no uniform marker of the terrestrial surface, such as the organic rich peaty layer identified at Pagham Harbour by Cundy et al. (2002), was identified. In each sample where a sub-surface unconformity was detected, a lower pre-reclamation sediment unit was also detected. PCA allowed, in the most cases, (partial) discrimination of samples based on the physical and geochemical sediment properties at different depths, as opposed to a single indicator such as loss on ignition or changes in particle size, into groups which corresponded to one of the three vertical sediment units.

The reclamation of saltmarshes results in modification to sediment structure and properties (e.g. Crooks et al., 2002; Hazelden and Boorman, 2001) caused by de-watering and organic matter mineralisation, decreasing the porosity and increasing the bulk density. After the re-introduction of intertidal conditions through MR, the legacy of these changes can still be detected, with low moisture contents still being found at depth several decades after site inundation (Spencer et al., 2017). Analysis of sites of different former land use, 16 months after site inundation, at Medmerry indicate similar bulk densities and porosities within the terrestrial unit. However, moisture content and loss on ignition were higher in samples taken from Sites 2a and 3, areas which previously had not been subjected to arable agricultural practices (i.e. ploughing).

Prior to site inundation, Site 1 had not been used for arable agriculture. Yet, lower moisture contents were found in the sub-surface environment below heavily water logged surface sediment. This site was flattened and heavily disturbed during site construction which may have resulted in a physical barrier, or aquiclude, forming between the terrestrial and post-breach units (Crooks and Pye, 2000; Hazelden and Boorman, 2001). The presence of an aquiclude has been associated with reduced hydrological connectivity (Tempest et al., 2015) and restricted penetration by burrowing invertebrates and vertical roots (Spencer et al., 2017) at other MR sites, which may have consequences for saltmarsh colonisation as long vertical roots are important for seedlings to successfully become established (Balke et al., 2011). Re-sampling of Sites 2b, 3 and 5, 36 months after site inundation, indicated that these broad trends had been preserved.

Detailed examination of the 3D sediment structure through the use of μCT allowed for relative comparisons of the morphology and connectivity of the macro-porosity. At Site 2b, which was previously used occasionally (and usually unsuccessfully) for agriculture, pore networks were more complex with greater connectivity. The surface of the sediment was cracked and desiccated, with no sub-surface differences in sediment structure as observed at Site 5 (see below), or by Spencer et al. (2017) at Orplands Farm Managed Realignment Site. Analysis of a second core, taken in 2016, indicated that the macro-pores had elongated and lower interconnectivity, implying reduced transportation of water through the sub-surface.

Terrestrial and post-breach units were detected in the first 3D sediment structural analysis performed from Site 5. The top unit consisted of laminar sediment deposits, which had accreted post-site inundation, and no evidence of macro-pores. This site had previously been used intensively for arable farming (Table 8.1) and was harvested two weeks before site inundation. The legacy of the agricultural activity was clear in the macro-porosity of the lower unit; the system was dominated by a large horizontal pore with low connectivity, indicating inefficient sub-surface transfer of water. In the second sample taken from Site 5, in 2016, neither the two sediment units nor the isolated horizontal macro-pore were present. The macro-porosity consisted of a single vertical

pore, possibly a root or burrow cast, and areas of isolated flattened pore space, indicative of continued low vertical sub-surface water transfer.

8.4.2 Implications for Geochemical Profile Development at Managed Realignment sites

Typical vertical saltmarsh profiles are controlled by strong physicochemical gradients in pH and redox potential, and microbially mediated organic matter breakdown using electron acceptors such as O_2, MnO_2 and $Fe(OH)_3$ (e.g. Koretsky et al., 2005; Spencer et al., 2003). Following reclamation and ploughing large-scale precipitation of Fe oxyhydroxides and other Fe-rich minerals would be anticipated (Auxtero et al., 1991; Violante et al., 2003). When re-introduced to intertidal conditions remobilisation of Fe by the saline water is expected through dissimilatory reduction of sulphate or dissolved Fe being re-distributed by advection caused by the local hydrology (Burton et al., 2011; Johnston et al., 2011). However, impeded vertical solute and porewater transport caused by the presence of an aquiclude may result in inadequate drainage, stagnant porewater and a lack of aeration. The occurrence of these conditions will inevitably prevent the formation of suitable oxic conditions for re-precipitation of Fe, and Mn, at the sediment surface (Spencer et al., 2008).

No evidence of an aquiclude was found in either of the samples taken from Site 3 in 2015. In the non-vegetated sample, Fe peaked at the terrestrial boundary, corresponding to a peak in loss on ignition values. The high concentration of Fe may well be caused by high concentrations of organic matter, present on the terrestrial surface before site inundation, available for sulphate reducing bacteria resulting in the enrichment of Fe. Through the rest of the sample no major trends were detected in Fe content, whereas the sediment showed clear red mottling, implying variability in the water table caused by tidal inundation (Cundy and Croudace, 1995). Fe fluctuated through the red mottled sample from the vegetated surface at Site 3, indicating a fluctuating water table through the sub-surface sediment.

The second sample from the non-vegetated surface at Site 3 was visibly darker in the intertidal and terrestrial units, decreasing in S and increasing in Fe and Mn to the boundary between the units. The sharp nature of this boundary, and the peak in moisture content (albeit from a parallel core so appears slightly below the boundary marked from the sedimentary log), may indicate reduced vertical conveyance of water through the unconformity. The fluctuations in Fe, and to a lesser extent Mn, in the pre-reclamation intertidal unit could be caused by trapping by authigenic carbonate / sulphide formation (Cundy and Croudace, 1995). In the second sample from the vegetated surface at Site 3, the distribution of Fe continued to indicate a fluctuating water column.

Broad and intensive scale analysis suggests evidence of bacterial reduction of sulphate in the surface of the first sample taken from Site 2b, although an algal mat was present allowing for accelerated diagenesis and accumulation of S (e.g. Nedwell and Abram, 1978). Below this unit the red mottled sediment and Fe profile implied a variable water column facilitated by the extensive inter-connected macro-pore network indicated by µCT analysis. An increase in the Mn / Fe ratio in the middle of the sample (Figure 8.33) suggests redox mobilisation of Mn, which is more sensitive to redox changes than Fe. Despite the differences in sediment structure at Site 5, there was still evidence of Fe enrichment. The macro-pore network was dominated by a large horizontal pore which corresponded to an increase in the intensity of Mn and the Mn / Fe ratio in ITRAX data, possibly the result of enrichment via lateral through flow. These trends were maintained when sites were re-sampled in 2016, with no sub-surface unconformity detected at Site 5. Broad and intensive scale results presented here differ from the geochemical and redox profiles observed in older MR sites (Spencer et al., 2008), and natural saltmarsh and mudflat environments within the Solent (e.g. Cundy and Croudace, 1995). It remains to be seen if the geochemical profiles evolve in a similar manner to other MR sites such as or a more typical intertidal setting, compared schematically in Figure 8.36, and the timescales required for this development.

<table>
<tr><th colspan="2">Medmerry Managed Realignment Site (West Sussex, United Kingdom)</th><th>Orplands Farm Managed Realignment Site (Essex, United Kingdom)</th><th>Natural Saltmarsh (Hamble estuary, Hampshire, United Kingdom)</th></tr>
<tr><td>Post-site inundation intertidal</td><td rowspan="3">Physical properties varied in terrestrial unit but mottled oxic conditions were found throughout suggesting a variable water table and that vertical solute transfer is not inhibited</td><td>Poorly consolidated unit with abundant root material</td><td>Thin (mm) oxidised surface layer rich in plant litter</td></tr>
<tr><td>Terrestrial</td><td rowspan="2">Firmer sediment layer, lower in organic and moisture content. Geochemical and hydrological evidence to suggest reduced solute transfer</td><td>Mottled oxic zone with evidence of a fluctuating water table</td></tr>
<tr><td>Pre-reclamation intertidal</td><td rowspan="2">Black unit with reducing anoxic conditions</td></tr>
</table>

Figure 8.36: Schematic comparison of the sub-surface physicochemical properties of the sediment found at the Medmerry Managed Realignment Site (this study), Orplands Farm Managed Realignment Site (Spencer et al., 2017; Spencer et al., 2008; Tempest et al., 2015) and a typical natural saltmarsh (Cundy and Croudace, 1995).

8.4.3 Influence of the Former Land Use and Site Construction

Previous studies have demonstrated differences in the physical, geochemical and hydrological characteristics of saltmarshes in MR sites, particularly at the Orplands Farm site, compared to natural marshes (Spencer et al., 2017; Spencer et al., 2008; Tempest et al., 2015). It has been proposed that these differences are the cause of water-logging and poor drainage, which have been attributed to poor saltmarsh species abundance and diversity within MR sites (e.g. Mossman et al., 2012). Clear differences in sediment structure for sites of different former land use were found at the Medmerry Managed Realignment Site. Therefore, it would be anticipated that sites with reduced porosity and pore connectivity would have lower subsurface flow, stagnant water and anoxic sediment. The findings from the Medmerry Managed Realignment Site, however, do not match this expectation.

Medmerry is still a developing site and, therefore, has not experienced a large accretion of intertidal sediment over the terrestrial boundary, particularly compared to Orplands Farm where up to 8 cm of sediment have accreted since the site was breached in 1995 (Spencer et al., 2017). It remains to be seen how the geochemical profiles develop following further accretion of sediment. However, the reduced levels of accretion appear to have postponed, or prevented, the formation of an aquiclude, allowing drainage through the terrestrial unit apart from at the non-vegetated area of Site 3. In the second sample taken from this site sediment appeared black and anoxic, with evidence of water pooling at the terrestrial boundary and reduced hydrological connectivity through the contact between the unit. These findings suggest that hydrological and geochemical differences found in MR sites compared to natural saltmarshes are not caused by sub-surface differences owing to the former land use, but by the formation and contact between two units in the sediment column as a result of (a) the accretion of sediment, and (b) sharp physicochemical contrasts between the accreted upper unit and the underlying sediment. It is also possible that the formation of the anoxic unit, at Site 3, has been driven by the decay of terrestrial vegetation trapped and buried under the accreted sediment following site inundation (French, 2006).

8.5 Summary

Variations in the sub-surface structure and physicochemical properties of sites with different former land use histories have been investigated at the Medmerry Managed Realignment Site in this chapter. Using a novel combination of repeated broad and intensive scale analysis, differences in the subsurface sediment structure and geochemical evolution in the three years following site inundation have been assessed. Results indicate clear discrepancies in the sediment structure and properties as a result of differences in the former land use.

Previous studies (e.g. Spencer et al., 2017; Tempest et al., 2015) have associated modifications, compaction and a reduction in the number and connectivity of pore networks, caused by a site's agricultural history, to differences in the hydrological regime and geochemical framework compared to natural saltmarshes. However, reduced drainage and anoxic conditions were not found at sites which had experienced higher levels of agricultural disturbance. Evidence of reduced hydrological connectivity (i.e. anoxic conditions caused by stagnant water) were only found at the site which had experienced the highest level of accretion. These findings indicate that the formation of an aquiclude reducing vertical solute transfer between units in MR sites is the result of the accretion of sediment, coupled with sharp physicochemical contrasts between the accreted upper layer and the underlying sediment. Many MR sites are designed to accumulate sediment, but these findings highlight the need for improved awareness of sediment accretion in decision making during the design of MR sites. Sites either need to be designed to encourage rapid accumulation of intertidal sediment, burying the terrestrial boundary and minimising the effect of an aquiclude or, as results presented here indicate, reduce sediment accumulation to allow the terrestrial soil to convert following the introduction of intertidal conditions. Alternatively, predictions need to be adjusted to anticipate reduced saltmarsh diversity abundance until sufficient sediment has been accreted.

9 Synthesis and Wider Implications

9.1 Introduction

The results and discussion presented in Chapters 5 to 8 of this thesis lead to an enhanced understanding of the evolution of the sediment regime in managed realignment (MR) sites through analysis of: the change in bed elevation, surface sediment properties and cohesive strength; rhythms of sedimentation and fluxes in suspended sediment in response to site hydrodynamics; the formation and evolution of embryonic creeks: and the change in subsurface sediment structure and the physicochemical evolution for areas of differing former land use, site design and construction processes (outlined in Table 3.1) at the Medmerry Managed Realignment Site. The key findings from this study are presented in Figure 9.1. This chapter amalgamates these results and discussions from the previous four chapters to present an overall synthesis of the research results, and discusses their wider implications for the design and construction of future sites. The factors influencing the evolution of the sediment regime in MR sites (reviewed in Chapter 2) are presented in Figure 9.2, with the issues evaluated in this thesis indicated. Findings from this investigation are now discussed following the structure of Figure 9.2.

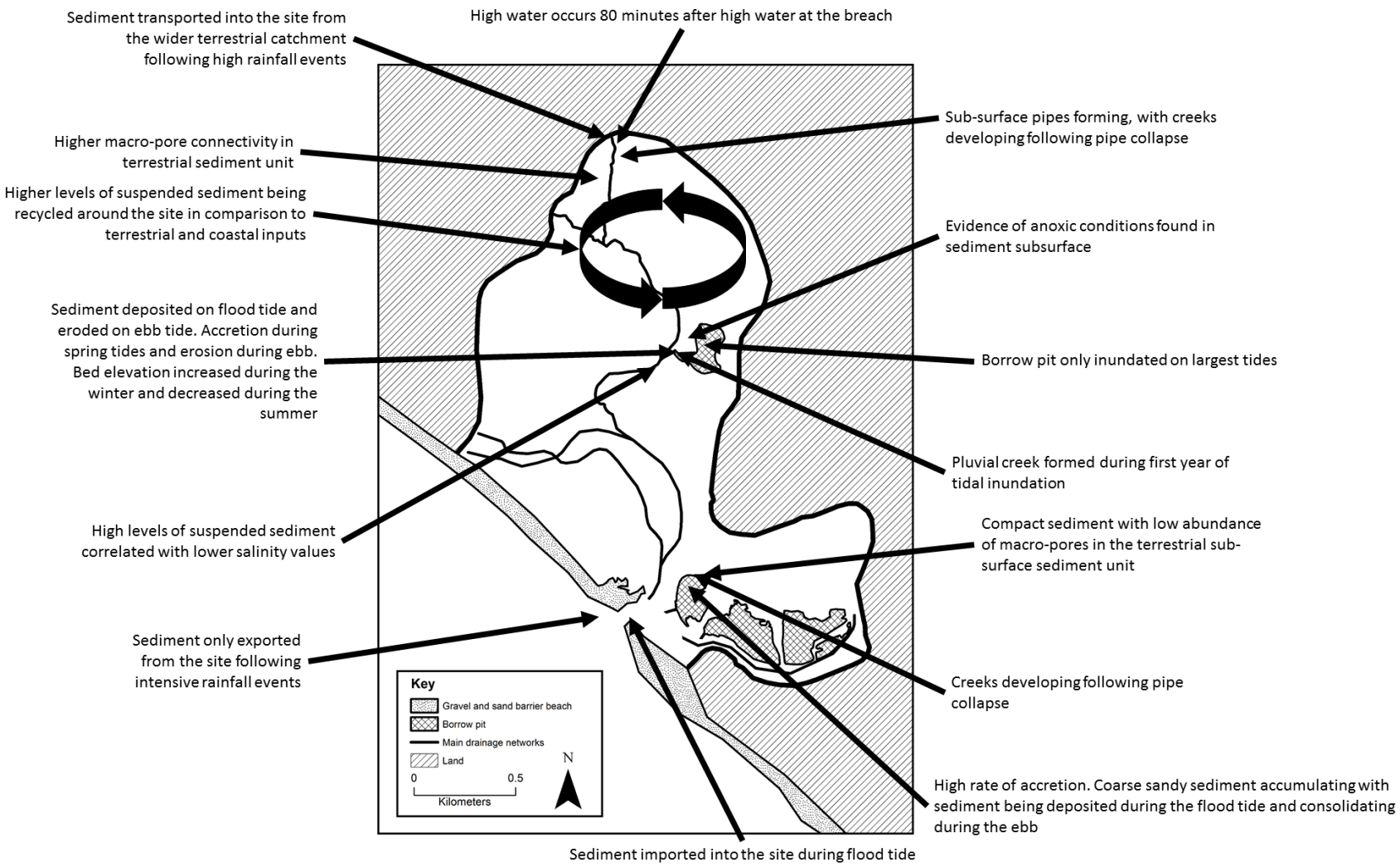

Figure 9.1: Schematic representation of the key findings in this thesis.

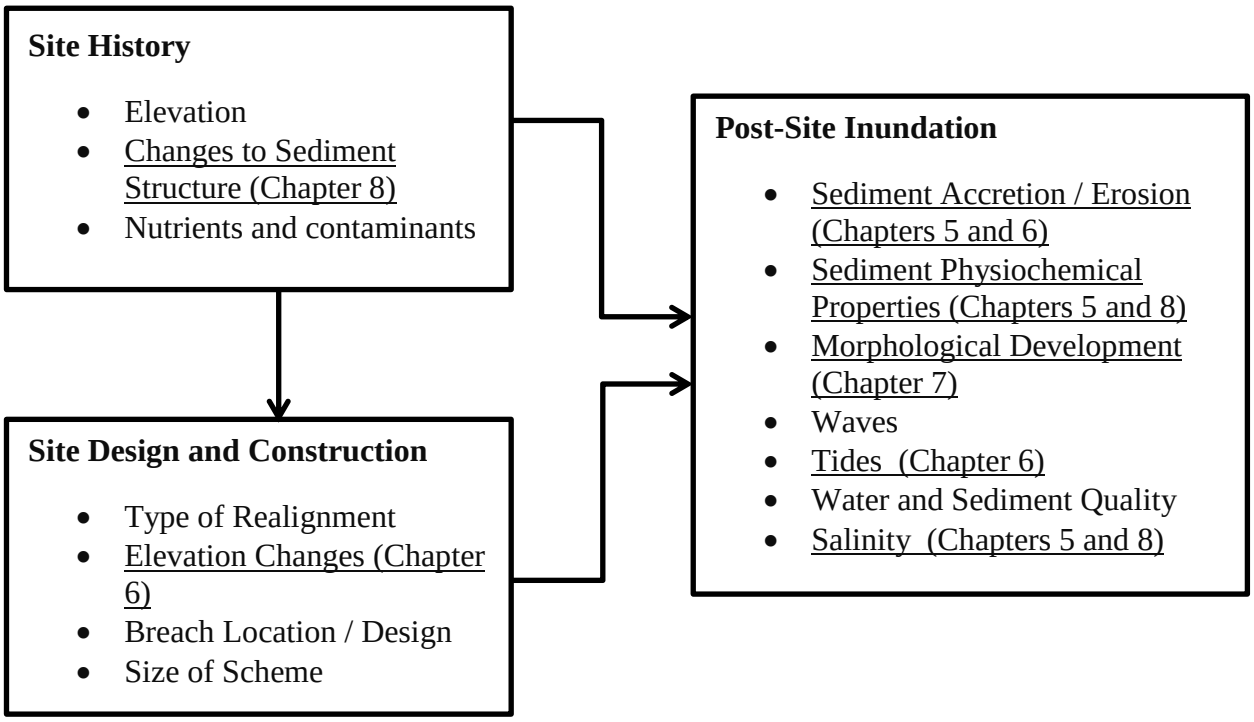

Figure 9.2: An overview of the factors influencing the evolution of the sediment regime in managed realignment sites (modified from Figure 2.2, see Chapter 2 for discussion), the factors examined in this thesis (underlined), and the corresponding chapters.

9.2 Synthesis of Key Results and Findings

9.2.1 Site History

Site history, as indicated by the results and observations presented in Chapters 5 to 8, was found to play an important role in the evolution of the sediment at the Medmerry Managed Realignment Site. Visual observations of plough lines (Site 5), tyre tracks (Site 2b) and different sub-surface sediment units (all sites) indicate that the Holocene evolution and the historical to recent land use (< 300 years) have left a physical, geomorphic and sedimentary signature on the landscape, which influence the evolution of the sediment regime following site inundation. The identified influence of the site's history on the evolution of the sediment regime in each results chapter is summarised in Figure 9.3. Differences in former land use can been seen to lead to different levels of compaction, demonstrated by the sediment bulk density and moisture concentration identified in Chapter 5 for sites of no (Site 3), low intensity and infrequent (Site 2b), and frequent high intensive (Site 5) arable agriculture. The source of 15.2 cm of accretion measured in the borrow pit at Site 5 (Chapter 6) was related to the erosion of

the relict terrestrial banks and hedgerows which run around the site, and has resulted in the rapid infill (and loss) of an area designed to encourage lower elevation intertidal habitat.

Land use histories also influence the morphogenesis and evolution of the creek networks. The creek networks which have formed in the Medmerry site have been influenced by differences in the sediment structure caused by the changes in land use (Chapter 7). For example, the different sediment units found in the bank at Site 2b have appeared to influence the piping process (proposed as the mechanism for creek formation), with piping occurring in the upper terrestrial soil (more organic, friable, unconsolidated) unit but not the lower former intertidal (higher moisture concentration and mud concentration, consolidated) unit. Differences in sub-surface sediment properties have also influenced the evolution of the creeks which have formed at Site 3 (by pluvial runoff) and Site 5 (through piping). At both these sites, the creek networks have eroded into a more compact sediment layer and have been unable to deepen any further, matching the observations of Vandenbruwaene et al. (2012).

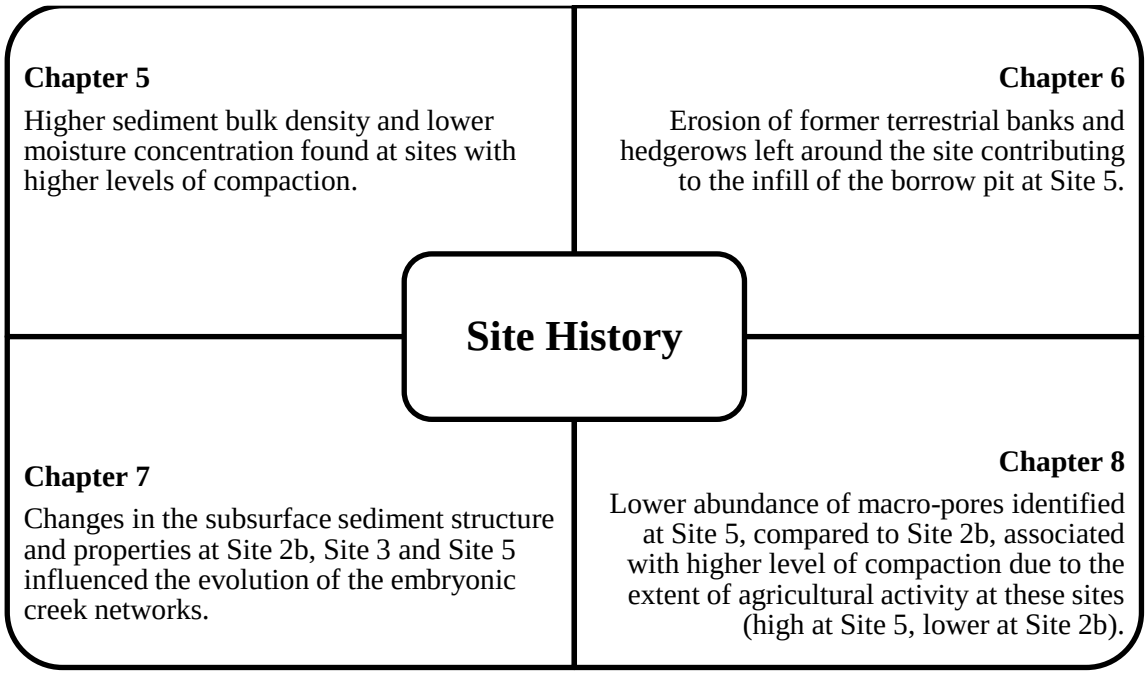

Figure 9.3: Summary of the findings associated with the site's history identified in each results chapter.

Changes in land use history influence the structure and physicochemical evolution of the sediment sub-surface. Terrestrial and pre-reclamation sedimentary units were

preserved at all sites apart from Site 5 in 2016 (Chapter 8), with visual, structural and physical differences found in the terrestrial units at the sites of different former land use. Results in Chapter 8 suggested anoxic conditions were only present at the site which had experienced the highest level of accretion (discussed in Section 9.2.3). Previous studies have related alterations caused by the former land use to reduced hydrological connectivity and solute transfer (e.g. Tempest et al., 2015), resulting in anoxic conditions and inhibited saltmarsh development (Spencer et al., 2017) following site inundation. This is due to the presence of an aquiclude (e.g. Crooks and Pye, 2000; Hazelden and Boorman, 2001; Tempest et al., 2015), inhibiting subsurface drainage across the interface between the terrestrial and the post-site inundation intertidal units. The formation of an aquiclude has been associated with compaction and a reduced number, and connectivity, of pore networks within the terrestrial unit, due to physical disturbances caused by arable agricultural activity (e.g. Spencer et al., 2017). However, results presented here indicate that an aquiclude will only form providing there has been a sufficient amount of sediment accreted on top of the terrestrial surface.

Changes in elevation, caused by compaction and dewatering, following reclamation were not evaluated as only the Medmerry Managed Realignment Site was investigated in this thesis; the extent of any changes are assumed to be relatively constant across the site. The influence of re-introducing intertidal conditions on nutrient and contaminant release has been investigated in detail by Kadiri (2010), and was not considered in this investigation as all measurements were taken during the second and third year of site inundation (i.e. after a year of percolation and sub-surface drainage of tidal waters).

9.2.2 Site Design and Construction

The results in Chapters 5 to 8 indicate that, in addition to site history, the site design and construction influence the evolution of the sediment regime in MR sites (as outlined in Figure 9.4). Surface elevation is considered to be the most important physical / structural factor in the design of MR sites (Howe et al., 2010), as elevation controls the hydroperiod, and therefore plant zonation and colonisation. Elevation can be modified during site construction to target the development of specific habitats, either by

applying additional material or by creating borrow pits through the excavation of material. Borrow pits were created at Medmerry, with the material excavated being used to construct the new earth embankment coastal flood defence. Differences in the sediment moisture concentration and bulk density were observed at Site 3 (Chapter 5), associated with compaction caused by the overburden of material removed in the construction of the channel leading up to the borrow pit. However, the high borrow pit in which Site 4 is located (Section 3.3.5) created a channel for pluvial water to drain, resulting in the formation of the creek at Site 3 (Burgess et al., 2016). The excavation of material during site construction also created the differential in hydraulic head and was therefore likely to encourage pipe formation, proposed in Chapter 7 as the mechanism of creek formation at Site 2b and Site 5.

In Chapter 6, different rates of sedimentation were measured in two of the borrow pits. At Site 3, 4.4 cm of accretion was measured over the two year monitoring period, whereas rapid infill (15.2 cm over a year) was measured in the borrow pit at Site 5, resulting in the loss of the areas of lower elevation and the habitat intended (Dale et al., 2017). The use of tidal gates on the drainage outlets appeared to influence site hydrodynamics, trapping freshwater and suspended sediment within the site. Visual observations during the flood tide indicate that the flood tidal velocities are reduced and reflected by the physical barriers. These gates may also be influencing the input of sediment to the site, as fresh water, and therefore terrestrial sediment, may only enter the site through the drainage outlets during low water. During the flood tide the gates close, resulting in a build-up of water and sediment transported from the wider catchment on the terrestrial side. As the gates open, during the ebb tide, the freshwater drains into the site transporting the sediment with it, trapping the sediment within the site and preventing the sediment from being subject to flood and ebb currents, normally experienced in estuarine environments.

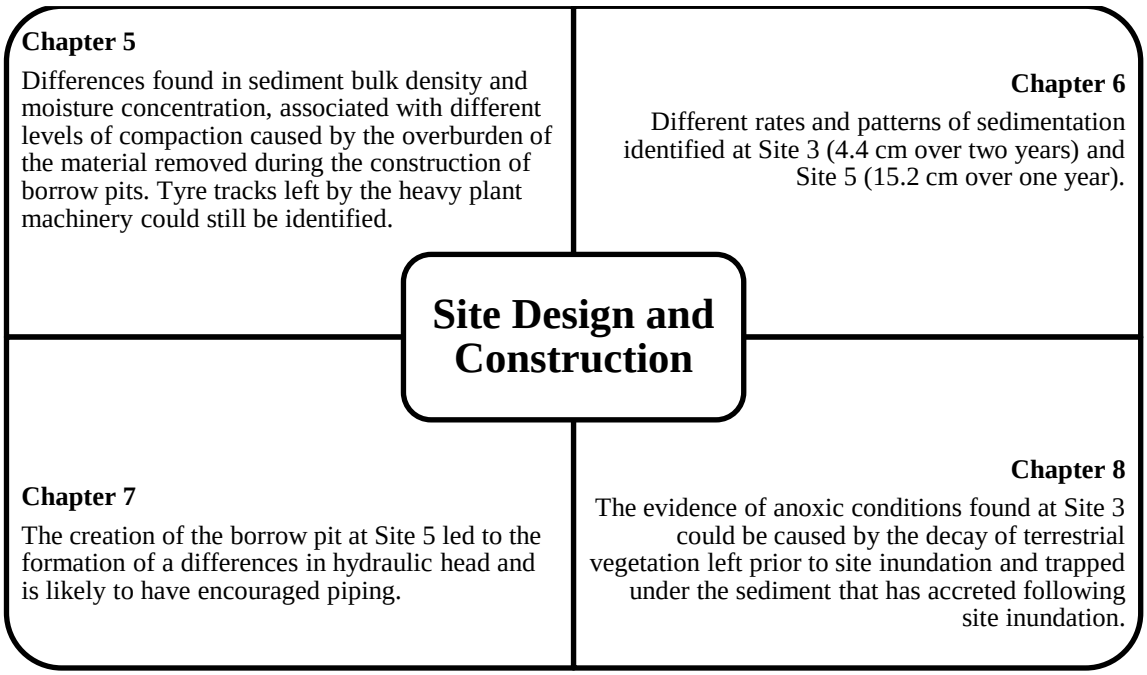

Figure 9.4: Summary of the findings associated with the site's design and construction identified in each results chapter.

The evidence of anoxic conditions found at Site 3 at Medmerry may be caused by decay of terrestrial vegetation buried under the intertidal sediment which has been deposited following site inundation. MR sites are often left vegetated in order to increase the stability of the terrestrial soil, and to encourage deposition of intertidal sediment, following site inundation. However, the decay of this vegetation will encourage anoxia, and in doing so be detrimental to the establishment of intertidal vegetation (French, 2006). As this thesis presents field data and laboratory analysis of samples from the second and third year of site inundation at the Medmerry site, comparisons of different types and sizes of MR sites, and different breach designs and locations, were not considered.

9.2.3 Post-Site Inundation

The evolution of the sediment regime is driven by tidal forcing following the introduction of intertidal conditions to the site. Figure 9.5 highlights the key findings in this thesis at the Medmerry Managed Realignment Site in response to site inundation. Tidal data, presented in Chapter 6, indicated that it takes approximately 80 minutes for

high water to propagate through the site. Near constant saline conditions were measured in the breach and at Site 5. Salinity values varied at Site 3, whereas at Site 2b the salinity remained relatively low except during the summer during periods of lower freshwater input. In Chapter 5, measurements of the accretion and erosion of sediment demonstrated seasonality in the change in bed elevation, associated with the availability of sediment and the absorption of water, and therefore the swelling of clay particles within the bed.

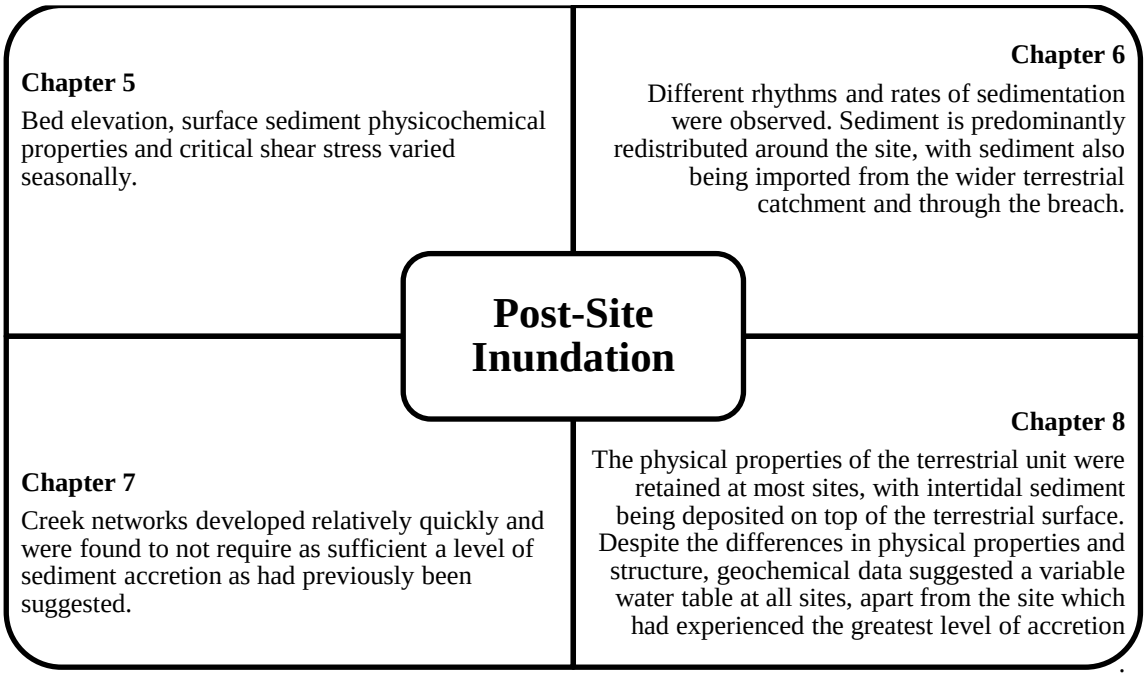

Figure 9.5: Summary of the findings associated with the site's response to tidal inundation identified in each results chapter.

At a number of previous MR schemes, the response to intertidal inundation has differed to the required or anticipated response, resulting in secondary degradation and failure to achieve the original design objectives at these sites. For example, Paull Holme Strays (Humber, United Kingdom) accreted more sediment than predicted, resulting in the loss of the targeted range of lagoon, mudflat and saltmarsh habitat (Wolanski and Elliott, 2016). In Chapter 6, patterns of accretion and erosion at Medmerry were investigated at Site 3 and Site 5, with different rhythmic sedimentation patterns, or rhythmites (Dale et al., 2017), being detected. Sediment was deposited during the flood tide, and consolidated during the ebb tide, at Site 5. In contrast to Site 5, sediment was accreted during the flood tide and eroded during the ebb tide at Site 3. This pattern was superimposed onto a pattern of accretion and erosion which matched the spring / neap

semi-lunar tidal cycle, and (in the second year) the seasonality. The source of sediment to Site 3 was identified to be predominately internal redistribution, with sediment also being transported into the site from the wider terrestrial catchment following rainfall events. The site was recognised to import sediment from the wider catchment, and only export sediment following extended periods of high suspended sediment. The Medmerry site was also found to be resistant to storm events, with sediment being imported and exported, and bed elevation recovering to a similar, pre-storm, elevation within two to three tidal cycles.

In the sediment sub-surface (Chapter 8), although different sediment units were identified visually, through X-Ray microtomography and analysis of the physical sediment properties, broad and intensive scale geochemical analysis suggests a variable water column in all sites apart from the site which had experienced the highest level of accretion. At this site, evidence of poor vertical hydrological connectivity was associated with the accretion of sediment and the physicochemical contrast between the two units. Therefore, sites either need to be designed to encourage rapid accretion to reduce the impact of the terrestrial unit, or to reduce accretion and allow the sub-surface to transition from terrestrial to intertidal conditions (rather than being buried under an intertidal unit) following site inundation. Analysis of the formation and growth of embryonic creek systems, presented in Chapter 7, indicated that creeks will develop relatively quickly (in three years following site inundation), but are influenced by changes in sub-surface sediment type and characteristics. Creeks were found to develop providing there was uncompact sediment, differing from the previous understanding that creeks would only form providing there had been a sufficient level of accretion (Watts et al., 2003).

9.3 Recommendations for the Design, Management and Science of Future Managed Realignment Projects

MR is an example of an ecological engineering technique (Type A) designed to create, or re-create, intertidal habitat by restoring coastal and estuarine systems through the (re)introduction of tidal inundation (e.g. Wolanski and Elliott, 2016) via a regulated

shift in the land / sea border (French, 2006). Such schemes are being implemented in order to improve the level and sustainability of local coastal flood defences (Esteves, 2013), and to compensate for the loss, reduction and degradation of intertidal habitats. Implementation of these schemes is frequently driven by legislative requirements to improve and protect marine biodiversity, such as the European Union (EU) Habitats Directive (European Parliament and the Council of the European Commission, 1992). These legislations are derived from a complex web of international, national, regional and private initiatives (Boyes and Elliott, 2014), with the EU playing a dominant role in such polices; the EU has adopted more than 200 pieces of legislation over a five decade period that have direct repercussions for policy and the management of marine environments. It remains to be seen what implications the current constitutional and political changes in the United Kingdom (e.g. Boyes and Elliott, 2016) have for the protection, and rehabilitation, of our coastal environments.

There is increasing evidence that suggests MR sites have lower biodiversity and delivery of ecosystem services than anticipated (e.g. Mazik et al., 2010; Mossman et al., 2012; Esteves, 2013), which may have implications for ecosystem functioning (Doherty et al., 2011). Despite these shortcomings being associated with differences in the physical structure and functioning of the sediment processes in MR sites (e.g. Spencer et al., 2008; Vandenbruwaene et al., 2012; Tempest et al., 2015), there remains a shortage of data regarding sedimentary processes within these sites (Esteves, 2013). The work presented in this thesis, and of others (e.g. Rotman et al., 2008; Spencer and Harvey, 2012; Tempest et al., 2015; Spencer et al., 2017), addresses this knowledge gap through advancing the understanding of the sedimentary processes, the evolution of the sediment regime and the physical structure and functioning of MR sites, which now needs to be implemented in the design and construction of future sites.

9.3.1 Selecting the Location for Managed Realignment

The size and design of MR schemes is often limited by the presence of infrastructure, land availability and finances (Wolanski and Elliott, 2016). As a result, schemes are often partial restorations rather than fully restoring conditions as they were prior to

reclamation. For example, in order to fully restore the Medmerry area back the original (pre-reclamation) system, analysed in this thesis, tidal inundation would be required via Pagham Harbour, through the B2145 and local sewage works, essentially isolating the town of Selsey from the mainland, and therefore making such a scheme unviable.

Former intertidal, previously reclaimed land is generally considered to be a prerequisite when deciding where to carry out managed realignment (French, 2006), re-creating, rather than creating new, intertidal environments (Elliott et al., 2007). However, physical disturbances to the sediment caused by agricultural activity following reclamation, resulting in the collapse of pore space, have been associated with issues regarding the biodiversity following the reintroduction of intertidal conditions, caused by reduced hydrological connectivity and therefore anoxic conditions (e.g. Spencer et al., 2008; Spencer and Harvey, 2012; Spencer et al., 2017). Therefore, it is probable that sites which have experienced higher intensity agricultural activity are likely to be less suitable for MR. Although analysis of the sub-surface sediment at the Medmerry site in this study (Chapter 8) found differences in physical properties and structure for areas of different levels of agricultural activity, geochemical analysis (Chapter 8) found no evidence of anoxia (implicit of stagnant water and reduced hydrological connectivity) apart from at the site which experienced the greatest level of accretion. This suggests that reduced hydrological connectivity is the result of the accretion of sediment and the contrasting physicochemical properties of the buried former terrestrial layer and the intertidal sediments accreted following site inundation. Therefore, despite concerns regarding the suitability of areas of the coastal hinterland for MR following physical disturbances caused by intensive arable agriculture, more attention to the sedimentary processes (including the rate of accretion) following site inundation is required.

9.3.2 Designing Managed Realignment Sites

The findings in this thesis further the understanding of the evolution of the sediment regime, providing a new insight through high frequency and regular measurements in a newly inundated MR site. These results provide a new temporal element (i.e. high

frequency, long term, and from one year after site inundation) to hydrodynamic, surface and sub-surface sediment structure and properties, and morphological development datasets from MR sites (as opposed to the short-term studies of heavily researched sites such as Orplands Farm (e.g. Macleod et al., 1999; Spencer et al., 2008; Tempest et al., 2015; Spencer et al., 2017) which was breached in 1995). Nonetheless, the design of MR sites is still based on aesthetics, accessibility (such as the Herringbone design at the Steart Managed Realignment Site to allow cattle to retreat to higher ground during the flood tide), and is derived using numerical models (e.g. Pontee, 2015). These models consider the hydrodynamic response to differences in elevation and pre-breach landscaping, and therefore the hydroperiod. However, many schemes are implemented with tenuous model validation, little ground truthing, and no consideration of inconsistencies between the modelled and implemented site design necessitated by changes made during site construction, as was the case at Medmerry (Burgess et al., 2016).

Models which consider the behaviour of sediment and morphological evolution in MR sites do exist (Spearman, 2011), but differences in sediment structure and functioning, and therefore the drainage and hydrological regime, are generally not included in the site design. Whilst it may be challenging to incorporate these factors into site design models (Spencer et al., 2017), their inclusion will optimise site design and construction in terms of the delivery of ecosystem services. Results presented in this thesis demonstrate differences in the surface and sub-surface sediment structure and evolution of the sediment regime for areas of different design and former land use (as summarised in Sections 9.2 to 9.4), within a single large open coast MR site. These differences now need to be compared to other sites, including managed (design and constructed) and non-managed (non-engineered) realignment sites. Although this will incorporate wider coastal and oceanographic differences, such as sediment availability and tidal regime, current comparisons of neighbouring managed and non-managed MR sites (e.g. Spencer et al., 2017) have evaluated sites of contrasting ages. As a result, it is possible that differences caused by the site design and construction may be missed, as older sites would have had longer (decades) to develop.

9.4 Conclusions and Recommendations for Future Work

This thesis aimed to evaluate how former land use, site design and construction influence the evolution of the sediment regime in managed realignment (MR) sites, through analysis of measurements and samples taken from the Medmerry Managed Realignment Site, West Sussex, United Kingdom. This has been achieved through repeat or near-continuous high frequency, and high resolution, measurements of the sedimentation processes and changes in sediment structure and properties, taken over a two-year period. The evaluation and discussion of these results addresses the knowledge gaps identified in Section 2.5.

The main findings in this thesis, presented in Figure 9.1, are;

- Bed elevation, surface physicochemical properties and cohesive strength measurements in Chapter 5 (Objective 1) demonstrated signs of seasonal variability, with some relationships found spatially and temporally between the physicochemical properties although the relationships between sediment properties varied between sites. Variability between sites was found to be greater than the within site variability, highlighting the need for analysis of a number of sites to represent the evolution of the sediment regime. Higher bulk densities and lower moisture concentrations were found at sites which were expected to have more compact sediment due to the intensity of agricultural activity and physical disturbances during site construction.
- In Chapter 6, different rates and rhythms of sedimentation were measured in the borrow pits at Site 3 and Site 5 (Objective 2). Near-constant accretion of sediment was observed at Site 5, as would be expected according to predictive models of sediment accretion (e.g. Allen, 2000), whereas at Site 3 sedimentary rhythmites typical of a developed natural sheltered intertidal mudflat (Deloffre et al., 2007) were observed. Sediment was imported into the site from terrestrial and coastal sources, although suspended sediment was mainly derived from internal reworking of sediment.
- Creek morphogenesis occurred before, and within, the study period (second and third year of site inundation), prior to the accretion of sediment exceeding a critical depth as suggested by Watts et al. (2003). The evolution of the creeks

did, however, appear to be influenced by sub-surface sedimentological conditions (Chapter 7, Objective 3), matching the observations of Vandenbruwaene et al. (2012).

- Clear differences in sediment structure and properties were identified in Chapter 8. However, evidence of poor drainage and anoxia were only found at the site which had experienced the highest level of accretion (Objective 4). These results suggest that the reduced sub-surface hydraulic connectivity observed at other MR sites (e.g. Tempest et al., 2015) may be caused by the accretion of intertidal sediment following site inundation, and the sharp contact between the deposited sediment and the underlying terrestrial units.
- The influence of the former land use, site design and construction have on the measured and observed evolution of the sediment regime have been discussed and evaluated in terms of the considerations required in the design and construction of future sites (Chapter 9, Objective 5). Elevation, and therefore the hydroperiod, is the focus in the design of MR sites, yet results presented in this thesis demonstrate that following site inundation sediment is imported, exported and redistributed around the site inevitably changing the elevation. At present, there is no requirement for hindcasting or validation of site design models following site inundation, resulting in little or no quality assurance for future modelling. Differences in the sediment structure need to be incorporated into site design models to provide accurate estimates of the evolution of a site, including: drainage, vegetation colonisation, the level of coastal flood defence, and the delivery of ecosystem services.

9.4.1 Further Research Requirements

Results and discussion within this thesis highlight the need for future research to better understand the evolution of the sediment regime in order to maximise the delivery of ecosystem services from MR sites. Some examples of future work that could address this need include;

1) Comparing managed (engineered) realignment sites, such as Medmerry, to recently breached non-managed (non-engineered) realignment sites to evaluate further the influence of parameters associated with site design and construction.

2) Hindcasting site construction models to validate the predictions of site evolution. This will facilitate sensitivity analysis of the key site construction and post-site inundation factors (e.g. breach size, location, number or the design of the main drainage channels) influencing site evolution and preventing secondary degradation by sustaining the intended intertidal habitat.
3) Identifying adjustments that can easily be made during site construction to improve the functioning of the sediment regime in MR sites to maximise the delivery of ecosystem services. Possible adjustments include leaving sites vegetated, ploughing, constructing small shallow trenches or importing dredged material, and can be investigated through experimentation at future MR sites and through further analysis of the pre-existing sites.

Advances in the understanding of the response of the sediment regime in MR sites to site design, construction and the historic influences on the landscape caused by the former land use can be attained through continued long-term monitoring. Therefore, improvements can be made to site design and construction, with a focus on engineering sites to restoration of the entire system, including the hydrological regime. This will ensure MR schemes provide the maximum and long-term delivery of ecosystem services through suitable and sustainable intertidal habitat restoration, compensating for previous, and current, habitat loss elsewhere, and locally enhancing the protection offered by coastal flood defences.

10 References

ABPmer, 2017. Online Marine Registry.

Alaoui, A., Lipiec, J., Gerke, H.H., 2011. A review of the changes in the soil pore system due to soil deformation: A hydrodynamic perspective. Soil & Tillage Research 115, 1-15.

Allen, J., Pye, K., 1992. Coastal saltmarshes: their nature and importance, in: Allen, J., Pye, K. (Eds.), Saltmarshes: Morphodynamics, conservation and engineering significance. Cambridge University Press, Cambridge, pp. 1-18.

Allen, J.R.L., 2000. Morphodynamics of Holocene salt marshes: a review sketch from the Atlantic and Southern North Sea coasts of Europe. Quaternary Science Reviews 19, 1155-1231.

Allen, L.G., Gibbard, P.L., 1993. Pleistocene evolution of the Solent River of southern England. Quaternary Science Reviews 12, 503-528.

American Public Health Association, American Water Works Association, 1981. Standard methods for the examination of water and wastewater: selected analytical methods approved and cited by the United States Environmental Protection Agency. American Public Health Association.

Amos, C.L., Droppo, I.G., Gomez, E.A., Murphy, T.P., 2003. The stability of a remediated bed in Hamilton Harbour, Lake Ontario, Canada. Sedimentology 50, 149-168.

Andrews, J.E., Burgess, D., Cave, R.R., Coombes, E.G., Jickells, T.D., Parkes, D.J., Turner, R.K., 2006. Biogeochemical value of managed realignment, Humber estuary, UK. Science of the Total Environment 371, 19-30.

Anisfeld, S.C., Tobin, M., Benoit, G., 1999. Sedimentation rates in flow-restricted and restored salt marshes in Long Island Sound. Estuaries 22, 231-244.

Auxtero, E., Shamshuddin, J., Paramananthan, S., 1991. Mineralogy, morphology and classification of acid sulfate soils in Pulau Lumut, Selangor. Pertanika 14, 43-51.

Baily, B., Pearson, A.W., 2007. Change detection mapping and analysis of salt marsh areas of central southern England from Hurst Castle Spit to Pagham Harbour. Journal of Coastal Research 23, 1549-+.

Balke, T., Bouma, T.J., Horstman, E.M., Webb, E.L., Erftemeijer, P.L.A., Herman, P.M.J., 2011. Windows of opportunity: thresholds to mangrove seedling establishment on tidal flats. Marine Ecology Progress Series 440, 1-9.

Balmford, A., Bruner, A., Cooper, P., Costanza, R., Farber, S., Green, R.E., Jenkins, M., Jefferiss, P., Jessamy, V., Madden, J., Munro, K., Myers, N., Naeem, S., Paavola, J., Rayment, M., Rosendo, S., Roughgarden, J., Trumper, K., Turner, R.K., 2002. Ecology - Economic reasons for conserving wild nature. Science 297, 950-953.

Barbier, E.B., Hacker, S.D., Kennedy, C., Koch, E.W., Stier, A.C., Silliman, B.R., 2011. The value of estuarine and coastal ecosystem services. Ecological Monographs 81, 169-193.

Bates, M.R., Parfitt, S.A., Roberts, M.B., 1997. The chronology, palaeogeography and archaeological significance of the marine quaternary record of the west Sussex coastal plain, southern England, UK. Quaternary Science Reviews 16, 1227-1252.

Baxter, P.J., 2005. The east coast Big Flood, 31 January-1 February 1953: a summary of the human disaster. Philosophical Transactions of the Royal Society a-Mathematical Physical and Engineering Sciences 363, 1293-1312.

Bendle, J.M., Palmer, A.P., Carr, S.J., 2015. A comparison of micro-CT and thin section analysis of Lateglacial glaciolacustrine varves from Glen Roy, Scotland. Quaternary Science Reviews 114, 61-77.

Bergen, S.D., Bolton, S.M., L. Fridley, J., 2001. Design principles for ecological engineering. Ecological Engineering 18, 201-210.

Berrow, M.L., Stein, W.M., 1983. Extraction of metals from soils and sewage sludges by refluxing with aqua regia. Analyst 108, 277-285.

Black, K.S., Paterson, D.M., 1997. Measurement of the erosion potential of cohesive marine sediments: a review of current in situ technology. Journal of Marine Environmental Engineering 4, 43-83.

Blackwell, M.S.A., Yamulki, S., Bol, R., 2010. Nitrous oxide production and denitrification rates in estuarine intertidal saltmarsh and managed realignment zones. Estuarine Coastal and Shelf Science 87, 591-600.

Bockstael, N.E., Freeman, A.M., Kopp, R.J., Portney, P.R., Smith, V.K., 2000. On measuring economic values for nature. Environmental Science & Technology 34, 1384-1389.

Bone, A.E., 1996. The shaping of the Selsey coastline: a review of the geomorphology, archaeology and history. Tertiary Research 16, 5-14.

Boorman, L., 1992. The environmental consequences of climatic change on British salt marsh vegetation. Wetlands Ecology and Management 2, 11-21.

Boorman, L., Hazelden, J., 1995. Saltmarsh creation and management for coastal defence, in: Healy, M.G., Doody, J.P. (Eds.), Directions in European Coastal Management. Samara Publishing Limited, Cardigan, pp. 175-184.

Borja, A., Dauer, D.M., Elliott, M., Simenstad, C.A., 2010. Medium- and Long-term Recovery of Estuarine and Coastal Ecosystems: Patterns, Rates and Restoration Effectiveness. Estuaries and Coasts 33, 1249-1260.

Bowron, T., Neatt, N., van Proosdij, D., Lundholm, J., Graham, J., 2011. Macro-Tidal Salt Marsh Ecosystem Response to Culvert Expansion. Restoration Ecology 19, 307-322.

Boyes, S.J., Elliott, M., 2014. Marine legislation – The ultimate 'horrendogram': International law, European directives & national implementation. Marine Pollution Bulletin 86, 39-47.

Boyes, S.J., Elliott, M., 2016. Brexit: The marine governance horrendogram just got more horrendous! Marine Pollution Bulletin 111, 41-44.

Brampton, A.H., 1992. Engineering significance of British saltmarshes, in: Allen, J.R.L., Pye, K. (Eds.), Saltmarshes: Morphodynamics, conservation and engineering significance. Cambridge University Press, Cambridge, pp. 115-122.

British Geological Survey, 2017. Geology of Britain Viewer.

Brossler, A., 2010. Medmerry Managed Realignment - West Sussex. Cultural Heritage Desk Based Assessment. Environment Agency, Bristol.

Burd, F., 1989. Saltmarsh survey of Great Britain: an inventory of British Saltmarshes. Nature Conservancy Council, Peterborough.

Burgess, H., Kilkie, P., Callaway, T., 2016. Understanding the Physical Processes Occurring Within a New Coastal Managed Realignment Site, Medmerry, Sussex, UK, Coastal Management, pp. 263-272.

Burton, E.D., Bush, R.T., Johnston, S.G., Sullivan, L.A., Keene, A.F., 2011. Sulfur biogeochemical cycling and novel Fe-S mineralization pathways in a tidally re-flooded wetland. Geochimica Et Cosmochimica Acta 75, 3434-3451.

Carter, D., Bray, M., 2004. Coastal sediment transport study, Report to SCOPAC by RACER, 2nd ed.

Castillo, C., Perez, R., James, M.R., Quinton, J.N., Taguas, E.V., Gomez, J.A., 2012. Comparing the Accuracy of Several Field Methods for Measuring Gully Erosion. Soil Science Society of America Journal 76, 1319-1332.

Castleden, R., 1998. Classic landforms of the Sussex coast, 2nd ed. Geographical Association, Sheffield.

Chang, Y.H., Scrimshaw, M.D., Macleod, C.L., Lester, J.N., 2001. Flood defence in the Blackwater Estuary, Essex, UK: The impact of sedimentological and geochemical changes on salt marsh development in the Tollesbury Managed Realignment site. Marine Pollution Bulletin 42, 470-481.

Chester, R., 2009. Marine geochemistry. John Wiley & Sons.

Clapp, J., 2009. Managed realignment in the Humber estuary: factors influencing sedimentation. University of Hull.

Cnudde, V., Boone, M.N., 2013. High-resolution X-ray computed tomography in geosciences: A review of the current technology and applications. Earth-Science Reviews 123, 1-17.

Cochran, J.K., Hirschberg, D.J., Wang, J., Dere, C., 1998. Atmospheric deposition of metals to coastal waters (Long Island Sound, New York USA): Evidence from saltmarsh deposits. Estuarine Coastal and Shelf Science 46, 503-522.

Cook, K.L., 2017. An evaluation of the effectiveness of low-cost UAVs and structure from motion for geomorphic change detection. Geomorphology 278, 195-208.

Cooper, N.J., 2005. Wave dissipation across intertidal surfaces in the Wash tidal inlet, eastern England. Journal of Coastal Research 21, 28-48.

Cope, S., 2004. Breaching of UK coarse-clastic barrier beach systems methods developed for predicting breach occurrence, stability and flooded hinterland evolution. University of Portsmouth.

Cope, S., Bradbury, A., Gorczynska, M., 2008. Solent Dynamic Coast Project: Main Report; A tool for SMP2, New Forest District Council and the Channel Coastal Observatory.

Cornu, C.E., Sadro, S., 2002. Physical and functional responses to experimental marsh surface elevation manipulation in Coos Bay's South Slough. Restoration Ecology 10, 474-486.

Costanza, R., d'Arge, R., deGroot, R., Farber, S., Grasso, M., Hannon, B., Limburg, K., Naeem, S., O'Neill, R.V., Paruelo, J., Raskin, R.G., Sutton, P., van den Belt, M., 1997. The value of the world's ecosystem services and natural capital. Nature 387, 253-260.

Cox, T.J.S., Maris, T., De Vleeschauwer, P., De Mulder, T., Soetaert, K., Meire, P., 2006. Flood control areas as an opportunity to restore estuarine habitat. Ecological Engineering 28, 55-63.

Crooks, S., Pye, K., 2000. Sedimentological controls on the erosion and morphology of saltmarshes: implications for flood defence and habitat recreation, in: Pye, K., Allen, J.R.L. (Eds.), Coastal and Estuarine Environments: Sedimentology, Geomorphology and Geoarchaeology, pp. 207-222.

Crooks, S., Schutten, J., Sheern, G.D., Pye, K., Davy, A.J., 2002. Drainage and elevation as factors in the restoration of salt marsh in Britain. Restoration Ecology 10, 591-602.

Croudace, I.W., Rindby, A., Rothwell, R.G., 2006. ITRAX: description and evaluation of a new multi-function X-ray core scanner. Geological Society, London, Special Publications 267, 51-63.

Cundy, A.B., Croudace, I.W., 1995. Sedimentary and geochemical variations in a salt-marsh mud flat environment from the mesotidal Hamble estuary, southern England. Marine Chemistry 51, 115-132.

Cundy, A.B., Croudace, I.W., 1996. Sediment accretion and recent sea-level rise in the Solent, southern England: Inferences from radiometric and geochemical studies. Estuarine Coastal and Shelf Science 43, 449-467.

Cundy, A.B., Croudace, I.W., Cearreta, A., Irabien, M.J., 2003. Reconstructing historical trends in metal input in heavily-disturbed, contaminated estuaries: studies from Bilbao, Southampton Water and Sicily. Applied Geochemistry 18, 311-325.

Cundy, A.B., Hopkinson, L., Lafite, R., Spencer, K., Taylor, J.A., Ouddane, B., Heppell, C.M., Carey, P.J., Charman, R., Shell, D., Ullyott, S., 2005. Heavy metal distribution and accumulation in two Spartina sp.-dominated macrotidal salt marshes from the Seine estuary (France) and the Medway estuary (UK). Applied Geochemistry 20, 1195-1208.

Cundy, A.B., Long, A.J., Hill, C.T., Spencer, C., Croudace, I.W., 2002. Sedimentary response of Pagham Harbour, southern England to barrier breaching in AD 1910. Geomorphology 46, 163-176.

Cundy, A.B., Sprague, D., Hopkinson, L., Maroukian, H., Gaki-Papanastassiou, K., Papanastassiou, D., Frogley, M.R., 2006. Geochemical and stratigraphic indicators of late Holocene coastal evolution in the Gythio area, southern Peloponnese, Greece. Marine Geology 230, 161-177.

Daily Mail, 2008. Britain braced for new storm front as forecasters warn 'the worst is yet to come'.

Dale, J., Burgess, H.M., Cundy, A.B., 2017. Sedimentation rhythms and hydrodynamics in two engineered environments in an open coast managed realignment site. Marine Geology 383, 120-131.

D'Alpaos, A., Lanzoni, S., Marani, M., Bonornetto, A., Cecconi, G., Rinaldo, A., 2007a. Spontaneous tidal network formation within a constructed salt marsh: Observations and morphodynamic modelling. Geomorphology 91, 186-197.

D'Alpaos, A., Lanzoni, S., Marani, M., Rinaldo, A., 2007b. Landscape evolution in tidal embayments: Modeling the interplay of erosion, sedimentation, and vegetation dynamics. Journal of Geophysical Research-Earth Surface 112.

Davy, A.J., Brown, M.J.H., Mossman, H.L., Grant, A., 2011. Colonization of a newly developing salt marsh: disentangling independent effects of elevation and redox potential on halophytes. Journal of Ecology 99, 1350-1357.

Defew, E.C., Tolhurst, T.J., Paterson, D.M., 2002. Site-specific features influence sediment stability of intertidal flats. Hydrology and Earth System Sciences 6, 971-981.

DEFRA, 2005. Making Space for Water. Department for Environment, Food and Rural Affairs, London.

Deloffre, J., Verney, R., Lafite, R., Lesueur, P., Lesourd, S., Cundy, A.B., 2007. Sedimentation on intertidal mudflats in the lower part of macrotidal estuaries: Sedimentation rhythms and their preservation. Marine Geology 241, 19-32.

Dent, D.L., Downing, E.J.B., Rogaar, H., 1976. Changes in structure of marsh soils following drainage and arable cultivation. Journal of Soil Science 27, 250-265.

Dixon, M., Morris, R.K.A., Scott, C.R., Birchenough, A., Colclough, S., 2008. Managed realignment - lessons from Wallasea, UK. Proceedings of the Institution of Civil Engineers-Maritime Engineering 161, 61-71.

Doherty, J.M., Callaway, J.C., Zedler, J.B., 2011. Diversity-function relationships changed in a long-term restoration experiment. Ecological Applications 21, 2143-2155.

Doherty, J.M., Miller, J.F., Prellwitz, S.G., Thompson, A.M., Loheide, S.P., Zedler, J.B., 2014. Hydrologic Regimes Revealed Bundles and Tradeoffs Among Six Wetland Services. Ecosystems 17, 1026-1039.

Doody, J.P., 1992. Sea defense and nature conservation - threat or opportunity. Aquatic Conservation-Marine and Freshwater Ecosystems 2, 275-283.

Doody, J.P., 2004. 'Coastal squeeze' - an historical perspective. Journal of Coastal Conservation 10, 129-138.

Doody, J.P., 2008. Saltmarsh conservation, management and restoration. Springer.

Doody, J.P., 2013. Coastal squeeze and managed realignment in southeast England, does it tell us anything about the future? Ocean & Coastal Management 79, 34-41.

Dyer, K.R., 1986. Coastal and Estuarine Sediment Dynamics. Wiley, Chichester.

Edwards, A.M.C., Winn, P.S.J., 2006. The Humber Estuary, Eastern England: Strategic planning of flood defences and habitats. Marine Pollution Bulletin 53, 165-174.

Edwards, K.R., Proffitt, C.E., 2003. Comparison of wetland structural characteristics between created and natural salt marshes in southwest Louisiana, USA. Wetlands 23, 344-356.

Ekwall, E., 1960. The Concise Oxford Dictionary of English Place-Names, 4th ed. Oxford University Press, Oxford.

Elliott, M., Burdon, D., Hemingway, K.L., Apitz, S.E., 2007. Estuarine, coastal and marine ecosystem restoration: Confusing management and science - A revision of concepts. Estuarine Coastal and Shelf Science 74, 349-366.

Elliott, M., Mander, L., Mazik, K., Simenstad, C., Valesini, F., Whitfield, A., Wolanski, E., 2016. Ecoengineering with Ecohydrology: Successes and failures in estuarine restoration. Estuarine, Coastal and Shelf Science 176, 12-35.

Environment Agency, 2007. Pagham to East Head Coastal Defence Strategy, Worthing.

Environment Agency, 2015. Medmerry Managed Realignment - March 2015 report, Bristol.

Esteves, L.S., 2013. Is managed realignment a sustainable long-term coastal management approach? Journal of Coastal Research Special Issue 65, 933-938.

Esteves, L.S., 2014. Managed Realignment : A Viable Long-Term Coastal Management Strategy? Springer, Netherlands.

European Parliament and the Council of the European Commission, 1992. Council directive 92/43/EEC of 21 May 1992 on the conservation of natural habitats and of wild fauna and flora. Official Journal of the European Communities Series L206, 22.12.2000.

Fagherazzi, S., Furbish, D.J., 2001. On the shape and widening of salt marsh creeks. Journal of Geophysical Research-Oceans 106, 991-1003.

Fettweis, M., Sas, M., Monbaliu, J., 1998. Seasonal, neap-spring and tidal variation of cohesive sediment concentration in the Scheldt Estuary, Belgium. Estuarine Coastal and Shelf Science 47, 21-36.

Flemming, B.W., Delafontaine, M.T., 2000. Mass physical properties of muddy intertidal sediments: some applications, misapplications and non-applications. Continental Shelf Research 20, 1179-1197.

Foster, N.M., Hudson, M.D., Bray, S., Nicholls, R.J., 2013. Intertidal mudflat and saltmarsh conservation and sustainable use in the UK: A review. Journal of Environmental Management 126, 96-104.

Foster, N.M., Hudson, M.D., Bray, S., Nicholls, R.J., 2014. Research, policy and practice for the conservation and sustainable use of intertidal mudflats and saltmarshes in the Solent from 1800 to 2016. Environmental Science & Policy 38, 59-71.

French, C.E., French, J.R., Clifford, N.J., Watson, C.J., 2000. Sedimentation-erosion dynamics of abandoned reclamations: the role of waves and tides. Continental Shelf Research 20, 1711-1733.

French, J.R., Stoddart, D.R., 1992. Hydrodynamics of salt marsh creek systems: Implications for marsh morphological development and material exchange. Earth Surface Processes and Landforms 17, 235-252.

French, P.W., 1999. Managed retreat: a natural analogue from the Medway estuary, UK. Ocean & Coastal Management 42, 49-62.

French, P.W., 2006. Managed realignment - The developing story of a comparatively new approach to soft engineering. Estuarine Coastal and Shelf Science 67, 409-423.

Friend, P.L., Collins, M.B., Holligan, P.M., 2003. Day-night variation of intertidal flat sediment properties in relation to sediment stability. Estuarine Coastal and Shelf Science 58, 663-675.

Friess, D.A., Möller, I., Spencer, T., Smith, G.M., Thomson, A.G., Hill, R.A., 2014. Coastal saltmarsh managed realignment drives rapid breach inlet and external creek evolution, Freiston Shore (UK). Geomorphology 208, 22-33.

Gambrell, R.P., Wiesepape, J.B., Patrick, W.H., Duff, M.C., 1991. The Effects of pH, Redox, and Salinity on Metal Release from a Contaminated Sediment. Water Air and Soil Pollution 57-8, 359-367.

Gedan, K.B., Silliman, B.R., Bertness, M.D., 2009. Centuries of Human-Driven Change in Salt Marsh Ecosystems. Annual Review of Marine Science 1, 117-141.

Goodburn, D.M., 1987. Medmerry - a reassessment of a migration period site on the south coast of England, and some of its finds. International Journal of Nautical Archaeology 16, 213-224.

Grabowski, R.C., Droppo, I.G., Wharton, G., 2010. Estimation of critical shear stress from cohesive strength meter-derived erosion thresholds. Limnology and Oceanography-Methods 8, 678-685.

Grabowski, R.C., Droppo, I.G., Wharton, G., 2011. Erodibility of cohesive sediment: The importance of sediment properties. Earth-Science Reviews 105, 101-120.

Granek, E.F., Polasky, S., Kappel, C.V., Reed, D.J., Stoms, D.M., Koch, E.W., Kennedy, C.J., Cramer, L.A., Hacker, S.D., Barbier, E.B., Aswani, S., Ruckelshaus, M., Perillo, G.M.E., Silliman, B.R., Muthiga, N., Bael, D., Wolanski, E., 2010. Ecosystem Services as a Common Language for Coastal Ecosystem-Based Management. Conservation Biology 24, 207-216.

Gutierrez, M., Sancho, C., Benito, G., Sirvent, J., Desir, G., 1997. Quantitative study of piping processes in badland areas of the Ebro Basin, NE Spain. Geomorphology 20, 237-253.

Haigh, I., Nicholls, R., Wells, N., 2009. Mean sea level trends around the English Channel over the 20th century and their wider context. Continental Shelf Research 29, 2083-2098.

Haigh, I., Nicholls, R., Wells, N., 2011. Rising sea levels in the English Channel 1900 to 2100. Proceedings of the Institution of Civil Engineers-Maritime Engineering 164, 81-92.

Hazelden, J., Boorman, L.A., 2001. Soils and 'managed retreat' in South East England. Soil Use and Management 17, 150-154.

Head, K.H., 1992. Manual of soil laboratory testing: Soil classification and compaction tests, 2nd ed. Pentech Press, London.

Hodge, M., Johnson, D., 2007. Constraint mapping as a means of further refining saltmarsh re-creation opportunities for the UK Solent region. Coastal Management 35, 483-498.

Horton, B.P., Rahmstorf, S., Engelhart, S.E., Kemp, A.C., 2014. Expert assessment of sea-level rise by AD 2100 and AD 2300. Quaternary Science Reviews 84, 1-6.

Howe, A.J., Rodriguez, J.F., Spencer, J., MacFarlane, G.R., Saintilan, N., 2010. Response of estuarine wetlands to reinstatement of tidal flows. Marine and Freshwater Research 61, 702-713.

Howes, B.L., Goehringer, D.D., 1994. Porewater drainage and dissolved organic-carbon and nutrient losses through the intertidal creekbanks of a New-England salt-marsh. Marine Ecology Progress Series 114, 289-301.

Hughes, R.G., Paramor, O.A.L., 2004. On the loss of saltmarshes in south-east England and methods for their restoration. Journal of Applied Ecology 41, 440-448.

Hvorslev, M.J., 1949. Subsurface exploration and sampling of soils for civil engineering purposes. Waterways Experiment Station, Vicksburg, Mississippi.

Jacobs, S., Beauchard, O., Struyf, E., Cox, T.J.S., Maris, T., Meire, P., 2009. Restoration of tidal freshwater vegetation using controlled reduced tide (CRT) along the Schelde Estuary (Belgium). Estuarine Coastal and Shelf Science 85, 368-376.

James, M.R., Robson, S., 2012. Straightforward reconstruction of 3D surfaces and topography with a camera: Accuracy and geoscience application. Journal of Geophysical Research-Earth Surface 117.

James, M.R., Robson, S., 2014. Mitigating systematic error in topographic models derived from UAV and ground-based image networks. Earth Surface Processes and Landforms 39, 1413-1420.

Javemick, L., Brasington, J., Caruso, B., 2014. Modeling the topography of shallow braided rivers using Structure-from-Motion photogrammetry. Geomorphology 213, 166-182.

Johnston, S.G., Keene, A.F., Bush, R.T., Burton, E.D., Sullivan, L.A., Isaacson, L., McElnea, A.E., Ahern, C.R., Smith, C.D., Powell, B., 2011. Iron geochemical zonation in a tidally inundated acid sulfate soil wetland. Chemical Geology 280, 257-270.

Kadiri, M., 2010. Physicochemical changes to soil and sediment in managed realignment sites following tidal inundation. Queen Mary's University, Queen Mary's University.

Kadiri, M., Spencer, K.L., Heppell, C.M., Fletcher, P., 2011. Sediment characteristics of a restored saltmarsh and mudflat in a managed realignment scheme in Southeast England. Hydrobiologia 672, 79-89.

Kennish, M.J., 2002. Environmental threats and environmental future of estuaries. Environmental Conservation 29, 78-107.

Kentula, M.E., 2000. Perspectives on setting success criteria for wetland restoration. Ecological Engineering 15, 199-209.

Kesel, R.H., Smith, J.S., 1978. Tidal creek and pan formation in inter-tidal salt marshes, Nigg Bay, Scotland. Scottish Geographical Magazine 94, 159-168.

Ketcham, R.A., Carlson, W.D., 2001. Acquisition, optimization and interpretation of X-ray computed tomographic imagery: applications to the geosciences. Computers & Geosciences 27, 381-400.

King, S.E., Lester, J.N., 1995. The value of salt-marsh as a sea defense. Marine Pollution Bulletin 30, 180-189.

Kirwan, M.L., Murray, A.B., 2007. A coupled geomorphic and ecological model of tidal marsh evolution. Proceedings of the National Academy of Sciences of the United States of America 104, 6118-6122.

Kirwan, M.L., Temmerman, S., Skeehan, E.E., Guntenspergen, G.R., Fagherazzi, S., 2016. Overestimation of marsh vulnerability to sea level rise. Nature Climate Change 6, 253-260.

Koretsky, C.M., Van Cappellen, P., DiChristina, T.J., Kostka, J.E., Lowe, K.L., Moore, C.M., Roychoudhury, A.N., Viollier, E., 2005. Salt marsh pore water geochemistry does not correlate with microbial community structure. Estuarine, Coastal and Shelf Science 62, 233-251.

Krawiec, K., 2017. Medmerry, West Sussex, UK: Coastal Evolution from the Neolithic to the Medieval Period and Community Resilience to Environmental Change. The Historic Environment: Policy & Practice 8, 101-112.

Krawiec, K., in press. Medmerry Managed Realignment Scheme, West Sussex: a Holocene deposit model of a coastal environment, in: Carey, C., J, Corcoran, J., Howard, A., Knight, D., Heathcote, J. (Eds.), Deposit Modelling for Archaeological Projects. Short Run Press, Exeter.

Leggett, D.J., Harvey, R., Cooper, N., 2004. Coastal and estuarine managed realignment: design issues. London: CIRIA.

Liu, Y.B., 2012. Prediction Methods to Determine Stability of Dam If There is Piping, in: Lee, G. (Ed.), 2012 International Conference on Mechanical, Industrial, and Manufacturing Engineering, pp. 131-137.

Long, N., Millescamps, B., Guillot, B., Pouget, F., Bertin, X., 2016. Monitoring the Topography of a Dynamic Tidal Inlet Using UAV Imagery. Remote Sensing 8, 18.

Luther, G.W., Church, T.M., 1988. Seasonal cycling of sulfur and iron in porewaters of a Delaware salt-marsh. Marine Chemistry 23, 295-309.

Macleod, C.L., Scrimshaw, M.D., Emmerson, R.H.C., Chang, Y.H., Lester, J.N., 1999. Geochemical changes in metal and nutrient loading at Orplands Farm Managed Retreat site, Essex, UK (April 1995-1997). Marine Pollution Bulletin 38, 1115-1125.

Marani, M., Belluco, E., D'Alpaos, A., Defina, A., Lanzoni, S., Rinaldo, A., 2003. On the drainage density of tidal networks. Water Resources Research 39.

Marani, M., Silvestri, S., Belluco, E., Ursino, N., Comerlati, A., Tosatto, O., Putti, M., 2006. Spatial organization and ecohydrological interactions in oxygen-limited vegetation ecosystems. Water Resources Research 42.

Maris, T., Cox, T.J.S., Temmerman, S., De Vleeschauwer, P., Van Damme, S., De Mulder, T., Van den Bergh, E., Meire, P., 2007. Tuning the tide: creating ecological conditions for tidal marsh development in a flood control area. Hydrobiologia 588, 31-43.

Masselink, G., Hanley, M.E., Halwyn, A.C., Blake, W., Kingston, K., Newton, T., Williams, M., 2017. Evaluation of salt marsh restoration by means of self-regulating tidal gate – Avon estuary, South Devon, UK. Ecological Engineering 106, Part A, 174-190.

Mazik, K., Musk, W., Dawes, O., Solyanko, K., Brown, S., Mander, L., Elliott, M., 2010. Managed realignment as compensation for the loss of intertidal mudflat: A short term solution to a long term problem? Estuarine, Coastal and Shelf Science 90, 11-20.

McRobie, A., Spencer, T., Gerritsen, H., 2005. The big flood: North Sea storm surge. Philosophical Transactions of the Royal Society a-Mathematical Physical and Engineering Sciences 363, 1263-1270.

Mehta, A.J., Hayter, E.J., Parker, W.R., Krone, R.B., Teeter, A.M., 1989. Cohesive Sediment Transport 1: Process Description. Journal of Hydraulic Engineering-Asce 115, 1076-1093.

Miller, H., Croudace, I.W., Bull, J.M., Cotterill, C.J., Dix, J.K., Taylor, R.N., 2014. A 500 Year Sediment Lake Record of Anthropogenic and Natural Inputs to Windermere (English Lake District) Using Double-Spike Lead Isotopes, Radiochronology, and Sediment Microanalysis. Environmental Science & Technology 48, 7254-7263.

Mitchell, S.B., Burgess, H.M., Pope, D.J., 2006. Stratification and fine sediment transport mechanisms in a semi-enclosed tidal lagoon (Pagham Harbour, West Sussex). Water and Environment Journal 20, 248-255.

Mitchell, S.B., Burgess, H.M., Pope, D.J., Theodoridou, A., 2008. Field studies of velocity, salinity and suspended solids concentration in a shallow tidal channel near tidal flap gates. Estuarine Coastal and Shelf Science 78, 385-395.

Mitsch, W.J., Gosselink, J.G., 2000. Wetlands. John Wiley & Sons, New York.

Moller, I., 2006. Quantifying saltmarsh vegetation and its effect on wave height dissipation: Results from a UK East coast saltmarsh. Estuarine Coastal and Shelf Science 69, 337-351.

Moller, I., Kudella, M., Rupprecht, F., Spencer, T., Paul, M., van Wesenbeeck, B.K., Wolters, G., Jensen, K., Bouma, T.J., Miranda-Lange, M., Schimmels, S., 2014. Wave attenuation over coastal salt marshes under storm surge conditions. Nature Geoscience 7, 727-731.

Moller, I., Spencer, T., 2002. Wave dissipation over macro-tidal saltmarshes: Effects of marsh edge typology and vegetation change. Journal of Coastal Research, 506-521.

Moller, I., Spencer, T., French, J.R., Leggett, D.J., Dixon, M., 1999. Wave transformation over salt marshes: A field and numerical modelling study from north Norfolk, England. Estuarine Coastal and Shelf Science 49, 411-426.

Moller, I., Spencer, T., French, J.R., Leggett, D.J., Dixon, M., 2001. The sea-defence value of salt marshes: Field evidence from north Norfolk. Journal of the Chartered Institution of Water and Environmental Management 15, 109-116.

Morris, R.K.A., 2013. Managed realignment as a tool for compensatory habitat creation - A re-appraisal. Ocean & Coastal Management 73, 82-91.

Mossman, H.L., Brown, M.J.H., Davy, A.J., Grant, A., 2012a. Constraints on Salt Marsh Development Following Managed Coastal Realignment: Dispersal Limitation or Environmental Tolerance? Restoration Ecology 20, 65-75.

Mossman, H.L., Davy, A.J., Grant, A., 2012b. Does managed coastal realignment create saltmarshes with 'equivalent biological characteristics' to natural reference sites? Journal of Applied Ecology 49, 1446-1456.

Nedwell, D.B., Abram, J.W., 1978. Bacterial sulfate reduction in relation to sulfur geochemistry in two contrasting areas of saltmarsh sediment. Estuarine and Coastal Marine Science 6, 341-351.

Ni, W., Wang, Y.P., Symonds, A.M., Collins, M.B., 2014. Intertidal flat development in response to controlled embankment retreat: Freiston Shore, The Wash, UK. Marine Geology 355, 260-273.

Nolan, M., Larsen, C., Sturm, M., 2015. Mapping snow depth from manned aircraft on landscape scales at centimeter resolution using structure-from-motion photogrammetry. Cryosphere 9, 1445-1463.

Paterson, D.M., 1989. Short-term changes in the erodibility of intertidal cohesive sediments related to the migratory behavior of epipelic diatoms. Limnology and Oceanography 34, 223-234.

Paterson, D.M., Black, K.S., 2000. Temporal variability in the critical erosion threshold of saltmarsh and upper intertidal sediments, in: Sherwood, D.M., Gardiner, B.M., Harris, T. (Eds.), British Saltmarshes. Forrest Text for the Linnean Society of London, London, pp. 51-63.

Pearce, J., Khan, S., Lewis, P., 2011. Medmerry managed realignment–sustainable coastal management to gain multiple benefits, ICE Coastal Management. Innovative Coastal Zone Management: Sustainable Engineering for a Dynamic Coast., Belfast, UK.

Pendleton, L., Donato, D.C., Murray, B.C., Crooks, S., Jenkins, W.A., Sifleet, S., Craft, C., Fourqurean, J.W., Kauffman, J.B., Marba, N., Megonigal, P., Pidgeon, E., Herr, D., Gordon, D., Baldera, A., 2012. Estimating Global "Blue Carbon" Emissions from Conversion and Degradation of Vegetated Coastal Ecosystems. Plos One 7.

Pethick, J., 1992. Saltmarsh Geomorphology, in: Pye, K., Allen, J.R.L. (Eds.), Saltmarshes: morphodynamics, conservation and engineering significance. Cambridge University Press, Cambridge, pp. 41-62.

Pethick, J., 2002. Estuarine and tidal wetland restoration in the United Kingdom: Policy versus practice. Restoration Ecology 10, 431-437.

Pontee, N., 2013. Defining coastal squeeze: A discussion. Ocean & Coastal Management 84, 204-207.

Pontee, N., 2014. Accounting for siltation in the design of intertidal creation schemes. Ocean & Coastal Management 88, 8-12.

Pontee, N.I., 2015. Impact of managed realignment design on estuarine water levels. Proceedings of the Institution of Civil Engineers-Maritime Engineering 168, 48-61.

Reed, D.J., Spencer, T., Murray, A.L., French, J.R., Leonard, L., 1999. Marsh surface sediment deposition and the role of tidal creeks: Implications for created and managed coastal marshes. Journal of Coastal Conservation 5, 81-90.

Reid, M.K., Spencer, K.L., 2009. Use of principal components analysis (PCA) on estuarine sediment datasets: The effect of data pre-treatment. Environmental Pollution 157, 2275-2281.

Rodwell, J.S., 2001. British Plant Communities: Volume 5 - Maritime Communities and Vegetation of Open Habitats, in: Rodwell, J.S. (Ed.). Cambridge University Press, Cambridge.

Rotman, R., Naylor, L., McDonnell, R., MacNiocaill, C., 2008. Sediment transport on the Freiston Shore managed realignment site: An investigation using environmental magnetism. Geomorphology 100, 241-255.

Rowell, D.L., 1994. Soil science: Methods & applications. Longman Scientific & Technical, Harlow, Essex.

Ruocco, A.C., Nicholls, R.J., Haigh, I.D., Wadey, M.P., 2011. Reconstructing coastal flood occurrence combining sea level and media sources: a case study of the Solent, UK since 1935. Natural Hazards 59, 1773-1796.

Rupp-Armstrong, S., Nicholls, R.J., 2007. Coastal and estuarine retreat: A comparison of the application of managed realignment in England and Germany. Journal of Coastal Research 23, 1418-+.

Sanford, L.P., 2008. Modeling a dynamically varying mixed sediment bed with erosion, deposition, bioturbation, consolidation, and armoring. Computers & Geosciences 34, 1263-1283.

Saunders, J.E., 2008. Measuring and understanding biogenic influences upon cohesive sediment stability in intertidal systems. University of St Andrews, University of St Andrews.

Schile, L.M., Callaway, J.C., Parker, V.T., Vasey, M.C., 2011. Salinity and Inundation Influence Productivity of the Halophytic Plant Sarcocornia pacifica. Wetlands 31, 1165-1174.

Seeberg-Elverfeldt, J., Schlüter, M., Feseker, T., Kölling, M., 2005. Rhizon sampling of porewaters near the sediment-water interface of aquatic systems. Limnology and Oceanography: Methods 3, 361-371.

Shi, Z., Lamb, H.F., Collin, R.L., 1995. Geomorphic change of salt-marsh tidal creek networks in the Dyfi Estuary, Wales. Marine Geology 128, 73-83.

Spearman, J., 2011. The development of a tool for examining the morphological evolution of managed realignment sites. Continental Shelf Research 31, S199-S210.

Spencer, K.L., Carr, S.J., Diggens, L.M., Tempest, J.A., Morris, M.A., Harvey, G.L., 2017. The impact of pre-restoration land-use and disturbance on sediment structure, hydrology and the sediment geochemical environment in restored saltmarshes. Science of the Total Environment 587–588, 47-58.

Spencer, K.L., Cundy, A.B., Croudace, I.W., 2003. Heavy metal distribution and early-diagenesis in salt marsh sediments from the Medway Estuary, Kent, UK. Estuarine Coastal and Shelf Science 57, 43-54.

Spencer, K.L., Cundy, A.B., Davies-Hearn, S., Hughes, R., Turner, S., MacLeod, C.L., 2008. Physicochemical changes in sediments at Orplands Farm, Essex, UK following 8 years of managed realignment. Estuarine Coastal and Shelf Science 76, 608-619.

Spencer, K.L., Harvey, G.L., 2012. Understanding system disturbance and ecosystem services in restored saltmarshes: Integrating physical and biogeochemical processes. Estuarine Coastal and Shelf Science 106, 23-32.

Spencer, T., Friess, D.A., Moeller, I., Brown, S.L., Garbutt, R.A., French, J.R., 2012. Surface elevation change in natural and re-created intertidal habitats, eastern England, UK, with particular reference to Freiston Shore. Wetlands Ecology and Management 20, 9-33.

Stark, J., Plancke, Y., Ides, S., Meire, P., Temmerman, S., 2016. Coastal flood protection by a combined nature-based and engineering approach: Modeling the effects of marsh geometry and surrounding dikes. Estuarine, Coastal and Shelf Science 175, 34-45.

Symonds, A.M., Collins, M.B., 2005. Sediment dynamics associated with managed realignment; Freiston shore, the wash, UK.

Symonds, A.M., Collins, M.B., 2007. The establishment and degeneration of a temporary creek system in response to managed coastal realignment: The Wash, UK. Earth Surface Processes and Landforms 32, 1783-1796.

Temmerman, S., Bouma, T.J., Van de Koppel, J., Van der Wal, D.D., De Vries, M.B., Herman, P.M.J., 2007. Vegetation causes channel erosion in a tidal landscape. Geology 35, 631-634.

Temmerman, S., Govers, G., Meire, P., Wartel, S., 2003. Modelling long-term tidal marsh growth under changing tidal conditions and suspended sediment concentrations, Scheldt estuary, Belgium. Marine Geology 193, 151-169.

Tempest, J.A., Harvey, G.L., Spencer, K.L., 2015. Modified sediments and subsurface hydrology in natural and recreated salt marshes and implications for delivery of ecosystem services. Hydrological Processes 29, 2346-2357.

Thomas, S., Ridd, P.V., 2004. Review of methods to measure short time scale sediment accumulation. Marine Geology 207, 95-114.

Tolhurst, J., Defew, E.C., Perkins, R.G., Sharples, A., Paterson, D.M., 2006a. The effects of tidally-driven temporal variation on measuring intertidal cohesive sediment erosion threshold. Aquatic Ecology 40, 521-531.

Tolhurst, T.J., Black, K.S., Paterson, D.M., Mitchener, H.J., Termaat, G.R., Shayler, S.A., 2000a. A comparison and measurement standardisation of four in situ devices for determining the erosion shear stress of intertidal sediments. Continental Shelf Research 20, 1397-1418.

Tolhurst, T.J., Black, K.S., Shayler, S.A., Mather, S., Black, I., Baker, K., Paterson, D.M., 1999. Measuring the in situ erosion shear stress of intertidal sediments with the Cohesive Strength Meter (CSM). Estuarine Coastal and Shelf Science 49, 281-294.

Tolhurst, T.J., Defew, E.C., de Brouwer, J.F.C., Wolfstein, K., Stal, L.J., Paterson, D.M., 2006b. Small-scale temporal and spatial variability in the erosion threshold and properties of cohesive intertidal sediments. Continental Shelf Research 26, 351-362.

Tolhurst, T.J., Friend, P.L., Watts, C., Wakefield, R., Black, K.S., Paterson, D.M., 2006b. The effects of rain on the erosion threshold of intertidal cohesive sediments. Aquatic Ecology 40, 533-541.

Tolhurst, T.J., Friend, P.L., Watts, C., Wakefield, R., Black, K.S., Paterson, D.M., 2006c. The effects of rain on the erosion threshold of intertidal cohesive sediments. Aquatic Ecology 40, 533-541.

Tolhurst, T.J., Riethmuller, R., Paterson, D.M., 2000b. In situ versus laboratory analysis of sediment stability from intertidal mudflats. Continental Shelf Research 20, 1317-1334.

Tonkin, T.N., Midgley, N.G., 2016. Ground-Control Networks for Image Based Surface Reconstruction: An Investigation of Optimum Survey Designs Using UAV Derived Imagery and Structure-from-Motion Photogrammetry. Remote Sensing 8.

Townend, I., Pethick, J., 2002. Estuarine flooding and managed retreat. Philosophical Transactions of the Royal Society a-Mathematical Physical and Engineering Sciences 360, 1477-1495.

Tucker, W., 2017. Crossrail project: the execution strategy for delivering London's Elizabeth line. Proceedings of the Institution of Civil Engineers-Civil Engineering 170, 3-14.

Turner, R.K., Daily, G.C., 2008. The ecosystem services framework and natural capital conservation. Environmental & Resource Economics 39, 25-35.

UK National Ecosystem Assessment, 2011. UK National Ecosystem Assessment: Chapter 11 Coastal Margins, Cambridge.

Van Huissteden, J., Van de Plassche, O., 1998. Sulphate reduction as a geomorphological agent in tidal marshes ('great marshes' at Barnstable, Cape Cod, USA). Earth Surface Processes and Landforms 23, 223-236.

van Loon-Steensma, J.M., Vellinga, P., 2013. Trade-offs between biodiversity and flood protection services of coastal salt marshes. Current Opinion in Environmental Sustainability 5, 320-326.

Vandenbruwaene, W., Bouma, T.J., Meire, P., Temmerman, S., 2013. Bio-geomorphic effects on tidal channel evolution: impact of vegetation establishment and tidal prism change. Earth Surface Processes and Landforms 38, 122-132.

Vandenbruwaene, W., Meire, P., Temmerman, S., 2012. Formation and evolution of a tidal channel network within a constructed tidal marsh. Geomorphology 151, 114-125.

Vant, W.N., Daviescolley, R.J., 1984. Factors affecting clarity of New-Zealand Lakes. New Zealand Journal of Marine and Freshwater Research 18, 367-377.

Vardy, S., Saunders, J.E., Tolhurst, T.J., Davies, P.A., Paterson, D.M., 2007. Calibration of the high-pressure cohesive strength meter (CSM). Continental Shelf Research 27, 1190-1199.

Viles, H.A., Naylor, L.A., Carter, N.E.A., Chaput, D., 2008. Biogeomorphological disturbance regimes: progress in linking ecological and geornorphological systems. Earth Surface Processes and Landforms 33, 1419-1435.

Violante, A., Barberis, E., Pigna, M., Boero, V., 2003. Factors affecting the formation, nature, and properties of iron precipitation products at the soil-root interface. Journal of Plant Nutrition 26, 1889-1908.

Vranken, M., Oenema, O., Mulder, J., 1990. Effects of tide range alterations on salt-marsh sediments in the eastern Scheldt, SW Netherlands. Hydrobiologia 195, 13-20.

Wadey, M.P., Nicholls, R.J., Haigh, I., 2013. Understanding a coastal flood event: the 10th March 2008 storm surge event in the Solent, UK. Natural Hazards 67, 829-854.

Wadey, M.P., Nicholls, R.J., Hutton, C., 2012. Coastal Flooding in the Solent: An Integrated Analysis of Defences and Inundation. Water 4, 430-459.

Wang, S., Chen, J.-s., He, H.-q., He, W.-z., 2016. Experimental study on piping in sandy gravel foundations considering effect of overlying clay. Water Science and Engineering 9, 165-171.

Wass, P.D., Leeks, G.J.L., 1999. Suspended sediment fluxes in the Humber catchment, UK. Hydrological Processes 13, 935-953.

Watts, C.W., 2008. Further Monitoring of the Strength and Stability of Sediments and Soils on the Tollesbury Managed Realignment Site, London.

Watts, C.W., Tolhurst, T.J., Black, K.S., Whitmore, A.P., 2003. In situ measurements of erosion shear stress and geotechnical shear strength of the intertidal sediments of the experimental managed realignment scheme at Tollesbury, Essex, UK. Estuarine Coastal and Shelf Science 58, 611-620.

Weeks, A.R., Simpson, J.H., Bowers, D., 1993. The relationship between concentrations of suspended particulate material and tidal processes in the Irish Sea. Continental Shelf Research 13, 1325-1334.

Westoby, M.J., Brasington, J., Glasser, N.F., Hambrey, M.J., Reynolds, J.M., 2012. 'Structure-from-Motion' photogrammetry: A low-cost, effective tool for geoscience applications. Geomorphology 179, 300-314.

Widdows, J., Friend, P.L., Bale, A.J., Brinsley, M.D., Pope, N.D., Thompson, C.E.L., 2007. Inter-comparison between five devices for determining erodability of intertidal sediments. Continental Shelf Research 27, 1174-1189.

Wilson, A.M., Evans, T., Moore, W., Schutte, C.A., Joye, S.B., Hughes, A.H., Anderson, J.L., 2015. Groundwater controls ecological zonation of salt marsh macrophytes. Ecology 96, 840-849.

Wilson, A.M., Morris, J.T., 2012. The influence of tidal forcing on groundwater flow and nutrient exchange in a salt marsh-dominated estuary. Biogeochemistry 108, 27-38.

Winterwerp, J.C., van Kesteren, W.G.M., 2004. Introduction to the Physics of Cohesive Sediment in the Marine Environment. Elsevier.

Wolanski, E., Elliott, M., 2016. Estuarine Ecohydrology (Second Edition). Elsevier, Boston.

Wolters, M., Garbutt, A., Bakker, J.P., 2005. Salt-marsh restoration: evaluating the success of de-embankments in north-west Europe. Biological Conservation 123, 249-268.

Wolters, M., Garbutt, A., Bekker, R.M., Bakker, J.P., Carey, P.D., 2008. Restoration of salt-marsh vegetation in relation to site suitability, species pool and dispersal traits. Journal of Applied Ecology 45, 904-912.

Xin, P., Jin, G.Q., Li, L., Barry, D.A., 2009. Effects of crab burrows on pore water flows in salt marshes. Advances in Water Resources 32, 439-449.

Young, E.J., 2012. dGPS, in: Clarke, L.E., Nield, J.M. (Eds.), Geomorphological Techniques, Online ed. British Society for Geomorphology, London.

Zwolsman, J.J.G., Berger, G.W., Vaneck, G.T.M., 1993. Sediment accumulation rates, historical input, postdepositional mobility and retention of major elements and trace-metals in salt-marsh sediments of the Scheldt estuary, SW Netherlands. Marine Chemistry 44, 73-94.

Appendices

Appendix 1

Methods of measuring rates of sediment accretion and erosion in the intertidal zone.

Method	Example	Description	Reported Resolution	Advantages	Disadvantages
ALTUS	Jestin et al. (1998); Dale et al. (2017)	A submersible autonomous echo-sounder altimeter device which is deployed in a tripod frame and includes separate pressure sensor.	± 2 mm	• Tripod reduces scour of study area • Autonomous so can be deployed in isolated areas • Provides constant high frequency measurements	• Only measures an area of 2.5 to 3 cm in diameter • Relatively expensive • Risk of fouling around instrument • Only measures when submerged
Anchored Tile	Pasternack and Brush	Rod inserted into sediment and a detachable tile fastened	0.001 to 0.002 μm	• Inexpensive • Can obtain multiple	• Only measures sediment accretion

	(1998)	on flush with the sediment surface. Material deposited on the tile then collected, dried and weighed.	depending on sediment collection and processing	measurements	• Potential for influence by disturbances
Filter Paper	Reed (1989)	Same as Anchored Tile method by using pre-weighed filter papers.	0.001 to 0.002 µm depending on sediment collection and processing	• Inexpensive • Can obtain multiple measurements	• Filter paper could be washed away • Only measures sediment accretion • Potential for influence by disturbances
Light Detecting and Ranging (LiDAR)	Clapp (2009)	The distance between the bed and a laser, usually mounted on an aeroplane, is measured by illuminating a target and analysing the light reflected.	Up to 100 mm	• Can cover a large area relatively quickly	• Large resolution too high for small scale measurements • Frequency of data collection can depend on

					conditions such as suitable weather
Marker Horizon	Cahoon and Turner (1989)	Layer of clay, sand, feldspar or sediment with rare element spread over the sediment. Cores taken at intervals to measure amount of sediment that has accumulated over layer.	± 1 mm	• Inexpensive • Can cover a large area • Can duplicate sampling for spatial comparisons	• Large quantity of material required • May have negative impact on environment • Layer may be disturbed by for example biofilms • Layer may be smeared whilst coring • Layer could be lost through erosion • Only measures accretion of sediment
Metal Plate	Allen and Duffy (1998)	Similar to the Marker Horizon technique, a metal plate is buried and the depth	± 1 mm	• Relative simple • Provides scope for repeat measurements and	• Plate could sink through sediment if denser • Sediment can be disturbed

		of sediment above the plate is measured.		comparisons	whilst burying plate
Stakes/Pins/ Pegs	Clapp (2009); Ni et al. (2014)	Metal or wooden pins are pushed into the sediment and the changing bed level can be measured by either measuring the distance from the top of the pin to the sediment or by placing pins in pairs and measuring the distance to the sediment at set intervals.	± 1 mm	• Inexpensive • Simple • Robust • Measures accretion and erosion • No environmental impact if lost or damaged	• Can be influenced by scour and disturbances around the base of the peg • Limited opportunity for temporal variability analysis • Susceptible to damage such as snapping
Sediment Erosion Table	Boumans and Day (1993)	The table is placed on a permanently installed mount, levelled and pins from the table are lowered to the sediment surface. The	± 1.4 to ± 2 mm	• Relatively inexpensive • Large samples size • Measures accretion and erosion	• Complicated and time consuming set-up and measurement procedure • High level of accuracy required in set-up

		distance between the top of the pins and table are measured directly relate to changes in distance between the sediment surface and the table.		• Limited opportunity of temporal variability analysis
Short-term Radionuclides/ Radiometric Dating	Cundy et al. (2002)	Sediment cores taken and sampled for presence of radionuclides to determine the duration since the sediment has been present on the surface.	• Range of temporal resolutions possible	• Expensive • Limited by the abundance of radionuclides

Sedimeter	Erlingsson (1991)	Series of sideways orientated infrared transmitters and optical backscatter sensors in a transparent rod. Rod is inserted into the sediment with more or fewer sensors receiving a signal as the bed elevation changes.	100 µm reported under laboratory conditions	• Measures accretion and erosion • Can measure constant rapid changes over very small temporal scale	• Expensive • Can interfere with flow of water
Photo-electronic erosion pins	Mitchell et al. (2003)	Similar to the Sedimeter but uses connected photosensitive sells in a transparent rod.	*c*. 2 mm	• Measures erosion and accretion • Can be used to compare elevation changes with influence of tides and wind	• Scouring around instrument • Fouling of sensors limiting potential for long deployment • Expensive • Resolution too high for small scale measurements

Appendix 2

The components and characteristics of the ALTUS data logger and altimeter used in this study.

	Component	Characteristics
Data Logger Characteristics	Data Logger	Built on a single double face 27 x 111 mm electronic board in Surface Mounted Components technology, managed by an 8 bit Philips 87C54 microcontroller driven at a 14.745 HMz frequency.
	Memory	Data are stored on a 32 Kbyte static memory.
Altimeter Characteristics	Altimeter	Uses the same technology as the data logger. It has an accuracy of ± 2 mm and resolution of 0.6 mm when measuring altitudes between 20 to 70 cm and an accuracy of ± 5 mm and resolution of 0.6 mm when measuring between 20 to 200 cm.
	Transducer	Acts as both the transmitter and the receiver and consists of a piezoelectric crystal which is excited at a frequency of 2 MHz. The overall diameter is 25 mm, of which the active cell consists of 10.2 mm. The Conical beam width is 3.6° giving an enlighted area of 2.5 cm when the transducer is located less than 30 cm above the bed. The cell is mounted in a 57 mm long and 54 mm diameter waterproof crystalline polyester container and is connected to the plug of a waterproof Jupiter connector by a 9 mm diameter and

	5 m long armoured polyurethane cable.
Pressure Sensor	Consists of a small piezoresistive Keller pressure gauge with both the diaphragm and the case made of hastelloy. The measurement range is 0 to 20 m of water above the sensor and the non-permanent survival depth is approximately 60 m.
Energy	Powered by four coupled parallel/series mounted lithium batteries and should theoretically power the altimeter for four years if recording at a 15 minute recording rate of two years if recording every 2 minutes.
Pressure Case	Made with ‘Ertalyte’ crystalline polyester and the screws of marine standard stainless steel, designed to withstand deployment in a harsh muddy environment. Designed to withstand 100 metres of immersion and can be easily dug into the sediment. The overall diameter is 84 mm and the overall length in 240 mm.
Non-connection Communication System	To communicate between the device and a PC a ‘data pencil’ has been developed. The device works by approaching the system with the data pencil, meaning there is no need to disconnect and reconnect part to the device whilst in the field. The system is also able to start an interrupted data transfer from where communication was lost without losing any data.

Appendix 3

The specification for the EXO2 Sonde probes used in this study.

EXO2 Sonde		Conductivity	Temperature	Depth	Turbidity
Sensor Type		Four Electrode Nickel Cell	Thermistor	Stainless Steel Strain Gauge	Optical, 90° Scatter
Default Units		microSiemens/centimetre (mS/cm)	Degrees Celsius (°C)	PSI, Depth (meters, feet, bar)	Formazin Nephelometric Units (FNU)
Temperature	Operating	-5 to +50 °C	-5 to +50 °C	-5 to +50 °C	-5 to +50 °C
	Storage	-20 to +80 °C	-20 to +80 °C	-20 to +80 °C	-20 to +80 °C
Range		0 to 200 mS/cm		Shallow: 0 to 10 m. Medium: 0 to 100 m. Deep: 0 to 250 m.	0 to 4000 FNU
Accuracy		0 to 100 mS/cm: ± 0.5 % of reading or 0.001 mS/cm, whichever is greater 100 to 200 mS/cm: ± 1 % of reading	-5 to +35 °C: ± 0.01°C +35 to +50 °C: ± 0.05 °C	Shallow: ± 0.004 m Medium: ± 0.04 m Deep: ± 0.1 m	0 to 999 FNU: 0.3 FNU or ± 2 % of reading, whichever is greater 1000 to 4000 FNU: ± 5 % of reading

Response	< 2 seconds	< 1 second	< 2 seconds	< 2 seconds
Resolution	0.0001 to 0.01 mS/cm (range dependent)	0.001 °C	0.001 m	0 to 999 FNU: 0.01 FNU 1000 to 4000 FNU: 0.1 FNU

Appendix 4

Calibration coefficients for Inductively Coupled Plasma-Optical Emission Spectrometer analysis.

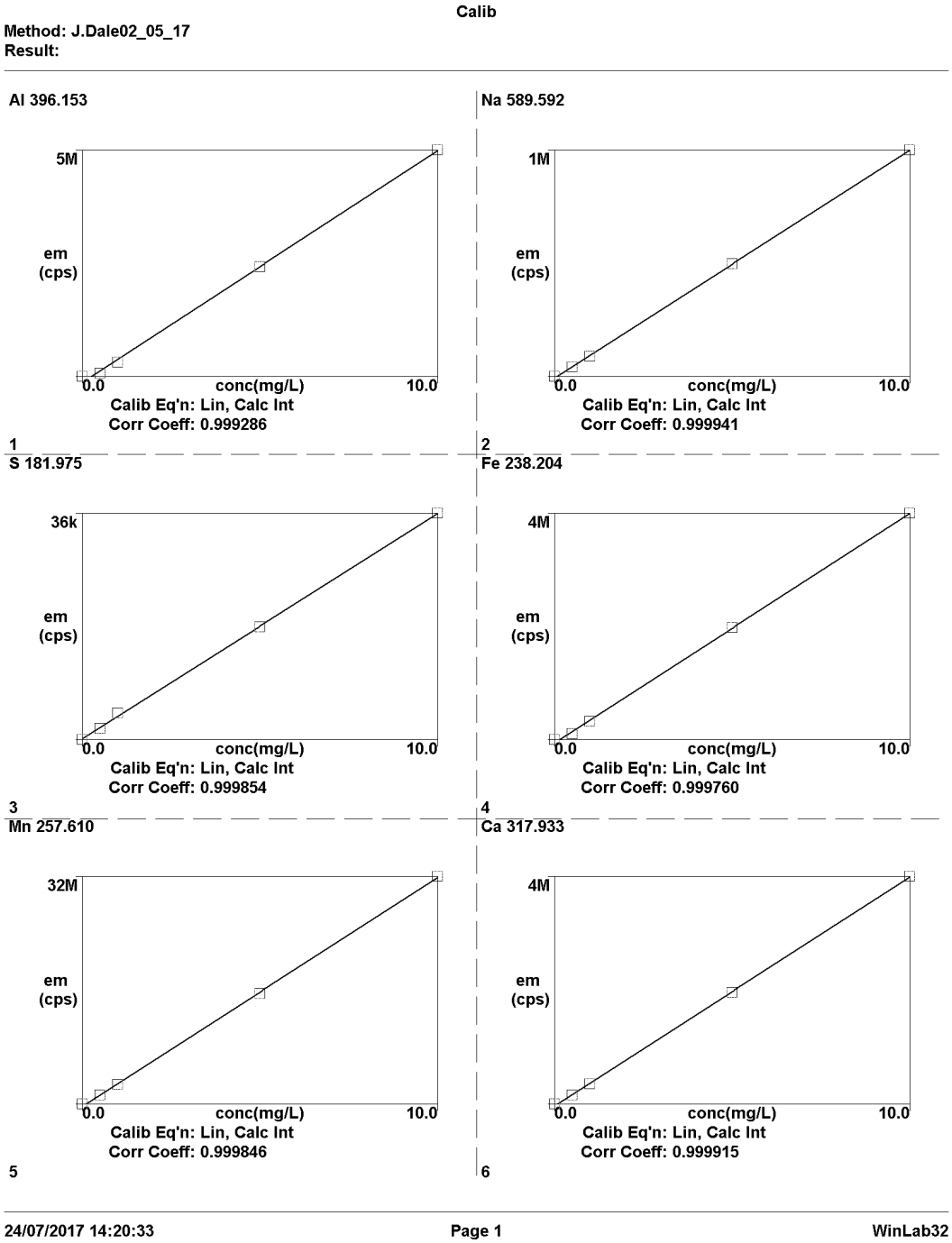

Appendix 5

Recovery values (percent) for the Mess-4 Marine Sediment Certified Reference Material digested alongside samples for Inductively Couples Plasma-Optical Emission Spectrometer analysis.

	Al	**Na**	**S**	**Fe**	**Mn**	**Ca**
Sample 1	74.98	74.20	109.33	77.45	112.77	94.05
Sample 2	75.80	79.78	106.12	75.03	110.79	90.52
Sample 3	78.84	89.22	126.00	90.12	130.70	108.44
Sample 4	73.57	64.96	93.78	64.66	95.12	78.34
Sample 5	75.34	74.98	107.01	76.09	111.77	91.97
Sample 6	76.83	79.36	104.06	74.82	115.13	89.68
Average	75.89	77.08	107.72	76.36	112.71	92.17
Standard Deviation	1.79	7.99	10.46	8.14	11.34	9.68

Appendix 6

Reconstruction of draining tidal waters through the pipes at Site 2b. See disc attached to back cover.